

## CATALYSIS IN DIRECT LIQUEFACTION OF COAL

R.D. Srivastava and S.V. Gollakota  
Burns and Roe Services Corporation  
Pittsburgh, PA 15236  
and

M.J. Baird, E.B. Klunder, S.R. Lee, and G.V. McGurl  
Pittsburgh Energy Technology Center  
Pittsburgh, PA 15236

Keywords: Direct Liquefaction, Catalysis, Dispersed Catalysts

### INTRODUCTION

In view of the recent National Research Council study (1) and the present National Energy Strategy (2), the Pittsburgh Energy Technology Center (U.S. Department of Energy) is actively pursuing the Direct Liquefaction Program to develop technologies for producing low-cost liquid fuels from coal. A brief overview of the ongoing Direct Liquefaction Program is given below. This program broadly encompasses laboratory and bench-scale developments of promising new concepts, as well as proof-of-concept evaluation in pilot-scale, two-stage liquefaction units. Of the various areas being studied in this program, improved catalysts could play a major role in lowering thermal severity, improving product yields/selectivity, and improving process configuration. Thus, the catalysts used in the ongoing two-stage liquefaction studies and some of the current activities in the catalysis research are outlined in this paper.

### OVERVIEW OF THE DIRECT LIQUEFACTION PROGRAM

The overall objective of the Pittsburgh Energy Technology Center's (PETC) Direct Liquefaction Program is to bring the liquefaction technology to commercial readiness in an environmentally acceptable manner, and some of the current activities directed toward this objective are outlined below.

#### Two-Stage Liquefaction Program

Direct liquefaction process testing is continuing at Hydrocarbon Research Inc. (HRI) and Amoco Oil Company. Future research will focus on the effects of coal cleaning/pretreatment, dispersed catalysts, preconversion processing, solids separation methods, bottoms processing, on-line hydrotreating, and solvent quality improvement.

#### Advanced Process Concepts Program

One of the main objectives of this program is to conduct fundamental studies and exploratory research to develop improved process configurations in direct liquefaction. The work being performed by some PETC contractors is briefly outlined as follows. The University of Kentucky Research Foundation is focusing on a two-stage low-rank coal liquefaction process that has oil agglomeration, fluid coking, and solvent dewaxing as the main features. Improvements in process operation, coal conversion, and product yields are anticipated. SRI is evaluating novel dispersed catalysts and improved reaction chemistry (e.g., use

of CO+H<sub>2</sub>) for low-rank coals. This program will focus on reducing regressive reactions and increasing product quality in liquefaction. HRI is studying the merits of integrating two-stage liquefaction with fixed-bed hydrotreating to give improved products. Amoco Oil Company is evaluating the following processing steps to improve process operability during liquefaction of low-rank coals: conventional coal cleaning, coal pretreatment with aqueous SO<sub>2</sub> solutions to remove alkali metals from coal, impregnation of coal with a catalyst, and bottoms processing (e.g., deasphalting, coking). The Canadian Energy Development, Inc. (with Alberta Research Council) is evaluating a two-stage process consisting of oil agglomeration, coal slurry pretreatment, and hydroconversion. In this study, use of a dispersed catalyst and CO+H<sub>2</sub>O system in a counter-flow reactor is proposed for process improvement.

#### Baseline Design and System Analysis

A conceptual baseline design of a two-stage direct coal liquefaction process, sponsored by PETC, is being performed by Bechtel and Amoco. This baseline study includes development of a process simulation model applicable over a certain range of capacities and process options involving coal cleaning, reactor configuration, vacuum bottoms processing, and hydrogen production methods. The model simulates a commercial liquefaction facility to predict yields and economics for different processing schemes. The data obtained at the Wilsonville Advanced Coal Liquefaction Research and Development Facility in Run 257 with Illinois No. 6 coal from Burning Star No. 2 mine and Amocat-1C catalyst in a two-stage catalytic liquefaction process is being utilized as the base case.

#### Coprocessing Program

Coprocessing, in which coal is processed along with a heavy petroleum residuum, is considered to be a variation of direct liquefaction. Some of the present studies in coprocessing are focusing on understanding possible synergism between coal and petroleum residuum, merits of dispersed catalysts, and recycle effects. Bench-scale studies are being carried out at UOP in a slurry reactor and at HRI in a two-stage ebullated-bed reactor system. These studies are being assessed for their technical and economic merits.

#### Refining, Upgrading, and End-Use Testing Program

Although the current two-stage liquefaction products are lower in heteroatom contents and higher in hydrogen compared to previous single-stage products, the two-stage products require additional refining/upgrading to meet commercial fuel specifications. Studies will be performed to produce refinery feeds and specification products in order to assess the technology required for refining and also to test the products for their emission properties.

#### Generic Bench-Scale Unit

An integrated, continuous-flow bench-scale unit (BSU) will be built at PETC to screen, develop, and improve new process concepts in direct liquefaction. This unit will have a capacity of 200 pounds of coal feed per day. This BSU will have the flexibility to operate over a wide range of conditions with different ranks of coals and different reactor types (i.e., slurry, ebullated-bed, fixed-bed). It is anticipated that this unit will be ready for operation by 1993. During the design and construction of this generic BSU, promising new approaches being developed by PETC contractors will be evaluated for testing in this unit.

## TWO-STAGE LIQUEFACTION CATALYSTS

Catalysis plays a major role in determining coal and resid conversions and distillate selectivity in direct liquefaction. Although the inherent mineral matter in coal itself has some catalytic activity, external catalysts must be provided to obtain satisfactory reaction rates and specification products. A description of the status of liquefaction catalysis and catalysts was given in some recent reviews (3, 4). In the catalytic two-stage liquefaction process that was studied at Wilsonville and HRI in the recent past, alumina-supported transition metal catalysts were used in the ebullated-bed reactors to facilitate coal liquefaction and solvent hydrogenation. A brief description of the two-stage liquefaction process is given below to better understand the role and importance of catalysts in each reactor.

### Process Description

In the close-coupled two-stage liquefaction, two ebullated-bed reactors are in series followed by a solids separation system. The pulverized feed coal is mixed with coal-derived recycle solvent and hydrogen and preheated before entering the first stage. The slurry in the first stage is continuously recirculated by the use of a pump while the catalyst extrudates are ebullated in an upflow stream. Typical reactor inlet hydrogen partial pressures and reactor average temperatures would be in the ranges of 2300 to 2500 psig and 750 to 810°F, respectively. About 90 wt% of a bituminous coal conversion generally occurs in the first stage, and the degree of hydrogenation and distillate production depend on the operating conditions such as temperature, pressure, catalyst type/charge/age, and space velocity. Depending on the liquefaction conditions, the catalyst could deactivate due to factors such as coking, deposition of minerals and basic compounds, pore mouth plugging, and sintering. To sustain steady catalytic activity in the reactor, some deactivated catalyst must be withdrawn and replaced with fresh catalyst. Because high catalyst deactivation rates require high catalyst replacement rates, developing catalysts that are resistant to rapid deactivation is desirable. Maintaining good catalyst activity in the first stage could facilitate obtaining higher coal conversions, higher solvent quality, and higher resid cracking/hydrogenation.

The first-stage products, which are gases, distillate, resid (resid is typically non-distillable at 850°F and 1 atm), unconverted coal, and ash, may be passed through an interstage separator for removing heteroatom gases (i.e., gases containing sulfur, nitrogen, and oxygen), light hydrocarbon gases, and some distillate before entering the second stage. Separating the heteroatom gases could allow maintaining higher hydrogen partial pressures in the second stage. In addition, undesirable reactions such as methanation could be minimized, especially in low-rank coal operations. The second stage is usually operated under conditions that are favorable for heteroatom removal and further upgrading of coal liquids. Depending on the operating mode, i.e., high/low or low/high, the second stage conditions could be, to some extent, in the range given above for the first stage. The second-stage products are sent to various vapor-liquid and liquid-solid separation systems for product recovery and recycle solvent preparation (5-9).

### Supported Catalysts

Generally, in two-stage liquefaction, supported catalysts were used in both

stages for bituminous coals (7-9). On the other hand, a supported catalyst was used in only one stage at Wilsonville in most of the low-rank coal liquefaction studies; some tests with subbituminous coals were, however, made both at HRI and Wilsonville using supported catalysts in both stages.

At Wilsonville, Criterion 324 (Shell 324) unimodal Ni-Mo catalyst was frequently used in recent runs. In addition, Ni-Mo bimodal catalysts were also tested in some runs, e.g., Shell 317 in Run 254, Amocat-1C in Run 257, and EXP-AO-60 in Run 261 (8, 9). These catalysts typically contain 10 to 13 wt% molybdenum and 2 to 3 wt% nickel on alumina. The pore volumes in unimodal and bimodal catalysts are typically in the ranges of 0.4 to 0.5 and 0.7 to 0.8 cc/g, respectively (9). The diameters of small pores in both types of catalysts are usually in hundreds of angstroms (e.g., 100-200 Å); however, the bimodal catalysts are distinguished by the presence of additional pores having diameters in thousands of angstroms (e.g., 1000-2000 Å). The larger pores in bimodal catalysts could facilitate diffusion of large asphaltene molecules and reduce pore mouth plugging.

Satisfactory performance of Criterion 324 was observed, when it was used as the second-stage catalyst in thermal/catalytic mode, in Wilsonville subbituminous coal runs 258 and 260 (8, 10). In these runs, the catalyst replacement rate was in the range of 1.5 to 3 lb/ton coal. Significantly improved performance of the catalytic stage was observed when Criterion 324 was used in the first stage in catalytic/thermal mode in Run 260 (8). It may be pointed out that in these runs, an iron precursor was introduced with coal-solvent slurry to catalyze coal conversion.

High distillate yields and good product qualities were obtained with a deep-cleaned Pittsburgh seam coal, in Wilsonville Run 259, using Criterion 324 catalyst in both stages at a total catalyst replacement rate of 8 lb/ton coal (9). In Run 261, tests were performed with Illinois No. 6 coal using EXP-AO-60 and Criterion 324 catalysts (8). The total catalyst replacement rates in this run were in the range of 3 to 6 lb/ton coal. In Runs 259 and 261, increasing slurry viscosities limited the extent of batch deactivation with Criterion 324 catalyst. Satisfactory process performance was obtained using EXP-AO-60 catalyst at a total catalyst replacement rate of 3 lb/ton coal (8). The physical strength of the bimodal catalysts was of some concern in ebullated-bed reactor operation. For example, when 1/12-inch Amocat-1C cylindrical extrudates were used in Wilsonville Run 257, a significant amount of the initially charged catalyst was found to be broken at the end of the tests (11). However, it appeared that some other bimodal catalysts, i.e., 1/16-inch EXP-AO-60 cylindrical pellets tested in Run 261 and 1/20-inch Shell 317 trilobe pellets tested in Run 254, did not exhibit significant breakage (8, 12).

HRI developed a catalytic two-stage liquefaction process operating in low/high temperature mode using nickel-molybdenum supported catalysts (7). Some of the catalysts tested were 1/32-inch Davison Amocat-1C catalyst, 1/20-inch UOP spherical catalyst, and 1/32-inch Shell 317 cylindrical catalyst. An Illinois No. 6 coal and an Ohio No. 5/6 coal (both bituminous) and a Wyodak subbituminous coal were tested in this process development. In this low/high process, the first-stage catalytic ebullated-bed reactor was operated at low temperatures (about 750°F). At these mild temperatures, coal is thought to dissolve slowly in the recycle solvent allowing the rate of catalytic hydrogenation reactions that regenerate the solvent to be somewhat similar to the rate of coal conversion. Further conversion and upgrading of first-stage products occur in

the second stage operated at higher temperatures. Higher distillate yields and extinction recycle conversion of heavy oils (750°F+ vacuum gas oil) were said to be some of the major achievements in this low/high mode (7).

Some of the recent supported catalyst work at HRI was focused on on-line hydrotreating. On-line hydrotreating with Shell 424, NiMo catalyst, was effective in reducing the heteroatom content in the distillate product. For example, when a distillate having an end-point of about 550°F was hydrotreated, the nitrogen and sulfur contents were reduced from 1280 to 9 ppm and 230 to 14 ppm, respectively. In additional tests, the hydrotreating efficiency was found to be dependent on the feed end-point (13).

#### Dispersed Catalysts

At Wilsonville, a readily available iron oxide (minus 325 mesh powder) in combination with a sulfiding agent was used routinely in the liquefaction of subbituminous coals. Although this gave satisfactory operation with two-stage coal conversions in the range of 90 to 95 wt%, the iron dispersion might not have been optimum under the liquefaction conditions. In the recent past, a molybdenum precursor was used at Wilsonville in the liquefaction of the Black Thunder mine subbituminous coal (8, 14). The precursor was a complex organic compound (commercial name is Molyvan L) containing molybdenum, sulfur, phosphorous, carbon, and hydrogen. It was used primarily to test the effectiveness of dispersed molybdenum in limiting the solids buildup frequently observed at Wilsonville during the liquefaction of subbituminous coals. Based on preliminary results, it appeared that the solids buildup was mitigated to some extent when the dispersed molybdenum was used (14). Again, as was the case with the iron oxide, it was not certain that the selected molybdenum precursor, Molyvan L, gave optimum active metal dispersion.

HRI recently tested some iron precursors in combination with a supported catalyst. These iron compounds were magnetite (an oxide magnetic pigment) and a pyrrhotite. It was concluded that these compounds had limited catalytic effect (15).

The effectiveness of supported catalysts in obtaining high distillate yields (up to 75-78 wt% maf coal) and good product qualities was demonstrated both at Wilsonville and HRI; however, the application of dispersed catalysts in pilot-scale two-stage liquefaction is yet to be thoroughly examined. Some of the current activities in dispersed catalyst development are outlined below.

#### CATALYST DEVELOPMENT

As stated earlier, due to high deactivation rates of supported catalysts currently used in pilot-scale process development, aged catalysts must be continually replaced to sustain good catalytic activity. High catalyst replacement rates could contribute significantly to the operating costs in a commercial process. Although regeneration of these catalysts could reduce costs, effective procedures for catalyst regeneration are yet to be demonstrated in pilot-scale operations. In addition, recovery of the metals from spent catalysts is a significant process expense. Hence, PETC is sponsoring research on the development of new and improved catalysts and catalytic processes. Some of these activities are briefly described below.

### Finely Dispersed Iron and Molybdenum Catalysts: In-House Research at PETC

Researchers at PETC are developing advanced procedures to obtain finely divided forms of iron and molybdenum to yield highly active catalysts for direct coal liquefaction applications. Demonstrating the effectiveness of dispersed catalysts in pilot-scale liquefaction units could allow using slurry reactors in place of ebullated-bed reactors at lower capital and operating costs.

Commercially available, low-cost iron compounds could be used as precursors for disposable liquefaction catalysts. However, the activity of catalysts derived from readily available iron oxides and iron sulfides could be low due to poor initial dispersion, low surface area, and the tendency to aggregate. PETC is focusing on preparing ultrafine particles that have significantly larger surface area and higher activity compared to the conventional catalysts.

The well-dispersed iron catalysts can exhibit superior characteristics for use in a coal dissolution reactor. In one preparation method, an initial incipient wetness impregnation of the feed coal with ferric nitrate was carried out. Subsequently, the high dispersion and interaction with the coal surfaces was maintained by conversion of the added iron to an insoluble hydrated iron oxide. Then, activation of this dispersed hydrated iron oxide at about 525°F was shown to result in an effective disposable catalyst for coal conversion (16, 17).

Under proper activation conditions, two sulfided molybdenum compounds -- ammonium tetrathiomolybdate and molybdenum trisulfide -- are very good candidates as precursors for a slurry catalyst. In contrast to alternative non-sulfided molybdenum catalyst precursors, use of these precursors could reduce the activation steps and external sulfur requirements while resulting in a highly active molybdenum disulfide catalyst. Preliminary studies at PETC indicated that both precursors thermally decompose to a high surface area molybdenum disulfide if the thermal transition was rapid. The catalytic activity was sufficient to sustain high coal conversions at molybdenum concentrations as low as 200 to 300 parts per million (18).

Laboratory liquefaction tests were made at PETC to evaluate the aforementioned iron and molybdenum catalysts. Using iron concentrations as low as 2500 ppm (based on coal), liquefaction tests were conducted with Illinois No. 6 coal slurried with coal-derived solvents. Conversions of the coal to distillate and soluble products at 425°C in H<sub>2</sub>+3% H<sub>2</sub>S atmosphere for 1 hr compared favorably with conversions obtained under the same conditions using 1500 ppm of molybdenum (16). HRI is also currently testing these dispersed iron catalysts prepared at PETC. Further development of these catalysts is in progress.

### Hydrous Metal Oxide Catalysts

Researchers at Sandia National Laboratories are developing catalysts based on hydrous titanium oxide (HTO) ion exchangers for application in direct liquefaction. The hydrous metal oxide ion-exchangers are amorphous inorganic compounds of metals such as Ti, Zr, Nb, and Ta. They offer significant advantages as supports in the preparation of catalysts. The following are some properties of these ion-exchange compounds that make them desirable as supports for active metals: several active metals or mixtures of metals can be atomically dispersed over a wide range of concentrations; the ion exchange capacity of the materials is large, permitting high loadings of active metals; solution chemistry

can be used to provide control of the oxidation state of the active metal; and, these materials have high surface areas. For example, hydrous titanium oxide catalysts were prepared by a technique that consisted of the synthesis of sodium hydrous titanate ion exchange material followed by exchanging the sodium for active metal ions (19).

Preliminary tests indicated that the HTO catalysts, even at low active metal loadings of 1 wt%, were as effective in converting coal to low molecular weight products as a commercial Ni-Mo/Al<sub>2</sub>O<sub>3</sub> catalyst containing 15 wt% active metals. In addition, for the same oil yield, the HTO catalysts used less hydrogen than the commercial catalyst (19). In recent tests at Amoco, a NiMo HTO catalyst gave similar performance compared to a commercial catalyst, but at only half of the active metal loading (20). This result suggested good dispersion of Ni and Mo on the HTO catalyst.

#### Metal Carbide and Nitride Catalysts

Researchers at Clarkson University are developing carbides and nitrides of transition metals to be used as catalysts specifically for nitrogen removal from coal liquids. The metal carbides and nitrides are hard, refractory materials that are resistant to corrosion. In a typical procedure, Mo<sub>2</sub>C was prepared from MoO<sub>3</sub> using a CH<sub>4</sub>/H<sub>2</sub> reactant gas. Initially, the precursor MoO<sub>3</sub> was reduced to MoO<sub>2</sub> producing water. In the next step, further reduction and carburization occurred giving Mo<sub>2</sub>C having a surface area of about 50-90 m<sup>2</sup>/g while forming additional water. When ammonia was used in place of CH<sub>4</sub>/H<sub>2</sub>, Mo<sub>2</sub>N having a surface area as high as 225 m<sup>2</sup>/g was produced (21).

Amoco recently compared the performances of a bulk molybdenum nitride and an alumina-supported molybdenum carbide with Amocat-1B (Mo/Al<sub>2</sub>O<sub>3</sub>) and Shell 324 (NiMo/Al<sub>2</sub>O<sub>3</sub>). These tests were conducted in packed-bed reactors (14/20 mesh catalyst size) under the following conditions: 760°F, 2000 psig total pressure, 10000 SCFB hydrogen flow rate. The feed material was a mixture of a coal-derived resid and Panasol (a refinery by-product). Coal-derived distillates were also used in some tests. This preliminary study seemed to indicate that the molybdenum carbide and nitride catalysts gave products that were better than those obtained using Shell 324 and Amocat-1B (20). Moreover, these carbide and nitride catalysts seemed to have higher activity on a per-site basis (turnover rate) compared to the commercial catalysts (21).

#### SUMMARY

PETC is actively pursuing an advanced, novel concepts research program in direct liquefaction to bring the technology to commercial readiness in the near future. Of the various areas being studied in this program, improved catalysts could play a major role in lowering thermal severity, improving product yields and selectivity, and improving process configuration. The catalysts used in the recent two-stage liquefaction studies at Wilsonville and HRI, and the current activities in catalysis research have been briefly reviewed. The commercial supported catalysts were found to be effective in two-stage liquefaction. Because of high deactivation rates and the need for using ebullated-bed reactors, PETC is also focusing on developing dispersed catalysts which will lead to the use of less capital intensive slurry reactors. Preliminary work at PETC was successful in obtaining finely dispersed, highly active iron and molybdenum catalysts. The PETC Project Office will continue to focus on the development of advanced liquefaction reactor systems to improve the overall economics.

## REFERENCES

1. "Fuels to Drive Our Future," National Research Council, National Academy Press, Washington, D.C., 1990.
2. "National Energy Strategy," U.S. Department of Energy, Washington, D.C., First Edition, February 1991.
3. Srivastava, R.D., "Catalysis in Direct Liquefaction - A Research Needs Assessment," Technical Report, Prepared by Burns and Roe Services Corp. Under DOE Contract No. DE-AC22-89PC88400, February 1991.
4. Derbyshire, F., "Catalysis in Coal Liquefaction: New Directions for Research," IEA Coal Research, IEACR/08, London, 1988.
5. Rao, S.N.; Schindler, H.D.; McGurl, G.V., "Advances and New Directions in Direct Liquefaction," Prepr. Am. Chem. Soc. Div. Fuel Chem. 145, 33(3), 1988.
6. Gollakota, S.V.; Lee, J.M.; Davies, O.L., "Process Optimization of Close-Coupled Integrated Two-Stage Liquefaction by the Use of Cleaned Coals," Fuel Proc. Tech., 205, 22, 1989.
7. Comolli, A.G.; Duddy, J.E.; Johanson, E.S.; Smith, T.O., "Low Severity Catalytic Two-Stage Liquefaction Process," Final Report by Hydrocarbon Research, Inc. Under DOE Contract No. AC22-85PC80002, Sept. 1988.
8. Gollakota, S.V.; Vimalchand, P.; Davies, O.L.; Lee, J.M.; Cantrell, C.E.; Corser, M.C., "Wilsonville CC-ITSL Process Development," Proceedings of Liquefaction Contractors' Review Meeting, September 1991, Pittsburgh, PA.
9. "Run 259 with Pittsburgh No. 8 (Ireland Mine) Coal," Technical Progress Report Prepared by Southern Electric International Under DOE Contract No. DE-AC-82PC50041, May 1991.
10. "Run 258 with Subbituminous Coal," Technical Progress Report Prepared by Southern Electric International Under DOE Contract No. DE-AC-82PC50041, May 1991.
11. "Run 257 with Illinois No. 6 Coal," Technical Progress Report Prepared by Southern Electric International Under DOE Contract No. DE-AC-82PC50041, February 1991.
12. "Run 254 with Ohio No. 6 Coal," Technical Progress Report Prepared by Southern Electric International Under DOE Contract No. DE-AC-82PC50041, February 1990.
13. Comolli, A.G.; Johanson, E.S.; Panvelkar, S.V.; Popper, G.A., "Recent Advances in Direct Coal Liquefaction," Proceedings of the 16th International Conference on Coal & Slurry Technologies, April 1991, Clearwater, FL.
14. Wilsonville 113th Technical Review Meeting, Birmingham, AL, November 1991.

15. Comolli, A.G.; Johanson, E.S.; Panvelkar, S.V., "CTSL™ Process Studies," Proceedings of Direct Liquefaction Contractors' Review Meeting, September 1990, Pittsburgh, PA.
16. Cugini, A.V.; Krastman, D.; Hickey, R.F., "The Use of Hydrated Iron Oxide Catalysts in Coal Liquefaction," Proceedings of the 8th Annual International Pittsburgh Coal Conference, October 1991, Pittsburgh, PA.
17. Cugini, A.V.; Utz, B.R.; Krastman, D.; Hickey, R.F.; Balsone, V., "Effect of Activation Conditions on Dispersed Iron Catalysts in Coal Liquefaction," Prepr. Am. Chem. Soc. Div. Fuel Chem. 91, 36(1), 1991.
18. PETC Review, Office of Fossil Energy, U.S. Department of Energy, 51, 2, September 1990.
19. Stohl, F.V.; Dosch, R.G.; Stephens, H.P., "Development of Hydrous Metal Oxide Catalysts for Direct Coal Liquefaction," Proceedings of Direct Liquefaction Contractors' Review Meeting, October 1988, Pittsburgh, PA.
20. Sajkowski, D.J., "Second-Stage Catalyst Testing," Proceedings of Direct Liquefaction Contractors' Review Meeting, September 1990, Pittsburgh, PA.
21. Oyama, S.T., "Catalytic Hydrodenitrogenation by Molybdenum Carbide and Nitride," Proceedings of Direct Liquefaction Contractors' Review Meeting, September 1990, Pittsburgh, PA.

## CATALYSIS OF LOW TEMPERATURE LIQUEFACTION BY MOLYBDENUM SULFIDES

B. C. BOCKRATH, E. G. ILLIG, AND M. J. KELLER, III

U. S. DEPARTMENT OF ENERGY  
PITTSBURGH ENERGY TECHNOLOGY CENTER  
PO BOX 10940  
PITTSBURGH, PA 15236

**KEYWORDS:** Liquefaction, dispersed catalysts, molybdenum disulfide

### INTRODUCTION:

The use of molybdenum sulfide catalysts in the direct liquefaction of coal is well known. Nonetheless, the development and application of more effective catalysts, particularly in first-stage liquefaction reactors, remains a high priority goal<sup>1</sup>. When used as unsupported catalysts in first-stage reactors, molybdenum sulfides are often intended to promote the conversion of coal and to provide better quality products for further refining. Typically, temperatures ranging from 400° to 465° C are used in first-stage reactors to promote the formation of distillable products. Molybdenum catalysts used at these temperatures generally increase coal conversion and the yield of distillates, and reduce the content of heteroatoms, principally sulfur and oxygen. Results described below suggest that molybdenum catalysts might play additional roles. The conversion of coal to soluble products at low temperatures, generally around 350° C, may be promoted by active catalysts, possibly through the prevention of retrogressive reactions<sup>2</sup>. With this in mind, the activity of molybdenum catalysts in low temperature liquefaction was investigated. The results indicate that it is of value to have the catalyst present in an active form when the liquefaction feed stock is brought to temperatures above 300° C.

### EXPERIMENTAL:

Small-scale liquefaction reactions were carried out in 316 stainless steel autoclaves of about 40 mL capacity. A set of five microautoclaves was heated and shaken (60 cps) in a sandbath. In these experiments, the reactors were brought to temperature slowly by heating the sandbath at about 6° C/min. The usual charge was 3.5 g Illinois No. 6 coal, 7 g coal-derived liquefaction solvent, and 1200 psig hydrogen at room temperature. Larger scale experiments were carried out in a 316 stainless steel stirred autoclave of 1/2 L capacity. Typical charges were 70 g coal, 140 g solvent, and 1200 psig hydrogen at room temperature. The heating rate was about 8° C/min. Rapid cooling was achieved by flowing water through an internal cooling coil.

Coal conversions were calculated on an maf basis from weights of dry residues recovered after vacuum filtration on 8u paper with cyclohexane followed by tetrahydrofuran (THF). The catalyst was added to the coal by mixing it with about 40% of its weight of an aqueous solution of ammonium heptamolybdate or ammonium tetrathiomolybdate followed by drying in a vacuum oven at 60° C. In one case, the catalyst was simply added to the reactor as a powder without impregnation. The coal was from Burning Star mine, and had the following elemental composition: C=78.4%; H=5.1%; N=1.6%; O=11.4% (by diff.) on an maf basis with total S=3.2%. The ash content was 10.4% on a moisture free basis. The liquefaction solvent was a hydrotreated distillate (V-178) obtained from the Advanced Coal Liquefaction R & D Facility at Wilsonville, Alabama. Its carbon and hydrogen contents were C=88.2% and H=9.6%. By

D-1160 distillation, 84% distilled below 850° F.

#### RESULTS AND DISCUSSION:

The use of unsupported molybdenum sulfides as liquefaction catalysts is well known<sup>1</sup>. Nonetheless, at the outset of this work, it was useful to establish whether or not catalyst activity could be observed at low temperatures, in this case about 350° C. Two sets of experiments were used to verify catalyst activity. In the first, coal conversion (THF) was measured as a function of catalyst activity. The residence time at liquefaction temperature (350° C) was 60 min. The conversion values shown in Fig. 1 increase with catalyst loading until a plateau is reached at around 2000 ppm molybdenum. Conversions with either ammonium heptamolybdate and ammonium tetrathiomolybdate were generally similar except at the lowest concentration. These differences aside, the more important observation is that the precursors may be activated and perform a catalytic function at low temperature.

In addition to increasing the conversion of coal, a catalyst may be expected to increase the rate of hydrogen consumption. In these experiments, we have no direct, real-time indication of changes in hydrogen partial pressure. However, the microautoclaves were equipped with pressure transducers allowing total pressure to be recorded as a function of reaction time. The time/temperature and time/pressure profiles for a set of autoclaves heated together in the sandbath are given in Figure 2. The pressure increased with temperature, as expected. A peak in total pressure is observed a short time after the temperature reached 350° C. Thereafter, total pressures declined.

The pressure profiles shown result from a composite of the effects of temperature changes, hydrogen uptake, and production of other gases or vapors. Despite this complexity, important information may still be derived from the profiles. Peak pressure developed shortly after reaching liquefaction temperature, indicating that the major portion of gas formation is rapid, being almost complete within several minutes of reaching reaction temperature. Analysis of the gases recovered at the end of the run indicates that the major component of the non-condensable gases evolved is CO<sub>2</sub>, with a lesser amount of CH<sub>4</sub>. Once gas evolution slows, a gradual decrease in total pressure is observed. This decrease is reasonably attributed to hydrogen uptake. Although the decrease is larger when catalyst has been added, it is evident even when it has not. It is possible that a native catalytic effect of coal mineral matter may contribute to the pressure decrease. Indeed, the Illinois No. 6 coal used in this work has a high iron content (1.1 wt%, mf).

The changes in total gas pressure reflect the effects of both temperature changes and chemical reactions. An attempt to factor out the former was made by estimating the pressure change that would be due to the temperature change. This estimate was based on a least squares fit of the temperature/pressure data using the first three points covering the temperature span from 15 to 219° C. The resulting linear equation was then used to calculate expected pressures for higher temperatures. This estimation assumes that the evolution of gases below 219° C is negligible. The difference between the calculated and observed pressures is a rough estimate of the combined effects of gas production and hydrogen uptake. Pressure differences calculated from the data in Figure 2 are plotted versus time in Figure 3.

The difference between catalyzed and non-catalyzed liquefaction is readily apparent. In the catalyzed cases, the pressure peak is reduced and hydrogen uptake begins to dominate within the first 15 minutes at 350° C. Coal conversions were also somewhat higher, being 91-92% for all catalyzed cases as opposed to 87% without catalyst. By cyclohexane extraction, conversions with catalyst ranged from 12% to as high as 21%

for 5000 ppm Mo. The value without catalyst was only 7%. Clearly the precursor was activated at 350° C and the resulting catalyst played an important role in the early stages of the liquefaction reaction.

The relative rates of hydrogen uptake at times beyond the pressure peak are also interesting. The rates are nearly identical for catalyst loadings of 1000 and 5000 ppm Mo. At these levels, the rate of hydrogenation seems to be limited by factors other than the amount of catalyst present. It is also apparent that the rate of hydrogen uptake falls off with time until it approaches that observed in the absence of added catalyst. This observation was grounds for asking whether or not the catalyst was progressively deactivated.

To determine if the catalysts were in fact deactivated, the tetrahydrofuran insoluble residues recovered after product work-up were mixed with fresh coal slurry and a second cycle of liquefaction was performed. For comparison, simultaneous experiments were made with and without the addition of ammonium molybdate powder. The temperature/pressure-difference profiles are shown in Figure 4. The experimental conditions were the same as the initial liquefaction experiment, except that the temperature was increased to 425° C after 120 minutes at 350° C. The pressure differences were calculated as before. As may be seen in the Figure, catalytic activity is quite apparent for the material recovered from the previous experiment. Improvements in coal conversion were also obtained by using the liquefaction residue. Values determined by THF extraction were 95% with liquefaction residue, 86% with ammonium molybdate, and 85% without catalyst. Measured by cyclohexane extraction, the values were 64%, 36%, and 38%, respectively.

It is important to note that the liquefaction residue demonstrated catalytic activity as soon as the temperature reached 350° C. The recovered catalyst was not only active, but able to participate in liquefaction reactions during the first few critical minutes. A pattern of hydrogen uptake similar to that seen in the previous experiment is repeated here. With added liquefaction residue, the rate of hydrogen uptake diminished with time until it approached that for the non-catalyzed case. However, when the temperature was increased to 425° C, the apparent hydrogen uptake was much greater in the presence of the liquefaction residue. From the results of temperature programming, it seems the catalyst acts as a cofactor in processes that are initiated by thermal reactions. Thus, as the temperature is brought up to each plateau, a new but limited burst of catalyzed hydrogen uptake initiated. These observations are in accord with the concept of catalytically controlled thermal cracking postulated for petroleum residua and other heavy hydrocarbons<sup>3</sup>. In that concept, MoS<sub>2</sub> was pictured as hydrogenating thermally produced free radicals, thus inhibiting the formation of coke.

Comparison of the addition of the liquefaction residue with addition of ammonium molybdate in the form of a powder illustrates the importance of dispersing the catalyst precursor. The added ammonium molybdate powder performed only marginally better than coal without added catalyst, even though twice as much molybdenum was added in the form of the powder as in the liquefaction residue. This relatively poor performance most likely resulted because no effort was made to disperse the catalyst precursor. By contrast, the precursor used to generate the catalyst in the liquefaction residue had been dispersed on the coal in the first liquefaction experiment. Thus, a major benefit of dispersing a precursor on coal is that more effective catalysts may be produced. This benefit is separate from any derived by improved contact between coal and catalyst brought about by dispersing the precursor. It should be emphasized that in the second liquefaction experiment, the added catalyst was physically associated with the liquefaction residue from the previous experiment. The degree of contact with fresh coal was then governed by the extent of mixing in the reactor. Experiments directed

toward improving the contact between the coal and catalyst thus need to take into account the effect the chosen method of dispersing the precursor might have on the physical properties of the resulting catalyst. It is also apparent that tailoring the conditions of the preparation of an unsupported catalyst may have a large effect on its performance in a process that makes use of catalyst recycle.

The recovery of the catalytic material in the previous experiments entailed the solvent separation of the liquefaction products. Thus, the catalyst was exposed to several laboratory operations that could have degraded its performance in the subsequent liquefaction cycle. These extraneous influences make it more difficult to conduct a systematic program to improve the preparation of these catalysts. A way around this problem was devised by preparing catalysts under liquefaction conditions in a microautoclave, then transferring them without work-up to a 1/2 L stirred autoclave for performance testing. In this way, a small volume of liquid product containing active catalyst can be mixed with a larger volume of fresh feed slurry before liquefaction. In this testing scheme, the precursor loading in the preparation stage must be high in order to supply enough catalyst for the performance test in the stirred autoclave. Initially, 20,000 ppm of ammonium molybdate on coal was used in the preparation, which reduced to 1000 ppm Mo after dilution with 20 times as much fresh coal in the performance test.

Initial tests of this preparation/testing scheme revealed that the introduction of active catalyst to the stirred autoclave often led to exothermic reactions as the temperature approached about 350° C. In general, the extent of these exotherms varied according to the type and amount of catalyst used. Thus, the temperature profiles were not reproducible. To obtain better control, a temperature staged testing program was adopted. One such temperature profile for a noncatalyzed liquefaction experiment in the 1/2 L stirred autoclave is illustrated in Figure 5. In this example, 20 minutes was spent at 300° C, followed by 60 minutes at 325° C, then 50 minutes each at 350° and 375° C. The total pressure rose until 10 minutes after reaching 325° C. Expected pressures were calculated based on the initial pressure change as done before. The difference between expected and observed pressures is plotted in Figure 6. For comparison, the pressure difference profile for a case with added catalyst is presented in Figure 7. The heating program was closely similar to the non-catalyzed example, but they are not identical. Several important observations may be made by comparing the two pressure difference profiles. First, in the non-catalyzed case, the onset of the pressure peak is evident as the temperature approaches the first plateau, 315° C, and it is much larger in magnitude than in the catalyzed case. This apparent increase in hydrogen uptake is further evidence that the catalyst carried in the liquefaction products of the previous run is able to function during the initial stage of the liquefaction reaction. Second, the pressure difference at the end of the heating program is much more negative with than without added catalyst. Third, the rate of pressure change in the presence of catalyst is nearly constant once the pressure peak has passed. It is striking that the rate of uptake does not seem to be affected by the changes in temperature. This is somewhat different than the profile from the microautoclave experiment shown in Figure 4, which exhibited a distinct change in rate as the temperature increased to the next plateau. It may be that the smaller temperature changes in the stirred autoclave experiment combined with a fortuitous choice of intervals between temperature changes produced a constant rate of uptake.

#### CONCLUSIONS:

The results obtained in this work indicate several factors are

important to using unsupported molybdenum sulfide catalysts more effectively in the first stage of liquefaction. Since catalysts are able to participate in liquefaction reactions at low temperatures, it is important that they be present in an active form rather than allow this one-time opportunity to pass while a precursor undergoes transformation. One approach to this objective is demonstrated here, namely, preparation of a catalyst from a precursor dispersed on coal in a small reactor followed by mixing the entire liquefaction product with fresh slurry for use in a larger reactor. Impregnation of the precursor on coal seems to be of benefit to generating a better catalyst. Such a prepared catalyst is able to perform well in subsequent liquefaction tests even though it is only physically mixed with coal, not impregnated in any way. It is also clear that evaluation and comparison of liquefaction catalysts is complicated by the fact that performance is governed by many factors, not just catalyst activity. For example, during typical liquefaction experiments, the catalytic properties of a precursor added with the feed undergo considerable change during the course of the reaction. For this reason, the results given above are taken as measures of overall catalyst performance rather than catalyst activity. In the present context, the latter may not be a static characteristic.

**ACKNOWLEDGEMENT:**

We gratefully acknowledge the assistance of Harold M. Boyer in carrying out many of the liquefaction experiments.

**REFERENCES:**

1. Derbyshire, F.; *Energy and Fuels*; **3**, 273 (1989).
2. Solomon, P. R.; Serio, M. A.; Deshpande, G. V.; Kroo, E.; *Am. Chem. Soc. Div. Fuel Chem., Preprints*, **34(3)**, 803 (1989).
3. Bearden, R; Aldridge, C. L.; *Energy Progress*, **1**, 44 (1981).

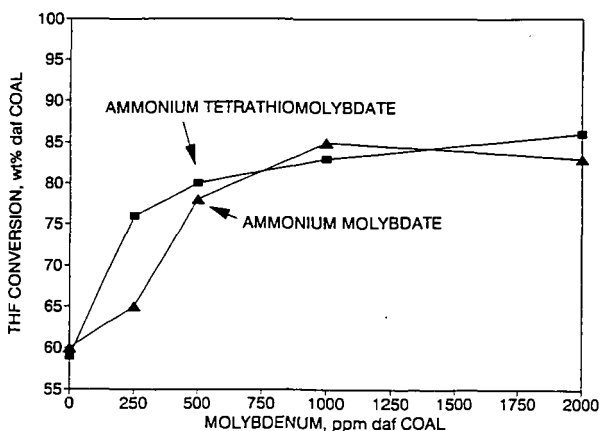


Fig. 1. Conversion versus molybdenum loading.

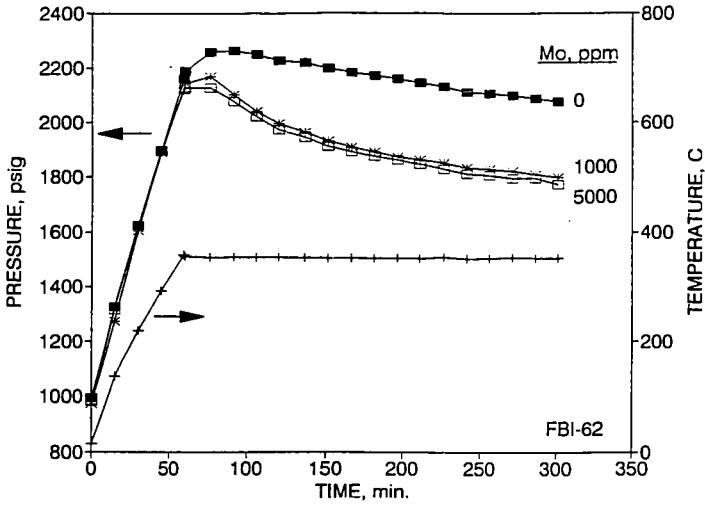


Fig. 2. Temperature and total pressure profiles.

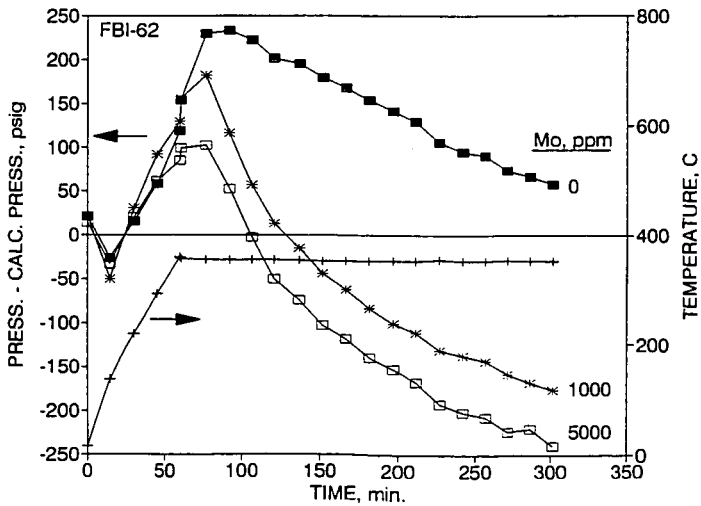


Fig. 3. Differences between calculated and total pressure.

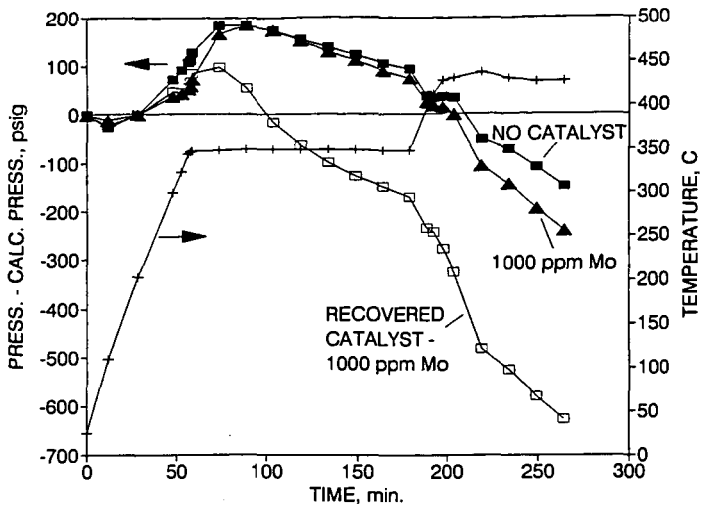


Fig. 4. Pressure difference profiles with and without catalyst.

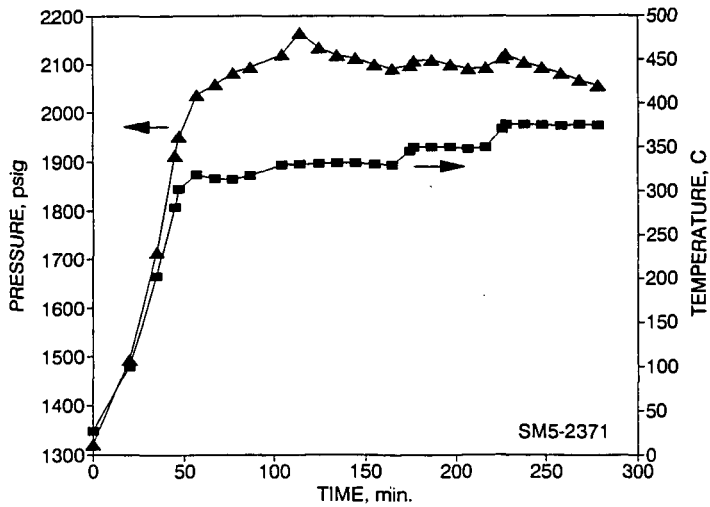


Fig. 5. Temperature and pressure profiles without added catalyst.

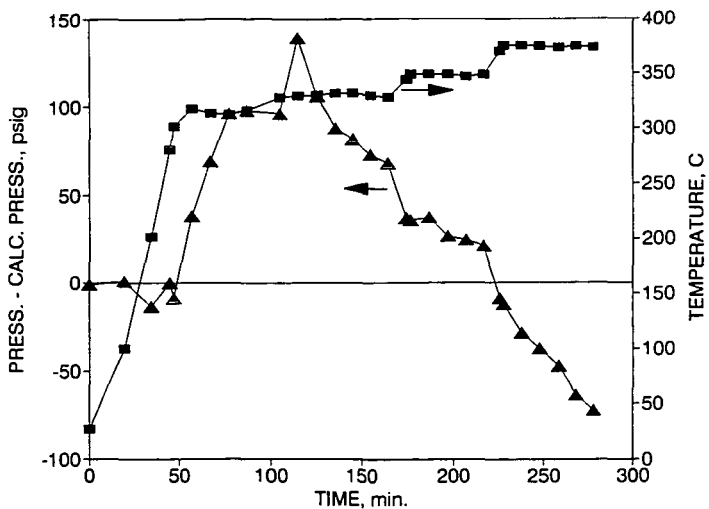


Fig. 6. Pressure difference without added catalyst.

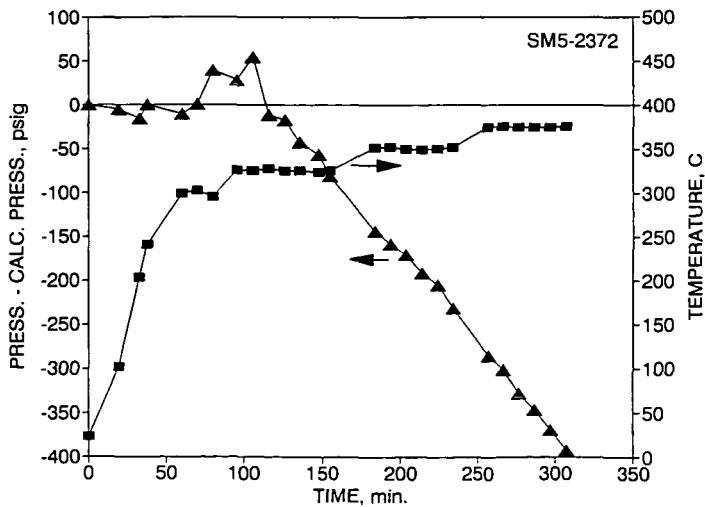


Fig. 7. Pressure difference with 1000 ppm Mo added.

## DEVELOPMENT OF THIN FILM HYDROUS METAL OXIDE SUPPORTED CATALYSTS FOR DIRECT COAL LIQUEFACTION\*

R. G. Dosch, L. I. McLaughlin, H. P. Stephens  
Process Research Division

and T. J. Headley  
Electron Optics Division

Sandia National Laboratories  
Albuquerque, New Mexico

### INTRODUCTION

In order to achieve optimum yields of distillate, current two-stage liquefaction processes, as evaluated in pilot research facilities consume as much 4 to 8 lbs of catalyst per ton of moisture-free coal fed to the reactors. The cost of catalyst for these replacement rates ranges from \$4 to \$6 per barrel of distillate product. If the cost of disposal of spent catalyst is considered, the cost could be substantially more. Thus a very important factor in achieving \$30/bbl liquids from coal is the development of less expensive catalysts or catalysts with better activity, selectivity and life.

The goal of this project is to develop catalysts, based on hydrous metal oxide (HMO) ion exchangers, that improve the efficiency and economics of conversion of coal to distillate products. Continuous reactor tests performed by AMOCO [1,2] have shown that preliminary formulations of one member of this class of catalysts, NiMo hydrous titanium oxide (HTO) catalysts were comparable or superior to 25 other commercial and novel formulations tested by AMOCO for second-stage upgrading of coal-derived resid. Thus efforts have focused on optimizing HTO supported catalysts, and recent research has resulted in formulation of NiMo/HTO catalysts with lower active metal loadings and increased activity. This paper reports the status of recent HTO catalyst research, especially the development of thin-film HTO-coated supports.

Although other HMOs, based on Zr, Nb or Ta may also provide good catalyst supports, HTO supports were chosen for initial development because the raw materials required to form HTOs are more readily available and less expensive than those required for other HMOs. A promising method to produce inexpensive catalysts with properties tailored to a specific process is the application of HTO catalysts as thin film coatings on other support structures. Development effort has concentrated on molybdenum as the major active metal in both the bulk and thin-film HTO catalysts. The choice of molybdenum as the major active component is based

---

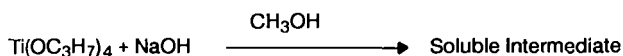
\* This work was supported by the US Department of Energy at Sandia National Laboratories under contract DE-AC04-76DP000789

on the fact that the most successful liquefaction catalysts currently in use (e.g. Shell 324M and Amocat 1C) contain molybdenum as the major active metal. Catalysts developed in this program have been evaluated with laboratory micro-scale reactors, and will ultimately be evaluated with bench-scale units, such as the PETC Generic Unit, and a large-scale process development unit.

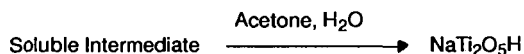
### CATALYST PREPARATION

Hydrous titanium oxide catalysts are prepared by a technique that consists of synthesis of sodium hydrous titanate ion exchange material followed by ion exchange of the sodium for active metal ions [3]. The synthesis involves three steps:

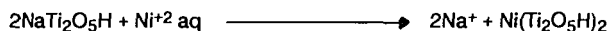
- (1) Reaction of tetraisopropyl titanate with sodium hydroxide in alcohol solution to form a soluble intermediate:



- (2) Hydrolysis of the soluble intermediate in acetone/water mixtures to form the hydrous metal oxide ion exchange material:



- (3) Ion exchange of the sodium for active metal ions in aqueous solution to form the catalyst:



In addition to the capacity to exchange metal cations, contact of the ion-exchangers with acidic solutions results in exchange of hydrogen ions, which alters the acidity and catalytic activity of the material. The materials can also function as anion exchangers in acidic solutions, allowing adsorption of metals that exist as aqueous oxygenated anions; molybdates, for example.

Catalyst preparation by coating inert supports with a thin film of a hydrous metal oxide ion-exchanger offers the potential of tailoring catalyst activity and selectivity by appropriate choice of active metal combinations and substrate physical properties such as strength, surface area, and pore size. Additionally, an excellent dispersion of active metals may be achieved by this technique.

Preparation of coated-support catalysts involves three steps:

- (1) Synthesis of the water or alcohol soluble hydrous titanium oxide as in step (1) above;

- (2) Deposition of an ion exchange coating by contacting the support with an aqueous or alcoholic solution of the soluble hydrous titanium oxide ion exchanger;
- (3) Ion exchange of the cations of the HTO coating for those of a catalytically active metal in aqueous solution as in step (3) above.

Because active metals are dispersed on HTO catalysts by ion exchange, they are chemically associated with the HTO support. Therefore activation techniques must result in release of the active metal components from the HTO support. For example, activation [4] of Mo-based HTO catalysts is performed in two steps: (1) calcination in air at 500°C to release the Mo and promoter ions from the HTO structure, followed by (2) sulfidation at 425°C with a 10% mixture of H<sub>2</sub>S in H<sub>2</sub>.

## CATALYST TESTING

Initial tests have been conducted on powdered (-100 mesh) and particulate catalysts (granular, extrudate, or spherical) using batch microautoclaves for rapid screening of a large number of preparations to determine their activity for model reactions such as pyrene hydrogenation and dibenzothiophene desulfurization. The batch microautoclaves have liquid reactant capacities of 2 cc and a gas-phase volume of 25 cc. Four reactors can be operated simultaneously. A typical experiment is carried out as follows. After being charged with the catalyst and reactant, the reactors are heated to temperature in a fluidized sand bath while being shaken with a wrist-action motion at 200 cycles/min. Temperatures and pressures are recorded with a digital data acquisition system during the course of the experiments. Following the heating period, the reactors are rapidly quenched to ambient temperature, a gas sample is taken and the products are removed for analysis by various techniques, including gas and liquid chromatography and elemental composition. For sulfided NiMo catalysts, pyrene hydrogenation tests are typically carried out at 300°C and 500 psig cold charge hydrogen pressure, and dibenzothiophene desulfurization at 350°C and 1200 psig. For the more active noble metal catalysts such as Pd/HTO, pyrene hydrogenation experiments are typically performed at 100°C and 100 psig.

## RESULTS AND DISCUSSION

### Bulk-Phase NiMo/HTO Catalysts

The development of NiMo/HTO catalysts has progressed to the point where the hydrogenation activity of HTO-supported materials, as measured by the hydrogenation of pyrene, is significantly higher than that of commercially available NiMo/Al<sub>2</sub>O<sub>3</sub> catalysts used for coal liquefaction. NiMo/HTO catalysts exhibiting pseudo-first-order rate constants for pyrene hydrogenation of 0.19 sec<sup>-1</sup> g cat<sup>-1</sup> (1.66 sec<sup>-1</sup> g Mo<sup>-1</sup>) for the powdered catalyst (-100 mesh) can be routinely prepared.

This hydrogenation activity can be compared to that of  $0.16 \text{ sec}^{-1} \text{ g cat}^{-1}$  ( $1.21 \text{ sec}^{-1} \text{ g Mo}^{-1}$ ) for powdered Shell 324M in tests run under identical conditions.

Further advances in catalytic activity have been made via a combination of HTO substrate modification and changes in metal loading techniques. Addition of tetraethylorthosilicate in the first step of the synthesis to achieve a Ti/Si ratio of 0.2 for the ion-exchanger was found to further increase activity. The  $\text{Na}_{0.5}\text{Ti}/0.2\text{Si}$  supports were converted to the  $\text{H}_{0.5}\text{Ti}/0.2\text{Si}$  form prior to metal loading. Mo was introduced onto the support via an ion exchange reaction. Following drying at  $100^\circ\text{C}$ , Ni was introduced by wetting with a minimum amount of aqueous  $\text{Ni}(\text{NO}_3)_2$  solution. With this method, most, but probably not all of the Ni is fixed on the support via ion exchange. After the Ni loading step, the materials were dried at  $100^\circ\text{C}$ , pelleted, calcined at  $500^\circ\text{C}$ , and sulfided at  $425^\circ\text{C}$  prior to testing. The powdered form of this catalyst (8.69% Mo, 2.95%Ni) was found to have a pseudo-first-order rate constant for pyrene hydrogenation of  $0.22 \text{ sec}^{-1} \text{ g cat}^{-1}$  ( $2.32 \text{ sec}^{-1} \text{ g Mo}^{-1}$ ). The catalyst weight basis desulfurization activity as measured by the pseudo-first-order rate constant for dibenzothiophene desulfurization ( $0.027 \text{ sec}^{-1} \text{ g cat}^{-1}$ ) was found to be the same as that for freshly sulfided, -200 mesh Shell 324M (0.027). However, on a weight of Mo basis, the desulfurization activity is about 50% greater, because of the lower Mo loading on the Si modified HTO catalyst. It appears that the increase in activity due to silicon addition is achieved, in part, by the stabilizing effect that Si has on the surface area of the calcined and sulfided catalysts. Catalysts containing silicon have approximately 60% higher surface area than preparations without silicon (150 vs  $90 \text{ m}^2/\text{g}$ ).

Transmission electron microscopy (TEM) of the sulfided NiMo/HTO and commercial NiMo/alumina catalysts has shown that the greater activity of the HTO catalysts appears to result from a better dispersion of the Mo sulfide crystallites. Whereas the alumina catalysts appear to contain 50 to 70 angstrom-size stacks of 4-6  $\text{MoS}_2$  layers supported on amorphous alumina (figure 1), the HTO catalysts contain 50 to 70 angstrom-size crystallites of only 1-2  $\text{MoS}_2$  layers supported on 100 to 150 angstrom diameter anatase crystallites (figure 2) formed during the calcination process.

#### HTO-Coated Catalyst Supports

The information obtained from the development of bulk-phase HTO catalysts was found to be directly applicable to the preparation of thin-film NiMo/HTO catalysts on pre-formed supports. Application of HTO catalysts as thin films on support material is a promising approach to preparing inexpensive catalysts, because smaller amounts of HTO ion-exchanger material and active metals are required, and inexpensive supports may be used. Initially thin-film NiMo/HTO catalysts supported on a material referred to as controlled pore glass (CPG), available in -20 mesh granular form, were prepared. Results of experiments performed to compare the hydrogenation activities of bulk-phase and thin-film Pd/HTO-coated and NiMo/HTO-coated CPG catalysts showed that the thin-film catalysts had comparable or greater activities on a weight of active metal basis.

Recently NiMo/HTO-coated catalysts have been prepared using a porous silica support in spherical form, 1.5 mm in diameter. The silica spherical support has a surface area of 55 m<sup>2</sup>/g, an average pore diameter of 77 nm, and a total pore volume of 1.00 cc/g. The spheres were first coated with a thin film of HTO followed by exchange of Mo and Ni onto the thin film to achieve nominal Mo loadings of 1% and Ni loadings of 0.3%. Following calcination and sulfidation, the catalysts were tested for their activity for hydrogenation of pyrene to 4,5-dihdropyrene at 300°C, and desulfurization of dibenzothiophene at 350°C. These spherical silica NiMo/HTO-coated catalysts had weight basis rate constants for pyrene hydrogenation of 0.032 ± 0.003 sec<sup>-1</sup>-g cat<sup>-1</sup> as compared to 0.041 for Shell 324M extrudate (0.78 mm diameter by 4 mm long) and 0.038 for Amocat 1C extrudate (1.59 mm diameter by 6 mm long). On a weight of active metal (Mo) basis, the rate constants ranged from 2.6 to 3.5 sec<sup>-1</sup> g Mo<sup>-1</sup>, a factor of ten greater than that of 0.31 for Shell 324M. For dibenzothiophene desulfurization, rate constants of 0.0081 ± 0.0003 sec<sup>-1</sup> g cat<sup>-1</sup> were determined for the NiMo/HTO-coated silica spheres, compared to 0.016 for Shell 324M. Thus the HTO-coated silica sphere catalysts, which contained only one-tenth as much active metal as Shell 324M, exhibited half of the dibenzothiophene desulfurization activity on a weight of catalyst basis. On a weight of Mo basis, because of the low active metal loadings, the HTO coated sphere catalysts had activities six times that of Shell 324M.

The high activity, on a weight of Mo basis, for these spherical silica HTO-coated catalysts is due, in part, to their high effectiveness factor (ratio of the rate constant for the catalyst spheres to that of the powdered catalyst), which was determined to be 0.75 (for hydrogenation), compared with the much smaller values of 0.27 and 0.22 for Shell 324M and Amocat 1C. This result is undoubtedly due, in part, to differences in the effective diffusivity resulting from the more open pore structures of the silica spheres. A factor contributing to the higher Mo weight basis activity of the NiMo/HTO-silica sphere catalysts is the better dispersion of MoS<sub>2</sub> achieved by the HTO coating process. TEM analysis (figures 3 and 4) has shown that, as with the case for the bulk-phase HTO catalysts, the MoS<sub>2</sub> crystallites for the coated catalysts consist of 50-70 angstrom-size crystallites of 1-2 layers of MoS<sub>2</sub> attached to small anatase crystallites. These results demonstrate that the HTO coating method can be used to produce a catalyst with a low active metal loading, satisfactory activity, and a geometry amenable to existing reactor systems.

## CONCLUSIONS

Hydrous titanium oxides are extremely versatile materials for preparation of coal liquefaction catalysts. Screening tests of catalyst activity with feeds that model coal liquefaction reactions have shown that bulk HTO catalysts with activities significantly greater than commercial NiMo/alumina catalysts can be prepared. Preliminary formulations of bulk-phase NiMo/HTO catalysts have also performed well in continuous microreactor tests [1] for upgrading coal-derived resid. In addition, catalysts prepared from HTO-coated supports, containing one-tenth the active metals of commercial alumina-supported catalysts, have been found to exhibit high

hydrogenation and desulfurization activities on a weight of Mo basis. Thus, HTO-coated support materials offer a promising method to produce cost-effective catalysts with mechanical, physical and catalytic properties tailored to specific direct liquefaction process applications.

## REFERENCES

1. D. J. Sajkowski, "Second Stage Catalyst Testing," Proceedings of the 1990 Direct Liquefaction Contractors' Review Meeting, U. S. Department of Energy, Pittsburgh Energy Technology Center, Pittsburgh, PA, September 24-26, 1990, p. 76.
2. R. G. Dosch, F. V. Stohl, and H. P. Stephens, "Development of Hydrous Metal Oxide-Supported Catalysts for Direct Liquefaction, Proceedings of the 1990 Direct Liquefaction Contractors' Review Meeting, U. S. Department of Energy, Pittsburgh Energy Technology Center, Pittsburgh, PA, September 24-26, 1990, p. 56.
3. R. G. Dosch, H. P. Stephens, F. V. Stohl, B. C. Bunker, and C. H. F. Peden, "Hydrous Metal Oxide-Supported Catalysts: Part I. Preparation Chemistry and Physical and Chemical Properties," SAND89-2399, Albuquerque: Sandia National Laboratories, February 1990.
4. R. G. Dosch, F. V. Stohl, and J. T. Richardson, "Activation of Hydrous Oxide-Supported Catalysts for HDS, and HDO Reactions," Novel Materials in Heterogeneous Catalysis, ACS Symposium Series 437, Edited by R. T. K. Baker and L. L. Murrell, pp. 279-288, 1990.



Figure 1. Transmission Electron Micrograph of sulfided NiMo/alumina catalyst containing 13.2% Mo and 2.7% Ni. A typical crystallite containing a "stack" of 4 MoS<sub>2</sub> layers (dark lines) is shown within circled area. Many other "stacks" of 4-6 MoS<sub>2</sub> layers can be observed.

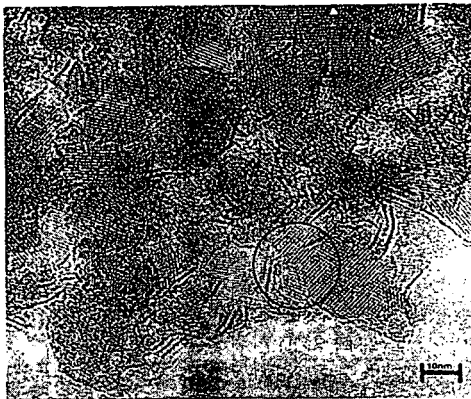
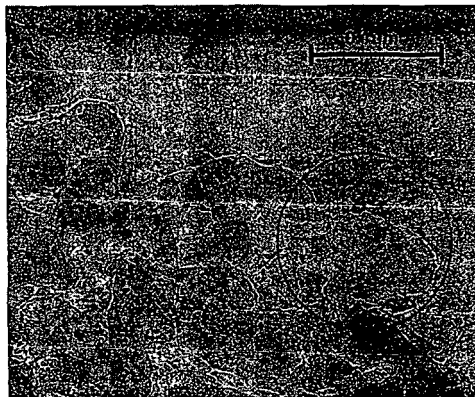
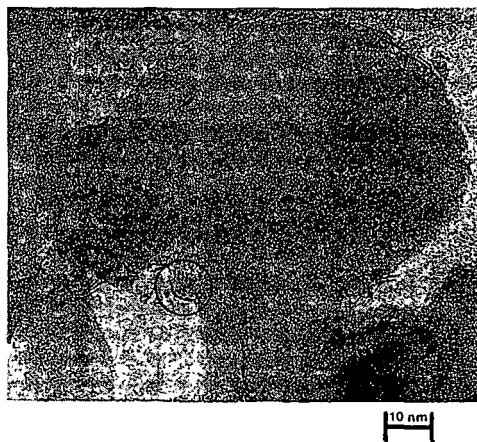


Figure 2. Transmission Electron Micrograph of sulfided NiMo/HTO catalyst containing 10.2% Mo and 3.4% Ni. Typical crystallites containing one MoS<sub>2</sub> layer (dark line) conforming to the shape of an anatase crystallite is shown within circled area. Many other crystallites of one MoS<sub>2</sub> layer can be observed.



**Figure 3.** Transmission Electron Micrograph of sulfided NiMo/HTO supported on porous silica. This catalyst contains 1.3% Mo and 0.2% Ni. The silica support is seen as the larger irregularly shaped material (circled), approximately 100 nm in size. The smaller material (10 nm in size, darker spots) on the silica are crystallites of anatase with MoS<sub>2</sub> attached. The circled area is shown magnified by a factor of 3 in Figure 4.



**Figure 4.** Transmission Electron Micrograph of sulfided NiMo/HTO supported on porous silica. The circled area shows a typical crystallite of anatase with a crystallite containing a single layer of MoS<sub>2</sub> (dark line) attached.

## DISPERSED MOLYBDENUM CATALYSTS FOR LIQUEFACTION OF ILLINOIS NO. 6 COAL

April J. Swanson  
Amoco Oil Co., H-2, P. O. Box 3011  
Naperville, IL 60566-8460

Keywords: Coal, Molybdenum, Catalyst

### ABSTRACT

Supported Ni/Mo catalysts have been used successfully for liquefaction of Illinois No. 6 bituminous coal at the Advanced Coal Liquefaction facility in Wilsonville, AL. In Run 261, coal conversions of 92-93% and C<sub>4</sub>+ distillate yields of 64-65% were obtained with Akzo's EXP-A060 catalyst or Shell 324. These results are excellent, however, process costs could be decreased by use of a dispersed catalyst in a slurry reactor. Research was undertaken to evaluate dispersed Mo catalysts for liquefaction of Illinois No. 6 coal under DOE Contract DE-AC22-88PC88819.

Resid conversion improved when oil-soluble Molyvan L replaced Amocat™ LC catalyst in the first stage (192 ppm Mo/coal). Raising the first stage temperature from 800°F to 820°F increased resid conversion further. Use of Molyvan L or Mo octoate (84-192 ppm Mo) as the only catalyst also gave high resid conversion. Furthermore, about the same yield structure was obtained at half the residence time and higher temperature. With the oil-soluble Mo catalysts, distilled fractions contained more heteroatoms, which must be removed in a subsequent hydrotreating step. Based on these tests, oil-soluble Mo catalysts are recommended for liquefaction of Illinois No. 6 coal.

### INTRODUCTION

Illinois No. 6 coal has served as the reference liquefaction feedstock at the Advanced Coal Liquefaction facility in Wilsonville, Alabama for several years. The process has evolved over time from single-stage high-severity to two-stage, moderate severity. Significant improvements have been made in coal conversion, energy rejection during solids separation, distillate yield, and coal throughput. The best results to date were obtained using a new catalyst, EXP-AO-60, with a pore structure similar to Amocat™ catalysts, in the two stage catalytic process. It is becoming increasingly difficult to develop a new supported catalyst that gives a large beneficial effect on process economics. Improvements are more likely to come from significant process changes. With this in mind, oil-soluble molybdenum catalysts for liquefaction of Illinois No. 6 coal were tested in this work in place of the supported catalyst in one or both stages. Use of oil-soluble catalysts would simplify reactor design and decrease reactor cost. Molyvan L (8% Mo, \$3.20/lb.) and molybdenum octoate (8% Mo, \$2.00/lb.) are commercially-available oil-soluble lubricant additives. Molyvan L was used as a first stage catalyst for liquefaction of Black Thunder coal in Wilsonville run 262 (Shell 324 in stage 2) and the only catalyst in Wilsonville run 263. This paper describes use of Molyvan L and molybdenum octoate for liquefaction of Illinois No. 6 coal. Results were very promising, suggesting that oil-soluble molybdenum compounds are good alternative catalysts for a Wilsonville-type process with Illinois No. 6 coal feed.

### EXPERIMENTAL

Analyses of the Illinois No. 6 coal feed, from Wilsonville Run 257, is given in Table 1. Liquefaction solvent was a blend of V-1074 and V-203 liquids from Wilsonville Run 257. The analysis is given in Table 2. The bench-scale liquefaction runs were made in AU-135L continuous, two-stage pilot plant with 1-liter stirred autoclave reactors. Feed slurries consisted of 33/67 mixtures of

coal/liquefaction solvent. Molyvan L or molybdenum octoate were added to the feed tank without additional sulfiding agent. Two runs with dispersed catalyst were completed, one with Molyvan L added to the feed as the first stage catalyst and Amocat™ 1C catalyst in the second reactor, and one with Molyvan L or molybdenum octoate and no supported second stage catalyst. Amocat™ 1C catalyst was presulfided with 8% hydrogen sulfide in hydrogen before use. Product solubility was determined by millipore filtration, distillate yields were determined by modified D-86 and D-1160 distillation, and distilled fractions were analyzed for C, H, S, N, and O. Unconverted solids were analyzed for metals by ICP (inductively coupled plasma spectroscopy).

#### Molyvan L Catalyst in Stage 1/Amocat™ 1C Catalyst in Stage 2

Liquefaction of Illinois No. 6 coal may place greater demands on the catalyst for hydrogenation of aromatics than liquefaction of Black Thunder coal. This test used Molyvan L in the first stage and Amocat™ 1C catalyst in the second stage to keep hydrogenation activity high. Feed slurries contained 800 ppm of Molyvan L (192 ppm molybdenum as a fraction of coal). Operating temperatures were 800-820 °F for the first stage, and 760 °F for the second stage. Nominal residence times were 1.5 hour in each stage or 3 hours overall. The run was operated with slurry feed for 15 days, and then with solvent-only feed for 6 days.

#### RESULTS

Product yields are compared to those from Amocat 1C in Table 3. The run with Molyvan L in the first stage is labelled "T/C" and the run with Amocat™ 1C catalyst in the first stage is labelled "C/C". At 800°F, the resid yield was lower with Molyvan L than with Amocat™ 1C first stage catalyst (15% vs. 28%). Resid yield decreased to 7% with Molyvan L when the first stage temperature was raised from 800 to 820°F. Yields of 650-935°F distillate increased from 5% to 13% with Molyvan L, and yields of 360-650°F distillate increased from 35% to 43% at the higher first stage temperature. Hydrocarbon gas yields and hydrogen consumption increased only slightly at 820°F.

Analyses of distilled products are given in Table 5. Amocat™ 1C catalyst in the first stage gave better hydrogenation and heteroatom removal in the lightest (360-650°F) fraction than Molyvan L. This result is not surprising because smaller pore catalysts are most effective for hydrotreating light distillate fractions. The Molyvan L acts like a very large-pore catalyst.

Spent second stage catalyst analyses are given in Table 6. With Molyvan L in the first stage, second stage catalyst was in worse shape than when it was protected by Amocat™ 1C first stage catalyst. Carbon levels were higher (25% vs. 8%), the surface area was lower (84 vs. 151 m<sup>2</sup>/g), the pore volume was lower (0.21 vs. 0.38 cc/g), and metal deposits were higher. Solids appear to deposit on the first supported catalyst that is available. In fact, spent second stage catalyst from the run with Molyvan L is similar to spent first stage Amocat™ 1C catalyst. The second stage catalyst replacement rate would have to increase if Molyvan L was used in the first stage.

#### Dispersed Molybdenum Catalysts in Stages 1-2

Molyvan L or molybdenum octoate were tested without supported catalyst for liquefaction of Illinois No. 6 coal at 192 ppm and 84 ppm Mo:coal (64 and 26 ppm Mo:slurry) for Molyvan L, and 96 ppm Mo:coal (32 ppm Mo:slurry) for molybdenum octoate. Operating temperatures were 800-820°F for both reactors. The nominal residence times were 0.75-1.5 hour in each stage or 1.5-3.0 hours overall. Each set of conditions was maintained for 3 days to obtain representative samples.

At the end of the run, a solvent-only feed was processed with Molyvan L catalyst (48 ppm Mo:solvent).

## RESULTS

Product yields from all conditions were good, see Table 3, columns labelled "slurry". Resid yields were 3-8%, C<sub>4</sub>-935°F distillate yields were 66-72%, and coal conversions were 94-96%, which was as least as good as from the first stage test with Molyvan L. Hydrogen consumption were somewhat lower (4.8-5.7%) than from Amocat™ 1C (5.6%) or for first stage Molyvan L (5.4-6.1%).

Product yields did not change when the molybdenum level was decreased from 192 ppm to 84 ppm. Product yields were also unchanged when and the residence time was decreased from 3 to 1.5 hours and the temperature was raised from 800 to 820°F. Molybdenum octoate gave less resid than Molyvan L at the same conditions, and would be the preferred oil-soluble molybdenum catalyst because it is less expensive.

Distillate product quality, Table 4, was not as good as when Amocat™ 1C catalyst was present, however. Nitrogen and oxygen levels were higher, but sulfur and hydrogen levels were about the same. It is interesting to note that the resid plus solid fraction has a higher H/C ratio (0.98) with Molyvan L catalyst at 800°F than with Amocat™ 1C catalyst (0.95-0.96). Better hydrogenation of the heaviest components by Molyvan L is indicated. At reactor temperatures of 820°F, the H/C ratio of the resid plus solids fraction dropped to 0.92, reflecting a shift in equilibrium toward dehydrogenation. Molybdenum octoate was not as active for hydrogenation of resid plus solids, giving a H/C ratio of 0.91 at 800°F.

## CONCLUSIONS

### Molyvan L Catalyst in Stage 1

Overall, a process with Molyvan L catalyst in the first stage and Amocat™ 1C catalyst in the second stage gave a higher distillate yields than a process with Amocat™ 1C catalyst in both stages. Because Molyvan L catalyst can be used in a less expensive slurry reactor, it would be the preferred first stage catalyst for liquefaction of Illinois No. 6 coal. With Molyvan L in the first stage, deactivation is more rapid for supported second stage catalyst, and the catalyst addition rate would have to be increased. Also, hydrogenation of light distillate was not as good, which would require additional hydrotreating.

### Molyvan L Catalyst in Stage 1/Amocat™ 1C Catalyst in Stage 2

A process with dispersed molybdenum compounds as the only catalyst offers several advantages over liquefaction with Amocat™ 1C catalyst, including less expensive reactor design and simpler operation of the reactors. Product was better than when Amocat™ 1C catalyst was used in both reactors and as good as when Amocat™ 1C was used in stage 2 with Molyvan L in stage 1. Low levels of molybdenum, 84 ppm Mo:coal, were effective. Production of a low-resid product at 1.5 hours residence time and 820°F was demonstrated. Molybdenum octoate, a less expensive dispersed molybdenum catalyst, performed well, perhaps because of the high sulfur content of Illinois No. 6 coal. Use of dispersed molybdenum catalysts for liquefaction of Illinois No. 6 coal is recommended.

## ACKNOWLEDGEMENTS

This work was completed with funding from the United States Department of Energy under contract number DE-AC22-88PC88819.

TABLE 1  
COAL ANALYSES

Coal	Illinois No. 6
As Received, Wt% H <sub>2</sub> O	6.05
Dry, Wt%	
C	69.54
H	4.56
N	1.17
S	3.26
O (Difference)	12.03
Ash	9.44
Fe	1.19
Na	0.05
K	0.18
Ca	0.37
Mg	0.06
Al	0.99
Ti	0.05
Si	2.15

TABLE 2  
SOLVENT ANALYSES

Wilsonville Run	257
Wilsonville Coal	Illinois No. 6
Elemental Analyses, Wt%	
C	89.26
H	8.83
N	0.57
S	0.08
O	1.26
Distillation, Wt%	
IBP-650°F	0.36
650-935°F	58.26
935+°F	40.45
Solubility, Wt%	
THF Insolubles	0.12
Toluene Insolubles	1.07
Hexane Insolubles	7.96

TABLE 3.  
Liquefaction of Illinois No. 6 Coal: Distilled Product Yields

Process	C/C	T/C	T/C	Slurry	Slurry	Slurry	Slurry
Residence Time, Hours	3	3	3	3	3	1.5	3
Stage 1, °F	790	800	820	800	800	820	800
Stage 2, °F	760	760	760	800	800	820	800
Molyvan L, ppm	0	192	192	192	84	84	0
MoOctoate, ppm	0	0	0	0	0	0	96
Catalyst Age, Hours	180	150	310				
Yields, Wt% of MAF Coal							
C <sub>1</sub> -C <sub>3</sub>	8.9	9.3	10.1	8.5	9.1	11.0	10.5
C <sub>4</sub> -360°F	7	7	12	7	10	11	8
360-650°F	35	35	43	40	39	41	43
650-935°F	5	13	12	21	19	16	22
935°F+	28	15	7	8	8	5	3
C <sub>4</sub> -935°F	47	56	67	68	66	68	72
Conversion	93.2	91.1	93.9	94.6	96.3	95.7	94.5
H <sub>2</sub> Consumption	5.6	5.4	6.1	5.1	5.7	4.9	4.8

C - With Amocat™ 1C catalyst T - Without Amocat™ 1C catalyst

TABLE 4.  
Liquefaction of Illinois No. 6 Coal: Product Analyses

Process	C/C	T/C	T/C	Slurry	Slurry	Slurry	Slurry
Residence Time, Hours	3	3	3	3	3	1.5	3
Stage 1 °F	790	800	820	800	800	820	800
Stage 2 °F	760	760	760	800	800	820	800
Molyvan L, ppm	0	192	192	192	84	84	0
MoOctoate, ppm	0	0	0	0	0	0	96
Catalyst Age, Hours	150	150	310				
Analyses, Wt%							
<u>360-650°F</u> Aromatic C	32	40	40	43	43	43	43
H/C	1.61	1.49	1.49	1.47	1.48	1.46	1.45
N	.25	.41	.48	.65	.56	.54	.51
O	1.5	2.3	2.4	2.9	3.3	3.1	3.1
<u>650-935°F</u> Aromatic C	42	47	47	47	48	50	51
H/C	1.28	1.28	1.27	1.25	1.27	1.22	1.22
S	.06	.07	.07	.08	.09	.09	.09
N	.30	.36	.47	.60	.61	.52	.49
O	.5	.8	.9	1.1	1.2	1.1	1.0
<u>935°F+, Solids</u>							
H/C	.96	.95	.96	.98	.98	.92	.91
S	.96	1.00	.92	1.01	.88	.35	.95
N	1.07	1.14	1.18	.97	1.06	1.09	1.12

C - With Amocat™ 1C catalyst T - Without Amocat™ 1C catalyst  
Nominal residence time was about 3 hours for these periods.

TABLE 5.  
 Analyses of Spent Amocat™ 1C Catalyst Samples:  
 Illinois No. 6 Liquefaction

Stage	Fresh	1	2	2
Temperature, °F		790	760	760
Process		C/C	C/C	T/C
Oil-Soluble Mo, ppm				192
Run Length, Days	0	20	20	20
<u>Elemental Analyses, Wt%</u>				
<u>Primary Metals</u>				
Mo	9.10	5.9	8.10	6.50
Ni	2.22	1.25	1.63	1.37
Al	35.40	23.50	31.60	25.10
Si	1.39	.98	1.22	.99
<u>Deposits</u>				
C	--	25.35	7.86	24.98
H	--	1.59	1.50	1.42
S	.20	4.78	5.86	4.97
Ti	.00	1.54	.14	.58
Fe	.02	.44	.14	.17
Na	.08	.12	.11	.15
Mg	.00	.05	.01	.01
Ca	.00	.00	.00	.00
<u>Pore Properties</u>				
Vol. <1200 Å Diam., cc/g	.59	.16	.38	.21
BET Surface Area, m <sup>2</sup> /g	200	65	151	84

## TRANSITION METAL CARBIDES AND NITRIDES AS HYDROPROCESSING CATALYSTS

S. Ted Oyama<sup>1,2</sup>, Rajat Kapoor<sup>1</sup>  
Departments of Chemical Engineering<sup>1</sup> and Chemistry<sup>2</sup>  
Clarkson University  
Potsdam, New York 13699-5705

Chakka Sudhakar  
Texaco, Inc.  
Research and Development  
Beacon, New York 12508

### INTRODUCTION

The removal of nitrogen and sulfur from petroleum and coal feedstocks is an essential step in their refining to transportation fuels. Traditional catalysts have been sulfides of Co, Mo, W and Ni in various combinations supported on alumina. Although other transition metal sulfides have been found to be more effective in hydrodesulfurization (Os, Ru, Ir, Rh), their high cost has precluded their use as commercial catalysts (1). The resemblance of early transition metal carbides and nitrides to Group 8 metals (2,3) suggested their possible application in hydroprocessing. The objective of this study was to compare the catalytic activity of selected carbides and nitrides to a commercial sulfided Ni-Mo-P/Al<sub>2</sub>O<sub>3</sub> catalyst in the hydroprocessing of a diesel feedstock.

### EXPERIMENTAL

The transition metal carbides and nitrides were prepared by a temperature-programmed method in which a precursor oxide was treated in a flowing reactive gas stream as the temperature was progressively raised (4,5,6). The catalysts were passivated in a stream of 0.5 mol% O<sub>2</sub>/He after preparation. The surface areas of the catalysts were determined in a flow system by the 1-point BET method and were found to be 66 m<sup>2</sup>g<sup>-1</sup> for Mo<sub>2</sub>C, 59 m<sup>2</sup>g<sup>-1</sup> for

Mo<sub>2</sub>N, and 60 m<sup>2</sup>g<sup>-1</sup> for VN. Prior to catalytic evaluations the catalysts were reduced *in situ* at 723 K (450 °C) for 3h.

The performance of the carbides and nitrides was compared to that of a state-of-the-art commercial catalyst containing 14 wt% Mo, 3 wt% Ni, and 4-6 wt% P, supported on alumina. The surface area of the catalyst was 175 m<sup>2</sup>g<sup>-1</sup>. This catalyst was sulfided in 10 mol% H<sub>2</sub>S/H<sub>2</sub> at 623 K (350 °C) for 2 hours before the start of the reaction.

The catalysts were evaluated in a standard high pressure flow reactor system equipped with electronic flow and temperature controllers. The feedstock used for the evaluations was a finished diesel from a west coast refinery containing 0.02% S, 82 ppm N and 27 wt% aromatics. Hydrodenitrogenation was determined as N removed as ammonia as measured by the Antek N analysis of the product. Hydrodearomatization (HDA) was measured by the open column liquid chromatography (OCLC, ASTM D# 2549) method. The catalysts were compared at two conditions, moderate and severe, applied in succession to the same catalyst batch. The moderate conditions consisted of a LHSV of 3.0 h<sup>-1</sup>, 4.8 MPa (700 psig), 573 K (300 °C) and a H<sub>2</sub> flow of 2000 SCFB. The severe conditions comprised a LHSV of 1.0 h<sup>-1</sup>, 10.3 MPa (1500 psig), 653 K (380 °C), and a H<sub>2</sub> flow of 4000 SCFB. All catalysts were compared on an equal volume basis.

## RESULTS AND DISCUSSION

The results of the catalytic evaluations are reported in Table 1 and 2. The tables also report the amounts of catalyst loaded in volume and weight. The comparisons are made at constant values of liquid hourly space velocity (LHSV), so that the hydrodenitrogenation activity (%HDN) of the different catalysts are on the basis of *equal volume*. For analysis, samples were collected at the reported time intervals, sometimes with mixing of aliquots.

Table 1 compares the performance of the catalysts at moderate conditions. The Mo<sub>2</sub>C catalyst shows a decline in activity over the 64 h of test time. Such initial deactivation is normal in most hydroprocessing catalysts. In contrast, Mo<sub>2</sub>N does not manifest any substantial deactivation and maintains its initial activity. The VN catalyst shows no catalytic activity at these conditions. The commercial Ni-Mo-P-S/Al<sub>2</sub>O<sub>3</sub> catalyst shows the greatest HDN activity per unit volume.

Table 1  
Catalytic Performance of Catalysts at Moderate Conditions  
(Reactant N = 84 ppm, P = 4.8 MPa, T = 573 K, LHSV = 3.0 h<sup>-1</sup>, H<sub>2</sub> flow = 2000 SCFB)

Catalyst	Volume cm <sup>3</sup>	Weight g	Product N ppm	HDN %	HDA %	Comments
Mo <sub>2</sub> C	4.3	5.2	68	17	-	24 h, cuts 1-3
			74	9.8	-	40 h, cuts 4,5
			77	6.1	-	64 h, cuts 6,7
Mo <sub>2</sub> N	3.2	5.1	70	17	-	24 h, cuts 1,2
			71	16	-	48 h, cuts 3,4
VN	5.8	5.2	84	0	-	24 h, cuts 1-3
			84	0	-	40 h, cuts 4,5
			84	0	-	64 h, cuts 6,7
Ni-Mo-P	15	12.8	25	70	-	24 h, cuts 1,2

Table 2 reports the performance of the catalysts at severe hydroprocessing conditions. At these conditions all catalysts are active, including VN. Of the carbides and nitrides Mo<sub>2</sub>N remains the most active, equalling the performance of the commercial Ni-Mo-P-S/Al<sub>2</sub>O<sub>3</sub> in HDN and approaching it in hydrodearomatization. Interestingly, the carbide and nitride catalysts showed increased HDN activity with the progression of the test. This is contrary to what is generally found in hydroprocessing and suggests that the catalysts were not properly activated in the initial tests. This may explain the lower performance of these catalysts compared to the commercial Ni-Mo catalyst at the moderate conditions (Table 1).

It should be pointed out that comparisons of catalyst performance in HDN at the severe conditions employed in Table 2 may be misleading because of the high conversions achieved. This would tend to eliminate differences between catalysts. However, it should also be noted that in all comparisons a *volume* basis was employed. If correction is made for the surface areas of the catalysts, the carbides and nitrides would manifest higher activities.

Table 2  
Catalytic Performance of Catalysts at Severe Conditions  
(Reactant N = 84 ppm, P = 10.3 MPa, T = 653 K, LHSV = 1.0 h<sup>-1</sup>, H<sub>2</sub> flow = 4000 SCFB)

Catalyst	Volume cm <sup>3</sup>	Weight g	Product N ppm	HDN %	HDA %	Comments
Mo <sub>2</sub> C	4.3	5.2	4	95	22	24 h, cut 8
			2	98	18	50 h, cut 9
Mo <sub>2</sub> N	3.2	5.1	17	80	31	30 h, cut 5
			1	99	41	100h, cut 6
VN	5.8	5.2	27	68	6	24 h, cut 8
			14	83	11	50 h, cut 9
Ni-Mo-P	15	12.8	1	99	43	24 h, cut 3
			1	99	61	50 h, cut 4

#### ACKNOWLEDGEMENTS

This paper was written with support from the Center for Advanced Materials Processing at Clarkson University and from the U.S. Department of Energy under the Advanced Coal Research at U.S. Universities Program, Grant no DE-FG22-91PC91298. The authors also thank Texaco, Inc. for permission to publish these results.

#### LITERATURE CITED

- (1) Chianelli, R. R., *Catal. Rev.-Sci. Eng.*, 26, 361 (1984).
- (2) Oyama, S. T. and Haller, G. L., *Catal. Spec. Period. Rep.*, 5, 333 (1982).
- (3) Oyama, S. T., *Catal. Today*, In press.
- (4) Lee, J. S., Oyama, S. T. and Boudart, M., *J. Catal.*, 106, 125 (1987).
- (5) Oyama, S. T., Schlatter, J. C., Metcalfe, J. E. and Lambert, J., *Ind. Eng. Chem. Res.*, 27, 1639 (1988).
- (6) Kapoor, R. and Oyama, S. T., *J. Solid State Chem.*, In press.

## HIGH-SEVERITY CO-PROCESSING

J. G. Gatsis, R. W. Roemisch, M. A. Miller,  
C. A. Piasecki, and H. E. Fullerton

UOP  
Des Plaines, Illinois

Keywords: co-processing, liquefaction, coal, petroleum resid

### INTRODUCTION

UOP is continuing bench-scale research and development of coal and petroleum resid co-processing technology under the sponsorship of U.S. Department of Energy. Earlier work, under completed contract DE-AC22-84PC70002, has been reported in a series of papers and reports (1-7). The overall objectives, to evaluate the technical feasibility of the co-processing concept and to establish a co-processing data base, were met. The concept of single-stage, slurry-catalyzed co-processing was successfully demonstrated in laboratory batch experiments (1) and in continuous bench-scale operations (2). Good long-term operability with the UOP vanadium-based catalyst was demonstrated for nearly 2,000 hours on-stream (3). A method of recovering the catalyst was developed and demonstrated on a laboratory scale. Based on the long-term operability and catalyst recovery studies, a conceptual commercial design was completed for a co-processing unit integrated into a 100,000 BPSD conventional refinery (3,4).

The primary objective of the current contract, DE-AC22-87PC79818, is to extend and optimize the single-stage, slurry-catalyzed co-processing scheme. Catalyst economics plays a major role in determining the overall profitability of slurry-phase co-processing. Consequently, much work has been devoted to exploring new catalyst systems and improving catalyst activity, dispersion, and recovery techniques. Most of the early development work was done using a vanadium-based slurry catalyst. A newer molybdenum-based slurry catalyst has been developed. In autoclave testing, the molybdenum-based catalyst gave equivalent conversions and yields as the vanadium-based catalyst at one-tenth the metal concentration (8). This molybdenum-based catalyst has been evaluated in the continuous bench-scale unit. Plant modifications, including the addition of a recycle loop, have made bench-scale operations possible at much higher severities than were previously possible. Good plant operations have been achieved at temperatures up to 470°C and with catalyst concentrations as low as 500 ppm molybdenum (9). Processing at high severities for short durations has demonstrated high nondistillable conversion without excessive carbon loss to retrograde reactions and light-ends yield. This important advancement in co-processing should significantly improve the process economics. A long-term operability study at high-severity conditions was needed to demonstrate that high-severity co-processing is feasible and can be run for extended periods without major operational problems. This paper reviews the results of a recent long-term operability study at high severity.

### Continuous Bench-Scale Operations

A simplified block diagram of the pilot plant is shown in Figure 1. The unit contains many of the essential features of the commercial flow scheme and is equipped to quantitatively measure the hydrogen consumption in the operations. The slurry feed (finely ground coal, petroleum vacuum resid, and catalyst) is combined with a hydrogen-rich recycle gas and is preheated before it enters the bottom of an upflow reactor. The products from the reactor are separated into gas and oil streams in the high-pressure separator (HPS). The gas stream from the HPS is combined with makeup hydrogen before being recycled back to the incoming fresh feed. A portion of the oil stream

from the HPS is recycled back to the incoming fresh feed, and the remainder is sent to a stripper. The lighter hydrocarbon stream from the stripper is sent to a debutanizer, where it is separated into  $C_4$  and  $C_5$  products. The heavier hydrocarbon stream from the stripper is sent to a vacuum fractionator to recover an overhead stream (light oil and vacuum gas oil) and a bottoms stream containing catalyst, coal minerals, insoluble carbonaceous material, and nondistillable hydrocarbons.

The addition of a recycle loop to the plant, i.e., the recycle of a portion of the HPS liquid back to the fresh feed, has greatly improved plant operability, especially at temperatures greater than 440°C. A recycle ratio of greater than 5:1 (based on recycle to fresh feed) is typically used. The space velocity of the fresh feed is maintained constant. The recycle results in increased liquid velocities and backmixing in the reactor. The improved mixing may help to eliminate the wall effect associated with a small bench-scale reactor. The liquid recycle also has a "flywheel" effect that helps to better withstand upsets in the fresh feed rate.

Prior to the introduction of liquid recycle, the reactor temperature in the bench-scale unit was limited to a maximum of about 425°C. As the operating temperature was increased beyond 425°C, a rapid decrease in heptane insolubles followed by coking and plugging problems made the plant increasingly difficult to operate (2).

With the addition of liquid recycle, the bench-scale unit can be run at much higher temperatures without developing coking problems (9). Temperatures of up to 470°C were achieved. The increased severity had little effect on the maximum coal conversion, which was still about 92%, but did result in about 20% increase in maximum asphaltene conversion (as measured by heptane insolubles) and an almost 30% increase in the 510°C+ nondistillable conversion.

The mechanism for improved high-temperature plant operability and conversions with liquid recycle may be due to better contacting of the reactive coal fragments with hydrogen and catalyst as a result of improved reactor backmixing or to the decrease in the relative contact between the coke precursors and the hot reactor walls as a result of greater superficial liquid velocities in the reactor. Hydrodynamic differences resulting from recycle may have also affected the flow regime, heat transfer characteristics, or gas void volume in the reactor. Further reactor modeling studies are needed to thoroughly understand these phenomena.

### **Feedstocks**

The feedstocks used for this study were reference feedstocks Lloydminster vacuum resid, designated as R10, and Illinois No. 6 coal, designated as Cl.4. Feed properties are given in Tables 1 and 2. Lloydminster vacuum resid (950°F<sup>+</sup>, 120-150 Pen.) was obtained from a commercial refinery in Canada. Illinois Coal No. 6 was obtained by the Kentucky Center for Energy Research Laboratory from the Burning Star Mine. Grinding (thru 200 mesh) and drying were done by Empire Coke Company of Holt, Alabama. The preparation procedure and equipment have been previously described (5).

### **TEMPERATURE SURVEY STUDY**

An important part of the single-stage, slurry-catalyzed processing program is to determine the optimum conversion level that produces high liquid yields by selective catalytic conversion as opposed to thermal conversion. A temperature survey study was conducted to determine the highest processing temperature attainable without excessive carbon loss to retrograde reactions and light ends (9). Standard operating conditions were used: 3000 psig, 5:1 minimum liquid recycle ratio, base WHSV, 2:1 mixture of petroleum resid to coal, and 0.12% molybdenum catalyst concentration.

The run was started at 427°C, and the temperature was increased in a stepwise manner. Six test conditions (427, 432, 438, 446, 451, and 459°C) were run. The plant operated well, even at the higher processing temperatures, and showed no evidence of either thermal degradation or reactor fouling. The conversion showed a steady increase with temperature and no sign of decrease even at 459°C. The unconverted coal showed a steady decrease with temperature (Figure 2), and the heptane-insoluble conversion increased with temperature (Figure 3). The greatest impact of the higher temperature was the 30 wt-% increase in nondistillable conversion (Figure 4) without significant carbon loss to retrograde reactions and only about 6% increase in light-ends yields (Figure 5). Table 3 compares the yields and product properties at 427, 446, and 459°C. The product distribution shows the expected trends when temperature was increased: an increase of lighter fractions (C<sub>1</sub>-C<sub>4</sub>, C<sub>5</sub>-177°C, and 177-343°C) and a decrease of heavier fractions (343-510°C and 510+°C). The quality of the liquid product improved with increasing temperature. The API gravity and hydrogen content of the product increased; and heptane insolubles, sulfur, and nitrogen levels decreased.

#### LONG-TERM OPERABILITY STUDY

A long-term operability study at high-severity conditions was undertaken to determine if high-severity co-processing could be run continuously for extended periods without major operational problems or the gradual buildup of coke in the reactor. The run was conducted at standard operating conditions: 3,000 psig, 5:1 minimum liquid recycle ratio, base WHSV, 2:1 mixture of petroleum resid to coal, and 0.090% molybdenum catalyst concentration. The reactor temperature was held at 455°C during the initial three weeks of operation, then increased to 465°C, and maintained for 17 days. During the operation, daily weight balances were conducted to ensure the integrity of the operation.

Catalyst and coal ash balances were followed to monitor fouling or deposition in the pilot plant. Product recoveries, H<sub>2</sub> consumption, and catalyst and ash balances indicated stable operation. The weight recoveries versus hours on-stream are shown in Figure 6 and can be compared with the average value, shown as a solid line. The weight recoveries were good and averaged 100.3 wt-%. The average reactor bed temperature for the 455 and 465°C operation versus hours on-stream is shown in Figure 7: the solid line on the figure represents the average temperature of 455.5°C and 464.7°C. The run was ended by a planned shutdown after 38 days on-stream without any significant operational problem. Upon disassembling the reactor, the walls were found to be free of coke or any deposits.

Conversions, product distribution, and total liquid product properties are shown in Tables 4 and 5 for the 455°C operations and in Tables 6 and 7 for the 465°C operation. The average coal, heptane-insoluble, and nondistillable conversions were 90.5, 74.6, and 78.9 wt-%, respectively, for the 455°C temperature and 91.9, 86.3, and 84.2 wt-%, respectively, for the 465°C temperature. As shown in Figures 8, 9, 10, and 11 the conversions and yields are comparable to those obtained at the same temperature in the temperature survey study.

#### CONCLUSIONS

Long-term operability of co-processing at high-severity conditions was demonstrated. Plant operations and performance were extremely good, and no major operational problems were encountered. High nondistillable conversion was obtained without excessive carbon loss to retrograde reactions and light-end yields. The operability of co-processing at high severity represents an important advance that may significantly improve the process economics.

#### REFERENCES

1. J. G. Gatsis, et al., "Coal Liquefaction Co-Processing," Proceedings of DOE Direct Liquefaction Contractors' Review Meeting, Nov. 19-21, 1985.
2. J. G. Gatsis, et al., "Continuous Bench-Scale Single-Stage Slurry Catalyzed Co-Processing," Proceedings of DOE Direct Liquefaction Contractors' Review Meeting, Oct. 20-22, 1986.
3. J. G. Gatsis, et al., "Continuous Bench-Scale Single-Stage Slurry Catalyzed Co-Processing," Proceedings of DOE Direct Liquefaction Contractors' Review Meeting, Oct. 6-8, 1987.
4. D. A. Nafis, et al., "Bench-Scale Co-Processing," Proceedings of DOE Direct Liquefaction Contractors' Review Meeting, Oct. 4-6, 1988.
5. C. P. Luebke, et al., "Coal Liquefaction Co-Processing Topical Report Number 1," Prepared for the United States Department of Energy under Contract No. DE-AC22-84PC70002, June 1, 1987.
6. J. G. Gatsis, et al., "Coal Liquefaction Co-Processing Topical Report Number 2," Prepared for the United States Department of Energy under Contract No. DE-AC22-84PC70002, Aug. 19, 1988.
7. D. A. Nafis, et al., "Coal Liquefaction Co-Processing Final Report," Prepared for the United States Department of Energy Under Contract No. DE-AC22-84PC70002.
8. D. A. Nafis, et al., "UOP Co-Processing Developments," Proceedings of DOE Direct Liquefaction Contractors' Review Meeting, Oct. 2-4, 1989.
9. C. A. Piasecki, et al., "Single-Stage Slurry-Catalyzed Co-Processing with Liquid Recycle," Proceedings of DOE Direct Liquefaction Contractors' Review Meeting, Sept. 24-26, 1990.

**Table 1**  
**Analysis of Lloydminster Vacuum Resid (R10)**

API Gravity	6.6
Specific Gravity	1.0246
Distillation, °C:	
IBP, vol-%	379
5	455
10	473
20	509
EP	512
Vol-% over at EP	22.0
Analysis, wt-%:	
Carbon	83.6
Hydrogen	10.3
Sulfur	4.77
Nitrogen	0.59
Heptane Insolubles	13.56
Carbon Residue (MCRT)	17.39

**Table 2**  
**Analysis of Illinois No. 6 (CL4)**

Proximate Analysis: (AR Basis), wt-%	
Volatile Matter	38.84
Fixed Carbon <sup>a</sup>	45.80
Moisture	4.08
Ash	11.28
Ultimate Analysis (AR Basis), wt-%	
Carbon	66.75
Hydrogen <sup>b</sup>	4.66
Sulfur	2.91
Nitrogen	1.34
Oxygen <sup>a</sup>	8.98
Ash	11.28
Moisture	4.08

<sup>a</sup> By difference

<sup>b</sup> Corrected for Moisture

**Table 3**  
**Effect of Severity on Yields and Product Properties**

Temperature, °C	427	446	459
<b>Yields, wt-% MAFF:</b>			
H <sub>2</sub> O + CO <sub>2</sub>	6.7	4.0	4.3
H <sub>2</sub> S	1.6	3.3	3.5
NH <sub>3</sub>	0.2	0.4	0.8
C <sub>1</sub> -C <sub>4</sub> (Light Ends)	2.5	5.5	9.1
C <sub>5</sub> -177°C (Naphtha)	5.4	12.0	14.5
177-343°C (Distillate)	17.6	24.0	36.0
343-510°C (VGO)	29.3	26.1	22.9
510+°C (Resid)	34.0	24.2	10.3
Unc. MAF Coal	5.6	3.6	2.3
H <sub>2</sub> Consumption	(2.8)	(2.9)	(3.6)
Total	100.0	100.0	100.0
<b>C<sub>5+</sub> Total Liquid Product:</b>			
MAFF, wt-%	86.2	86.3	83.7
API Gravity	12.9	17.0	19.9
Carbon, wt-%	84.7	84.0	84.4
Hydrogen, wt-%	10.0	10.3	11.0
Sulfur, wt-%	2.1	1.4	1.1
Nitrogen, wt-%	0.9	0.8	0.4
Heptane Insolubles, wt-%	9.8	9.1	3.1
MCRT, wt-%	12.7	11.2	6.2

**Table 4**  
**Conversion and Product Distribution**  
**of 455°C High-Severity Co-Processing**

Normalized Conversion	Wt-%
Coal	90.5
Heptane Insolubles	74.6
Nondistillable, 510+ °C	78.9
Product Distribution	Wt-% MAFF
H <sub>2</sub> O, CO <sub>2</sub> , CO	3.2
H <sub>2</sub> S	4.7
C <sub>1</sub> -C <sub>4</sub>	7.5
C <sub>5</sub> -177°C	13.8
177-343°C	25.8
343-510°C	24.0
510+ °C	17.7
Unc. MAF Coal	3.3
H <sub>2</sub> Consumption	(1.6)
Total	100.0

**Table 5**  
**Total Liquid Product Properties**  
**of 455°C High-Severity Co-Processing**

API Gravity	17.2
Carbon, wt-%	85.1
Hydrogen wt-%	10.4
Sulfur, wt-%	1.3
Nitrogen, wt-%	0.4
Heptane Insolubles, wt-%	9.9
MCRT, wt-%	9.3

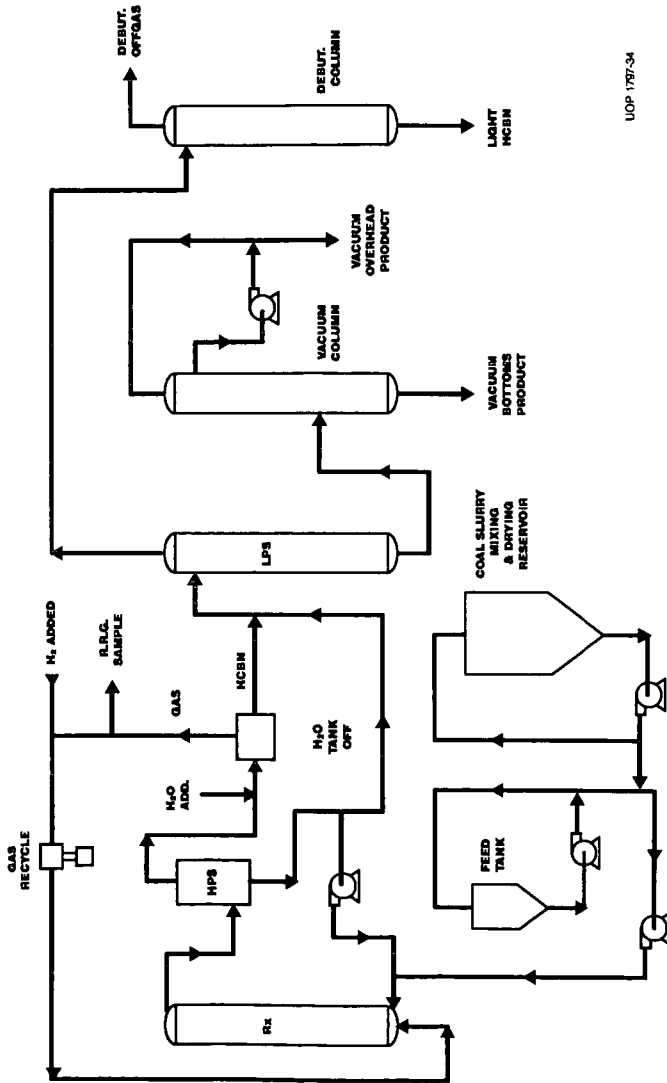
**Table 6**  
**Conversion and Product Distribution**  
**of 465°C High-Severity Co-Processing**

Normalized Conversion	Wt-%
Coal	91.9
Heptane Insolubles	86.3
Nondistillable, 510+ °C	84.2
Product Distribution	Wt-% MAFF
H <sub>2</sub> O, CO <sub>2</sub> , CO	5.0
H <sub>2</sub> S	5.9
C <sub>1</sub> -C <sub>4</sub>	9.9
C <sub>5</sub> -177°C	19.5
177-343°C	28.2
343-510°C	17.9
510+ °C	12.8
Unc. MAF Coal	2.9
H <sub>2</sub> Consumption	(2.1)
Total	100.0

**Table 7**  
**Total Liquid-Product Properties**  
**of 465°C High-Severity Co-Processing**

API Gravity	20.3
Carbon, wt-%	83.7
Hydrogen, wt-%	10.5
Sulfur, wt-%	1.0
Nitrogen, wt-%	0.4
Heptane Insolubles, wt-%	4.4
MCRT, wt-%	8.4

**FIGURE 1  
CO-PROCESSING PILOT PLANT**



UOP 1967-64

**FIGURE 2**  
**UNCONVERTED COAL YIELD**  
**vs. TEMPERATURE OF 0.12% Mo**

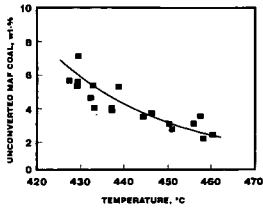


**FIGURE 3**  
**HEPTANE INSOLUBLE CONVERSION**  
**vs. TEMPERATURE OF 0.12% Mo**

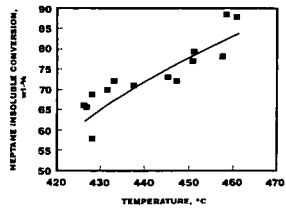


**FIGURE 4**  
**NONDISTILLABLE CONVERSION**  
**vs. TEMPERATURE OF 0.12% Mo**

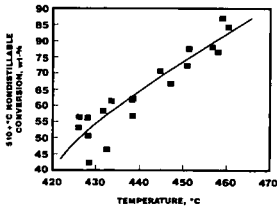


**FIGURE 5**  
**LIGHT-ENDS YIELDS**  
**vs. TEMPERATURE OF 0.12% Mo**

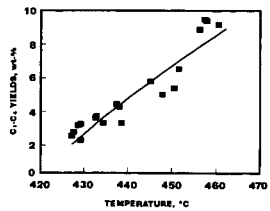


**FIGURE 6**  
**HIGH-SEVERITY CO-PROCESSING**  
**WEIGHT RECOVERIES**

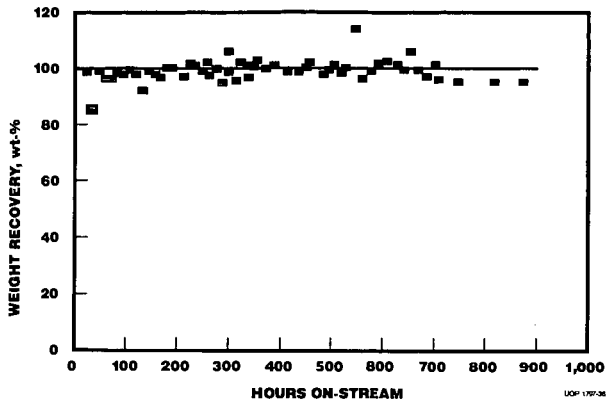


**FIGURE 7**  
**HIGH-SEVERITY CO-PROCESSING**  
**OPERATING TEMPERATURE**

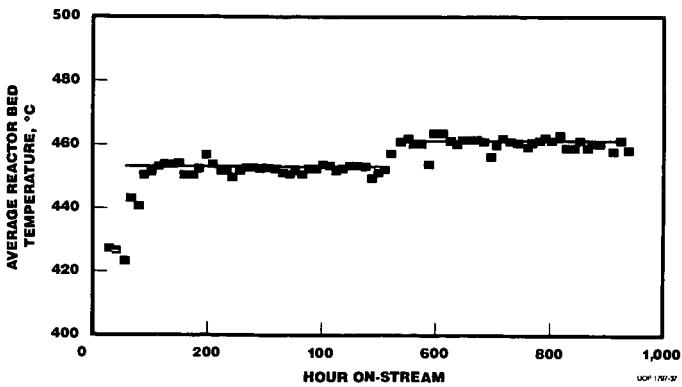


FIGURE 8  
UNCONVERTED COAL YIELD  
COMPARISON

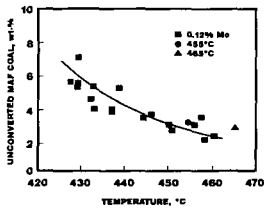


FIGURE 9  
HEPTANE INSOLUBLE CONVERSION  
COMPARISON

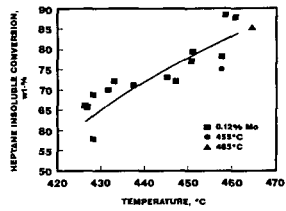


FIGURE 10  
NONDISTILLABLE CONVERSION  
COMPARISON

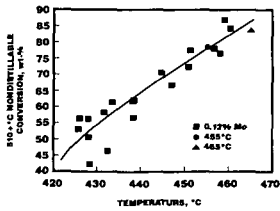
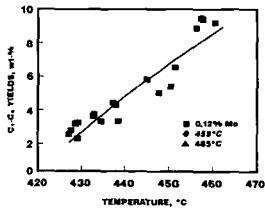


FIGURE 11  
LIGHT-ENDS YIELDS  
COMPARISON



## THE TWO-ALPHA VALUE FOR IRON FISCHER-TROPSCH CATALYSTS: FACT OR FICTION?

Burtron H. Davis  
Center for Applied Energy Research  
University of Kentucky  
3572 Iron Works Pike  
Lexington, KY 40511

Keywords: Fischer-Tropsch Synthesis, Selectivity, Two-Alpha Plots

### INTRODUCTION

The Fischer-Tropsch Synthesis may be viewed as a simple polymerization reaction, the monomer being CO or a C<sub>1</sub> species derived from it. Schulz (1,2) derived an equation for the distribution of molecular weights of polymers obtained by a free radical polymerization process, that is, through a one-by-one addition of monomer to a growing chain. The Schulz distribution function is applicable generally if there is a **constant** probability of chain growth,  $\alpha$ , and  $\alpha < 1$ ; the latter requirement applies when some reaction limits the chain growth. The probability for chain growth,  $\alpha$ , is defined as:

$$\alpha = r_p / (r_p + \Sigma r_t) \quad [1]$$

where  $r_p$  is the rate of chain propagation and  $r_t$  is the rate of chain transfer or chain termination. The probability of the chain growth step to take place P times without termination is

$$P_p = \alpha_1 \alpha_2 \alpha_3 \dots \alpha_p = \alpha^P \quad [2]$$

The number of molecules per degree of polymerization P,  $n_p$ , is proportional to the probability of their formation

$$n_p = \text{const } \alpha^P \quad [3]$$

The mass fraction  $m_p$  is proportional to  $n_p$  as well as the molecular weight of the components of the fraction ( $M_p = M_M P$ , where  $M_M$  is the molecular weight of the monomer)

$$m_p = A P \alpha^P \quad [4]$$

where A contains the constant  $M_M$ . The mass fraction is defined so that

$$\Sigma m_p = 1 \quad [5]$$

The mass fraction is considered to be a continuous function so that

$$\int_0^{\infty} m_p dP = A \int_0^{\infty} P \alpha^P dP = 1 \quad [6]$$

and

$$A = 1 / \int_0^{\infty} P \alpha^P dP \quad [7]$$

Solving the integral ( $\alpha < 1$ ,  $\alpha^{\infty} = 0$ ) and combining equations [4] and [7] leads to

$$m_p = (\ln^2 \alpha) P \alpha^P \quad [8]$$

Rearranging gives the more familiar form

$$\log(m_p/P) = \log(\ln^2 \alpha) + (\log \alpha) P \quad [9]$$

Thus, a plot of  $\log(m_p/P)$  versus  $P$  should result in a straight line.

Flory published a number of theoretical distribution functions for this and other types of macromolecular formation (e.g., reference 3). Thus, polymer scientists usually designate distributions as represented by [9] as conforming to a Schulz-Flory distribution.

Similar equations were derived, apparently independently, by catalysis scientists (4-6). Anderson continued his efforts to develop chain growth mechanisms and to account for the products formed by chain branching (7). Many catalysis scientists therefore recognize Anderson's contributions to the Fischer-Tropsch Synthesis by designating equation [9], and plots based upon it, as an Anderson-Schulz-Flory (ASF) equation or plot, and we shall follow this practice.

Anderson (8) summarized product distribution results up to about 1954. Included in this review were the results of the Schwarzheide tests using catalysts from Lurgi, Brabag, K.W.I., I.G. Farben, Ruhr Chemie, and Rheinpreussen as well as tests at the larger U.S. pilot plants, and Standard Oil Co. of New Jersey (figure 1). These results included operations with iron catalysts both in fixed and fluidized reactors. The results in figure 1 clearly indicate that a single  $\alpha$  value does not adequately describe the data. Up to carbon number 9 to 11 the data fit one alpha value for equation [9] very well; however, a second  $\alpha$  value is needed to describe those products higher than carbon number 9 to 11. These early workers did not have the benefit of gas chromatography to analyze the higher molecular weight products. Thus, while Anderson noted the need for two or more alpha values to describe the products from FTS using iron catalysts, it received little attention. Furthermore, FTS products from a cobalt catalyst were adequately described with a single alpha value.

Madon and Taylor (9) conducted extensive tests with a precipitated, alkali-promoted iron-copper catalyst. They reported a product distribution for the condensed products from FTS using a plug flow reactor that exhibited a two-alpha plot (figure 2) but the break occurred at a higher carbon number than those in figure 1. Madon and Taylor (9) noted that Anderson and coworkers (10) had obtained such a plot but with the break occurring at a lower carbon number. Madon and Taylor noted that Hall *et al.* (11) had suggested that in addition to stepwise growth

with a single carbon intermediate, multiple build-in of growing chains could occur and that this could affect the growth rate of heavy hydrocarbons. Madon and Taylor, after considering this explanation, suggested instead that chain growth takes place on at least two types of sites, each having a slightly different chain growth probability  $\alpha$ .

Novak *et al.* (12) considered the impact of readsorption of  $\alpha$ -olefins upon the products from a continuous stirred tank reactor (CSTR) and a plug flow reactor (PFR). They also considered that  $\alpha$ -olefins could only initiate chain growth, or that they can also isomerize to internal olefins as well as be hydrogenated. For the CSTR, these authors concluded that, even with such secondary reactions, the products still exhibit an ASF plot. For the PFR, the products deviate from an ASF plot when  $\alpha$ -olefins can undergo only chain initiation. If, however, as is the case in a more realistic situation, the  $\alpha$ -olefin also undergoes hydrogenation and isomerization in addition to chain initiation, the distribution rapidly becomes similar to an ASF distribution. Finally, these authors considered the case where the chain growth parameter was allowed to vary along the length of a PFR by forcing the  $C_1$  surface concentration to vary and found, in this case also, that the distribution is quite close to a Flory distribution.

Satterfield and Huff (13) initially concluded that the products for a doubly promoted catalyst (C-73, United Catalysts, Inc.) in a CSTR yielded a precise linear relationship between the log of the mole fraction of the products and the carbon number as predicted by an ASF distribution provided all products, including oxygenate species, were included. The linear relationship held over four orders of magnitude of the moles of products and for carbon numbers from 1 to about 20 over a wide range of gas compositions. The chain growth probability factor,  $\alpha$ , increased slightly from 0.67 at 269°C to 0.71 at 234°C.

Huff and Satterfield (14), after re-examination of their previous data and a consideration of new experimental data on three different iron catalysts, reported that in some cases, the ASF distribution plot can only be well represented by two straight lines with a marked break occurring at about  $C_{10}$ . However, when the products are considered on the basis of compound classes, the situation shown in figure 1 is an oversimplification. As shown in figure 3, Huff and Satterfield found that only the paraffins deviate from the ASF plot; oxygenates and alkenes appear to follow a single ASF plot with  $\alpha \sim 0.55$ .

Egiebor *et al.* (15) also reported that the break in the ASF plot was due to the alkanes. These authors showed that  $\alpha$ -olefins and cis- and trans- $\beta$ -olefins all show straight line plots with different slopes. They concluded that all these compounds are primary products. The fact that only paraffins show a break in the ASF slope proves that paraffins are not secondary products derived from  $\alpha$ -olefins. These authors advanced the view that growth of linear chains proceed at the same rate ( $\alpha$ ) for all species and that it is the termination event which is species specific. The break in the paraffin ASF plot is therefore caused by a sharp change in the rate of termination at about  $C_{13}$ . Since a number of investigators have found that the carbon number where the break occurs is about the same and since the break is observed with a variety of catalysts, they state that it may be that the phenomenon is governed by the nature of the  $C_{13}$  molecule as well as the catalyst.

Gaube and coworkers (16,17) also observed a two  $\alpha$  plot. For an iron catalyst the  $C_3 - C_{40}$  products exhibit a linear ASF plot that only required a single  $\alpha$  value (figure 4). However, when the catalyst contained alkali (added as  $K_2CO_3$ ), the ASF plot needed two  $\alpha$  values to adequately describe the data. However, others have found the need for two alpha values for catalysts that do not contain potassium or other alkali metals (e.g., 18-21).

Donnelly *et al.* (22) extended the chain growth theory to include two growth probabilities; thus, rather than equation [4] one should write

$$m_p = AP\alpha^P + BP\alpha^P \quad [10]$$

The contribution of each growing chain will be equal at the break point. They offer this as an improved equation for analyzing FTS product distributions, and show that this equation adequately described their data.

Dictor and Bell (18) found a two-alpha plot for both reduced and unreduced iron oxide catalysts. Furthermore, these authors found that the ASF plot for n-aldehydes yielded a two-alpha plot just as was the case for the hydrocarbon products. Furthermore, the break for the aldehydes was at the same carbon number as the hydrocarbons, provided the aldehyde ASF plot was based upon n-1 rather than  $\bar{n}$ , as was used for the hydrocarbons (figure 5). This was taken to support the view that aldehydes are formed by CO insertion into a growing surface alkyl group and subsequent reductive elimination of the acyl group (23,24); hydrocarbons on the other hand are believed to be formed in a termination step that occurs by elimination of a hydrogen from an alkyl group. Since the break occurs at  $\bar{n}$  for hydrocarbons and  $n + 1$  for the aldehydes, it appears that the oxygenate and hydrocarbon products are derived from a common surface species.

Donnelly and Satterfield (20) utilized a Ruhrchemie catalysts in a CSTR and found that both the n-alkanes and 1-alkenes fit a two-alpha ASF plot (figure 5) whereas earlier work from that laboratory (14) showed that only n-alkanes deviated from ASF. In contrast to Dictor and Bell (18), Donnelly and Satterfield (20) found that oxygenates followed a single alpha plot even though they now find, in contrast to earlier results, that both n-alkanes and 1-alkenes deviate from ASF. These data serve to illustrate the difficulty in deciding the one or two-alpha plot question.

Stenger (25) showed that the two site ASF equation used by Huff and Satterfield was equivalent to one based on a distributed-site model in its ability to fit the molecular weight product distribution from an iron catalyst promoted with potassium. In the promoted catalyst, a distribution of sites proportional to the concentration of potassium relative to iron is utilized. In his model, Stenger assumed a normal distribution of K on the surface and postulated an exponential dependence of alpha on the random distribution variable, X, that is proportional to the potassium distribution.

Inoui *et al.* (26) introduced a single criterion to differentiate between the two-site model (20) and a distributed site model (25). However, for typical values of  $\alpha_1$  and  $\alpha_2$  for iron catalysts ( $\sim 0.6$  and  $0.8$ , respectively) the fit to the ASF plot should make it difficult to distinguish the two models, even using the approach suggested by Inoui *et al.*

Kikuchi and Itoh (27) utilized an iron catalyst based upon ultrafine particles loaded with 1% K and found a break in the ASF plot at  $C_{10}$ . The data fit the model based upon two kinds of sites, A and B, with A exhibiting the lower and B exhibiting the higher growth probability. The fit of the experimental data and the calculated curve was satisfactory (figure 6).

Iglesia *et al.* (28) reported that olefins readsorb and initiate surface chains that are indistinguishable from those formed directly from CO/H<sub>2</sub>. Diffusion enhanced olefin readsorption leads to an increase in chain growth probability,  $\alpha$ , and in paraffin content with increasing pore

and bed residence time. Deviations from conventional (ASF) polymerization kinetics were quantitatively described by transport effects on the residence time of intermediate olefins within the liquid-filled catalyst pores without requiring the presence of several types of chain growth sites. The results reported for this study were obtained with a Ru catalyst, and not an iron catalyst.

Not all of the earlier studies require two or more  $\alpha$  values to describe the distribution of products from FTS with iron catalysts. Three examples of this will be noted. Zwart and Vink (29) report that the product from zeolite supported iron catalysts derived from iron carbonyl complexes produced a product distribution in the  $C_{3-20}$  range which obeyed ASF statistics in all cases. Eilers et al. (30) report that in a few hundred independent FTS experiments with various catalyst formulations under different operating conditions it was confirmed that the carbon number distribution were in close agreement with the ASF kinetics (figure 7). However, neither of the two data sets for the iron catalysts cover the total range of carbon numbers where the break in the ASF plot is observed. Cannella (31) reported a linear ASF plot that only required one alpha value to fit the  $C_{3+}$  products for an unsupported iron catalyst but that a two-alpha plot was required for the K-promoted catalyst. Linear ASF plots were always obtained for the  $C_3^+$  products produced over each of the supported iron catalysts.

Tau et al. (32) found that a doubly promoted C-73 catalyst incorporated  $^{14}C$  labeled 1-pentanol, added to the  $CO/H_2$  feed, into higher carbon number products. They found that product accumulation in the CSTR was not adequate to explain the deviation from a constant  $^{14}C$  activity/mole with increasing carbon number for higher carbon number alkane products.

$^{14}C$  labeled ethanol served only as a chain initiator; this is demonstrated by the constant  $^{14}C$  activity/mole for the  $C_2$  through  $C_4$  products (figure 8). The constant activity of  $C_3$  and  $C_4$  that is equal to ethanol indicates that only one  $C_2$  species derived from ethanol was incorporated into these products. These results are in agreement with the earlier data obtained by Emmett and coworkers (11, 33-37).

However, the data in figure 9 clearly indicate that the  $C_{10} - C_{14}$  paraffins exhibit a different  $^{14}C$  activity pattern with increasing carbon number than those in the  $C_2 - C_4$  range. The higher carbon number products are diluted by the products accumulated in the reactor prior to the addition of  $^{14}C$  labeled 1-pentanol. Analysis of the wax withdrawn from the reactor prior to the addition of the  $^{14}C$  tracer provided data to calculate the impact of these products in diluting the  $^{14}C$  content of higher carbon number products. Dilution did provide a minor contribution to the negative slope of the ASF plot in figure 9; however, the points corrected for accumulation ( $\blacklozenge$ ) provided only a modest correction toward that exhibited by the lower carbon number products where  $^{14}C/mole$  was constant with increasing carbon number (figure 8). Hence, the effect of accumulation alone cannot account for the experimental data.

Another explanation for the deviation from the ASF plot is that hydrogenolysis of higher carbon number compounds produce more lower carbon number hydrocarbon products than can be accounted for by ASF. Using the same C-73 catalyst, Huang et al. (38) used octacosane, labeled at the carbon-14 position of the chain, to show that a detectable amount of hydrogenolysis did not occur even after one week of operation at the same conditions as was used by Tau et al. (32). Thus, hydrogenolysis is eliminated as an explanation for the two-alpha ASF plot for a promoted iron catalyst.

Tau et al. (32) concluded that the two alpha values in figure 1 correspond to different product groupings. For the smaller alpha (about 0.62) the typical Fischer-Tropsch products are formed

(alkanes, alkenes, oxygenates, etc.). However, for the larger alpha (about 0.82) the only significant product obtained corresponds to alkanes. The data in figure 10, after first correcting for accumulation and then for the two different product groups, show a constant  $^{14}\text{C}/\text{mole}$ , causing the conclusion based upon the higher carbon alkane products to be consistent with the one based on the lower alkane products.

In conclusion, it is evident that many groups using a variety of iron catalysts have found that two or more alpha values are needed if ASF kinetics are to account for the FTS products. The summary of the two-alpha values (39) for eight studies emphasize this conclusion. It is possible for deficiencies in the analytical determinations or loss of certain carbon number ranges during sampling or testing could cause the break in the ASF plot. However, this is not possible for the  $^{14}\text{C}$  studies since the conclusion is based upon the  $^{14}\text{C}/\text{mole}$  rather than the total number of moles. Recent data using  $^{14}\text{C}$ -ethanol (40) and analysis of a wider carbon number range than in reference 32 provide additional support for the results reported by Tau *et al.* Furthermore, similar results are obtained for the addition of  $^{14}\text{C}$  labeled  $\text{C}_2$ ,  $\text{C}_3$ ,  $\text{C}_5$ ,  $\text{C}_6$  and  $\text{C}_{10}$  alcohols and  $\text{C}_2$ ,  $\text{C}_5$  and  $\text{C}_{10}$  alkenes (41,42). With emphasis on the  $^{14}\text{C}$  tracer studies, we conclude that it is likely that at least two chains are growing independently, and that these independent chains lead to different groups of products. These in turn require at least two-alpha values for the ASF to adequately describe the FTS data.

#### ACKNOWLEDGMENT

This work was supported with funding from the Commonwealth of Kentucky and the U.S. Department of Energy, Pittsburgh Energy Technology Center, through Contract No. De-AC22-84PC70029.

#### REFERENCES

1. G. V. Schulz, *Z. Phys. Chem.*, **29**, 299 (1935); **30**, 375 (1935).
2. G. V. Schulz, *Z. Phys. Chem.*, **30**, 375 (1936).
3. P. J. Flory, *J. Amer. Chem. Soc.*, **58**, 1877 (1936).
4. E. F. G. Herrington, *Chem. Ind.*, (1946) 347.
5. R. A. Friedel and R. B. Anderson, *J. Amer. Chem. Soc.*, **72**, 1212 (1950); **72**, 2307 (1950).
6. S. Weller and R. A. Friedel, *J. Chem. Phys.*, **17**, 801 (1949).
7. R. B. Anderson, "The Fischer-Tropsch Synthesis", Academic Press, New York, 1984.
8. R. B. Anderson in "Catalysis" (P.H. Emmett, ed.) Reinhold Pub. Corp., New York, 1956, Vol. IV, pp 22-256.
9. R. J. Madon and W. F. Taylor, *J. Catal.*, **69**, 32 (1981).
10. J. F. Schulz, W. K. Hall, B. Seligmon and R. B. Anderson, *J. Amer. Chem. Soc.*, **77**, 211 (1955).
11. W. K. Hall, R. J. Kokes and P. H. Emmett, *J. Amer. Chem. Soc.*, **82**, 1027 (1960).
12. S. Novak, R. J. Madon and H. Suhl, *J. Catal.*, **77**, 141 (1982).
13. C. N. Satterfield and G. A. Huff, Jr., *J. Catal.*, **73**, 187 (1982).
14. G. A. Huff, Jr. and C. N. Satterfield, *J. Catal.*, **85**, 370 (1984).
15. N. O. Egiebor, W. C. Cooper and B. W. Wojciechowski, *Canadian J. Chem. Eng.*, **63**, 826 (1985).
16. L. Konig and J. Gaube, *Chem. Ing. Tech.*, **55**, 14 (1983).
17. B. Schliebs and J. Gaube, *Ber. Bunsenges. Phys. Chem.*, **39**, 68 (1985).
18. R. A. Dictor and A. T. Bell, *J. Catal.*, **97**, 121 (1986).
19. L.-M. Tau, H. Dabbagh, B. Chawla and B. H. Davis, "Mechanism of Promotion of Fischer-Tropsch Catalysts", DOE/PC/70029-T1, Final Report, December 1987.

20. T. J. Donnelly and C. T. Satterfield, *Appl. Catal.*, **52**, 93 (1989).
21. H. Itoh, H. Hosaka and E. Kikuchi, *Appl. Catal.*, **40**, 53 (1988).
22. T. J. Donnelly, I. C. Yates and C. N. Satterfield, *Energy & Fuels*, **2**, 734 (1988).
23. H. Schulz and A. Zein El Deen, *Fuel Proc. Tech.*, **1**, 45 (1977).
24. P. Biloen, J. N. Helle and W. M. H. Sachtler, *J. Catal.*, **58**, 95 (1979).
25. H. G. Stenger, Jr., *J. Catal.*, **92**, 426 (1985).
26. M. Inoui, T. Miyake and T. Inui, *J. Catal.*, **105**, 266 (1987).
27. E. Kikuchi and H. Itoh, "Methane Conversion" (D. M. Bibby et al., eds.) Elsevier Sci. Pub., Amsterdam, 1988, pp 517-521.
28. E. Iglesia, S. C. Reyes and R. J. Madon, "Transport-Enhanced Olefin Readsorption Model of Hydrocarbon Synthesis Selectivity", 12th NAM of The Catalysis society, Abstract PC02, Lexington, KY, May 5-9, 1991.
29. J. Zwart and J. Venk, *Appl. Catal.*, **33**, 383 (1987).
30. J. Eilers, S. A. Posthuma and S. T. Sie, *Catal. Lett.*, **7**, 253 (1990).
31. W. J. Cannella, Ph.D. dissertation, U. of California, Berkeley, 1984.
32. L.-M. Tau, H. Dabbagh, S.-Q. Bao and B. H. Davis, *Catal. Lett.*, **7**, 127 (1990).
33. W. K. Hall, R. J. Kokes and P. H. Emmett, *J. Amer. Chem. Soc.*, **79**, 2983 (1957).
34. J. T. Kummer, T. W. DeWitt and P. H. Emmett, *J. Amer. Chem. Soc.*, **70**, 3632 (1948).
35. J. T. Kummer and P. H. Emmett, *J. Amer. Chem. Soc.*, **75**, 5177 (1953).
36. J. T. Kummer, H. H. Podgurski, W. B. Spencer and P. H. Emmett, *J. Amer. Chem. Soc.*, **73**, 564 (1951).
37. G. Blyholder and P. H. Emmett, *J. Phys. Chem.*, **63**, 962 (1959); **62**, 470 (1960).
38. C. S. Huang, H. Dabbagh and B. H. Davis, *Appl. Catal.*, **73**, 237 (1991).
39. D. K. Matsumoto and C. N. Satterfield, *Energy & Fuels*, **3**, 249 (1989).
40. Unpublished data.
41. L.-M. Tau, H. A. Dabbagh and B. H. Davis, *Energy & Fuels*, **5**, 174 (1991).
42. L.-M. Tau, H. A. Dabbagh and B. H. Davis, *Energy & Fuels*, **4**, 94 (1990).

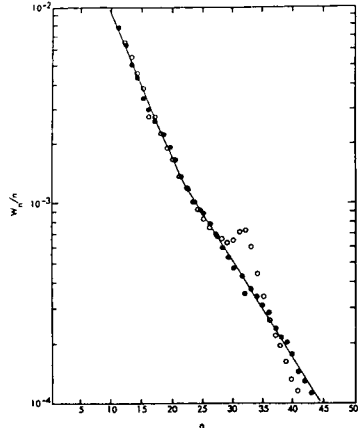
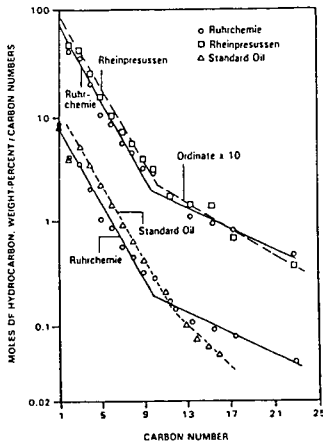


Figure 1. Anderson-Schulz-Flory (ASF) plots for the products from Schwarzheide for four sources and Standard Oil Company of New Jersey (reproduced from ref. (8), p. 208).

Figure 2. Plot of  $\ln W_n/n$  versus carbon number  $n$ . Open points, unsulfided catalysts; solid points, sulfided catalyst (reproduced from ref. (9)).

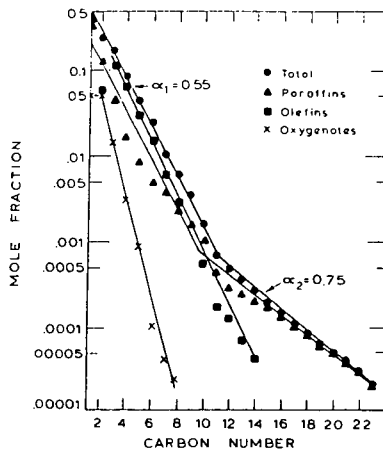


Figure 3. Flory distribution of MnO/Fe catalyst; 283°C, 1.24 MPa,  $(H_2/CO)_m = 1.19$  (reproduced from ref. (14)).

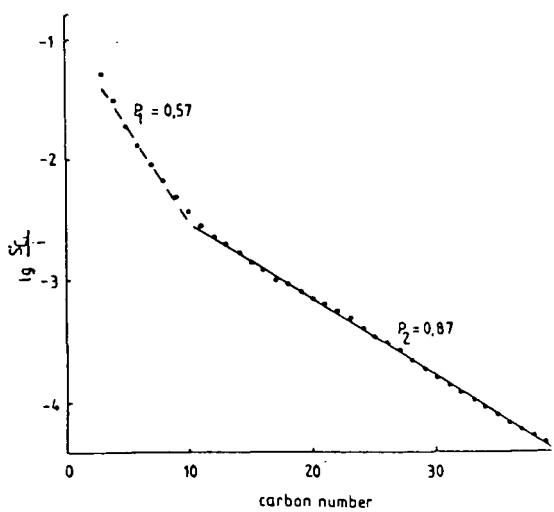
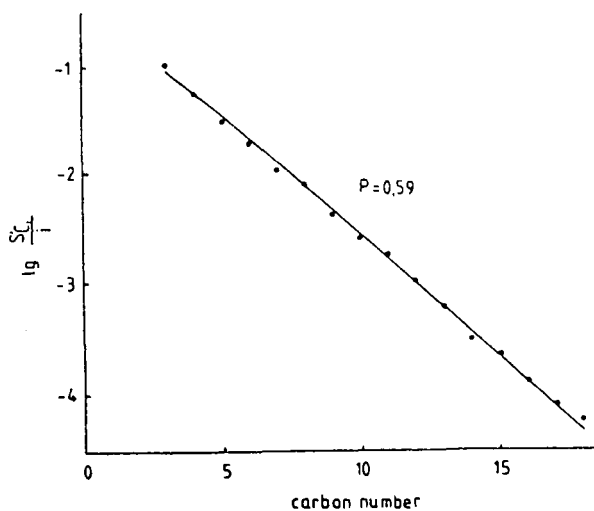


Figure 4. Product distribution from FTS using an iron (top) and potassium promoted iron catalyst (bottom) (redrawn from ref. (16)).

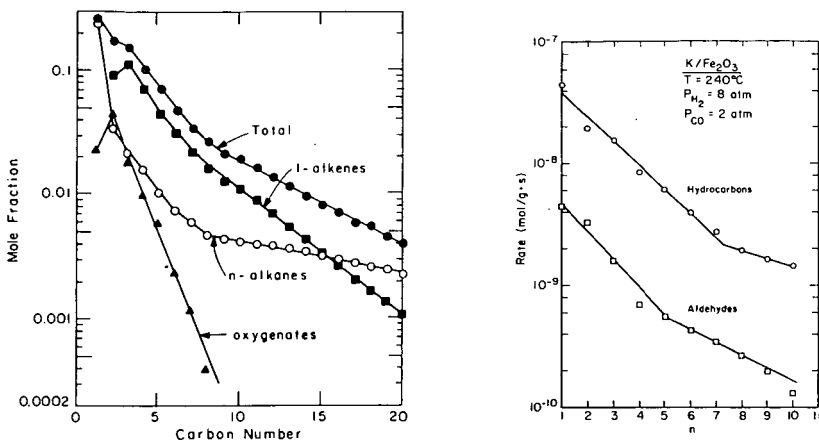


Figure 5. (left) Component Schulz-Flory diagram for overhead products. Ruhrchemie Catalyst MPa,  $0.034 \text{ Nl/min/g}_{\text{cat}}$ ,  $(\text{H}_2/\text{CO})_{\text{feed}} = 0.7$ , 600 hours-on-stream (reproduced from ref. (20)). (right) Distribution of hydrocarbons and aldehydes from a common effluent sample. Each point for hydrocarbons represents the sum of 1-olefin plus n-paraffin; only straight-chain aldehydes are measured (reproduced from ref. (18)).

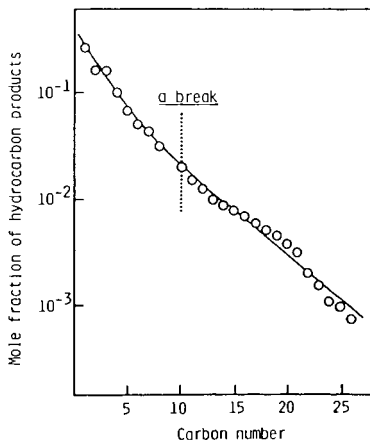


Figure 6. Flory plot of hydrocarbon products over potassium-promoted Fe UFP (ultrafine particle) catalyst. Reaction conditions: temperature,  $220^\circ\text{C}$ ; pressure, 30 atm;  $\text{H}_2/\text{CO}$ , 1 mol/mol; W/F, 300 g-cat.min/CO-mol. Potassium addition: 1 wt.% of catalyst. Solid line represents the simulated distribution based on two-site ASF equation (reproduced from ref. (21)).

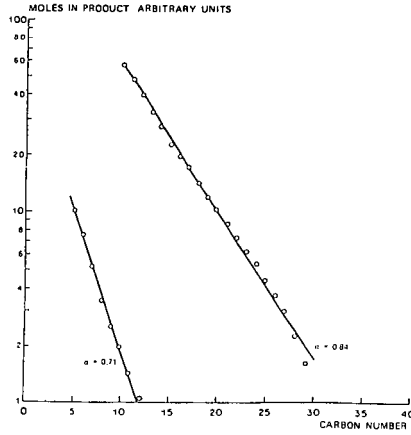


Figure 7. Typical carbon number distribution of the FTS using an iron catalyst (redrawn from ref. (30)).

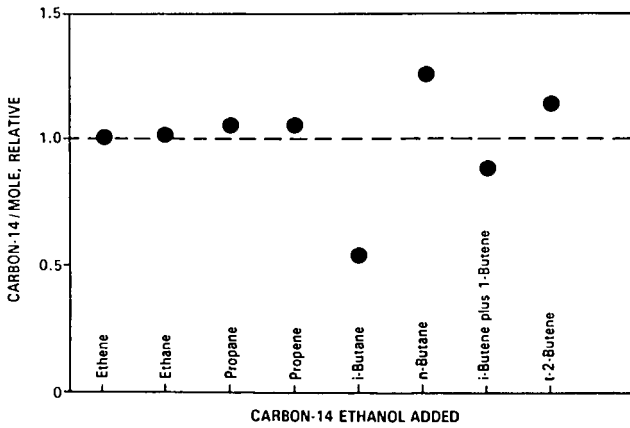


Figure 8. Relative <sup>14</sup>C/mole in gaseous products from the synthesis (7 atm, H<sub>2</sub>/CO = 1.2, 262°C) with 3-volume % (based on alcohol and CO) [<sup>14</sup>C-1]-ethanol was added during a 24 hour period (redrawn from ref. (32)).

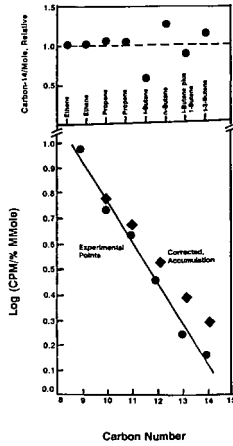


Figure 9. Composite figure showing relative radioactivity for the lower carbon number compounds (●); the measured values for the higher carbon number compounds (◆), and the values for the higher carbon number compounds (■) after correcting for reactor accumulation effects (redrawn from (41)).

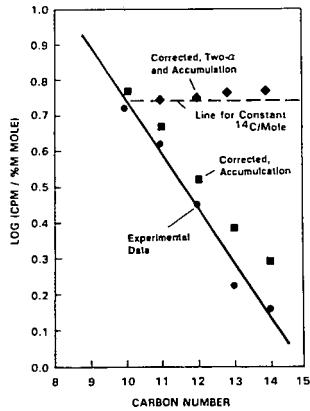


Figure 10. Radioactivity of the: alkane products (●); experimental data corrected for accumulation using data shown in Table 1 (■), and experimental data corrected for both accumulation and the two alpha mechanism (see text for details) (◆) (redrawn from ref. (41)).

## IRON-BASED CATALYSTS FOR SLURRY-PHASE FISCHER-TROPSCH SYNTHESIS

V. U. S. Rao, G. J. Stiegel, A. C. Bose and G. J. Cinquegrane  
U. S. Department of Energy  
Pittsburgh Energy Technology Center  
P. O. Box 10940  
Pittsburgh, PA 15236

and

R. D. Srivastava  
Burns and Roe Services Corporation  
P. O. Box 18288  
Pittsburgh, PA 15236

Keywords: Fischer-Tropsch, Indirect Liquefaction, Iron Catalysts

### Introduction

The Pittsburgh Energy Technology Center is responsible for implementing the U.S. Department of Energy's (DOE) Indirect Liquefaction program as part of the Coal Liquefaction program. The overall goal of the Coal Liquefaction program is to develop the scientific and engineering knowledge base to help industry market economically competitive and environmentally acceptable advanced technology for the manufacture of synthetic liquid fuels from coal.

This article examines the state of knowledge in iron-based catalysts for use in slurry-phase synthesis reactors used in the Indirect Liquefaction of coal. The advantages of using iron catalysts are (1) they are inexpensive, (2) specific activity for Fischer-Tropsch (FT) synthesis is high, and (3) some iron catalysts have high water-gas-shift activity and can convert low  $H_2/CO$  ratio synthesis gas without an external shift reaction step.

### Stoichiometry of the FT Reaction:

The intrinsic stoichiometry of the FT synthesis reaction is represented by eq 1. Many FT catalysts are also active for water-gas-shift (WGS) reaction represented by eq 2. Catalysts that are active for both reactions can be used to convert synthesis gas with hydrogen-to-carbon monoxide ratios as low as 0.5 into hydrocarbon products [see eq 3]. This point is significant because of the development of several advanced coal gasification processes that directly produce synthesis gas with approximately this ratio.



In current commercial practice (SASOL, South Africa), the indirect liquefaction route for the conversion of coal to liquid fuels involves four principal stages [1], namely, coal gasification, gas purification, hydrocarbon synthesis, and product upgrading.

Of these, the gasification step is the most expensive; hence, technological improvements associated with this step offer the greatest potential for reducing costs.

A number of advanced gasification processes (e.g., Texaco and Shell-Koppers), which are now in various stages of commercial development, significantly improve on SASOL technology [2] which uses the conventional Lurgi gasifier. The advanced gasifiers not only exhibit improved efficiencies but also produce a smaller proportion of undesirable by-products (e.g.,  $\text{CH}_4$ ,  $\text{CO}_2$  and  $\text{H}_2\text{S}$ ). At the same time, however, the hydrogen-to-carbon monoxide ratio of the synthesis gas produced is much lower (0.5-0.9, compared to 2.1 for Lurgi). It has been shown that hydrocarbon products can be produced at reasonable reaction rates from this low  $\text{H}_2/\text{CO}$  synthesis gas [3-5], provided the catalyst is active for both reactions 1 and 2.

Depending on the process configuration, the desired products from slurry-phase FT synthesis could be liquid fuels (e.g., gasoline, diesel, jet fuel), light olefins, and/or wax. The light olefins could be oligomerized to liquid fuels through known processes such as MOGD [6]. The wax could be treated by catalytic hydrocracking to provide liquid fuels [7].

**Slurry Phase FT Synthesis:** The development of a slurry-phase Fischer-Tropsch process using an iron-based catalyst has drawn considerable attention. The advantages of the slurry-phase reactor system are (1) the ability to use low  $\text{H}_2/\text{CO}$  ratio synthesis gas produced by the advanced gasification processes, (2) the ability of the liquid phase to withdraw heats of reaction efficiently and thereby control reaction temperature, (3) high catalyst and reactor productivity, (4) favorable conditions for catalyst regeneration, and (5) simple construction and low investment costs.

Initial evaluation of FT catalysts for slurry bubble column reactors is performed in bench-scale, mechanically-stirred, slurry reactors. These reactors offer excellent temperature control and flexibility in operating conditions. Descriptions of such reactors and their operation are available [8]. Since the internal composition of such reactors is uniform, they facilitate development of kinetic models without the complications involved in the analysis of integral data obtained in a fixed bed reactor. The kinetic models will permit the prediction of performance of the catalyst in a slurry-bubble column reactor.

The production of hydrocarbons using traditional FT catalysts, such as Fe or Co, is governed by chain growth or polymerization kinetics. This can be described by the Anderson formalism [9], which is related to the Schulz-Flory polymerization equation [10]. The nature of the product and the product distribution among the carbon numbers will depend upon the catalytic surface, composition ( $\text{H}_2/\text{CO}$  ratio) and the rate of flow of the feed gas, reaction pressure, and the temperature at which the FT synthesis reaction is performed. The above parameters will affect the rate of hydrogen and CO dissociation, hydrogenation, degree of polymerization, and desorption of the product species.

**Chain Growth Kinetics:** The chain growth probability is designated by the quantity  $\alpha$  and represents the probability that an oligomer with  $(r-1)$  carbon atoms will grow to an oligomer with  $r$  carbon atoms. The product distribution among the carbon numbers follows the polymerization equation

$$W_n = n(1-\alpha)^2 \alpha^{n-1} \quad (4)$$

The above expression, usually known as the Anderson-Schultz-Flory (ASF) polymerization equation, is written

$$\log(W_n/n) = n \log \alpha + \log[(1-\alpha)^2/\alpha] \quad (5)$$

One would then expect a linear relation between  $\log(W_n/n)$  and  $n$ , with slope  $\log \alpha$ , as shown in Fig. 1 [4]. The theoretical maxima for various hydrocarbon fractions in the FT product such as gas, naphtha, heavy distillate, and wax have been calculated [11] and can be seen in Fig. 2.

### Catalyst Synthesis

Varieties of iron catalysts have been examined for FT synthesis in slurry reactors. These include (1) precipitated iron catalysts [3-5,12,13], (2) fused iron catalysts [14-16], (3) ultrafine-particle catalysts [17-19], and (4) catalysts produced by laser pyrolysis [20,21].

The pioneering work of Kolbel in Germany to develop the Rheinpreussen slurry reactor process after World War II used a precipitated iron catalyst [3]. The results obtained by Kolbel were very favorable, and efforts are ongoing to reproduce the space-time yields or catalyst activities. Koppers [22] of Rheinprussen claimed slurry reactor space-time yields of up to 2800 kg/m<sup>3</sup> per day in a laboratory reactor, but all other studies published by his group reported considerably lower values (e.g., 940 kg/m<sup>3</sup> per day in a pilot-scale reactor and 740 kg/m<sup>3</sup> per day in a laboratory reactor [23]). These investigations and later work by the Mobil group [4,5] using precipitated iron catalysts in a slurry bubble column reactor (see Table 1) have resulted in a sustained interest in this type of catalyst. Accordingly, the effort in the DOE program has been centered on precipitated iron catalysts.

#### Precipitated Iron Catalysts:

The development of precipitated iron catalysts for slurry-phase synthesis was based on earlier work that was performed with iron catalysts intended for use in fixed-bed processes [1]. The feasibility of the use of precipitated iron catalysts has been demonstrated under relatively mild Arge-type conditions at SASOL [1,24]. Apart from the tests conducted on a limited scale at Rheinpreussen [3] and Mobil [4,5], these catalysts have not been sufficiently demonstrated in a slurry-bubble column reactor representative of commercial operation. The main reason for this is the lack of precise information in the public domain regarding the following factors influencing the activity, selectivity, and stability of the catalysts: (1) pH of precipitation, (2) concentration of Fe and other components such as Cu in the precipitation reactor, (3) temperature of precipitation, (4) residence time of Fe and other components in the precipitation reactor, (5) filtration rate of the hydrated gel, (6) washing rate of the hydrated iron oxide gel, (7) use of binders such as silica to provide mechanical strength, and (8) procedures such as spray drying to obtain uniform size spherical particles with a mean diameter of about 30 microns.

Under the DOE program an iron-based catalyst with the desired properties has been developed [25] for study in the Alternative Fuels Development Unit in LaPorte, Texas. Efforts are underway to scaleup the synthetic procedure in order to make about 2,000 pounds of the catalyst. Some features of the catalyst are (1) spherical particles of average diameter of about 30 microns, (2) FT and WGS activities that are higher than those of the commercial Ruhrchemie Fe catalyst, and (3) favorable suspension behavior in the slurry medium.

#### Kinetics of the Fischer-Tropsch Synthesis over Fe Catalysts

The CSTR is well-suited for measuring the intrinsic kinetics of the FT reaction as the influence of heat and mass transfer effects in this reactor can be ignored [8]. The kinetic models that have been proposed for the FT reaction will now be examined.

To date, no model can account for the reaction rate under all conditions. Each of the models agrees with the experimental results under certain conditions.

Anderson's rate expression [9]

$$-r_{CO-H_2} = \frac{k P_{H_2}}{1 + a P_{H_2O}/P_{CO}} \quad (6)$$

is applicable when the WGS activity is low. The rate expression is suggestive of a competition between water and CO for the available sites on the catalyst.

Ledakowicz et al. [26] have proposed that the rate expression

$$-r_{CO-H_2} = \frac{k P_{H_2}}{1 + a P_{CO_2}/P_{CO}} \quad (7)$$

could be used at high WGS activity. This rate equation implies that the influence of CO<sub>2</sub> is more important than that of H<sub>2</sub>O under these conditions.

Satterfield et al. [27] drew attention to the fact that water inhibits the FT synthesis rate more than does CO<sub>2</sub>. It was therefore reasonable to suppose that the concentration of H<sub>2</sub>O (or the H<sub>2</sub>O/H<sub>2</sub> ratio) is more important than the concentration of CO<sub>2</sub> (or the CO<sub>2</sub>/CO ratio) in affecting the oxidation state of the catalyst. It was suggested [28] that the inhibition attributed to CO<sub>2</sub> by Ledakowicz et al. [26] was instead actually caused by H<sub>2</sub>O formed by the reverse WGS reaction. Based on these arguments, the following rate equation [29] was favored:

$$-r_{CO-H_2} = \frac{k P_{H_2}}{1 + a P_{H_2O}/(P_{H_2} \cdot P_{CO})} \quad (8)$$

To use equation (8), it is important to have reliable methods for analyzing H<sub>2</sub>O and H<sub>2</sub>. H<sub>2</sub>O tends to tail in some GC columns, but methods to quantitatively determine the H<sub>2</sub>O concentration have been established [30]. The kinetics of the FT synthesis has recently been reviewed by Wojciechowski [31].

In addition to fluid dynamic data, the development of reliable kinetic rate expressions for iron catalysts is important for the prediction of the behavior of slurry bubble column reactors. The ongoing research to develop active and stable Fe FT catalysts for the slurry phase will stimulate additional work to develop accurate kinetic rate expressions.

#### Predicting Catalytic Performance in a Slurry Bubble Column Reactor

From CSTR data obtained on a precipitated iron catalyst, Abrevaya and Shah [12] have predicted the performance in an SBCR. The calculation was based on the CO+H<sub>2</sub> conversion measured in a CSTR at 265°C and 275°C at various feed flowrates (Fig 3). They assumed that the slurry bubble column reactor could be modelled as 11 slurry autoclave reactors-in-series operating at 8%, 16%, 24% ... 88% conversions. Since data were not available below 35% conversion at 265°C and 50% at 275°C (Fig 3), it was assumed that the reaction rate and selectivity at these temperatures did not

Table 1

## Comparative Catalyst Performance Data

Reactor Type*	SASOL (Dry, 1981)		Köbel et al. (1955) Rheinpreussen Plant	Sakai and Kunugi (1974) [32]	MOBIL (Kuo, 1985)	
	Arge Pptd. FB	Synthol Fused CFB			CT 256-3 Low Max	CT 256-13 High Max
Catalyst			100Fe/0.1Cu/.05-0.5% <sub>2</sub> O BCSR	100Fe/0.3Cu/.6-1.2% <sub>2</sub> O BCSR	Fe/Cu/K <sub>2</sub> O BCSR	Fe/Cu/K <sub>2</sub> O BCSR
Conditions						
Temperature, °C	220	325	268	273	260	258
Pressure, atm	25	25	12	10.8	15	15
SV, ML/g-Fe/h	--	--	3.4	12.1	2.6	2.4
H <sub>2</sub> :CO ratio	1.3-2.0	>2.0	0.67	0.52	0.67	0.67
Activity						
CO+H <sub>2</sub> conv. (%)	--	--	89.0	78.5 (CO)	86.8	82.2
mol/g-cat/h	--	--	.106	--	.070	.061
Nm <sup>3</sup> /kg-Fe/h	--	--	3.02	--	2.25	1.97
Selectivity, wt%						
C <sub>1</sub>	2.0	10.6	3.2 (CH <sub>4</sub> +C <sub>2</sub> H <sub>6</sub> )	2.3	7.8	2.7
C <sub>2</sub> -C <sub>4</sub>	11.2	35.2	31.3	8.2	24.5	11.1
C <sub>5</sub> -C <sub>11</sub>	18.6	42.5	53.6	4.7 (C <sub>5</sub> -C <sub>9</sub> )	41.9	18.1
C <sub>12</sub> -C <sub>18</sub>	14.5	7.5	10.0	12.8 (C <sub>10</sub> -C <sub>18</sub> )	15.4	10.2
C <sub>19</sub> **	53.7	4.2	1.9	71.9	10.8	57.9
C <sub>12</sub> **	68.2	11.7	11.9	84.7 (C <sub>10</sub> )	26.2	68.1
Product Yield						
g-HC/Nm <sup>3</sup> converted	--	--	178	151.8	197	206
g-HC/g-Fe/h	--	--	.57	--	.37	.41

\* FB - fixed bed, CFB - circulating fluidized bed, BCSR - bubble column slurry reactor

change below 35% and 50% conversion respectively. The calculations made using these assumptions are summarized in Table 2. Subsequent improvements in the catalyst resulted in catalyst performance that was much closer to the target performance.

Table 2

Performance of Precipitated Iron Catalyst [12] in  
11 Autoclave Reactors in Series at 21 ATM, 0.7 H<sub>2</sub>: CO Feed  
(wt-%)

	<u>265° C</u>	<u>275° C</u>	<u>Target</u>
C <sub>1</sub>	4.3	5.8	---
C <sub>2</sub> (Ethane + Ethylene)	4.6	6.0	---
C <sub>1</sub> + C <sub>2</sub>	8.9	11.8	7
Sv, nL/h-gFe	1.1	1.6	≥2

**Concluding Remarks:**

From the survey on Fe FT catalysts for slurry-phase operation, it is evident that additional research is needed for the development of reproducible synthesis of active and stable catalysts. A more complete understanding of the behavior of iron catalysts that can be obtained from modern surface and bulk analytic techniques is required. The correlation of catalyst properties with kinetic data will establish a sound basis for the commercial manufacture of Fe FT catalysts for slurry bubble column reactors.

References:

1. M.E. Dry, in J.R. Anderson and M. Boudart (Eds.), *Catalysis - Science and Technology*, Springer, Berlin, 1981, Vol. 1, pp. 159-255.
2. M. Teper, D.F. Hemming, and J.M. Holmes, *The Cost of Liquid Fuels from Coal, Part 1: Executive Summary*, International Energy Agency Report, November 1984.
3. H. Kolbel and M. Ralek, *Catal. Rev. - Sci. Eng.* **21**, 225 (1980).
4. J.C.W. Kuo, *Slurry Fischer-Tropsch/Mobil Two-Stage Process of Converting Syngas to High Octane Gasoline*, Final Report, DOE/PC/30022-10 (DE84004411), 1983.
5. J.C.W. Kuo, *Two Stage Process for Conversion of Synthesis Gas to High Quality Transportation Fuels*, Final Report, DOE/PC/60019-9, 1985.
6. S.L. Meisel, in "Methane Conversion" (Eds. D.M. Bibby, C.D. Chang, and R.F. Howe), *Studies in Surface Science and Catalysis*, **36**, 17 (1988).
7. P.P. Shah, M.J. Humbach, K.Z. Steigleder, and F.G. Padrta, UOP Des Plaines Technical Center, *Fischer-Tropsch Wax Characterization and Upgrading*, Final Report, DE-AC22-85PC80017, 1988.
8. T.J. Donnelly and C.N. Satterfield, *Appl. Catal.* **56**, 231 (1989).
9. R.B. Anderson, in "Catalysis," Volume 4 (P. H. Emmett, ed.), Reinhold, New York, 1956. See also R.B. Anderson, "The Fischer-Tropsch Synthesis," Academic Press, Orlando (1984).
10. G. Henrici-Olive and S. Olive, *Angew. Chem. Int. Ed.* **15**, 136 (1976).
11. J.H. Gregor, AIChE Spring National Meeting, Orlando, Florida, March 18-20, 1990.
12. H. Abrevaya and P.P. Shah, *Proc. DOE Indirect Liquefaction Contractors' Review Meeting*, Pittsburgh, 1990, p. 203.
13. M.F. Zarochak and M.A. McDonald, *Proc. DOE Indirect Liquefaction Contractors' Review Meeting*, Pittsburgh, 1986, p. 58.
14. G.A. Huff and C.N. Satterfield, *J. Catal.* **85**, 370 (1984).

15. D.M. Bukur and R.F. Brown, *Can. J. Chem. Eng.* **65**, 604 (1987).
16. H. Dabbagh, L.M. Tau, S. Bao, J. Halasz, and B.H. Davis, in "Catalysis Today" (J.W. Ward, Ed), Elsevier, 1988.
17. H. Itoh, H. Hosaka, T. Ono, and E. Kikuchi, *Appl. Catal.* **40**, 53 (1986).
18. E. Kikuchi and H. Itoh, in "Methane Conversion," (D.M. Bibby, C.D. Chang, R.F. Howe, and S. Yurchak, Eds.) Elsevier, 1988.
19. H. Itoh, H. Tanabe, and E. Kikuchi, *Appl. Catal.* **47**, L1 (1989).
20. R.A. Fiato, G.W. Rice, S. Misco, and S.L. Soled, U.S. Patent 4,687,753 (1987).
21. G.W. Rice, R.A. Fiato, and S.L. Soled, U.S. Patent 4,659,681 (1987).
22. H.H. Koppers, *Chem. Age India*, **12**, 7 (1961).
23. D.S. van Vuuren, Assessment of the Techno-economic Potential of Fischer-Tropsch Slurry Reactors, CSIR, South Africa, Report CENG 655 (1987).
24. M.E. Dry, *Catalysis Today*, **6**, 183 (1990).
25. F. Tungate, Private Communication.
26. S. Ledakowicz, H. Nettelhoff, R. Kokuun, and W.-D. Deckwer, *Ind. Eng. Chem. Process Dev.* **24**, 1043 (1985).
27. C.N. Satterfield, R.T. Hanlon, S.E. Tung, Z.-M. Zou, and G.C. Papaefthymiou, *Ind. Eng. Chem. Prod. Res. Dev.* **25**, 407 (1986).
28. I.C. Yates and C.N. Satterfield, *Ind. Eng. Chem. Research* **28**, 9 (1989).
29. G.A. Huff, Jr., and C.N. Satterfield, *Ind. Eng. Chem. Process Des. Dev.* **23**, 696 (1984).
30. G.A. Huff, Jr., C.N. Satterfield, and M.H. Wolf, *Ind. Eng. Chem. Fundam.* **22**, 258 (1983).
31. B. Wojciechowski, *Catal. Rev. - Sci. Eng.* **30**, 629 (1988).
32. T. Sakai and T. Kunugi, *Sekiyu Gakkai Shi*, **17**(10), 863 (1974).

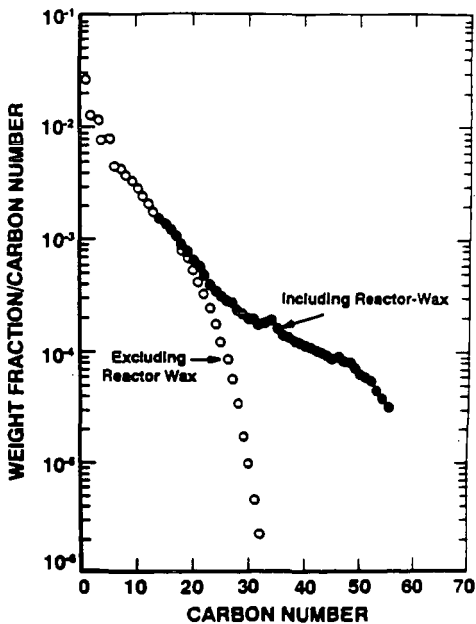


Figure 1. Schulz-Flory distribution for Fischer-Tropsch products from a slurry bubble column-reactor [4].

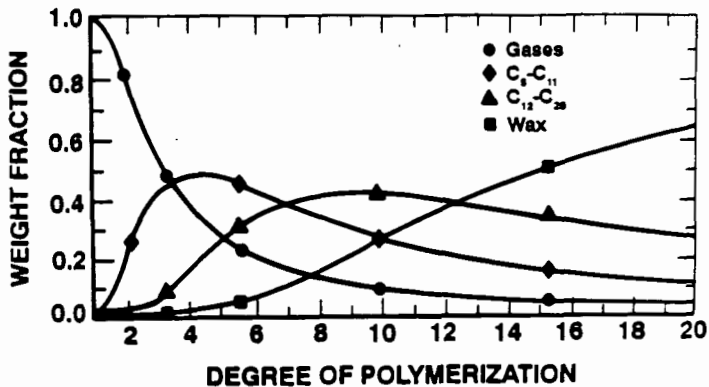


Figure 2. FT product distribution versus degree of polymerization [11].

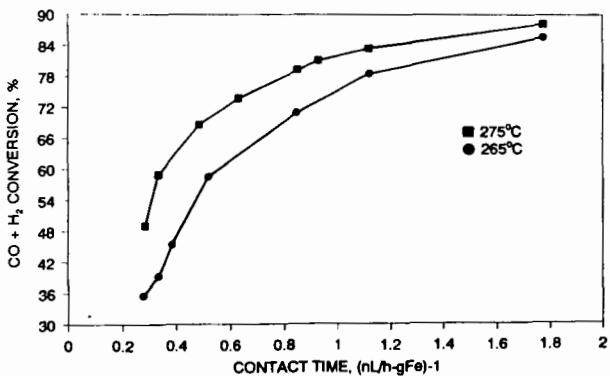


Figure 3. Conversion versus contact time for a precipitated iron catalyst [12] at 21 atm with feed H<sub>2</sub>/CO = 0.7.

HYDROGEN AND CARBON MONOXIDE TEMPERATURE PROGRAMMED DESORPTION  
STUDY OF Mn-Fe CATALYSTS

Y. Soong, V.U.S. Rao, M.F. Zaroachak, and R. J. Gormley  
Pittsburgh Energy Technology Center, U.S. Department of Energy,  
P.O. Box 10940, Pittsburgh, PA 15236

B. Zhang, Institute of Coal Chemistry, Academia Sinica,  
P.O. Box 165, Taiyuan, Shanxi, China

Keywords: manganese-iron, temperature-programmed desorption,

INTRODUCTION

Mn-Fe catalysts have been studied extensively during recent years, primarily because they can enhance the selectivity for low-molecular weight olefins in the Fischer-Tropsch (FT) synthesis (1-9). The reason for the increased selectivity towards light olefins on Mn-Fe catalysts remains controversial. A chemical and/or electronic promoter effect of Mn on the available iron surface has been proposed (4). The change in selectivity upon the addition of Mn to iron catalysts has also been attributed to a MnO species sitting on the Fe surface (1). Moreover, a surface spinel phase ( $\text{MnFe}_2\text{O}_4$ ) has been proposed to play an important role in providing high selectivity to light olefins (2,3,5,6). It is still an open question as to whether the spinel phase ( $\text{MnFe}_2\text{O}_4$ ) is responsible for the activity and selectivity during the FT synthesis.

In general, Mn-Fe catalysts were prepared by coprecipitation (or impregnation) of the corresponding nitrates. The degradation of a metal complex, a simple method employed in this study, has not been widely utilized. In this study,  $\text{MnFe}_2(\text{C}_2\text{O}_4)_3$  was decomposed to prepare the Mn-Fe catalysts. Some of the major advantages of this method are the following: (a) degradation of this complex can lead to the formation of various Mn-Fe oxides by calcination at different temperatures; and (b) pure Mn-Fe spinel can be prepared with the correct stoichiometric metal ratio,  $\text{Fe}/\text{Mn}=2$ .

Previous studies have reported that hydrogen adsorption on iron catalysts can be activated and dissociative, and carbon monoxide adsorption on iron catalysts includes both associative and dissociative adsorption (4,10,13,14). In an attempt to gain a better understanding of the role that the spinel phase ( $\text{MnFe}_2\text{O}_4$ ) plays in Mn-Fe catalysts, a TPD study of Mn-Fe catalysts was conducted.

EXPERIMENTAL

$\text{MnFe}_2(\text{C}_2\text{O}_4)_3$  was prepared as described by Wickhem (15). The catalyst precursor  $\text{MnFe}_2(\text{C}_2\text{O}_4)_3$  was calcined in air at different temperatures (1300, 1000, 700, and 500 °C) for 5 hours, followed by quenching in nitrogen.  $\text{Fe}_2\text{O}_3$  was prepared from the precursor  $\text{Fe}(\text{C}_2\text{O}_4)$  by calcining at 500 °C for 5 hours, followed by quenching

in nitrogen.

High purity argon, hydrogen, and carbon monoxide were used in this study. Gas flow rates of 30 ml/min were used for experiments conducted in this study. A temperature-programmed, catalyst characterization system (AMI-1) manufactured by Altamira Instruments, Inc., was used to obtain the TPD spectrum. A ramp of 15°C/min was used for all experiments in this study.

Catalyst samples were first exposed to a stream of argon gas at 120°C for one hour, then they were reduced in hydrogen at 350°C or 450°C for 12 hours. The catalyst was cooled under flowing hydrogen from the reduction temperature to ambient temperature, flushed in argon for one-half hour to remove the weakly held hydrogen, then heated to 650°C and held at 650°C for one-half hour. The TPD spectra obtained from this sequence are referred to as high temperature (HT) H<sub>2</sub>-TPD. After being purged with argon at 650°C for about one-half hour, the catalyst samples were then cooled to ambient temperature. The catalysts were exposed to adsorbate gas (H<sub>2</sub> or CO) at ambient temperature for one hour, followed by flushing in argon for one-half hour, and then heated in argon to 650°C and held for one-half hour. The TPD spectra obtained from this sequence are referred to as low temperature (LT) H<sub>2</sub> (or CO)-TPD.

## RESULTS AND DISCUSSION

The amount of hydrogen absorbed (or desorbed) was determined from the TPD spectra shown in Figs 1 to 3. The effects of varying calcination and reduction temperatures on hydrogen uptakes are presented in Table 1. For each catalyst, two hydrogen uptakes are measured. One is determined from the HT H<sub>2</sub>-TPD, and the other is calculated from the LT H<sub>2</sub>-TPD. Three to 50 times as much hydrogen uptake is obtained by comparing the HT H<sub>2</sub>-TPD to that of LT H<sub>2</sub>-TPD. Based on these two hydrogen uptakes at any reduction temperature, it is apparent that hydrogen adsorption is an activated process over Mn-Fe catalysts. These data are in agreement with previous studies that have shown hydrogen adsorption on iron catalysts can be highly activated (3,13). Noticeably, a high temperature of reduction significantly suppresses the amount of HT-H<sub>2</sub> uptake obtained from the MnFe1300 catalyst (Table 1). This result correlates well with our reaction data that there is a higher syngas conversion of 28% from the MnFe1300 catalyst with a lower reduction temperature, 350°C, versus that of 21% when the catalyst was reduced at 450°C (16). The lower uptakes of hydrogen obtained from higher reduction temperatures may be a result of catalyst sintering and/or MnO encapsulated with iron particles during the higher temperature of reduction. The MnO encapsulated with iron particles has been verified by our XPS observations (16).

XRD results obtained for each of the catalysts are also shown in Table 1. These results show that various phases can be formed by calcination at different temperatures, as anticipated. High calcination temperature (1300°C) favored the formation of a Mn-Fe

spinel before reduction. A mixture of spinel, manganese oxide, and iron oxide was observed when catalysts were calcined at 1000°C. Lower calcination temperatures (700 and 500°C) led to the formation of manganese oxide and iron oxides. Different reduction temperatures can also result in the formation of different phases. In general, two phases, MnO and Fe, were observed when catalysts were reduced at 450 and 350°C. However, the additional spinel phase ( $\text{MnFe}_2\text{O}_4$ ) formed when the catalysts were calcined at 1000 or 1300°C and reduced at 350°C. These results are consistent with previous studies on the effects of reduction temperature on spinel phases. Studies on the Mn-Fe catalysts, prepared by the coprecipitation method, indicated that reducing catalysts at a higher temperature than 375°C results in the complete decomposition of the spinel phase to MnO and metallic Fe phases. However, reduction at a lower temperature than 375°C results in a mixture of Fe, MnO, and mixed spinel phases (3,5-7,9). Fe was the only phase observed after the reduction of the Fe500 catalyst prepared using the oxalate precursor.

Figs 1 and 2 illustrate the effects of calcination and reduction temperature on HT  $\text{H}_2$ -TPD of Mn-Fe catalysts. Some general observations can be made by comparing the TPD spectra with the XRD results in Table 1. Two desorption peaks (90 to 120°C and 450 to 510°C) can be correlated with the Fe phase (Figs 1a, 2a). As indicated by XRD results, MnO and Fe phases were the only two phases present when catalysts were reduced at 450°C. By correlating TPD spectra in Figs 2b to 2e with XRD results, the MnO-related peaks can be assigned as those peaks with temperatures near 140 to 190°C and 570 to 630°C. These MnO-related peaks were also observed in Figs 1c and 1d. The XRD results also indicate that when catalysts are calcined at 1000 or 1300°C and reduced at 350°C, the spinel phase ( $\text{MnFe}_2\text{O}_4$ ) is present along with MnO and Fe phases. The shapes of the TPD spectra for these materials (Figs 1c and 1d) are significantly different from other spectra in Figs 1 and 2, in that they have an additional peak centered at 350°C. This additional peak, centered at 350°C, can be clearly correlated with the spinel phase ( $\text{MnFe}_2\text{O}_4$ ). The surface of the Mn-Fe catalyst is probably complex. However, through a systematic series of experiments, the Fe, MnO, and  $\text{MnFe}_2\text{O}_4$  related TPD spectra can be assigned. Fig. 3 shows the effects of calcination and reduction temperatures on LT  $\text{H}_2$ -TPD of Mn-Fe catalysts. Noticeably, the LT  $\text{H}_2$ -TPD spectra are much smaller than that in Figs 1 and 2. Combining the TPD spectra on Fig. 3 with the XRD information obtained in Table 1, the following conclusions were reached. The peak centered at 100°C is correlated with the Fe phase (Fig. 3). A broad desorption peak centered at 230°C may be correlated with the MnO phase (Figs 3a, 3b, and 3c). The spinel phase related peak (with peak temperature centered at 350°C in Figs 1c and 1d) was also observed in Figs 3-c and 3-d. Based on the information collected from Figs 1 to 3, the spinel phase does adsorb hydrogen and it is an activated process. Weatherbee et al. indicated that highly activated adsorption of hydrogen on reduced iron could lead to hydrogen-adsorption limiting kinetics and a hydrogen-poor surface resulting in the modification of the product distribution

during hydrogenation (13). Less adsorbed hydrogen that may be available for the hydrogenation on the Mn-Fe catalysts under reaction conditions thus could favor the formation of olefins. Moreover, an additional experiment was conducted to verify the hypothesis that the spinel phase does adsorb hydrogen. The pure spinel,  $MnFe_2O_4$ , was first heated to 650°C in argon to desorb any impurities that remained during the preparation. Then the catalyst was cooled to 280°C in argon, followed by exposure to hydrogen for 10 minutes at 280°C. It was cooled down to ambient temperature in hydrogen, then switched to argon. The TPD spectrum obtained from this experiment showed only one desorption peak, centered at 350°C, which was identified as the spinel phase related hydrogen desorption peak previously identified.

The LT CO-TPD spectra are shown in Fig. 4. It was found that all the desorption peaks consisted solely of carbon monoxide. Based on the observed peaks, two forms of desorbed CO could be distinguished; one type desorbed at a temperature of about 90 to 110°C and the other at about 590 to 630°C. Both desorption peaks can be correlated with the Fe phase. The lower temperature peak is probably related with the desorption of molecular CO, whereas the higher temperature peak might correlate with the recombination of surface carbon and surface oxygen. The two desorption peaks are consistent with previous studies (4,12). It is interesting to note that the relative ratio of the higher temperature peak versus the lower temperature peak is affected by the reduction temperature (Fig. 4b to 4d and 4e to 4c). A larger ratio is obtained from Fig. 4b and 4e, when the catalyst is reduced at 350°C, while a smaller ratio is observed from Fig. 4d and 4c, when the catalyst is reduced at 450°C. This difference in relative ratio correlates well with the reaction results (16). The CO conversion for the MnFe1300,350 catalyst (Fig. 4b) was 23%, while the conversion for the MnFe1300,450 catalyst (Fig. 4d) was 17%. These reaction results indicate that the lower reduction temperature catalyst has a higher CO conversion. The higher relative ratio of the two TPD peaks, obtained from the lower reduction temperature material (Fig. 4b) suggests that the CO dissociation is enhanced at lower reduction temperature. The peak around 230 to 250°C may be correlated with the MnO-related phase from Figs. 4c and 4d. No spinel phase related peak could be assigned in Fig. 4b and 4e. From the CO TPD spectra, it can be inferred that the spinel phase does not adsorb CO at room temperature. An additional experiment was also conducted to verify the hypothesis that the spinel phase does not adsorb CO. The pure spinel phase was first heated to 650°C in a stream of argon to remove any impurities. Then the catalyst was cooled to 280°C and the CO was introduced to the catalyst and held for 10 min followed by cooling to room temperature in CO. The flow was then switched to a stream of argon. The TPD spectrum obtained from this experiment showed no desorption of CO. An attempt was also made to verify whether or not the spinel phase alone is an active phase for syngas conversion. The  $MnFe_2O_4$ , which had been calcined at 1300°C for 5 hours from the spinel precursor, was exposed to synthesis gas at 280°C and 21 bar. In the absence of a reduction stage, it exhibited no activity during the 72-hour

testing period. The phase of the catalyst after calcination was shown to be a  $\text{MnFe}_2\text{O}_4$  spinel (Table 1). After exposing the catalyst to synthesis gas, the phase was still a  $\text{MnFe}_2\text{O}_4$  spinel, as determined by X-ray diffraction. These results suggest that the  $\text{MnFe}_2\text{O}_4$  spinel phase is not responsible for syngas conversion when it is present alone. It is speculated that the lower electron density on the catalyst surface is responsible for this effect. It is well known that the  $\text{MnFe}_2\text{O}_4$  spinel is a near normal spinel in structure.  $\text{Fe}^{+++}$  ions are distributed on both tetrahedral sites and octahedral sites in a 1:9 ratio.  $\text{Fe}^{+++}$  differs from  $\text{Fe}^0$  mainly in its lower electron density (11). Hence, electron back donation from the  $\text{Fe}^{+++}$  ions into the  $2\pi$  orbitals of CO is too weak to involve a metal-carbon bonding. A metal-carbon bonding is a prerequisite for syngas conversion, and therefore, no reaction takes place.

#### CONCLUSION

In the light of the TPD spectra, XRD results, and our reaction results, we have concluded that  $\text{MnFe}_2\text{O}_4$  may not be an active phase itself during FT synthesis, because it does not chemisorb CO. The  $\text{MnFe}_2\text{O}_4$  phase does chemisorb hydrogen in an activated process. The temperature of reduction determines the phases of the Mn-Fe catalyst. The hydrogen adsorption over the Mn-Fe catalysts is an activated process and at least three types of adsorption state may be assigned, namely Fe, MnO, and  $\text{MnFe}_2\text{O}_4$  related phases.

#### ACKNOWLEDGMENTS

The authors gratefully acknowledge the technical assistance by Mr. A.G. Blackwell and Mr. N.H. Haden.

#### REFERENCES

1. I.S.C. Hughes, J.O.H. Newman, Appl. Catal. 30,303,1987.
2. U. Lochner, M. Papp, M. Baerns, Appl. Catal. 23,339,1986.
3. J. Venter, M. Kaminsky, G.L. Geoffroy, and M.A. Vannice, J. Catal. 103,450,1987.
4. K.B. Jensen, and F.E. Massoth, J. Catal. 92,98,1985.
5. G.C. Maiti, R. Malessa, M. Baerns, Appl. Catal. 5,151,1983.
6. G.C. Maiti, R. Malessa, U. Lochner, H. Papp, M. Baerns, Appl. Catal. 16,215,1985.
7. J. Venter, M. Kaminsky, G.L. Geoffroy, M.A. Vannice, J. Catal. 105,155,1987.
8. K.M. Kreitman, M. Baerns, J.B. Butt., J. Catal. 105,319,1987.
9. R. Malessa, and M. Baerns, Ind. Eng. Chem. Res. 27,279,1988.
10. K.H. Huang, X.M. Zerg, J.T. Li, J. Catal. 81,259,1983.
11. H. Yoo and H. L. Tuller., J. Phys. Chem. Solid., 49,761,1988.
12. Y. Amenomiya, and G. Pleizier, J. Catal. 28,442,1973.
13. G.D. Weatherbee, J.L. Rankin, C.H. Bartholomew, Appl. Catal. 11,73,1984.
14. J.L. Rankin, C.H. Bartholomew, J. Catal. 100,533,1986.
15. D.G. Wickhem, "Inorganic Synthese"; Vol. 9,152,1967.
16. V.U.S. Rao, R.J. Gormley, S. Pollack, B. Zhong, in preparation

Table 1. Calcination and Reduction Temperature Effects on Catalyst Compositions and Hydrogen Uptakes.

Catalyst	Calcined Temp. °C	XRDC	Reduction Temp. °C	XRDC <sup>d</sup>	HT-H <sub>2</sub> <sup>a</sup> Uptake ml/g	LT-H <sub>2</sub> <sup>b</sup> Uptake ml/g
Fe500	500	Fe <sub>2</sub> O <sub>3</sub>	350	Fe	2.58	0.12
MnFe500	500	Fe <sub>3</sub> O <sub>4</sub> Mn <sub>2</sub> O <sub>3</sub>	350	MnO Fe	3.92	0.49
MnFe700	700	Mn <sub>2</sub> O <sub>3</sub>	350	MnO Fe	2.13	0.15
MnFe1000	1000	MnFe <sub>2</sub> O <sub>4</sub> Mn <sub>2</sub> O <sub>3</sub>	350	MnFe <sub>2</sub> O <sub>4</sub> MnO Fe	2.05	0.21
MnFe1300	1300	MnFe <sub>2</sub> O <sub>4</sub>	350	MnFe <sub>2</sub> O <sub>4</sub> MnO Fe	2.65	0.27
Fe500	500	Fe <sub>2</sub> O <sub>3</sub>	450	Fe	1.48	0.03
MnFe500	500	Fe <sub>3</sub> O <sub>4</sub> Mn <sub>2</sub> O <sub>3</sub>	450	MnO Fe	3.03	0.95
MnFe700	700	Mn <sub>2</sub> O <sub>3</sub>	450	MnO Fe	2.23	0.3
MnFe1000	1000	MnFe <sub>2</sub> O <sub>4</sub> Mn <sub>2</sub> O <sub>3</sub>	450	MnO Fe	2.48	0.11
MnFe1300	1300	MnFe <sub>2</sub> O <sub>4</sub>	450	MnO Fe	1.77	0.29

<sup>a</sup>Obtained after the temperature-activated adsorption from the stream of hydrogen at reduction temperature and cooling to ambient temperature in the stream of hydrogen (HT H<sub>2</sub>-TPD).

<sup>b</sup>Obtained after adsorption from the stream of hydrogen for one hour at ambient temperature (LT H<sub>2</sub>-TPD).

<sup>c</sup>Obtained after calcination.

<sup>d</sup>Obtained after the reduced samples were mixed with Dow Corning silicone grease in a glove box for preventing further oxidation.

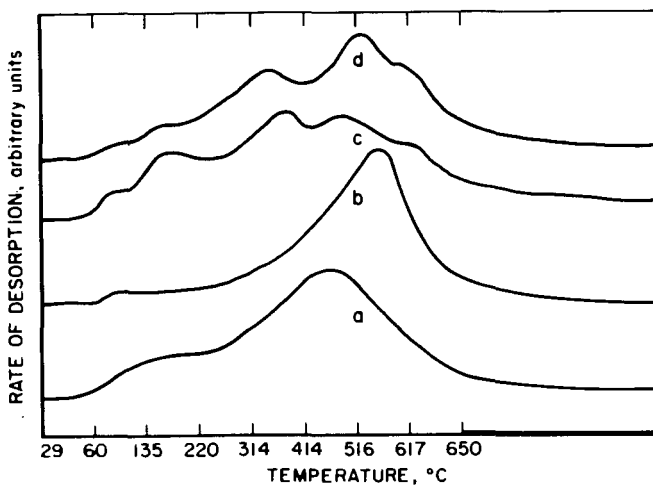


Fig. 1. Temperature-programmed desorption spectra of hydrogen (HT  $H_2$ -TPD) from catalysts as a function of calcination temperatures (catalysts were reduced at 350°C). (a)  $Fe_2O_3$  calcined 500°C; (b) MnFe500 calcined 500°C; (c) MnFe1000 calcined 1000°C; (d) MnFe1300 calcined 1300°C.

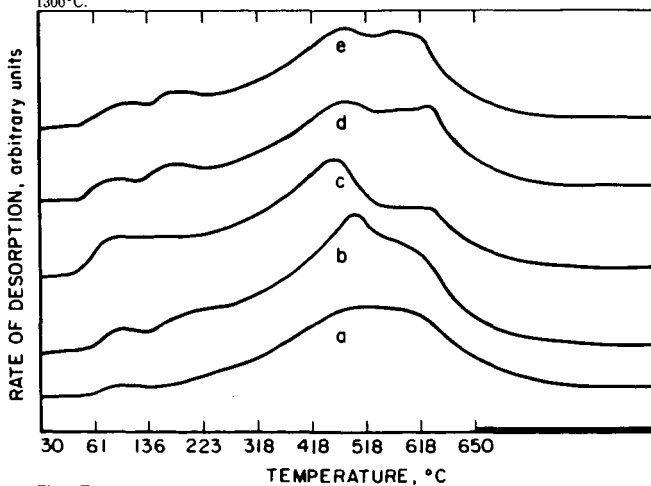


Fig. 2. Temperature-programmed desorption spectra of hydrogen (HT  $H_2$ -TPD) from catalysts as a function of calcination temperatures (catalysts were reduced at 450°C). (a)  $Fe_2O_3$  calcined 500°C; (b) MnFe500 calcined 500°C; (c) MnFe700 calcined 700°C; (d) MnFe1000 calcined 1000°C; (e) MnFe1300 calcined 1300°C.

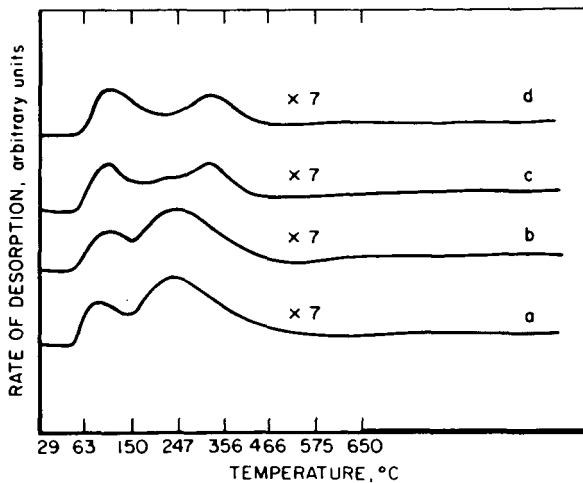


Fig. 3. Temperature-programmed desorption spectra of hydrogen (LT  $H_2$ -TPD) from catalysts as a function of calcination temperatures. (a) MnFe700 calcined 700°C, reduced 450°C; (b) MnFe1300 calcined 1300°C, reduced 450°C; (c) MnFe1000 calcined 1000°C, reduced 350°C; (d) MnFe1300 calcined 1300°C, reduced 350°C.

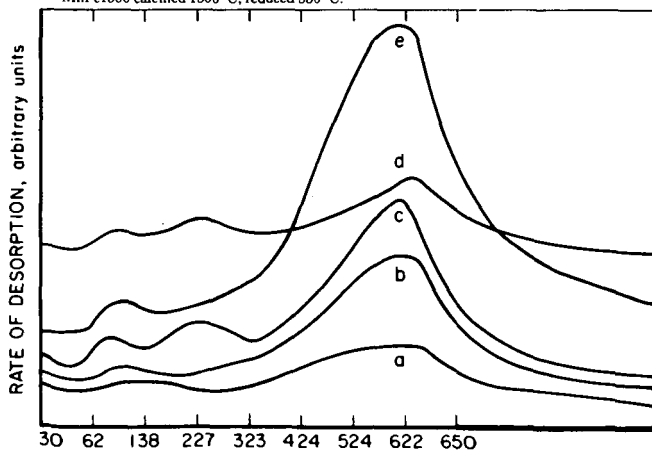


Fig. 4. Temperature-programmed desorption spectra of carbon monoxide (LT CO-TPD) from catalysts as a function of calcination temperatures and reduction temperatures. (a)  $Fe_2O_3$ , 350 calcined 500°C reduced 350°C; (b) MnFe1300, 350 calcined 1300°C reduced 350°C; (c) Mn-Fe1000, 450 calcined 1000°C reduced 450°C; (d) MnFe1300, 450 calcined 1300°C reduced 450°C; (e) MnFe1300, 350 calcined 1300°C reduced 350°C.

## RELATIONSHIPS OF COAL STRUCTURE TO MOLYBDENUM CATALYST ACTION IN LIQUEFACTION

Caroline E. Burgess, Levent Artok, and Harold H. Schobert  
Fuel Science Program  
The Pennsylvania State University  
University Park, PA 16802

Keywords: Molybdenum sulfide catalyst, low severity liquefaction, coal structure

### INTRODUCTION

Previous work in this laboratory has shown that the addition of ammonium tetrathiomolybdate catalyst precursor (ATTM) to coal at low severity conditions primarily increased the asphaltene yield from subbituminous coals, while for bituminous coals, ATTM primarily increased the oil yield [1]. For coals with higher crosslink density (lower rank coals), the catalyst promoted dissolution, while coals with lower crosslink density did not need catalyst to dissolve, and the catalyst instead mainly participated in the hydrogenation of asphaltenes to oils [1]. Our earlier work has now been extended to several additional coals to include liquefaction data with and without catalyst. This data will be compared with coal aromaticity data determined by  $^{13}\text{C}$  NMR and solvent swelling data in pyridine.

### EXPERIMENTAL

Two different catalyst precursors were used. Sulfided ammonium molybdate (SAM) was prepared, as described in several publications [1-6], by bubbling  $\text{H}_2\text{S}$  into a solution of ammonium heptamolybdate. Ammonium tetrathiomolybdate (ATTM) was purchased from Aldrich.

The coal was impregnated in the same manner as reported previously [1-8]. Coal was slurried with catalyst precursor solutions for 2 hours and dried to less than 1% moisture. Although several molybdenum sulfide precursors were used, previous data have shown that the predominant active catalyst species is  $\text{MoS}_2$  [1-8] and relative comparisons can be made about the effect of molybdenum catalysts on coal liquefaction. However, it should be recognized that the degree of dispersion of the precursors on coal could be different because two different catalyst precursors were used.

A total of eight coals was used. Data on the elemental composition of each coal are contained in Table 1. All reactions were carried out in 25 ml microautoclave (tubing bomb) reactors, and heating was accomplished in a temperature controlled fluidized sandbath. The catalyst loading was 1% expressed as weight of molybdenum (not of molybdenum compound) on a daf basis. The reactor was flushed three times with hydrogen, with the final addition pressurized to 6.9 MPa (cold). The reactor was vertically oscillated 2.5 cm at 200 cycles per minute. The coals PSOC-487, PSOC-831, PSOC-1379, and DECS-12 were reacted in a single stage reaction at 360°C for 1 h (PSOC-1488 for 350°C for 1 h). The solvent used was phenanthrene (naphthalene for PSOC-1488) at a 2/1 solvent-to-coal ratio, and the mass of the coal reacted was 2.5 g. The coal PSOC-1488 was reacted in a temperature-staged reaction (350°C for 1 h followed by 425°C for 10 min). A Texas lignite and a hvB bituminous coal used the following reaction conditions: phenanthrene solvent at a 1/1 solvent-to-coal ratio, with the coal mass 5 g, and the reaction was temperature-staged at 275°C for 30 min and 425°C for 30 min. The Çan (Turkish) coal was reacted in phenanthrene and dihydrophenanthrene (5 g of each of solvent and coal) in temperature-staged reactions of 275°C for 30 min and 425°C for 30 min.

For PSOC-1488, the cooled reactor was vented into a glass expansion bulb, and the contents were analyzed by gas chromatography using a Varian model 3700. The contents of the reactor were then rinsed with tetrahydrofuran (THF) into a dried Soxhlet thimble and extracted for about 12 h under nitrogen. The THF was removed by rotary evaporation. The solid residue was dried at 100°C

for 12 h before weighing. Conversion was calculated by subtracting the weight of the residue from the weight of the coal and dividing by the dmmf weight of the coal. Liquids were further separated into asphaltenes and oils by adding hexane to the THF-soluble portion. This mixture was refluxed for 12 h under nitrogen, followed by filtration into hexane-solubles and insolubles. The hexane was removed by rotary evaporation, and the samples were dried at 100°C for 1 h before weighing. The oil (hexane-soluble) yield was calculated by difference from the conversion percentages of the gas yield, THF solubles, and the THF insolubles.

For the rest of the coals, the work-up procedure was changed slightly. Gas percentages were not determined, so the calculated difference for the oils includes the gas yield as well. Gas yields vary only slightly, so any trend in oil plus gas really reflects changes in oil yield. Once the pressure was vented from the reactor, the contents of the tubing bomb were rinsed with hexane into a dried, weighed ceramic thimble and Soxhlet extracted for about 24 h under nitrogen. The hexane was removed from the extract by rotary evaporation. The hexane-insoluble residue was then Soxhlet extracted with toluene to separate asphaltenes from the residue. Toluene was removed from the extract by rotary evaporation. The toluene-insoluble residue was then Soxhlet extracted with THF to separate preasphaltenes from the residue. THF was removed from the extract by rotary evaporation. Preasphaltenes, asphaltenes, and residue were dried overnight under vacuum at 110°C. Conversion was calculated by subtracting the weight of the residue from the weight of the coal and dividing by the daf weight of the coal.

Solid state  $^{13}\text{C}$  NMR was performed using a Chemagnetics NMR Model M100S. The experiment was the standard CPMAS and pulsed Fourier transform (PFT) technique to collect the NMR spectrum. This technique was used for determination of  $f_a$  and to characterize the structure of each coal. The conditions used for this were: contact time, 1000  $\mu\text{s}$ ; acquisition count, 10,000; carbon frequency, 25 MHz; the time of the 90° pulse, 5.5  $\mu\text{s}$ ; and a pulse delay of 1 s. Table 2 contains  $f_a$  data.

Solvent swelling was performed according to the same procedure as Artok et al. [7] and Davis et al. [8]. About 1 g of coal (-60 mesh) was placed into a graduated centrifuge tube fitted with a screw cap. The coal was centrifuged for 30 min at 3000 rpm (room temperature), and the height of the coal ( $H_0$ ) was recorded. Pyridine (6-7ml) was added to the coal, and the sample was shaken to ensure that all the coal was wetted with the pyridine. The samples sat for ~24 h. The sample was again centrifuged for 30 min at 3000 rpm, and the new height of the coal ( $H_s$ ) was recorded. The solvent swelling index,  $Q$ , was calculated by  $H_s/H_0$ . Table 2 contains the results of this experiment.

## RESULTS AND DISCUSSION

It is important to mention that much of the data discussed in this paper were obtained as part of several different projects. Because each of the projects had somewhat different objectives, different reaction conditions were used to obtain the original data. Therefore it would be impossible to draw quantitative statistical conclusions. However, some useful qualitative comparisons can be discussed. Tables 2 and 3 contain the solvent swelling data, the aromaticity data, and the liquefaction data for all the coals. Table 2 contains single-stage data and Table 3 contains temperature-staged data. The first part of the discussion will focus on the low temperature single-stage data.

For the low temperature single-stage reactions, at every reaction condition, using molybdenum sulfide catalyst shows an increase in the total conversion, even at 275°C. The principal factor of concern in this paper is the change in the light fraction-to-heavy fraction ratio (L/H) compared to the coal rank, the solvent swelling index, and the aromaticity ( $f_a$ ). The L/H ratio is calculated by dividing the oil plus gas yield by the preasphaltene plus asphaltene yield. For all the subbituminous coals (PSOC-487, -1488, and DECS-1), the L/H ratio decreases when comparing the catalyzed reaction to the uncatalyzed reaction. It appears at low severity that the catalyst functions to depolymerize the coal, not to hydrotreat preasphaltenes and asphaltenes to oils and gas. For the bituminous coals (PSOC-831, PSOC-1379, DECS-6, and DECS-12), the L/H ratio increases when comparing the catalyzed reaction to the uncatalyzed reaction. It appears that the catalyst functions not only to depolymerize the coal, but also to hydrogenate asphaltenes to oils and gas. These data are

similar to data presented in the previous work [1]. It was shown by Burgess et al. [1] that earlier work by Weller and Pelipetz [9] and Garg and Givens [10] fits into this pattern.

There are some other comparisons that can be made for the liquefaction data at 350-360°C. The organic sulfur in the coals can be qualitatively classified as high ( $\geq 0.83\%$ ) or low; the crosslink density can be high ( $\sim 1.7$ ), medium ( $\sim 1.5$ ), or low ( $\sim 1.1$ ); organic oxygen can be high ( $\geq 15\%$ ) or low; and the solvent quality is high (phenanthrene) or low (naphthalene). For the uncatalyzed reactions, the two systems indicating the highest conversions - PSOC-831 and DECS-12 - share the following characteristics: high organic sulfur, a medium crosslink density, and low organic oxygen, while using a relatively good solvent during liquefaction. Organic sulfur is a point of macromolecular decomposition [11] and is important for liquefaction reactivity [12]. It seems odd that a coal with a medium crosslink density would be a better liquefying coal than one with a low crosslink density, but the coal with the medium crosslink density liquefies better than the coal with the high one (the fewer the crosslinks to cut, the easier the liquefaction). High organic oxygen can mean a high percentage of carboxyl groups, and it is thought that carboxyl groups play a role in preventing the hydrogenation of free radicals that can lead to retrogressive crosslinking during liquefaction [13].

For the single stage catalyzed reactions at 350-360°C, liquefaction reactions giving the highest conversions are PSOC-1379 and DECS-12. However, there is no apparent distinction for these coals based on coal properties (at least sulfur,  $f_a$ , oxygen, and Q). However, consider the comparison of PSOC-487 and -1379. These coals have comparable Q and oxygen. Note that the higher conversion is obtained with the higher sulfur coal, and furthermore, the higher sulfur coal gives a significant increase in oils. For PSOC-831 and DECS-12, both have comparable Q and oxygen, though lower Q and oxygen values than those of PSOC-487 and -1379. In this case, the coal with higher sulfur gives lower conversion. A possible explanation for these observations is that sulfur is not as important as a reactive site in the higher rank coals (Given found that sulfur was important for lignites [12]). When there is a lower oxygen content, there is less likelihood of retrogressive crosslinking at oxygen sites [13], and hence the intervention of  $H_2S$  (generated from hydrogenation of the sulfur compounds) is much less important. For the 487/1379 pair of coals, where sulfur is important, increased conversion comes largely from oils. In the 831/12 pair, where sulfur apparently has no effect, the increased conversion comes largely from asphaltenes and preasphaltenes. It is possible that  $H_2S$  facilitates conversion to oils [11, 12].

The discussion will now focus on temperature-staged reactions without catalyst. If PSOC-1488 and DECS-1 are compared, they both have similar oxygen contents, with DECS-1 giving much better liquefaction conversion. Notice the big increase in conversion is due to oils. The better conversion of DECS-1 is consistent with its relatively high organic sulfur content, although the effects of solvent quality and crosslink density must also be considered.

The reaction conditions of temperature-staging plus catalyst give comparable conversions for the three coals (not including the ultra-reactive high organic sulfur coal Çan). However, this is consistent with previous arguments [1], that if a sufficiently severe reaction condition is used (and in the context of the work discussed here catalytic temperature-staging is severe), then the severity of the reaction conditions simply overwhelms effects of coal structure and most coals can be driven to high conversions. The main difference in the reaction for the Çan coal is that the conversion in phenanthrene and catalyst is quite high (96.3% for total conversion and 62.0% for the oil + gas yield) and that the conversion in DHP without catalyst is quite high (93.8% for total conversion and 49.0% for the oil + gas yield). When reacting the Çan coal in DHP and catalyst, there isn't much otherwise reactive coal left to break apart, so the catalyst acts mainly in hydrogenating preasphaltenes and asphaltenes to oil and gas. It is also evident with the Çan coal that even without using catalyst or hydrogen donor solvent, the temperature-staged liquefaction conversion would be very good, hence the coal itself is quite reactive. The Çan coal is also very high in sulfur.

## CONCLUSIONS

For the single stage liquefaction experiments, using a catalyst with a subbituminous coal will likely be an asset to help depolymerize the coal, and using a catalyst with a bituminous coal will help

depolymerize the coal and hydrogenate asphaltenes to produce higher oil yields. For the temperature-staged data, there is no correlation for rank. There is no correlation for solvent swelling and aromaticity to the liquefaction data when comparing catalyzed experiments to uncatalyzed experiments. For the low rank coals, coals with higher sulfur content tend to have higher conversions, mainly in the oil fractions. For the bituminous coals, the effect of sulfur is minimal. Future work includes more extensive analysis of the structure of these coals as well some additional coals.

#### ACKNOWLEDGEMENTS

Various portions of this work have been supported by the U.S. Department of Energy, The Pennsylvania Research Corporation, and The Pennsylvania State University Mining and Mineral Resources Research Institute. The authors are pleased to acknowledge this support.

#### REFERENCES

1. Burgess, C.E., Artok, L., and Schobert, H.H. *Preprints for Div. Fuel Chem., American Chemical Society*, **36** (2), 462, 1991.
2. Epstein, M.J. M.S. Thesis, The Pennsylvania State University, 1987.
3. Derbyshire, F.J., Davis, A., Lin, R., Stansberry, P.G., and Terrer, M-T. *Fuel Proc. Tech.*, **12**, (7), 127, 1986.
4. Garcia, A.B. and Schobert, H.H. *Fuel*, **68**, 1613, 1989.
5. Burgess, C.E. and Schobert, H.H. *Preprints, Amer. Chem. Soc., Div. Fuel Chem*, **35**, (1), 31, 1990.
6. Burgess, C.E. and Schobert, H.H. *Fuel*, **70**, 372, 1991.
7. Artok, L., Schobert, H.H., Mitchell, G.D., and Davis, A. *Preprints for Div. Fuel Chem., American Chemical Society*, **36** (1), 36, 1991.
8. Davis, A., Schobert, H.H., Mitchell, G.D. and Artok, L. "Catalyst Dispersion and Activity Under Conditions of Temperature-Staged Liquefaction," DOE-PC-898-1-6, Progress Reports, 1989-1991.
9. Weller, S. and Pelipetz, M.G. *Ind. Eng. Chem.*, **43**, (5), 1243, 1951.
10. Garg, D. and Givens, E. *Preprints, Amer. Chem. Soc., Div. Fuel Chem*, **28**, (5), 200, 1983.
11. Garcia, A.B. and Schobert, H.H. In *Coal Science II* (Eds. H.H. Schobert, K.D. Bartle, and L.J. Lynch), American Chemical Society Symposium Series 461, 213, 1991.
12. Yarzab, R.F., Given, P.H., Spackman, W., and Davis, A. *Fuel*, **68**, 1613, 1980.
13. Solomon, P.R., Serio, M.A., Deshpande, G.V., Kroo, E., Schobert, H.H., and Burgess, C. In *Coal Science II* (Eds. H.H. Schobert, K.D. Bartle, and L.J. Lynch), American Chemical Society Symposium Series 461, 193, 1991.
14. Artok, L., Schobert, H.H., Davis, A., and Mitchell, G. Accepted for publication in *Fuel*, 1992.

Table 1: Data for Coal Samples.

Penn State Sample Bank No.	PSOC-487	PSOC-831	PSOC-1379	PSOC-1488	DECS-1	DECS-6	DECS-12	Çan
Scan	Bed # 53	Brazil Block	Colorado F	Deitz	Big Brown	Blind Canyon	Pitt #8	
State	Wyoming	Indiana	Colorado	Montana	Texas	Utah	Penn	
Country	USA	USA	USA	USA	USA	USA	USA	Turkey
ASTM Rank	Sub A	hvC b	hvC b	Sub B	Sub C	hvA b	hvA b	Sub A
Moisture (as received, w%)	11.55	13.02	11.99	23.66	30.00	4.70	2.40	20.20
Mineral Matter (dry, wt%)	6.89	4.16	5.09	6.05	7.62	6.67	11.88	8.80
<b>Elemental Composition</b>								
Carbon	75.91	83.28	76.74	76.57	75.90	81.72	84.75	77.00
Hydrogen	4.78	4.97	4.97	5.20	5.80	6.22	5.66	5.60
Nitrogen	1.21	1.61	1.69	0.95	1.50	1.56	1.39	2.00
Sulfur (organic)	0.42	0.94	0.63	0.51	1.10	0.40	0.83	3.30
Oxygen (by difference)	17.67	8.64	15.96	16.78	15.70	10.10	7.37	12.10
<b>Petrographic Composition</b>								
Virginite	89.60	79.20	92.20	88.60		69.10	83.00	n.d.*
Exinite	2.50	4.90	0.60	3.50		17.00	8.10	n.d.
Inertinite	7.90	15.90	7.20	7.90		13.60	8.90	n.d.

\* n.d. = not determined.

Table 2: Data for Solvent Swelling, Aromaticity, and Liquefaction Conversion for Single Stage Reactions.

Coal	Solvent Swelling Q (in pyridine)	f <sub>a</sub>	%O Org	%S Rank	Reaction Conditions	Tot Conv wt %	Oils + Gas wt %	Asph wt %	Preasph wt %	L/H <sup>a</sup>
PSOC-487	1.7	0.654	17.67	0.42	Sub A 360°C, phor <sup>b</sup> 360°C, phen, cat <sup>c</sup>	20.4 54.5	0.8 -4.8	7.3 18.6	12.2 40.8	0.04 -0.08
PSOC-831	1.5	0.658	8.64	0.94	hvC b 360°C, phen, cat	29.0 43.2	0.1 4.1	7.0 8.9	21.9 30.2	0.00 0.10
PSOC-1379	1.7	0.634	15.96	0.63	hvC b 360°C, phen, cat	18.1 65.8	3.5 16.2	5.4 19.7	9.3 29.9	0.24 0.32
DECS-12	1.5	0.633	7.37	0.83	hvA b 360°C, phen, cat	38.1 70.6	-0.2 8.1	23.2 18.0	15.3 44.5	-0.01 0.13
PSOC-1488	1.1	0.600	16.78	10.51	Sub B 350°C, naph <sup>d</sup> 350°C, naph, cat	18.3 47.8	11.2 14.0	7.1 33.9	1.58 0.40	
DECS-1 <sup>e</sup>	1.3	0.438	15.70	1.10	Sub C 275°C, phen, cat	6.6 9.0	1.6 1.5	2.2 3.6	2.8 3.9	0.32 0.20
DECS-6 <sup>e</sup>	2.0	0.598	10.10	0.40	hvA b 275°C, phen, cat	17.7 25.0	4.9 6.9	2.1 3.0	10.7 15.1	0.38 0.38

a L/H = Light-to-heavy ratio.

b phen = phenanthrene

c cat = catalyst

d naph = naphthalene

e Referenced data from [1], [7], [14].

Table 3: Data for Solvent Swelling, Aromaticity, and Liquefaction Conversion for Temperature-Staged Reactions.

Coal	Solvent Swelling Q (in pyridine)	$f_a$	%O	%S Org	Rank	Reaction Conditions	Tot Conv	Olis + Gas	Asph	Preasph	L/H <sup>a</sup>
PSOC-1488	1.1	0.600	16.78	0.51	Sub B	2-stg <sup>b</sup> , naph <sup>c</sup>	30.8	16.9	13.9		1.21
						78.5	21.7	57.7		0.38	
DECS-18	1.3	0.438	15.70	1.10	Sub C	2-stg, phen <sup>e</sup>	53.1	34.0	10.9	8.2	1.78
						78.9	49.0	19.3	10.6	1.63	
DECS-68	2.0	0.598	10.10	0.40	hvA b	2-stg, phen	48.0	27.2	8.5	12.3	1.31
						85.1	38.9	32.5	14.7	0.82	
Çan	1.7	12.10	3.30	Sub A	2-stg, phen, cat	96.3	62.0	27.8	6.5	1.81	
					2-stg, DHP <sup>f</sup>	93.8	49.0	27.8	16.9	1.10	
					2-stg, DHP, cat	98.4	74.1	22.6	1.7	3.05	

a L/H = Light-to-heavy ratio.

b 2-stg = temperature-stage, see text for temperatures and times

c naph = naphthalene

d cat= catalyst

e phen = phenanthrene

f DHP = dihydrophenanthrene

g Referenced data from [1], [7], [14].

## REACTANT AND CATALYST STRUCTURE/FUNCTION RELATIONSHIPS IN HYDROCRACKING OF BIPHENYL MOIETIES

Carole J. Read, Stephan Schwarz, and Michael T. Klein  
Center for Catalytic Science and Technology  
Department of Chemical Engineering, University of Delaware  
Newark, Delaware 19716

Keywords: hydrocracking, biphenyl, CoMo-Y-Zeolite

### 1.0 INTRODUCTION

Catalytic hydrocracking is a flexible refining process that can accommodate a wide range of feedstocks and generate a range of useful products. Part of this flexibility derives from the use of a bifunctional catalyst. A metal function allows for hydrogenation of polynuclear aromatics (PNA's) and dehydrogenation of alkanes to olefin intermediates. An acid function promotes isomerization and cracking. Acting in concert, these functions and the process conditions of temperature, hydrogen pressure, WHSV, etc., combine to lower the molecular weight and increase the H/C ratio of the feedstock.

Clearly the feedstock specifications also play a crucial role. For example, in PNA hydrocracking, the apparently subtle reactant structural feature of six versus five carbon-containing rings can lead to important process implications. The hydrocracking of PNA's containing exclusively six-carbon-membered rings, such as anthracene, phenanthrene and naphthalene, proceeds by the predominant patterns<sup>1-3</sup> of: terminal ring hydrogenation, followed by cyclohexyl ring isomerization, ring opening and dealkylation to yield a lower molecular weight aromatic product and light gases (e.g., C<sub>4</sub>). On the other hand, the reaction of the five-carbon-membered ring containing PNA fluoranthene (I) involves hydrogenation to tetrahydrofluoranthrene, center ring opening to 5-phenyl tetralin, and biphenyl bond cleavage to tetralin and benzene, as shown in Equation 1.<sup>4</sup>

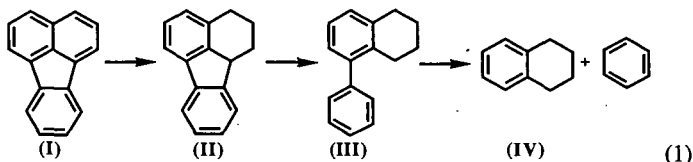


Table 1 summarizes important hydrocracking pathways of fluoranthene<sup>4</sup>, 9-ethyl fluorene, 9-phenyl anthracene, and 2-phenyl naphthalene deduced from reactions with H<sub>2</sub> and an industrial equilibrated NiMo/USY-Zeolite catalyst. These model compounds all generate structures that can undergo the direct biphenyl cleavage. Inspection of Table 1 reveals the minimum structural moiety for direct biphenyl cleavage. Fluoranthene, 2-phenyl naphthalene, and 9-phenyl anthracene, all fully aromatic, require hydrogenation and cracking steps before they have the structure capable of direct biphenyl cleavage which occurs from rows III to IV in Table 1. In contrast, 9-ethyl fluorene has aliphatic character and as a result requires fewer transformations before forming 2-propyl biphenyl, which can be directly cleaved.

It is also instructive to consider the reactions of related compounds that did not follow the efficient bond cleavage pathway. Fluorene, for example, ring opens to 1-phenyl toluene, which contains a benzylic hydride but not the additional  $\beta$  saturated carbon whose deprotonation to an olefin would allow hydrogenation to afford the final alkyl-substituted product<sup>5</sup>. 2-Methyl biphenyl likewise suffers from the same structural deficiency, and undergoes only isomerization reactions. Biphenyl does not directly cleave to form two moles of benzene per mole of biphenyl reacted; rather, it is postulated that cracking occurs via cyclohexyl benzene. Thus the *minimum structure necessary for efficient cleavage* is proposed to be a biphenyl moiety with an alkyl group,

comprising at least two carbons, bonded ortho to the biphenyl bond.

Additional experiments with the NiMo/USY-Z industrial catalyst and 9-ethyl fluorene revealed kinetically significant reactions: cleavage of the center fused cyclopentyl ring, transalkylation, and condensation reactions to form 9-methyl phenanthrene. Comparison of the 5-phenyl tetralin and 2-propyl biphenyl intermediates observed from reaction of fluoranthene and 9-ethyl fluorene, respectively, highlights the causes of these new pathways. The formal [1,5] shift is the only significant pathway for 5-phenyl tetralin. In contrast, the n-propyl group can participate in ring closure and transalkylation. Thus somewhat subtle changes in reactant structure can engender a wide range of available pathways. It is reasonable to expect similar sensitivity with regard to catalyst structure.

The reactions noted above comprise several key molecular transitions: hydrogenation, the net [1,5] biphenyl cleavage, center ring opening of cyclopentyl ring, isomerization, transalkylation, and ring closure. Each of these is influenced by the catalyst properties to a different degree. Herein, we report the preliminary work aimed to determine the catalyst function that influences the kinetics of each.

As a first step, the acidity of the catalyst was probed by varying the sodium content of the zeolite-Y support. The procedure used followed the early work of Ward<sup>6-9</sup> and Hansford and Ward<sup>10,11</sup>. These workers concluded that the concentration of Bronsted acid sites increases linearly with decreasing sodium content of the zeolite until 60-70% of the sodium ions have been replaced. They also found that o-xylene isomerization activity increased with decreasing sodium content. The activity per site also increased with decreasing sodium content.

The foregoing suggests that hydrocracking reactivity can be viewed as a rate functional,<sup>12</sup> which combines structure/function relations  $f(S)$  for both the catalyst ( $S_C$ ) and reactant ( $S_R$ ). Observed reactivity  $R$  is thus a function of both  $f(S_C)$  and  $f(S_R)$ , as in Equation (2).

$$R = R \{ f(S_C), f(S_R) \} \quad (2)$$

The objective of this paper is to report the results of hydrocracking experiments with a standard commercial catalyst and a range of reactant molecules, as a probe of  $f(S_R)$ , and also experiments involving a probe reactant (9-ethyl fluorene) and a range of carefully prepared catalytic materials that mimic aspects of the industrial catalyst. The goal is to lay a foundation for unraveling more quantitative aspects of  $R$ .

## 2.0 EXPERIMENTAL PROCEDURES

### 2.1 Material Synthesis

The catalysts prepared for the present work were designed as follows: both commercial (Strem Na-Y zeolite) and synthesized zeolite were used. Sodium zeolite Y was synthesized following an early patent by Breck<sup>13</sup>. Zeolite-Y was synthesized from an aged gel and then washed and filtered. The samples were dried overnight at 110°C and then calcined under a flow of air. The calcination program was heating at 350°C for three hours and then calcining at 500°C for four hours.

A series of acid supports was made by ion exchanging either commercial or synthesized zeolite-Y with ammonium nitrate solutions. The hydrogenation activity was provided by sulfided CoMo. The metal loading and introduction methods are as reported by Cid and co-workers<sup>14-16</sup>. The metal function was varied through the use incipient wetness impregnation, ion exchange/impregnation, and rotary vacuum impregnation.

### 2.1 Zeolite Characterization by XRD and TEM

X-Ray powder diffraction (XRD) of the zeolite samples was accomplished using a Philips XRG 3000 x-ray generator coupled to an APD 3520 controller. The radiation employed was CuK $\alpha$  with a wavelength of 1.540562 Å. All samples were scanned from 6° to 60° 2 $\theta$ . The peak heights above the background of the 5

largest peaks of calcined NaY were used to compute % crystallinity according to:

$$\% \text{ Crystallinity} = \frac{(\sum \text{hts. of 5 peaks})_{\text{sample}}}{(\sum \text{hts. of 5 peaks})_{\text{standard}}} \times 100$$

Metal oxide and metal sulfide species in the catalyst samples were identified using Table 2 which lists the characteristic peaks for each of the non-zeolitic phases.

Transmission electron microscopy (TEM) of the samples was accomplished using a Philips EM 400 transmission electron microscope. The sample was prepared for microscopy by dispersing some of the zeolite in n-hexane, transferring a drop of the suspension onto a copper grid and allowing the solvent to evaporate. The average crystal size of the parent zeolite,  $n$ , was obtained from micrographs by counting and measuring ~ 200 crystals. Note that  $n = \sum(d_i n_i) / \sum n_i$  where  $d_i$  is the diameter of the  $i$ th particle and  $n_i$  is the number of crystals of diameter  $i$ .

## 2.2 Catalytic Hydrocracking Reactions

The hydrocracking pathways and kinetics of 9-ethyl fluorene, 9-phenyl anthracene and 2-phenyl naphthalene in the presence of an equilibrated NiMo/Z-USY were studied at 310-380°C and 153 atm hydrogen. Experimental methods are detailed elsewhere <sup>4,17</sup>. In brief, hydrocracking experiments were conducted in a batch autoclave or in batch agitated tubing bombs. Experiments conducted in the stirred batch autoclave were in the presence of hexadecane solvent, whereas reactions in the tubing bombs were without.

Additionally, the hydrocracking of 9-ethyl fluorene, 1-phenyl naphthalene, biphenyl, and naphthalene in the presence of the synthesized catalytic materials were studied at 325°C and 153 atm. hydrogen pressure. These experiments were conducted in 12-cm<sup>3</sup> SS agitated tubing bombs in the absence of solvent.

For all types of experiments, the catalyst was ground to 80-100 mesh. It was then sulfided with 90% H<sub>2</sub>/10% H<sub>2</sub>S at flow rate of 30 cm<sup>3</sup>/min for 2 hours at 400°C. Gas chromatography and gas chromatography/mass spectrometry were used to identify liquid-phase reaction products.

## 3.0 RESULTS AND DISCUSSION

### 3.1 Zeolite Characterization

XRD analyses showed that CoMoO<sub>4</sub> was found in all samples whether the cobalt be introduced by impregnation or ion exchange. Co(imp)Mo(imp)NaY also showed evidence of Co<sub>3</sub>O<sub>4</sub>, but after exchange with NH<sub>4</sub><sup>+</sup> and subsequent calcination, this oxide could no longer be detected. MoO<sub>3</sub> could not be unambiguously assigned to any of the samples, except for Co(imp)Mo(imp)NaY, since its two strongest lines very nearly coincide with NaY lines <sup>15</sup>. The sulfided Co(ex)Mo(imp)NaY did not contain x-ray crystalline Co<sub>9</sub>S<sub>8</sub> or MoS<sub>2</sub>. Note, however, that since the detection limit of XRD is ~ 2nm, the above results do not necessarily imply that the oxide and sulfide species mentioned were absent.

Table 3 lists the crystallinities of the calcined materials. Clearly impregnation decreased crystallinity. This has also been reported by Cid et al. <sup>14,15</sup> who observed crystallinities < 40% for high Mo loadings (9% and above). The loss of crystallinity upon impregnation was ascribed to the partial destruction and distortion of the zeolite lattice by the interaction of molybdate anions with framework oxygen. It was noteworthy that impregnation by the rotary evaporation technique yielded slightly more crystalline materials than the incipient wetness technique. When Co was incorporated into the zeolite by aqueous ion exchange prior to Mo impregnation, the reduction in crystallinity was far less pronounced.

The results from the TEM showed an average crystal size of 0.7 μm, with a size range of 0.2 - 1.1 μm.

### 3.2 Reactant and Catalyst Structure/Function

Preliminary reactions are reported with the following materials: a CoMo impregnated Sirem sodium zeolite-Y (Co(I)Mo(I)/Na-Y), Co ion exchanged Mo impregnated Sirem sodium zeolite-Y (Co(ex)Mo(I)/Na-Y), and a CoMo impregnated onto a twice ammonium exchanged, calcined Sirem sodium zeolite-Y (Co(I)Mo(I)/Sirem 2X ex NaH-Y). All impregnations used the incipient wetness technique. Reactions with biphenyl, naphthalene, 9-ethyl fluorene, and 1-phenyl naphthalene reactants revealed broad trends. Under the reaction conditions of 325°C, 150 atm hydrogen, the main reaction product yield and selectivities are summarized in Table 4.

The first catalyst used was the Co(I)Mo(I)/Na-Y. Naphthalene, 1-phenyl naphthalene, 9-ethyl fluorene, and biphenyl were separately contacted. For naphthalene and 1-phenyl naphthalene, the main reaction was hydrogenation. Naphthalene hydrogenated to tetralin; no decalins were observed. The selectivity to tetralin formation was 54% after 30 minutes reaction time. The naphthalene moiety of 1-phenyl naphthalene was preferentially hydrogenated as the main product was 1-phenyl-1,2,3,4-tetrahydronaphthalene. The hydrogenation kinetics of naphthalene and 1-phenyl naphthalene were of the same order of magnitude. Biphenyl and 9-ethyl fluorene did not react over this catalyst.

The second catalyst examined was a Co(ex)Mo(I)/Sirem Na-Y. Naphthalene, 1-phenyl naphthalene, 9-ethyl fluorene, and biphenyl were individually reacted.

Naphthalene hydrogenated to tetralin with the cobalt exchanged catalyst; some transalkylation reactions occurred to form methyl naphthalenes. The selectivities for tetralin, 2-methyl naphthalene, and 1-methyl naphthalene were 59, 7.4, and 4.2%, respectively, after 25 minutes reaction time. The kinetics of hydrogenation were of the same order of magnitude as with the previous catalyst sample.

1-Phenyl naphthalene preferentially reacted to form 2-phenyl naphthalene (selectivity of 69%, 30 minutes). All four hydrogenation products of 1-phenyl and 2-phenyl naphthalene also formed. The temporal variation of products' yields showed that 1-phenyl and 2-phenyl-1,2,3,4 tetrahydronaphthalenes cleaved to form tetralin and benzene.

Biphenyl underwent predominantly transalkylation reactions to form methyl biphenyls and fluorene with the Co(ex)Mo(I)/Na-Y catalyst. No single ring cleavage products were observed.

Finally, 9-ethyl fluorene was exposed to the Co(ex)Mo(I)/Na-Y catalyst. The center cyclopentyl ring cleaved to form 2-propyl biphenyl (selectivity of 0.75%). No single ring aromatics or naphthenics were observed in the product spectrum. The intermediate 2-propyl biphenyl did undergo ring closure to form 9-methyl-9,10-dihydrophenanthrene and, ultimately, 9-methyl phenanthrene (selectivity of 1.8, 3.8%, respectively, 32 minutes). Transalkylation reactions were dominant, forming methyl, ethyl-fluorenes with a selectivity of 45%, 32 minutes.

The third catalyst was a Co(I)Mo(I)/2x(ex) NaH-Y. The reaction of 9-ethyl fluorene led to center ring cleavage and transalkylation as the predominant reactions. The selectivity to 2-propyl biphenyl was 2.6% (40 minutes). The selectivity for the transalkylation products was 11% after 40 minutes.

#### Acknowledgement:

We gratefully acknowledge the support of this work by Sun Refining and Marketing Company. Additional acknowledgements are to Mr. Ralph Bertolacini and Dr. Simon Kukes of Amoco Oil and Dr. James Lyons and Mr. Aris Macris of Sun Refining and Marketing Company.

#### References:

- (1) Lemberton, J.; Guisnet, M. *Applied Catalysis* **1984**, *13*, 181-192.
- (2) Martens, J. A.; Jacobs, P. A.; Weitcamp, J. *Appl. Catal.* **1986**, *20*, 283 - 303.

- (3) Haynes, H. W. J.; Parcher, J. F.; Helmer, N. E. *Ind. Eng. Chem. Proc. Des. Dev.* **1983**, *22*, 401 - 409.
- (4) Lapinas, A. T.; Klein, M. T.; Gates, B. C.; Macris, A.; Lyons, J. E. *Ind. Eng. Chem. Res.* **1987**, *26*, 1026 - 1033.
- (5) Lapinas, A. T.; Klein, M. T.; Gates, B. C.; Macris, A.; Lyons, J. E. *Ind. Eng. Chem. Res.* **1991**, *30*, 42 - 50.
- (6) Ward, J. W. *Journal of Catalysis* **1967**, *9*, 225-236.
- (7) Ward, J. W. *Journal of Catalysis* **1967**, *9*, 396-402.
- (8) Ward, J. W. *Journal of Catalysis* **1968**, *10*, 34-46.
- (9) Ward, J. W. *Journal of Catalysis* **1968**, *11*, 251-258.
- (10) Ward, J. W. and Hansford, R. C. *Journal of Catalysis* **1969**, *13*, 316-320.
- (11) Ward, J. W. and Hansford, R. C. *Journal of Catalysis* **1969**, *13*, 364-372.
- (12) Astarita, G. *Thermodynamics: An Advanced Textbook for Chemical Engineers*; Plenum Press: New York, 1989, pp pp.93-96.
- (13) Breck, D. W. In *Crystalline Zeolite Y*; 1964; U. S. Patent No. 3,130,007
- (14) Cid, R.; F. Orellana *Applied Catalysis* **1987**, *32*, 327-336.
- (15) Cid, R., F. J. Gil Lambias, J. L. G. Fierro, A. L. Agudo and J. Villaseñor *Journal of Catalysis* **1984**, *89*, 478-488.
- (16) Cid, R., J. Villaseñor, F. Orellana, J. L. G. Fierro, and A. L. Agudo *Applied Catalysis* **1985**, *18*, 357-372.
- (17) Lapinas, A. T. PhD Thesis, University of Delaware, 1989.

Table 1. Chemical Motives Susceptible to Efficient Biphenyl Cleavage

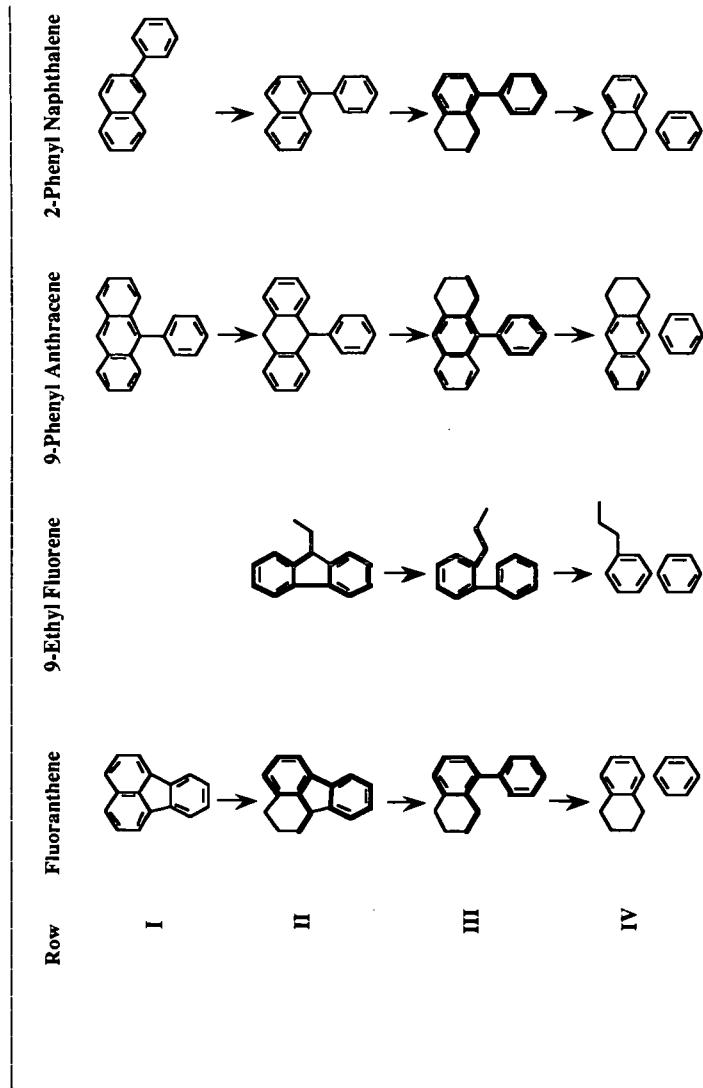


**Table 2: Identification of non-zeolitic phases**

Species	Largest peak (2 $\theta$ )	2nd largest peak (2 $\theta$ )
Co <sub>3</sub> O <sub>4</sub>	36.8°	31.3° (*)
MoO <sub>3</sub>	27.3° (*)	23.3° (*)
CoMoO <sub>4</sub>	26.5°	23.3° (*)
Co <sub>9</sub> S <sub>8</sub>	52.0°	29.9° (*)
MoS <sub>2</sub>	14.4°	39.5° (*)

(\*) : partial overlap with NaY peaks

**Table 3: XRD Crystallinities of metal-zeolite Y materials**

Catalyst	% Crystallinity
NaY	100
NaHY(2x exch.)	100
Co(imp)Mo(imp)NaY	25
Co(imp)Mo(imp)NaHY(2x exch.)	30
Co(imp)Mo(imp) rot. vap. NaY	45
Co(imp)Mo(imp) rot. vap. NaHY (1x exch.)	40
Co(ex)Mo(imp)NaY	90
Co(ex)Mo(imp)NaY, sulfided	70

Note: rot. vap. = impregnation by rotary evaporation. Other samples impregnated by incipient wetness

Table 4. Hydrocracking reaction selectivities for naphthalene, 1-phenyl naphthalene, 9-ethyl fluorene, and biphenyl

Reactant:	Naph	1-PN	Naph	1-PN	9-et $\Pi$	biphenyl	9-et $\Pi$
catalyst:	1	1	2	2	2	2	3
T, °C	325	325	325	325	325	325	325
P/atm (at T)	150	150	150	150	150	150	150
t, min	30	21	25	30	32	25	40
conversion of reactant	0.057	0.065	0.634	0.877	0.111	0.035	0.075
<b>Product Selectivities</b>							
benzene				6.71E-02		3.55E-02	
cyclohexyl benzene						2.84E-02	
methyl indans			3.11E-03				
tetralin	5.42E-01	2.79E-02	5.90E-01	7.14E-02			
naphthalene		1.89E-02		8.69E-03			
methyl tetralins			2.82E-02	1.16E-03			
2me naphthalene	1.60E-02		7.39E-02	6.01E-04			
1me naphthalene	5.46E-02		4.18E-02	5.04E-04			
2-methyl biphenyl						3.70E-02	
3-methyl biphenyl						1.35E-01	
4-methyl biphenyl						4.15E-01	
hexahydro fluorenes					2.46E-02		1.37E-01
2propyl biphenyl					7.54E-03		2.59E-02
mw 168's					1.21E-01		1.38E-01
hexahydro-9et-fluorenes					3.54E-02		1.89E-01
fluorene, 38.09					5.94E-03	1.20E-01	6.52E-02
9-me dihydro phenanthrene					1.78E-02		
methyl 9-et fluorenes					4.54E-01		1.10E-01
ethyl 9et fluorene, 53.18					4.50E-02		6.75E-02
9-me phenanthrene, 60.4					3.75E-02		5.99E-03
1-phenyl tetralin		3.51E-01		1.04E-02			
5-phenyl tetralin		9.74E-02		6.97E-03			
2-phenyl naphthalene				6.90E-01			
phenyl tetralins				1.88E-01			
methyl phenyl naphthalenes				1.02E-02			
1 = Co(I)Mo(I)/Na-Y							
2 = Co(E)Mo(I)/Na-Y							
3 = Co(I)Mo(I)2XNaH-Y							

## EFFECTS OF PORE STRUCTURE AND SUPPORT TYPE OF CATALYSTS IN HYDROPROCESSING OF HEAVY COAL LIQUIDS

**Chunshan SONG\*, Kouji HANAOKA<sup>+</sup> and Masakatsu NOMURA<sup>+</sup>**

\* Fuel Science Program, Department of Materials Science and Engineering, 209 Academic Project Building, The Pennsylvania State University, University Park, PA 16802, USA

<sup>+</sup> Department of Applied Chemistry, Faculty of Engineering, Osaka University Yamada-oka 2-1, Suita, Osaka 565, Japan

**Keywords:** Catalyst; Pore size; Support type; Coal liquids upgrading

### INTRODUCTION

Catalyst pore structure determines how easily the reactants can access the interior surface of the catalyst. The pore structure parameters include pore sizes and their distribution, pore volume and surface area. Various classification of pore sizes can be found in literature, but the International Union of Pure and Applied Chemistry (IUPAC) classifies pores of different sizes in the following manner: micropores, < 20 Å; mesopores, 20-500 Å; and macropores, > 500 Å in diameter. The IUPAC classification will be used in this paper. In general, hydrotreating catalysts are prepared by impregnation methods and the catalyst pore structure is determined mainly by the support. Earlier reports by Ho and Weller [1981], Bertolacini et al. [1978], and Shimada et al. [1984] have shown that pore diffusional limitation of reaction rates can be serious in hydroliquefaction of coals over supported catalysts. The catalyst pore structure is also very important for hydroprocessing of heavy coal liquids due to diffusional limitations [Tischer et al., 1985; Yoshimura et al., 1986; Song et al., 1988a, 1989a, 1991a]. However, systematic knowledge of pore size effects is still very limited for hydroprocessing of heavy coal-derived liquids. Reviews of previous work in this area may be found elsewhere [Derbyshire, 1988; Onuma, 1988; Song et al., 1991b].

The present work involves the upgrading of several solvent refined coals (SRC) derived from thermal liquefaction of coals, which contain both asphaltene and preasphaltene. This work attempts to provide a better understanding of the relationship of catalyst pore structure and support type to the conversion of asphaltene and preasphaltene, which in turn could lead to the development of more effective catalyst. This paper will describe 1) the effects of pore size of Ni-Mo/Al<sub>2</sub>O<sub>3</sub> catalysts on their performance in hydroprocessing of two different SRCs in terms of oil yields and conversions of heavy fractions, and the interactive chemistry involved in the pore-size dependence for simultaneous conversion of asphaltene and preasphaltene on catalyst surface, 2) the differences in reactivity of heavy fractions in several SRCs and their convertibility in catalytic runs, and 3) comparative examination of alumina- and silica-supported catalysts as well as carbon-coated catalysts.

### EXPERIMENTAL

**Catalyst Preparation.** The four gamma-Al<sub>2</sub>O<sub>3</sub> cylindrical extrudates are the same supports that have been in a previous work [Song, 1991a]. The SiO<sub>2</sub> supports were two spherical Cariact-50 and Cariact-10 beads from Fuji-Davison Chemical Company. Table 1 gives their properties provided by the manufacturers. Four Ni-Mo/Al<sub>2</sub>O<sub>3</sub> catalysts (NiO: 2.9, MoO<sub>3</sub>: 15.8 wt%) were prepared by co-impregnation of (NH<sub>4</sub>)<sub>6</sub>Mo<sub>7</sub>O<sub>24</sub>·4H<sub>2</sub>O and Ni(NO<sub>3</sub>)<sub>2</sub>·6H<sub>2</sub>O from their aqueous solution, followed by calcination and sulfidation [Song et al., 1991a, 1991b]. Two Mo/SiO<sub>2</sub> catalysts containing 15.8 wt% MoO<sub>3</sub> (Cat-SA, Cat-SB) were prepared by using the same procedure. Figure 1 shows the pore size distribution of the prepared Ni-Mo/Al<sub>2</sub>O<sub>3</sub> catalysts measured by using a Shimadzu AutoPore-9200 mercury porosimeter. The maximum intrusion pressure was 60,000 psi, which corresponds to pore radius of 18 Å as dictated by Washburn equation with contact angle and surface tension of mercury taken as 140° and 480 dyn/cm, respectively. A commercial catalyst, Akzo Ketjenfine 153S sulfided Ni-Mo/Al<sub>2</sub>O<sub>3</sub> [Song et al., 1988, 1991c] was also used in some experiments.

**SRC Upgrading.** Solvent refined coals (Table 2) derived from Wandoan subbituminous coal (Wan-SRC) and Akabira bituminous coal (Aka-SRC) were used as feedstocks. Aka-SRC was produced from Run 5511 at 420 °C for 34 minutes, and Wan-SRC from Run 5512 at 440 °C for 34 minutes in a 3 ton/day coal liquefaction plant at Sumitomo Coal Mining Co. [Hanaoka et al., 1988]. In some experiments we also used a SCT-SRC sample produced from short contact time pyrolytic liquefaction (SCT-PL) of Wandoan coal at 440-465 °C for 5 minutes in H-donor solvent under N<sub>2</sub> atmosphere [Song et al., 1989b]. The hydroprocessing was carried out in a 60 ml SUS-316 stainless steel rocking

autoclave at 425 °C for 1 h with 4.9 MPa H<sub>2</sub> (5 g SRC : 0.5 g catalyst : 5 g tetralin). The runs of SCT-SRC were carried out under the same conditions, but using 2.5 g SRC, 5 g tetralin, and 1 g catalyst.

**Product Separation and Analysis** The volume of gaseous products was measured by a continuous flow-type gas volume meter, through which the gases were introduced from the reactor into a plastic gas bag. The gases were analyzed by GC (Shimadzu GC-8A). The liquid and solid products were separated into oil (hexane soluble), asphaltene (hexane-insoluble but benzene-soluble) and BI or preasphaltene (benzene-insoluble). The concentrated oil plus the reaction solvent were analyzed by GC to determine the tetralin/naphthalene ratio. After the solvent has been removed by vacuum distillation (up to 115°C, 8 mmHg), the oil products were subjected to elemental and <sup>1</sup>H NMR analyses [Song et al., 1988c]. The catalysts that have been used once in SRC hydroprocessing were also analyzed (after benzene extraction and drying) by using scanning electron micrograph (SEM, Hitachi S-450) combined with electron probe microanalysis (EPMA, Horiba EMAX-1800E).

## RESULTS AND DISCUSSION

**Property and Reactivity of SRC.** As shown in Table 2, Wan-SRC and Aka-SRC have similar carbon and hydrogen contents, although Wandoan and Akabira coals differ significantly in elemental composition. Both SRCs contain a high proportion of heavy fractions such as asphaltene and preasphaltene. Wan-SRC contains less benzene-insolubles and more asphaltene and oil, as compared to Aka-SRC. Analysis of the fractions from both SRCs showed that the H content and atomic H/C ratio decrease, but N and O contents and the average molecular weights (MW) increase in the order of oil, asphaltene, and BI. The average MW values determined by vapor pressure osmometry are about 590-600 and 270-320 for asphaltene and oil fractions, respectively [Song et al., 1988a]. In addition, relative to the SRCs from long residence time runs in pilot plant, the SCT-SRC from laboratory SCT-PL has higher oil content and H/C ratio, and lower preasphaltene content.

Table 3 gives the data on the thermal runs and some catalytic runs at 425°C. The oil yields from Wan-SRC are generally higher than those from Aka-SRC. Relative to the raw SRCs, thermal runs increased oil yields by 16-18 % and produced 4-5 % gas. The use of a catalyst promoted the production of oil. It appears that the BI fraction of Aka-SRC is more reactive than that of Wan-SRC, and this trend becomes more remarkable when a catalyst was used. Probably this is due in part to the lower severity of conditions used for producing Aka-SRC than that for Wan-SRC. In addition, SCT-SRC of Wandoan coal (see below) appears to be much more reactive than both Wan-SRC and Aka-SRC in terms of higher BI and asphaltene conversions. These results demonstrated that the liquefaction conditions affects the reactivity of the products; the SRC derived from a lower-severity run exhibits a higher reactivity.

**Comparison of SiO<sub>2</sub>- and Al<sub>2</sub>O<sub>3</sub>-Supported Catalysts.** We examined two Mo/SiO<sub>2</sub> and a number of Ni-Mo/Al<sub>2</sub>O<sub>3</sub> catalysts. Since a SiO<sub>2</sub>-supported catalyst is less active as compared to a Al<sub>2</sub>O<sub>3</sub>-supported one for hydrotreating, and since a Ni- or Co-promoted Mo catalyst is more active than a unpromoted catalyst, one would expect a higher activity of Ni-Mo/Al<sub>2</sub>O<sub>3</sub> catalyst. As shown in Table 3, KF-153S and Cat-1 did afford higher asphaltene conversion than the SiO<sub>2</sub>-supported Cat-SB. However, it is very interesting to note that Cat-SB exhibited considerably higher effectiveness for converting BI fractions of both Wan-SRC and Aka-SRC. It is known that the acidity increases in the order of SiO<sub>2</sub> < Al<sub>2</sub>O<sub>3</sub> < SiO<sub>2</sub>-Al<sub>2</sub>O<sub>3</sub> [Satterfield, 1991]. Because Cariact-50 has much lower surface area than the Al<sub>2</sub>O<sub>3</sub> support (78 vs. 203 m<sup>2</sup>/g) and Cat-SB contains no Ni promoter, the observed superiority of Mo/SiO<sub>2</sub> catalyst over Ni-Mo/Al<sub>2</sub>O<sub>3</sub> in BI conversion can be attributed to the large pore diameter (507 Å) and/or lower surface acidity of the silica support.

Table 4 compares the results for runs of Wan-SRC at 400 °C using 20-32 mesh particles of two Mo/SiO<sub>2</sub> and KF-153S Ni-Mo/Al<sub>2</sub>O<sub>3</sub> catalysts. The data for Cat-SA and Cat-SB show that a large pore silica (Cariact-50) is better than a small pore silica (Cariact-10) in terms of higher BI conversion. Relative to the two Mo/SiO<sub>2</sub>, KF-153S Ni-Mo/Al<sub>2</sub>O<sub>3</sub> afforded higher oil yield and higher asphaltene conversion. However, the conversion of BI was substantially higher with Mo/SiO<sub>2</sub> than with KF 153S. Combination of data in Tables 3 and 4 reveals that using silica support is more effective for converting preasphaltene, the BI fraction, while the use of alumina gives higher conversion of asphaltene and in most cases, higher oil yields.

**Effect of Particle Size of Ni-Mo/Al<sub>2</sub>O<sub>3</sub>.** Table 5 shows the effects of crushing KF-153S Ni-Mo to <100 mesh particles for hydroprocessing of SCT-SRC. The higher oil yield and conversion with crushed catalyst provide another indication of the intraparticle diffusional limitations occurring during SRC hydroprocessing. In fact, relative to the thermal runs, the cylindrical KF-153S Ni-Mo and its 20-32 mesh (0.84-0.50 mm) particles promoted asphaltene conversion but did not improve BI conversion both for Wan-SRC (Tables 3 and 4) and for SCT-SRC (Table 5). However, the use of <100 mesh (<0.15 mm) KF-153S resulted in significant increase in BI conversion (Table 5).

These results indicate that improving mass transfer has greater impact on conversion of preasphaltene. The superiority of the fine catalyst particles can be attributed to greatly increased external surface area and decreased length of diffusional path, as compared to the 1.5 mm extrudate. In practice, the lowest catalyst sizes permitted in industrial fixed-bed operations are 0.8-1.6 mm. Described in the subsequent sections is SRC conversion using 0.8-1.5 mm cylindrical extrudate Ni-Mo/Al<sub>2</sub>O<sub>3</sub>.

**Effects of Pore Size of Ni-Mo/Al<sub>2</sub>O<sub>3</sub> on Product Distribution.** In order to examine the pore size effects on a unified basis, one should prepare the catalysts having unimodal and narrow pore size distribution, different median pore diameters, and similar chemical composition. As can be seen from Figure 1, the unimodal pore structure and the significantly different pore sizes of Cat-1 through Cat-4 prepared by using the same procedure, enabled us to evaluate the pore size effects.

Figure 2 presents the results for Wan-SRC hydroprocessing over a series of cylindrical Ni-Mo/Al<sub>2</sub>O<sub>3</sub> catalysts with different MPD. Also shown in Figure 2 are the data from the run with KF-153S sulfided Ni-Mo, which has a MPD value (90 Å) similar to that (100 Å) of the well known Shell 324M Ni-Mo [Baker et al., 1987, Lee et al., 1991]. All of these catalysts were used in the form of cylindrical extrudate. It should be noted that Cat-1 though Cat-4 is alumina-supported catalyst, while KF-153S contains 4.5 wt% SiO<sub>2</sub>. Relative to thermal run, each of the four prepared catalysts enhanced the production of oil. Figure 3 shows the results for Aka-SRC which originally contained more BI and less asphaltene and oil as compared to Wan-SRC. As can be seen from Figures 2 and 3, both for Wan-SRC and Aka-SRC, the conversion of SRC into benzene soluble products increased in the order of Cat-1 < Cat-2 < Cat-3 ≤ Cat-4. This order is contrary to that of catalyst surface area. The yields of asphaltene, however, decreased with increasing MPD in the small pore size region, but rose with further increase in MPD in the large pore range. The oil yields from catalytic runs of both SRCs with the four prepared Ni-Mo did not vary considerably, but the oil yield from Wan-SRC with KF-153S was lower. The gas yields were nearly constant in the runs of both SRCs.

**Pore-Size Effects on Conversion of Heavy Fractions and Interactive Chemistry.** Table 6 compares the product distribution and hydrogen consumption for typical runs of Aka-SRC in this work and its isolated asphaltene fraction Aka-Asp reported in previous paper [Song 1991]. The oil yields from thermal runs of Aka-SRC and Aka-Asp are relatively similar to each other, but the catalytic run of Aka-Asp with Cat-1 gave 11% higher, and that with Cat-3 afforded 17% higher oil yield than the corresponding values for runs of Aka-SRC. This is surprising because Aka-SRC originally contained about 32% oil but Aka-Asp contained no oil. The conversions of asphaltene as well as the consumption of gas phase H<sub>2</sub> are considerably higher in the runs of the isolated asphaltene than for the whole SRC. This comparison indicates that catalytic conversion of asphaltene into oil is suppressed during the runs of whole SRC. Probably the presence of preasphaltene inhibits the catalytic reaction of asphaltene.

Table 7 compares the results for hydroprocessing of Wan-SRC and its BI fraction Wan-BI. Apparently, the runs of whole SRC gave better product spectra than those of its BI fraction. This is because Wan-BI is composed of about 85 % preasphaltene and about 15 % quinoline insolubles (Table 2), which are the heaviest fractions in coal liquids. Taking into account the oil content of original Wan-SRC, the oil yields produced from Wan-BI with Cat-3 and Cat-4 are only 2-3% lower, and that with Cat-1 is about 6% lower than the corresponding values for net oil production from Wan-SRC. The net conversion of BI fraction appears to be higher for the runs of isolated Wan-BI than for the whole Wan-SRC. However, such a difference is much smaller as compared to that between the runs of whole SRC and asphaltene. Therefore, the negative impact of asphaltene on preasphaltene conversion is very limited, but preasphaltene materials appear to inhibit the catalytic conversion of asphaltene.

**Carbon-Coated Catalysts.** Analysis of the benzene-extracted spent catalysts that have been used once in runs of Wan-SRC by using SEM-EPMA showed that the deposition of carbonaceous materials and metal species such as Ca, Fe and Ti took place in the 1 h reaction, being consistent with the findings of Stiegel et al. [1983] and Stohl and Stephens [1987]. These catalysts are denoted as carbon-coated catalysts, in which the amounts of benzene-insoluble materials are estimated to be around 10 wt%. We also conducted the runs of Wan-SRC using the carbon-coated Ni-Mo/Al<sub>2</sub>O<sub>3</sub> catalysts. The consumption of gas-phase H<sub>2</sub> decreased and the oxygen content of oil and asphaltene products increased slightly, as compared to the runs with fresh Ni-Mo, which suggest a small decrease in catalytic activity. However, the conversion of BI fraction was substantially higher with the carbon-coated Ni-Mo than with the fresh Ni-Mo, while oil yields with each pair of fresh and carbon-coated Ni-Mo were similar to each other.

Figure 4 shows the relationship between MPD and conversions of BI and asphaltene for runs of Wan-SRC and Aka-SRC over fresh and carbon-coated Ni-Mo catalysts. Increasing catalyst MPD up to about 150 Å increased the conversion of both asphaltene and preasphaltene. Within this range, the BI has relatively less inhibiting effect on asphaltene conversion. Further increasing MPD leads to further increase in conversion of preasphaltene, but this results in decrease in asphaltene conversion. The decrease in the apparent asphaltene conversion is considered to be due

to two different effects: 1) increasing MPD increased conversion of preasphaltene, producing more asphaltene, as suggested by data in Table 7, and 2) diffusion and preferential adsorption of highly polar and polyaromatic BI materials on surface inside pores of large-pore catalysts, which inhibits the adsorption and conversion of asphaltene on catalyst surface, as revealed by the data in Table 6.

It is interesting to note that carbon-coated catalysts gave substantially higher conversion of BI than the fresh catalysts, but the fresh Ni-Mo gave higher asphaltene conversion. We also observed that pure SiO<sub>2</sub>-supported catalysts gave higher BI conversion. The KF-153S, which contains 4.5 wt% SiO<sub>2</sub> and is more acidic than pure alumina-supported Ni-Mo, did not improve BI conversion, as compared to the thermal runs. All of these results point to the conclusion that less acidic hydrogenation catalysts are more effective for conversion of BI materials into asphaltene. These observations are consistent with the findings of Derbyshire et al. [1988] and Masuyama et al. [1990] who reported the improved performance of carbon-coated alumina supported Mo catalysts or carbon-supported Mo catalysts and Ca-modified Ni-Mo, respectively, for hydrotreating of coal liquids. Ca addition serves to neutralize or passivate, and carbon coating covers the surface acidic sites. These results, however, are in distinct contrast with those of McCormick et al. [1989] who reported that relative to the other catalysts a Co-Mo/Al<sub>2</sub>O<sub>3</sub> catalyst containing 5% SiO<sub>2</sub> exhibits an extremely low coking tendency because of the Bronsted acid sites on the silicated alumina.

**A New Concept for Catalyst Design.** In industrial practice, a compromise between the need for high activity and for extended life can be achieved by using a bimodal pore size distribution. Some recently developed catalysts such as Shell 317, Amocat 1C and Amocat 1A are Ni-Mo or Co-Mo supported on bimodal Al<sub>2</sub>O<sub>3</sub> supports [Lee et al, 1991; McCormick et al., 1989]. Al<sub>2</sub>O<sub>3</sub>-supported bimodal catalysts have been shown to exhibit better apparent activity for coal liquids upgrading [Tischer, 1985]. However, the present results point to the conclusion that less acidic and larger-pore hydrogenation catalysts are more effective for preasphaltene conversion, but efficient conversion of asphaltene requires mild hydrocracking catalysts. These results suggest a new concept for design of coal liquids upgrading catalyst: two component-bimodal catalyst consisting of a moderately acidic mild hydrocracking component having mostly mesopores and a less acidic hydrogenating component with large mesopores or mostly macropores. This concept needs to be verified by further investigation.

#### ACKNOWLEDGEMENT

C. Song wish to thank Professor Harold H. Schobert of The Pennsylvania State University for his kind review and helpful comments.

#### REFERENCES

- Baker, J.R.; McCormick, R.L.; Haynes, H.W., Jr., *Ind. Eng. Chem. Res.* **1987**, *26*, 1895-1901.  
Bertolacini, R.J.; Gutberlet, L.C.; Kim, D.K.; Robinson, K.K. *ACS Fuel Chem. Prepr.* **1978**, *23*, 1-10.  
Derbyshire, F., *Catalysis in Coal Liquefaction*, IEA/CR, 1988, 66 pp, and references cited therein.  
Hanaoka, K.; Song, C.; Nomura, M. *Proc. 24th Coal Sci. Conf.*, Tokyo, **1988**, 222-225.  
Ho, P.N.; Weller, S.W. *Fuel Processing. Technol.* **1981**, *4*, 21-29.  
Lee, J.M.; Cantrell, C.E.; Gollakota, S.V.; Davies, O.L.; Corser, M.M.; Vimalchand, P., *ACS Fuel Chem. Prepr.* **1991**, *36* (4), 1915-1926.  
Masuyama, T.; Kageyama, Y.; Kawai, S. *Fuel* **1990**, *69*, 245-250.  
McCormick, R.L.; King, J.A.; King, T.R.; Haynes, H.W., Jr., *Ind. Eng. Chem. Res.* **1989**, *28*, 940-947.  
Onuma, K. *Shokubai* **1989**, *31*, 182-187.  
Satterfield, C.N. "Heterogeneous Catalysis in Industrial Practice". 2nd Ed., McGraw-Hill, New York, **1991**, Chapter 7., p.211-266.  
Shimada, H.; Kurita, M.; Sato, T.; Yoshimura, Y.; Kawakami, T.; Yoshitomi, S.; Nishijima, A., *Bull. Chem. Soc. Japan* **1984**, *57*, 2000-2004.  
Song, C.; Nihonmatsu, T.; Nomura, M. *Proc. 24th Japan Coal Sci. Conf.*, Tokyo, **1988a**, 226-228.  
Song, C.; Hanaoka, K.; Ono, T.; Nomura, M. *Bull. Chem. Soc. Japan* **1988b**, *61*, 3788-3790.  
Song, C.; Hanaoka, K.; Nomura, M. *Energy & Fuels* **1988c**, *2*, 639-644.  
Song, C.; Hanaoka, K.; Nihonmatsu, T.; Nomura, M. *Proc. 1989 Int. Conf. Coal Sci.*, Tokyo, **1989a**, 226-228. The median pore radius was erroneously written as median pore diameter in this paper.  
Song, C.; Hanaoka, K.; Nomura, M. *Fuel* **1989b**, *68*, 287-292.  
Song, C.; Nihonmatsu, T.; Hanaoka, K.; Nomura, M. *ACS Fuel Chem. Prepr.* **1991a**, *36* (2), 542-550  
Song, C.; Nihonmatsu, T.; Nomura, M., *Ind. Eng. Chem. Res.* **1991b**, *30*, 1726-1734.  
Stiegel, G.J.; Tischer, R.E.; Polinski, L.M. *Ind. Eng. Chem. Prod. Res. Dev.* **1983**, *22*, 411-420.  
Stohl, F.V.; Stephens, H.P., *Ind. Eng. Chem. Res.* **1987**, *26*, 2466-2473.  
Tischer, R.; Narain, N.K.; Stiegel, G.J.; Cillo, D.L. *J. Catal.* **1985**, *95*, 406-413. 8.  
Yoshimura, Y.; Sato, T.; Shimada, H.; Nishijima, A. *Fuel Sci. Technol. Int'l* **1986**, *4*, 621-642.

**Table 1.** Properties of Al<sub>2</sub>O<sub>3</sub> and SiO<sub>2</sub> Supports Used for Preparing the Supported Mo Catalyst

	SiO <sub>2</sub> Support		Al <sub>2</sub> O <sub>3</sub> Support				
	Cariact-10	Cariact-50	S-1	S-2	S-3	S-4	S-C <sup>a</sup>
Median pore diam, Å	90	507	115	120	280	750	90 <sup>b</sup>
Surface area, m <sup>2</sup> /g	267	78	203	174			255 <sup>b</sup>
Pore volume, mL/g	1.00	1.05	0.79	0.65	1.05	1.49	0.56 <sup>b</sup>

a) The Kejefine 153S catalyst contains 4.5 wt% SiO<sub>2</sub>. b) The values measured for the KF 153S catalyst.

**Table 2.** Representative Analyses of Samples

Sample	Elemental (wt%, daf)					Atomic H/C	Fractional (wt%, daf)				Ash (wt%)
	C	H	N	S	O <sup>a</sup>		Oil	Asp.	Preasp. <sup>b</sup>	QI or Pyl <sup>c</sup>	
Solvent Refined Coals											
Wan-SRC	85.7	6.1	1.5	0	6.7	0.85	35.7	33.1	26.4	4.8	0.9
Aka-SRC	84.9	6.2	1.8	0.3	6.8	0.87	31.5	27.0	39.9	1.6	0.5
SCT-SRC	86.3	6.7	1.2	0	5.8	0.93	46.0	34.1	19.9	0	—
Raw Coals											
Wandoan	78.3	5.9	1.0	0.1	14.7	0.90	0.9	4.7	1.7	92.7	7.3
Akabira	83.2	6.2	2.1	0.6	7.9	0.89	0.8	0.9	19.5	78.8	8.4

a) By difference; b) Quinoline or pyridine soluble; c) quinoline or pyridine insoluble.

**Table 3.** Results of Thermal and Catalytic Hydroprocessing of SRC at 425°C

Catalyst		Products (wt%)				Conv (wt%)		H Consum (wt%)	
Name	Composition	Gas	Oil	Asp	BI	Asp	BI	H <sub>2</sub>	Tetralin
Original Wan-SRC		—	35.7	33.1	31.2	0	0	—	—
None	None	4.6	54.4	22.9	18.1	30.8	42.0	0.7	0.6 <sup>a</sup>
KF-153S	Ni-Mo/Al <sub>2</sub> O <sub>3</sub>	6.2	58.7	14.6	20.6	55.9	34.0	1.4	0.3
Cat-1	Ni-Mo/Al <sub>2</sub> O <sub>3</sub>	3.6	65.2	15.4	15.8	53.5	49.4	1.6	0.8
Cat-SB	Mo/SiO <sub>2</sub>	3.9	61.5	23.0	11.6	30.5	62.8	1.6	0.3
Original Aka-SRC		—	31.5	27.0	41.5	0	0	—	—
None	None	5.0	48.2	23.7	23.1	12.2	44.3	0.7	0.9
Cat-1	Ni-Mo/Al <sub>2</sub> O <sub>3</sub>	4.3	59.2	20.7	15.8	23.0	61.9	1.4	0.4
Cat-SB	Mo/SiO <sub>2</sub>	5.4	58.7	25.4	10.5	5.9	74.7	1.3	0.3

a) This value seems to be lower than real value, as compared to the data in Table 4.

**Table 4.** Hydroprocessing of Wan-SRC over 20-32 mesh SiO<sub>2</sub>- and Al<sub>2</sub>O<sub>3</sub>-Supported Catalysts at 400°C

Catalyst		MPD (Å)	Yields (wt%)		Conv (wt%)		H consum (wt%)	
Name	Composition		Gas	Oil	Asp	BI	H <sub>2</sub>	Tetralin
None	None		1.9	45.9	16.9	20.8	0.7	1.0
Cat-SA	Mo/SiO <sub>2</sub>	90 <sup>a</sup>	1.8	49.7	21.2	28.2	0.9	0.4
Cat-SB	Mo/SiO <sub>2</sub>	507 <sup>a</sup>	1.9	51.3	19.0	35.9	1.1	0.4
KF-153S	Ni-Mo/Al <sub>2</sub> O <sub>3</sub>	90	1.9	55.5	44.4	22.4	ND	0.3

a) Median pore diameter of SiO<sub>2</sub> supports Cariact-10 and Cariact-50, respectively.

**Table 5.** Hydroprocessing of SCT-SRC over Cylindrical Extrudate and Finely Crushed KF-153S Ni-Mo/Al<sub>2</sub>O<sub>3</sub> Catalysts at 425°C

Catalyst		Gas + Oil (wt%)	Conv (wt%)	
Composition	Size		Asp	BI
Orig. SCT-SRC	—	46.0	0	0
None	—	70.9	40.5	55.8
Ni-Mo/Al <sub>2</sub> O <sub>3</sub>	1.5 mm cylinder	81.5	72.4	54.8
Ni-Mo/Al <sub>2</sub> O <sub>3</sub>	<100 mesh powder	87.8	80.6	71.9

**Table 6.** Comparison of Hydroprocessing of SRC and Its Asphaltene Fraction

Sulfided Ni-Mo/Al <sub>2</sub> O <sub>3</sub> MPD (Å)	Aka-SRC			Aka-Asp <sup>a</sup>		
	None	Cat-1 120	Cat-3 290	None	Cat-1 120	Cat-3 290
<b>Products (wt%)</b>						
Gas	5.0	4.3	4.3	5.7	5.2	5.1
Oil	48.2	59.2	62.5	50.7	69.8	80.3
Asphaltene	23.7	20.7	21.7	32.3	22.4	12.8
BI	23.1	15.8	11.5	12.2	2.6	1.8
<b>H Consumed (wt%)</b>						
H <sub>2</sub>	0.7	1.4	1.5	0.5	2.1	2.3
Tetrafin	0.8	0.5	0.3	0.4	0.3	0.2

a) Hexane-insoluble but benzene soluble fraction of Aka-SRC.

**Table 7.** Comparison of Hydroprocessing of SRC and Its Preasphaltene (BI) Fraction

Sulfided Ni-Mo/Al <sub>2</sub> O <sub>3</sub> MPD (Å)	Wan-SRC			Wan-BI <sup>a</sup>		
	Cat-1 120	Cat-3 290	Cat-4 730	Cat-1 120	Cat-3 290	Cat-4 730
<b>Products (wt%)</b>						
Gas	3.6	3.7	3.6	10.5	7.6	10.3
Oil	65.2	66.8	66.0	23.5	27.9	27.1
Asphaltene	15.4	18.2	19.6	24.8	30.1	33.1
BI	15.8	11.3	10.8	41.2	34.4	29.5
<b>H Consumed (wt%)</b>						
H <sub>2</sub>	1.6	1.7	1.7	1.7	1.7	1.9
Tetrafin	0.8	0.5	0.4	ND	ND	ND

a) Benzene insoluble fraction of Wan-SRC.

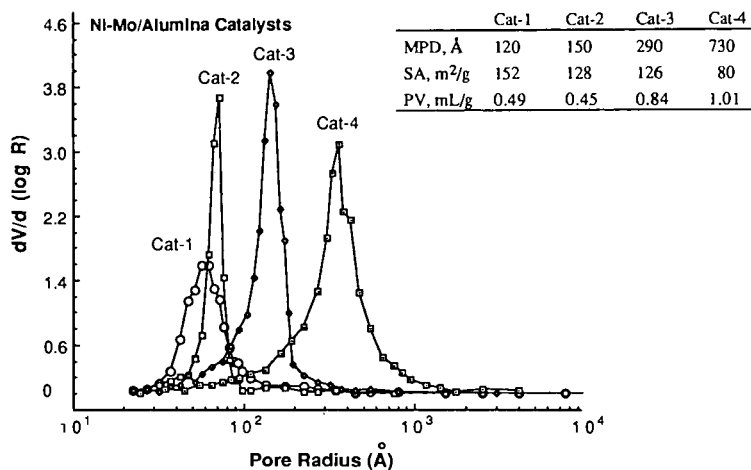


Figure 1. Pore size distribution of prepared Ni-Mo/Al<sub>2</sub>O<sub>3</sub> catalysts.

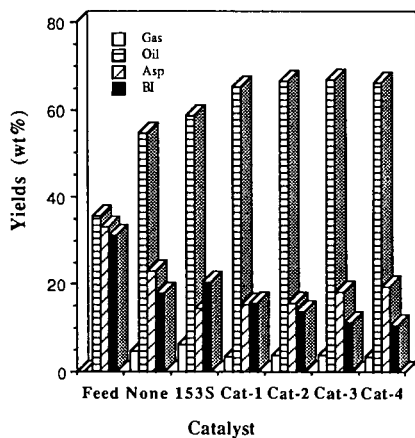


Figure 2. Hydroprocessing of Wan-SRC over unimodal Ni-Mo/Al<sub>2</sub>O<sub>3</sub> catalysts with different median pore diameter. See Figure 1 for MPD values.

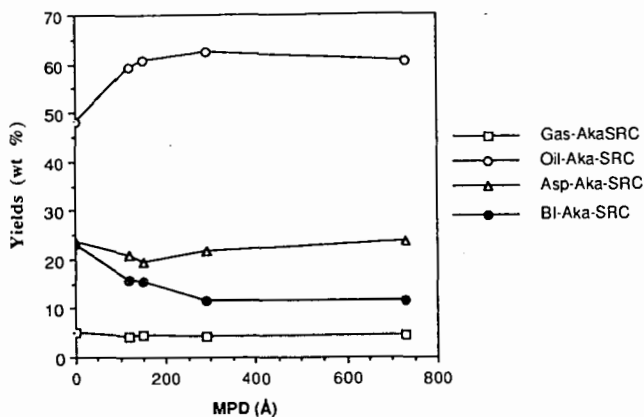


Figure 3. Effects of pore size of Ni-Mo/Al<sub>2</sub>O<sub>3</sub> catalysts on product distribution for hydroprocessing of a solvent refined coal (Aka-SRC).

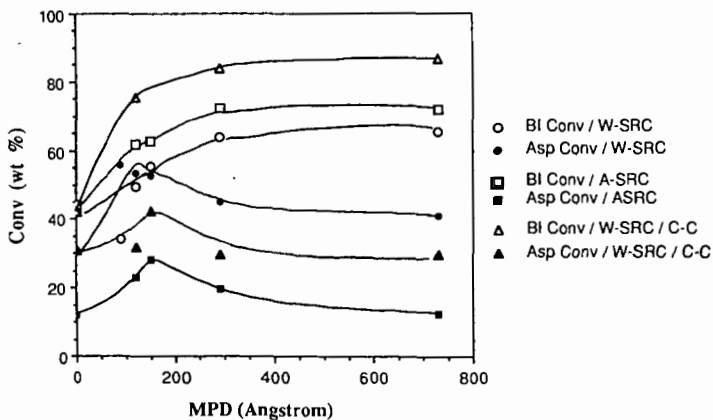


Figure 4. Relation between median pore diameter and conversion of BI and asphaltene with fresh and carbon-coated (C-C) Ni-Mo/Al<sub>2</sub>O<sub>3</sub> catalysts for hydroprocessing of Wan-SRC and Aka-SRC. Note that incorporation of the data with KF-153S Ni-Mo containing 4.5 % SiO<sub>2</sub> resulted in some deviation at MPD of 90 Å.

## TEMPERATURE-PROGRAMMED CATALYTIC LIQUEFACTION OF LOW RANK COAL USING DISPERSED Mo CATALYST

Lili Huang, Chunshan Song and Harold H. Schobert  
Fuel Science Program  
Department of Material Science and Engineering  
The Pennsylvania State University  
University Park, PA 16802

Keywords: temperature-programmed liquefaction, catalysts, conversion

### INTRODUCTION

In the presence of catalyst, the specific reaction conditions have a direct effect on conversion in coal liquefaction and on the product distribution [1]. At temperatures lower than 300°C, catalyst precursors such as ammonium tetrathiomolybdate may not be converted to a catalytically active form and thus have no benefit on liquefaction [2]. However, at severe reaction conditions, such as high temperature, retrogressive reactions will take place, and crosslinking or recombination of radicals generated in thermal cracking will reduce the possibility of breaking the coal macromolecule into smaller molecules. In an effort to achieve highest conversion and desired product distribution, low-severity processes have been studied by several research groups. It has been found that temperature-programmed and temperature-staged liquefaction are efficient to maximize the conversion and minimize the retrogressive reactions [3, 4, 5].

The objective of the work reported in this paper is to study the catalytic effect of ammonium tetrathiomolybdate, techniques to disperse this catalyst precursor onto coal, and the optimum reaction conditions for the highest conversion.

### EXPERIMENTAL

The coal sample was a Montana subbituminous (DECS-9, PSOC-1546) coal obtained from Penn State Coal Sample Bank. Its composition is summarized as follows: 24.68% moisture, 4.80% ash, 33.46% volatile matter and 37.06% fixed carbon on an as-received basis, 76.11% carbon, 5.14% hydrogen, 0.91% nitrogen, 0.33% organic sulfur and 17.50% oxygen on a dmmf basis. The coal was dried at 95°C in vacuum for two hours before use.

The catalyst precursor, ammonium tetrathiomolybdate (ATTM), was dispersed on coal by incipient wetness method. The loading was 1% of molybdenum on the basis of dmmf coal. Water and a mixture of H<sub>2</sub>O/THF (44 : 56) were employed as impregnation solvents. After loading of the catalyst precursor, the coal sample was dried in vacuum for two hours at 105°C, then removed and stored under a nitrogen atmosphere.

Liquefaction experiments were conducted in microautoclave reactors (tubing bombs) in a preheated fluidized sandbath. For each reaction, 4 grams of coal and 4 grams of Wilsonville Middle Distillate (WIMD) as reaction solvent were added to the reactor, following which hydrogen was purged three times, with a final pressure of 7 MPa at room temperature. The reactor was then plunged into the sandbath and agitated at 200 cycles per minute. The tubing bomb reached the reaction temperature in about three minutes. For a single-staged liquefaction (SSL), the tubing bomb was rapidly heated-up to 400°C and held for 30 minutes followed by rapid quench. For a temperature-programmed liquefaction (TPL), the tubing bomb was rapidly heated-up to a relatively low temperature (200°C-300°C) and soaked in sandbath at that temperature for 15 minutes. The

temperature was then gradually increased to a higher temperature level (400°C-450°C) and held for 30 minutes, followed by rapid quench. The rate of temperature increase was 30°C/min to 8.30°C/min, depending on the difference between the lower temperature and the higher temperature. The heat-up period was about 30 minutes, and the total reaction time was about 75 minutes. Temperature-staged liquefaction (TSL) was a different procedure from TPL. A tubing bomb was rapidly heated-up to a low temperature (200°C-300°C), soaked at that temperature for 15 minutes, then it was immediately (without a heating period) transferred to another sandbath of a higher temperature (400°C) and held for 30 minutes followed by rapid quench. Since there was no heating period between two temperature stages, the total reaction time was about 45 minutes, which is different from TPL.

After the reaction, the gaseous product was vented into a gas sample bag and later analyzed by gas chromatography. The liquid and solid products and residue were washed into a tared ceramic thimble using hexane. Then the products were separated under a nitrogen atmosphere by Soxhlet-extraction using hexane, toluene and THF as solvents, the products being classified as oil, asphaltene and preasphaltene respectively. Solvents were removed by rotary evaporation and the products were dried in vacuum at 110°C for about 12 hours, except for the hexane solubles. The solid residue was washed first by acetone and then by pentane several times and dried in the same procedure as the reaction products. The asphaltene, preasphaltene and residue were then weighed, and conversion and product distributions were calculated based on dmmf coal.

## RESULTS AND DISCUSSION

The effects of TPL and SSL are compared in Table 1. In the absence of a catalyst, TPL total conversion is 6.4 percentage units higher than SSL. This is mainly due to the gains in asphaltene and preasphaltene yields, while the oil yield remains almost identical in both cases, about 30.2%. In the presence of ATTM as catalyst precursor, total conversion increases again in TPL by 6.6 percentage units, similar to those experiments without catalyst. It is noticed that, different from non-catalytic liquefaction, the oil yield increases drastically by 8.8 percentage units in TPL, while asphaltene decreases by 4.9 percentage units. This may suggest that TPL, with presence of the catalyst, promotes the further cracking or hydrogenation of asphaltene to oil, though the detailed mechanism is not yet clear.

Another comparison is liquefaction with and without catalyst. In SSL runs, total conversion increases 32.2 percentage units by employing ATTM as catalyst. This is mainly due to an oil yield increase (by 12.5 percentage units) and an asphaltene yield increase (by 16.4 percentage units), and to a lesser extent, to a preasphaltene yield increase (by 3.3 percentage units). In TPL runs, catalytic liquefaction achieves 32.4 percentage units higher than non-catalyst run in total conversion. Gas and oil yield increases are the predominant (by 21.2%) contribution to the increase in total conversion. Asphaltene and preasphaltene increase by lesser amounts, 6.7 and 4.4 percentage units respectively. This comparison presents that the addition of ATTM as catalyst efficiently improves both the total conversion of liquefaction and the selectivity of products to the more desirable oils.

As mentioned in previous section, in the procedure of sample preparation, both H<sub>2</sub>O and H<sub>2</sub>O/THF (44 : 56) were employed as impregnation solvents. The volume of the H<sub>2</sub>O/THF mixture required to achieve incipient wetness is about three times of that of pure water. It is apparent that the mixture has higher affinity toward the coal surface than water. This difference in affinity may lead to a different dispersion of the catalyst precursor on coal, which will subsequently result in a difference of catalyst performance. Table 1 provides the conversion data to compare the solvent effect on liquefaction. For SSL runs, samples prepared using H<sub>2</sub>O/THF appear a bit more active than samples prepared using H<sub>2</sub>O. For TPL runs, the difference is more pronounced. By using H<sub>2</sub>O/THF as impregnation solvent, total conversion increases by 10.4 percentage units, which is due to the increase of gas and oil yield (by 10.3 percentage units). The asphaltene and

preasphaltene yields are identical within experimental error. This set of data supports the assumption that by employing H<sub>2</sub>O/THF, better catalyst dispersion will be achieved, thus leading to a better catalyst performance.

Temperature-programmed liquefaction may be advantageous over temperature-staged liquefaction because TPL provides a heating period which could slowly generated radicals and allow hydrogenation to take place. Table 2 compares TPL with TSL. For 200/400 runs (the first number indicates the first stage temperature and the second number indicates the second stage temperature), the total conversion increases slightly (1.5 percentage units) in TPL with a remarkable increase in gas and oil yield (7.5 percentage units). In contrast, the asphaltene and preasphaltene yields decrease slightly. For 300/400 runs, the same phenomenon is observed, though in 300/400 runs, both TPL and TSL achieve higher total conversion and gas oil yield. It is apparent that TPL is more favorable to achieve high conversion and better product selectivity. Consistent with the previous observations, the asphaltene yield decreases in TPL experiments. This again reflects the fact TPL promotes the interconversion of asphaltene to oils [6].

Figure 1 shows the conversion as a function of the temperature in the first stage in TPL runs. The curve starts at room temperature, which is in fact the SSL run. The total conversion reaches a maximum at 200°C (91%) and starts to decrease as temperature increases, 86.6% at 250°C and 89.7% at 300°C. The oil yield changes in a very similar way as total conversion, 51.5% at 200°C, 46.8% at 250°C and 50.6% at 300°C. The low temperature stage is used to allow time for the reaction solvent to penetrate into the interior of coal particles [3]. If the temperature of this stage is too high, the reaction solvent may evaporate before penetration. In this case, less solvent will be in the interior of coal and this could result in reduced H-transfer to the coal radicals, which will consequently cause poor liquefaction results. The temperature of the first stage may also affect the activation of catalyst precursor, but how this will subsequently affect the liquefaction is still unknown.

The effect of changing temperature of the second stage in TPL is shown in Figure 2. Although the total conversion, as well as the yields of asphaltenes and preasphaltenes, show a trend of decreasing, the gas and oil yields show a remarkable increase as the temperature increase from 400°C to 450°C (51.5% to 62.4%). This indicates that an increase of second stage temperature may not favor high total conversion of liquefaction, but it has some benefit in achieving high yield of oil and gas. The decrease of total conversion might be caused by retrogressive reactions. At temperatures as high as 450°C, radicals formed in thermal cracking immediately crosslink and recombine with one another to form some very stable compounds that are difficult to liquefy.

## CONCLUSIONS

Addition of ATTM as catalyst precursor will increase the total conversion substantially. In the impregnation procedure, using organic compounds in the impregnation solvent appears to lead to a better dispersion of catalyst precursor thus giving a higher conversion. Temperature-programmed liquefaction is advantageous over temperature-staged and single-staged liquefaction regardless of whether a catalyst is used. The change of first and second stage temperature in TPL will influence the conversion, though determining the reasons for these influences relies on future research.

## ACKNOWLEDGEMENTS

The authors are pleased to acknowledge the financial support provided by the United States Department of Energy for this work.

## REFERENCES

1. B. R. Utz, A. V. Cugini and E. A. Frommell, ACS Sym Ser. **1989**, 473, 289.
2. A. B. Garia and H. H. Schobert, Fuel, **1989**, 68, 1613.
3. C. Song, H. H. Schobert and P. G. Hatcher, ICCS, Sept 1991, Newcastle, United Kingdom.
4. C. E. Burgess and H. H. Schobert, Am. Chem. Soc. Div. Fuel Chem. Prepr., **1990**, 35(1), 31.
5. C. E. Burgess, L. Artok and H. H. Schobert, Am. Chem. Soc. Div. Fuel Chem. Prepr., **1991**, 36(2), 462.
6. F. J. Debyshire, A. Davis, R. Lin, P. G. Stansberry and M.-T. Terry, Fuel Processing Tech., **1986**, 12, 127.

Table 1. Comparison of TPL and SSL Effect on Liquefaction.

Sample	rxn Cond.	Tot Conv.	Gas + Oil	Asph.	Preasph.
Non-cat	SSL	52.22	30.21	12.46	9.55
	TPL	58.57	30.27	17.24	11.06
ATIM THF/H <sub>2</sub> O	SSL	84.4	42.73	28.86	12.82
	TPL	91	51.49	23.93	15.5
ATIM H <sub>2</sub> O	SSL	83.24	38.98	19.46	24.8
	TPL	80.57	41.18	23.4	15.42

Oil: hexane soluble.

Asphaltene: toluene soluble but hexane insoluble.

Preasphaltene: THF soluble but toluene insoluble

Table 2. Comparison of TPL with TSL.

Temperature	rxn Cond.	Tot. Conv.	Gas + Oil	Asph.	Preasph.
200/400	TPL	91	51.49	23.93	15.5
	TSL	89.46	43.98	27.62	17.87
300/400	TPL	89.67	50.61	22.67	16.4
	TSL	87.91	42.66	28.37	16.89

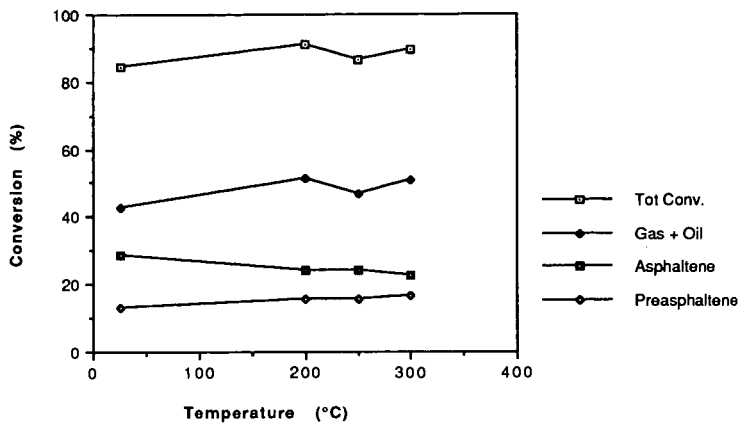


Figure 1. Conversion as a function of first stage temperature in TPL.

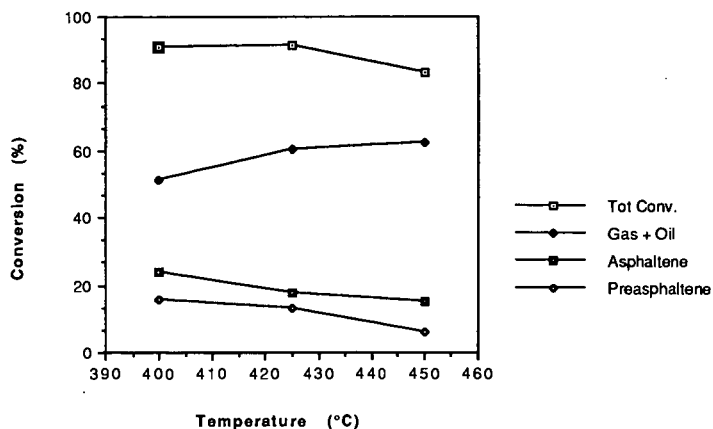


Figure 2. Conversion as a function of second stage temperature in TPL.

## EXAFS Studies of Mo, Ni-Y-Zeolite Catalysts

Qiwu Wang and Dale Sayers

Department of Physics, North Carolina State University, Raleigh, NC 27695

Miming Huang, Chunhua Yuan and Shiqiang Wei

Department of Modern Chemistry, University of Science and Technology of China, Hefei, Anhui, P. R. China

### Introduction

Bimetallic zeolite catalysts which contain Mo are of great interest as bifunctional catalysts<sup>1-4</sup>. However, there are difficulties in preparing such catalysts since it is difficult to exchange the cations of a zeolite for molybdenum ions directly because high valence cationic molybdenum can only exist in a very acidic solution where ion-exchange equilibria are unfavorable and many zeolites are unstable. Ion exchange with neutral and anionic species results in a large amount of surface loading. In order to overcome the difficulties of aqueous ion exchange, molybdenum is introduced into zeolites by a solid-ion exchange method. A special procedure was developed recently for initiating controlled immigration of  $\text{MoO}_2(\text{OH})_2$  into the pores of HY and NiY using  $\text{MoO}_3$  in the presence of water vapor.<sup>5</sup>

EXAFS is an effective physical method for determination of the local structure of specific atoms in complex systems such as highly dispersed supported metal catalysts. It has been successfully applied to some metal zeolite catalysts: viz. Pt-Y-zeolite<sup>6</sup>, Cd-Y-zeolite<sup>7</sup> and Ni, Mo-Y-zeolite<sup>8</sup> and other bimetallic catalysts<sup>9-10</sup>. In this work, we studied by EXAFS the change of the environment around Mo and Ni as a function of preparation of the Mo, Ni-Y-zeolite to follow the incorporation of Mo and Ni into the framework of the Y-zeolite and to see if there are any Mo-Ni interactions.

### Experimental

#### Samples

The HNaY was prepared by exchange of NaY with a 0.1 N  $\text{NH}_4\text{NO}_3$  solution at 365K for 1 hour, followed by a direct calcination at 823K for 5.5 hours in a closed vessel. The modified solid ion exchange was performed as following: a mixture of 27 g HNaY and 1.2g  $\text{MoO}_3$  was ground in a mortar (hereafter denoted as MoHY), placed in a quartz tube and then calcined at 723K, water vapor at 323K (118 torr) was carried through the mixture using  $\text{H}_2$  as vector gas with a flow of 45ml/min. The sample obtained after calcination was then denoted as MoHYR and that after dehydration at 673K as MoHYRD.

The NiY was prepared by ion exchange of HNaY in a 0.5N Ni(NO<sub>3</sub>)<sub>2</sub> solution at 318K for 3.5 hours, followed by washing and drying at 393K. To prepare one bimetallic catalyst, MoHYRD was subjected to the same ion exchange process in Ni(NO<sub>3</sub>)<sub>2</sub> solution. This sample was denoted as MoNiY (Mo 1.63 wt. %, Ni 2.09 wt. %). A second sample was prepared starting with NiY and using solid ion exchange to incorporate Mo. This sample is denoted NiMoY (Ni 2.07%, Mo 2.5%). After dehydration they are denoted as MoNiYD and NiMoYD respectively. The Mo and Ni contents of the samples were then analyzed by AAS and Na contents were determined by ICP, and X-ray powder diffraction measurements were made using a Cu-target x-ray tube.

#### X-ray Absorption Measurements

X-ray absorption experiments were performed on beam line X-11A of the National Synchrotron Light Source (NSLS), Brookhaven National Laboratory. The X-ray absorption spectra for Mo and Ni K-edges were recorded with the ring operating at 2.5 GeV beam energy and a beam current of 40-180 mA. The pressed powder samples were mounted on the holder and measured at liquid nitrogen temperature in the transmission mode.

Data analysis was carried out with using standard methods<sup>11</sup> and the fitting was done using experimentally determined Mo-O (from ZnMoO<sub>4</sub>), Mo-Mo (from metallic Mo) and theoretically calculated Mo-Si, Mo-Ni, Ni-Si, Ni-O and Ni-Ni (using FEFF)<sup>12</sup> phase shifts and backscattering amplitudes. Both single or multiple shell models were assumed for fitting the various filtered Fourier transform (FT) peaks.

#### **Results and Discussion**

##### Mo in Mo,Ni-Y-zeolites

As mentioned above, two different preparations were used: one put Mo into the zeolite first using solid-ion exchange and then introduces Ni cations by aqueous ion exchange. The other incorporates Ni first followed by Mo. Will the different order of incorporating Mo and Ni into Y-zeolite produce different local environments of Mo and Ni in these two catalysts? For these low loading and highly dispersed metal-zeolites, only EXAFS studies of the individual metal elements in them can give the answer to this question.

From Fig.1 it can be seen that the X-ray absorption profile of Mo in NiMoY and NiMoYD in which Mo was introduced into Ni-Y-zeolite are similar to those in MoO<sub>3</sub> and MoHY<sup>7</sup> having a clear pre-edge peak and the weak structure in the extended absorption region. The spectra of Mo in MoNiY and MoNiYD are virtually the same as those in MoHYR and MoHYRD<sup>7</sup>: no pre-

edge absorption and with a strong oscillation in the extended region which means prominent higher coordination shells.

Fourier transforms of  $k^3 \cdot \chi(k)$  for the Mo K-edge EXAFS of figure 1 shows that these differences are in both the first and higher shells (Fig.2). The Mo environment in NiMoY is very similar to MoO<sub>3</sub>. The clear decrease of a Mo-Mo feature and a longer Mo-O distance in NiMoYD, in comparison with NiMoY indicates that MoO<sub>3</sub> is further dispersed into the Ni-Y zeolite by the further calcination and dehydration. This is also consistent with the decrease in the higher (Mo-Mo and Mo-O) shells. The fitting results listed in Table 1 quantitatively demonstrate these changes. For both MoNiY and MoNiYD, where Mo was introduced into Y-zeolite by solid-ion exchange, the higher coordination shell structures surrounding Mo are similar and sharper than those in NiMoY and NiMoYD. It is also known that the infrared absorption spectra are nearly same for both MoNiY and MoNiYD.<sup>7</sup> The long metal oxygen bonds at around 2.6Å in both MoNiY and NiMoY (see Table 2) have been observed before in metal-zeolites.<sup>13</sup> A Mo-Mo interaction (R~3.63 Å) also was observed by EXAFS in MoO<sub>3</sub>/TiO<sub>2</sub> catalysts after calcination.<sup>14</sup> From fitting the experimental  $k^3 \chi(k)$  data for MoNiY and MoNiYD isolated from the shells between 2.86 and 3.74Å with Mo-Mo, Mo-Si and Mo-Ni models it can be demonstrated that the Mo has not only Mo and Si which are present in MoHYR and MoHYRD but also a small amount of Ni atoms as its neighbors. An example is shown in Figure 3 for the case of MoNiY. The presence of an interaction between Mo and Ni in Mo,Ni-Y-zeolites may be significant for the catalytic properties of these bimetallic zeolite catalysts.

#### Ni in Mo,Ni-Y-zeolites

The Ni K-edge absorptions for MoNiY, MoNiYD, NiMoY and NiMoYD all have a strong first X-ray absorption peak which can be related to the oxidation state of Ni (see Fig.4). However, further comparison indicates that there are slight differences in the edge region and a great change in the extended region between MoNiY and NiMoY in both the as-prepared and dehydrated forms. The Fourier transforms of the data in Figure 4 are shown in Figure 5 and clearly show the differences between the MoNi and NiMo forms. The local environment of Ni in MoNiY is very close to that of dispersed NiO (CN=6, R=2.04 Å). After dehydration, the oxygen coordination decreases because of the removal of bound waters, and the Debye-Waller factor decreases. However, the higher shell coordinations still could not be found. Ni<sup>2+</sup> is still present in a highly dispersed state with a simple oxygen coordination structure only. This is in agreement with other work.<sup>15</sup> The strong interaction between Mo and Ni, as indicated in the previous paragraph, will inhibit the growth of Ni metal particles and results in the

fine Ni particles which would relate to excellent activity and selectivity toward hydrodemethylation of toluene.<sup>13</sup> In NiMoY and NiMoYD the Ni-O first neighbors have overlapping contributions from higher shells. Multiple shell fitting showed that best fits were obtained for Ni-O, Ni-Si and Ni-Ni coordinations compared with those for Ni-O and Ni-Si or Ni-O and Ni-Ni only. An example of the results with Mo, Ni and O as the neighbors fitted to Fourier filtered data between 2.86-3.74 Å in NiMoY is shown in Figure 6. It indicates that Ni has not only O and Ni but also Mo as its coordination neighbors consistent with the Mo edge results on the same samples.

### Summary

From Mo and Ni K-edge EXAFS studies we have studied the difference between the local environments of Mo and Ni in Mo,Ni-Y-zeolites prepared by interchanging the order of introduction of metals into the zeolite. The results clearly indicate that significant differences occur. When Mo is introduced first it seems to be exchanged into the supercages as indicated by the coordination numbers and distances we have found. The subsequent addition of Ni seems to allow Ni to go into nearby cages where it can coordinate to Mo through oxygens. When Ni is added first it seems to go into a smaller cages in an aqueous phase. Subsequent addition of Mo does not affect this environment and the Mo seem to remain essentially as MoO<sub>3</sub>. This should not result in an effective interaction between Mo and Ni. These results clearly indicate the importance of the order of exchange of metals onto zeolites in the preparation of bimetallic zeolite catalysts.

### References

1. Meszaros-Kis, A. and Valyon, J., in "Zeolites as Catalysts, Sorbents and Detergent Builders" Edited by Karge H. G. and Weitkamp J., Elsevier, Amsterdam, 1989, p.251
2. Laniecki, M., *ibid* P. 259
3. Harris, I. M., Dwyer, J., Garforth, A.A., Mc Ateer, C. H. and Ball, W. J., *ibid* P.271
4. Howe, R. F. and Huang M., Proceeding of 9th International Conference on Catalysis, Canada, 1988, p. 1585
5. Huang, M. and Howe, R. F., *J. Catal.* 108 (1987) 283
6. Wang, Q., Sayers, D., Huang, M., Yuan, C. and Wei, S., abstract in this symposium
7. Moller, K., Eddy, M. M., Stucky, G.D., Herron, N. and Bein, T., *JACS.* 1989, 17, 1564
8. Clozza, A., Bianconi, A., Gareia, J., Corma, A and Burattini, E., *XAFS V*, Ed: Mustre de Leon, J., Stern, E. A., Sayers, D. E., Ma, Y. & Rehr, J.J., North-Holland, 1988, p.162
9. Wang Q. and Wei S., *Kehue Tongbao* 6, 435, (1990)
10. Wang Q. and Wei S., *Chinese J. Chem. Phys.* 3, 49, (1990)
11. Stern, E. A., Sayers, D. E. and Lytle, F. W., *Phys. Rev. B: Solid State II*, 4836-4845, 1975
12. Rehr, J. J., *Physica B* 158 (1989) 1-4 (XAFS V)
13. Huang, M., Yuan, C., Wei, S. and Wang, Q., *in press*
14. Koningsberger, D. C., *XAFS VI*, Ed. S. Hasnain, York, August, 1990, p.28
15. Soeya, T, Kim, D.S., Matsubayashi, N., Shimada, H., Nishijima, A. & Segawa, K., *Photon Factory Activity Report #7* 1989, P.80
16. Clozza, A., Bianconi, A., Garcia, J., *Physica B*, 158, 162, 1989

**Table 1 Mo Coordination Shells in Mo,Ni-Y-Zeolites**

MoNiY					MoNiYD			
Model	CN	R(Å)	DWF.10 <sup>2</sup>	d-E <sub>0</sub> (eV)	CN	R(Å)	DWF.10 <sup>2</sup>	d-E <sub>0</sub> (eV)
Mo-O	3.2±.2	2.03±.01	0.01±.00	-4.3±.6	2.2±.2	2.00±.01	-0.27±.02	-1.1±.1
Mo-O	1.4±.1	2.62±.01	-0.69±.06	-7.6±.7	0.7±.1	2.61±.01	-0.77±.04	8.4±.6
Mo-Ni	0.9±.2	3.54±.01	0.40±.03	7.1±.6	0.1±.0	3.63±.02	-0.83±.05	7.0±.6
Mo-Mo	3.4±.1	3.70±.02	-0.14±.01	6.1±.4	3.6±.3	3.68±.02	-0.05±.02	6.0±.4
Mo-Si	1.5±.1	4.05±.02	-0.02±.02	-3.0±.3	1.0±.1	4.00±.02	-0.40±.03	3.3±.3
NiMoY					NiMoYD			
Model	CN	R(Å)	DWF.10 <sup>2</sup>	d-E <sub>0</sub> (eV)	CN	R(Å)	DWF.10 <sup>2</sup>	d-E <sub>0</sub> (eV)
Mo=O	0.5±.1;	1.55±.01	-0.03±.01	13.5±3.	0.1±.0	1.53±.01	-0.37±.02	11.7±.9
Mo-O	3.2±.3	1.71±.01	0.04±.01	6.8±.7	2.3±.2	1.72±.01	-0.06±.01	6.8±.6
Mo-O	1.2±.2	1.98±.01	-0.48±.02	-12.6±.8				
Mo-Mo	2.2±.4	3.31±.01	-0.03±.01	3.7±.3				

**Table 2 Ni Coordination Shells in Mo,Ni-Y-Zeolites**

NiMoY					NiMoYD			
Model	CN	R(Å)	DWF.10 <sup>2</sup>	d-E <sub>0</sub> (eV)	CN	R(Å)	DWF.10 <sup>2</sup>	d-E <sub>0</sub> (eV)
Ni-O	4.3±.2	2.08±.01	0.01±.01	-0.6±.3	4.1±.3	2.07±.01	0.13±.01	2.4±.3
Ni-Si	2.7±.2	2.68±.01	0.22±.01	12.8±.9	1.9±.2	2.66±.01	0.10±.01	14.3±.9
Ni-Ni	2.3±.1	3.03±.01	0.77±.01	-1.2±.5	2.9±.2	2.98±.01	0.72±.04	5.5±.5
Ni-Ni	1.8±.1	3.94±.01	0.42±.01	8.2±.7	2.1±.2	3.96±.01	0.40±.01	3.9±.4
Ni-Mo	4.0±.4	4.51±.02	0.72±.01	14.2±.1.	4.0±.3.	4.53±.02	0.70±.08	15.0±1.2
Ni-O	2.1±.2	4.95±.02	-0.91±.01	-9.6±.3	2.9±.4	4.97±.02	-0.78±.0	-11.3±.4
MoNiY					MoNiYD			
Model	CN	R(Å)	DWF.10 <sup>2</sup>	d-E <sub>0</sub> (eV)	CN	R(Å)	DWF.10 <sup>2</sup>	d-E <sub>0</sub> (eV)
Ni-O	4.9±.2	2.04±.01	0.36±.01	6.5±.4.	3.2±.3	2.05±.01	-0.13±.01	9.3±.4

Note: The experimental standard data are used for fitting: Mo-O(CN=4,R=1.78) from ZnMoO<sub>4</sub> and Mo-Mo (CN=12,R=2.73Å) from Mo metal foil; FEFF program was used to calculate the standard data for Mo-Si(CN=12, R=2.69Å), Mo-Ni(CN=12, R=2.61Å), Ni-O(CN=6,R=2.09Å), Ni-Si(CN=12,R=2.69Å), Ni-Ni(CN=12,R=2.96Å) and Ni-Mo(CN=12, R=2.61Å).

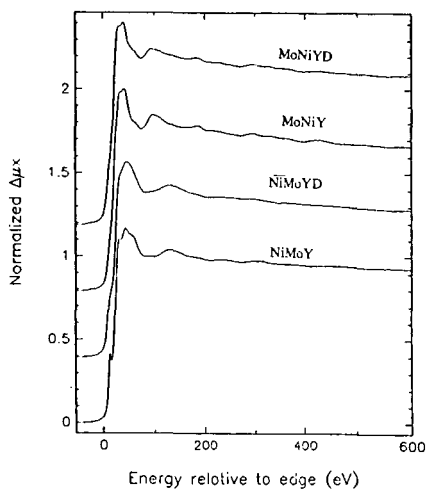


Fig.1 The normalized X-ray absorption spectrum versus energy for Mo in MoNiYD and MoNiY in which Mo were introduced first and in NiMoYD and NiMoY where Ni first. The energy scale is relative to the binding energy of the Mo 1s state (20,000 eV).

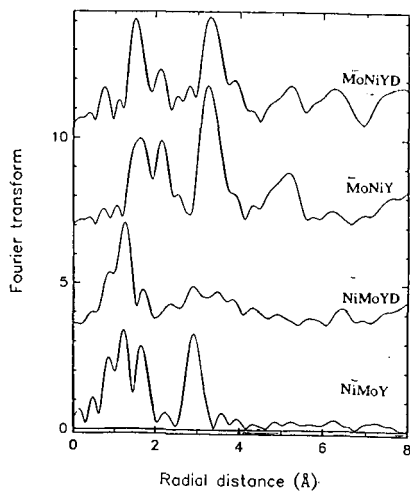


Fig.2 A comparison of the magnitudes of the Fourier transforms of the weighted Mo EXAFS for MoNiYD, MoNiY, NiMoYD and NiMoY zeolites versus R. The transforms are all of  $k^3X(k)$  and taken over a k-space range of  $3-14 \text{ \AA}^{-1}$ .

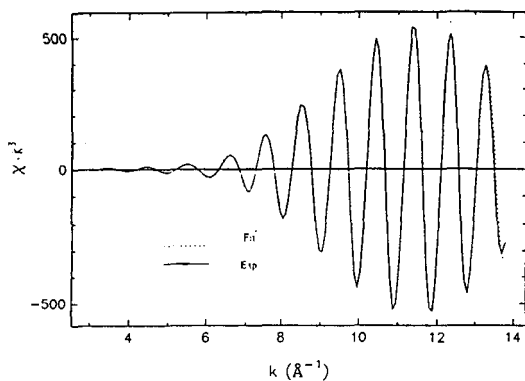


Fig.3 An overplot of the Fourier filtered  $k^3X(k)$  data of Mo in MoNiY and the best fitting results (see Table 1) versus R. The fitting range was from 2.86 to 3.74 $\text{\AA}$ . The fit included Mo-Mo, Mo-Ni and Mo-Si contributions.

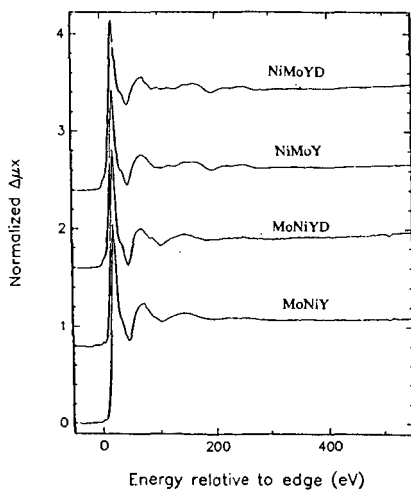


Fig. 4 The normalized X-ray absorption spectrum versus energy for Ni in NiMoYD and NiMoY in which Ni were introduced first and in MoNiYD and MoNiY where Mo first. The energy scale is relative to the binding energy of the Ni 1s state.

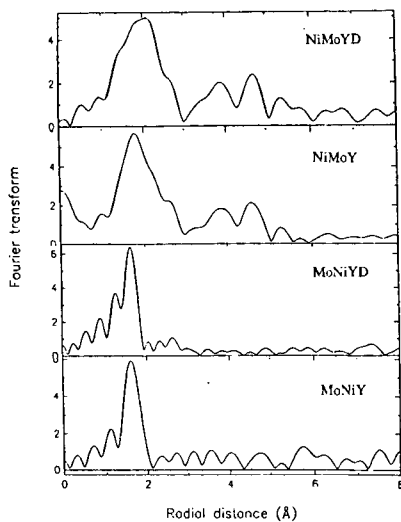


Fig.5 A comparison of the magnitudes of the Fourier transforms of the weighted Ni EXAFS for NiMoYD, NiMoY, MoNiYD and MoNiY zeolites versus R. The transforms are all of  $k^3X(k)$  and taken over a k-space range of  $3-14 \text{ \AA}^{-1}$ .

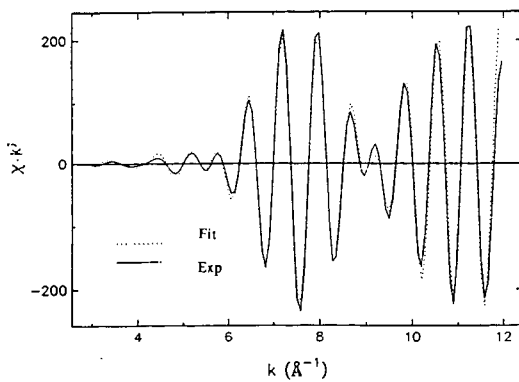


Fig.6 An overplot of the Fourier filtered  $k^3X(k)$  data of Ni in NiMoY and the best fitting results (see Table 2) versus R. The fitting range was from 3.0 to 5.1Å. The fit included Ni-Ni, Ni-Mo and Ni-O contributions.

**SYNTHESIS OF C<sub>5</sub> ETHERS FROM METHANOL AND 2-METHYL-1-PROPANOL  
(ISOBUTANOL)**

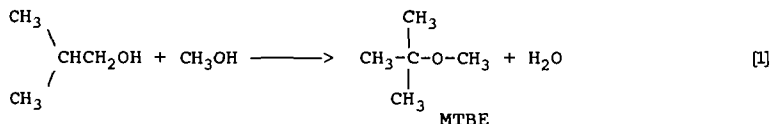
K. Klier, R.G. Herman, M.A. Johansson, and O.C. Feeley  
Department of Chemistry, S.G. Mudd #6  
Lehigh University, Bethlehem, PA 18015

Keywords: Alcohol dehydration, Ether synthesis

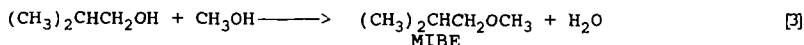
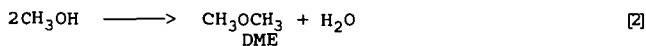
Introduction

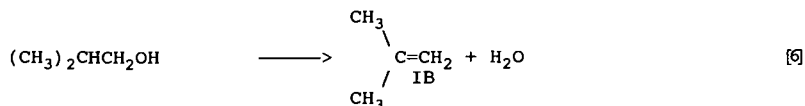
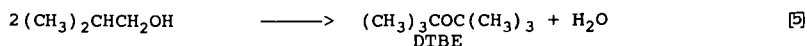
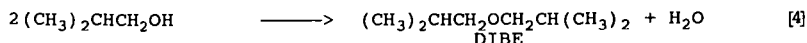
Methyl-tertbutyl ether (MTBE) and tertamyl-methyl ether (TAME) technology is well established with methanol and a branched olefin (iso-butene or 2-methyl-butene) as source feedstock (1,2). The recently announced engineering innovation of reaction with distillation led to a new process, ETHERMAX, by Dow-Hülse-Kohl (3), in which the thermodynamic equilibrium is shifted in favor of MTBE by the product removal directly in the catalytic reactor. Despite the very fast growth of the MTBE and TAME production capacity worldwide, there is a potential shortage of the feedstock olefins (4) and by some accounts of methanol (5), should MTBE/TAME be used as the principal oxygen additive and octane booster for partial replacement of aromatics in gasolines (3).

As isobutene can be obtained by dehydration of 2-methyl-1-propanol (isobutanol) and isobutanol can be directly synthesized from the syngas CO/H<sub>2</sub> (6,7), there is an alternative route to MTBE via the syngas-derived isobutanol. Still a more attractive route to MTBE would be via the direct coupling of alcohols,



if the selectivity of the process could be controlled so that reaction [1] is the dominant route. There are several other reactions that can occur in a system that couples isobutanol with methanol: coupling of two methanol molecules to dimethyl ether (DME) [2], of methanol and isobutanol to methyl-isobutyl ether (MIBE) [3] which is a low octane isomer of MTBE, of two isobutanol molecules to di-isobutyl ether (DIBE) [4] or di-tertbutyl ether (DTBE) [5], dehydration of isobutanol to isobutene (IB) [6], and oligomerization of isobutene to C<sub>8</sub>, C<sub>12</sub>, etc. hydrocarbons.

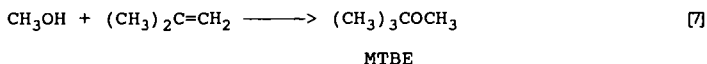




All of the above reactions [1] - [6] are acid-catalyzed, and the use of solid acids is preferred to that of acid solutions. The factors influencing selectivity are thermodynamic constraints, the concentration and strength of the catalyst acid sites, and mass transfer related phenomena such as shape- or diffusion controlled selectivity in zeolites. In this work we report on the selectivities of isobutanol-methanol coupling over two classes of catalysts, organic polymeric sulfonic acids and inorganic acids based on silica-alumina, mordenite, montmorillonite, and sulfate-modified zirconia.

#### Thermodynamic Considerations

The standard free energies for the key reactions involved in the set [1] - [6] are represented in Figure 1 for two temperatures, 298 and 400K. It is evident that at 400K and above, the synthesis of MTBE from methanol and isobutene [7]



becomes a thermodynamically uphill process while if the two alcohols are the reactants in reaction [1], the path to MTBE is exoenergetic. Further, the mixed ether isomer of MTBE, MIBE, that is readily formed over Nafion H (8), is a thermodynamically less favorable product than MTBE. Elevated pressure will favor the ether-forming reactions [1] - [5] over the dehydration of isobutanol [6] in which the molar volume increases when going from the left to the right.

#### Kinetic Considerations

Although kinetics of reactions [1] - [6] and related processes have been studied in detail only over Nafion H (9), it is important to summarize the main features of that kinetic behavior here, because the kinetic patterns provide guidelines for testing protocol over a wide range of catalysts. The results of kinetic studies of coupling methanol with isobutanol over Nafion H yield the following conclusions:

- (i) Dehydration of isobutanol to IB, reaction [6], requires two acid sites, one of which binds isobutanol and one that supplies an acid catalyzing function for the isobutanol dehydration. The consequence of this kinetic behavior is that at high pressures, isobutanol poisons its own

dehydration and the kinetic order becomes negative with isobutanol concentration. Methanol also exhibits a retarding effect on isobutanol dehydration by competitive adsorption and blocking of the acid sites.

- (ii) The formation of DME, reaction [2], and DIBE, reaction [4], requires two sites occupied by the respective alcohol, methanol for DME and isobutanol for DIBE. The consequence of this behavior is that at high pressures, the kinetics become "saturated" and the rates of DME or DIBE reach constant values.
- (iii) The formation of MIBE, reaction [3], requires two sites occupied by the two different alcohols. The consequence of this behavior is that there is a maximum rate at an optimum ratio of partial pressures of the two alcohols. Quantitative evaluation of the observed rates shows that isobutanol is approximately two times more strongly held by the acid sites of Nafion H than methanol.
- (iv) The conversion of MIBE to the thermodynamically more stable MTBE or isobutene and methanol is kinetically strongly hindered.

The dual site character of all catalyzed reactions involved imposes a requirement that the acid sites be highly concentrated on the surface of any prospective heterogeneous catalyst. Further, pressure is recognized as an important variable controlling the selectivity to ethers (high pressures) or isobutene (low pressures).

#### Organic Polymeric Catalysts

In this section, we compare the outcome of isobutanol-methanol coupling under standard test conditions developed in this laboratory. Reaction conditions were similar to those described in Nunan et al (8). The test reaction used 5 g of catalyst at 90°C under a total pressure of 1 atm. The flow rate of each alcohol was 1.72 mol/kg cat/hr and was achieved by pumping an equimolar mixture of isobutanol and methanol. The flow rate of He and N<sub>2</sub> is 16 mol/kg cat/hr. The catalyst bed was diluted to 20 cm<sup>3</sup> with Pyrex beads. The organic polymers were all sulfonic derivatives in their hydrogen form, and they are listed in Table I.

Steady state conversions were obtained within the first hour of the reaction. Data were collected for several hours time-on-stream during which no catalyst deactivation was detected. The results of the standard test over these polymers are summarized in Table II. The major products, excluding water, of the reaction of the two alcohols are given in this table. In addition, minor amounts of C<sub>6</sub> and C<sub>12</sub> hydrocarbons, formed from the di- and trimerization of isobutene, were detected. The order of activity of the catalyst was found to be Amberlyst ≈ Purolite > BioRad > Nafion.

Product selectivities for the different catalysts are illustrated by Figure 2. Water, which is, of course, the major product of these dehydration reactions, is not included in the selectivity analysis. Under the standard reaction conditions, Nafion-H appears to be the best catalyst for MIBE production. The other catalysts produce significant amounts of MTBE, along with other ethers, viz. DTBE, DIBE, and DME. The higher selectivity of Nafion towards MIBE formation may be due to the distinctly different nature

of the acid sites of Nafion. The sulfonic acid groups of perfluorinated Nafion contrast with the sulfonic acid groups of the other hydrocarbon based resins tested in this study.

#### Inorganic Solid Acid Catalysts

The following inorganic acid catalysts were tested: H-Mordenite (Norton),  $\text{SiO}_2/\text{Al}_2\text{O}_3$  (Davison), Montmorillonite K-10 (Aldrich), and  $\text{ZrO}_2$  treated with sulfuric acid, which will be designated as  $\text{ZrO}_2/\text{SO}_4$ .

The preparation of  $\text{ZrO}_2/\text{SO}_4$  was according to the work of Hino and Arata (10).  $\text{ZrOCl}_2 \cdot 8\text{H}_2\text{O}$  was added to aqueous ammonia to precipitate  $\text{Zr}(\text{OH})_4$  which was washed and dried at 100 °C overnight. The dried  $\text{Zr}(\text{OH})_4$  weighing 10 g was placed on a folded filter paper and 150 ml of 1N  $\text{H}_2\text{SO}_4$  was poured through it. The wet powder was dried at 110°C overnight and then calcined at 620 °C for 3 hr. Pretreatment of other catalysts consisted of calcination of Mordenite and  $\text{SiO}_2/\text{Al}_2\text{O}_3$  at 400°C, the Montmorillonite catalysts being used as received.

The reaction conditions and catalyst weight used for the inorganic catalysts were identical to those used for the organic catalysts mentioned above. In addition, in light of their much higher temperature stability, the inorganic catalysts were studied at reaction temperatures of 125°C, 150°C, 175°C, as well as 90°C.

The results of the standard test over these inorganic catalysts are summarized in Table IV.

The product selectivities of these catalysts are shown in Figures 3-6. Water, the coproduct of all the dehydration reactions, is not included in the selectivity calculations.

The patterns that emerge are the following:

- (i) H-mordenite is a selective catalyst for dehydration of methanol to DME. Isobutanol is not converted to any ethers or dehydrated significantly to isobutene over H-mordenite under the conditions used. Evidently the pore size or shape of H-mordenite restricts reactions of isobutanol; even though the isobutanol molecule is small enough to enter the larger channel pores of mordenite, its conversion is suppressed by one or all of the following three classic mechanisms of zeolite shape selectivity: (a) inaccessibility of acid centers that possibly reside primarily in the narrow side channels of the mordenite structure; this type of size exclusion in alcohol dehydration was first studied by Weisz et al. (11), however it should be noted that acid sites in mordenite are accessible to molecules as large as 1-methyl-2-ethylbenzene at higher temperatures (12) (b) retardation of isobutanol transport by preferential diffusion of methanol, diffusive selectivity was studied by Chen and Weisz (13) (c) size restrictions on the transition states involving isobutanol, isobutyl esters, and isobutyl oxonium ions. Csicsery first proposed the concept of restricted transition state selectivity in zeolites (12).

- (ii) Sulfate-modified zirconia is an efficient and highly selective catalyst for the dehydration of isobutanol to isobutene, with methanol dehydration to DME suppressed. The reasons for this selectivity pattern have not been established but it is tentatively suggested that isobutanol is more strongly bonded than methanol to the sulfate groups on the zirconia surface so that methanol activation is suppressed. The relative bonding strength of isobutanol and methanol to the sulfate-modified zirconia would have to be more markedly different than that on Nafion H because DME and MIBE are co-products with isobutene over Nafion H but not over the sulfate-modified zirconia.
- (iii) There is an overall order of activities for the dehydration reactions over the inorganic acids used,  
 $\text{ZrO}_2/\text{SO}_4^{2-} > \text{H-mordenite} > \text{SiO}_2/\text{Al}_2\text{O}_3 > \text{H-Montmorillonite}$
- (iv) The inorganic catalysts are generally less active than the organic polymeric catalysts at 90°C except for H-mordenite which is active and selective for methanol dehydration to DME. Higher temperatures are needed for significant alcohol dehydration with inorganic catalysts. In general, the organic polymeric catalysts are unstable at these higher temperatures.

#### Conclusions

Acid-catalyzed reactions of an equimolar mixture of methanol and 2-methyl-1-propanol (isobutanol) gave rise to homo- and heteroethers, as well as to isobutene, depending on the catalyst used. The organic polymeric acids were selective towards MIBE which is a low octane isomer of MTBE. A particularly high selectivity to DME was displayed by H-mordenite, evidently due to a combination of factors that are summarily termed "shape selectivity". The sulfate-modified zirconia proved to be a selective catalyst for isobutanol dehydration to isobutene, with ether formation suppressed. The inorganic catalysts displayed a lower activity than sulfonated organic resins and thus higher temperatures were needed, but the sulfate-modified  $\text{ZrO}_2$  has proven to be promising when isobutene is a desirable product of alcohol isobutanol dehydration in the mixture with methanol. The significant advantages of inorganic catalysts are their applicability at high temperatures and ease of regeneration.

#### Acknowledgements

This work was supported by the U.S. Department of Energy Grant No. DE-AC22-90PC90044.

#### References

1. Chase, J. D. and Galvez, B. B., *Hydrocarbon Process.*, 60(3) (1981) 89.
2. Chase, J. C., in "Catalytic Conversions of Synthesis Gas and Alcohols to Chemicals," ed. by R. G. Herman, Plenum Press, New York (1984) 307.
3. Ainsworth, S.J., *Chem. & Eng. News*, (June 10, 1991) 13.
4. Shearman, J., *Chem. Eng.*, (July 1991) 44v.
5. *Oil & Gas Journal*, (Aug. 19, 1991) 28.

6. Nunan, J. G.; Bogdan, C. E.; Klier, K.; Smith, K. J.; Young, C.-W.; and Herman, R. G., *J. Catal.*, 116 (1989) 195.
7. Nunan, J. G.; Herman, R. G.; and Klier, K., *J. Catal.*, 116 (1989) 222.
8. Nunan, J. G.; Klier, K.; and Herman, R. G., *J. Chem. Soc., Chem. Comm.*, (1985) 676.
9. Nunan, J. G.; Klier, K.; and Herman, R. G., to be submitted.
10. Hino, M. and Arata, K., *J. Chem. Soc., Chem. Commun.*, (1980) 851.
11. Weisz, P.B.; Frilette, V.J.; Maatman, R.W.; and Mower, E.B., *J. Catal.*, 1, (1962) 307.
12. Csicsery, S.M., *J. Catal.*, 19, (1970) 394.
13. Chen, N.Y.; Mazuik, J.; Schwartz, A.B.; and Weisz, P.B., *Oil & Gas Journal*, (Nov. 18, 1968) 154.

**TABLE I**  
**Organic Catalysts**

	Polymer base	Resin type	Decomposition Temperature
Amberlyst-15	Polystyrene	Macroreticular	≈120 °C
Purolite 150	Polystyrene	Macroreticular	≈120 °C
BioRad AG50WX2	Polystyrene	Gel	≈120 °C
Nafion-H	Fluorocarbon	Gel	>200 °C

**TABLE II**  
**Yields over Organic Catalysts**  
**(mol/kg cat/hr)**

	DME	Butenes	MIBE	MTBE	C8 ether
Amberlyst-15	0.042	0.041	0.053	0.013	0.014
Purolite 150	0.034	0.048	0.062	0.011	0.015
BioRad AG50WX2	0.015	0.011	0.040	0.004	0.008
Nafion-H	0.004	0.002	0.014	0.0003	0.003

TABLE III

Yields over Inorganic Catalysts  
(mol/kg cat/hr)

	T <sub>Reaction</sub>	DME	Butenes	MIBE	MTBE	C8 ether
H-Mordenite	90°C	0.060	-----	-----	-----	-----
	125°C	0.6599	-----	-----	-----	-----
	150°C	0.83	0.068	-----	-----	0.004
ZrO <sub>2</sub> /SO <sub>4</sub> <sup>=</sup>	90°C	-----	-----	0.003	-----	-----
	125°C	0.006	0.067	0.02	0.003	0.008
	150°C	0.027	0.696	0.068	0.009	0.017
	175°C	0.103	1.29	0.049	0.007	-----
SiO <sub>2</sub> /Al <sub>2</sub> O <sub>3</sub>	90°C	-----	-----	-----	-----	-----
	125°C	0.007	0.028	0.011	0.001	0.003
	150°C	0.021	0.225	0.032	0.005	0.014
	175°C	0.039	0.943	0.049	0.007	0.016
Montmorillonite	90°C	----	-----	-----	----	-----
	125°C	0.008	0.008	0.008	----	0.004
	150°C	0.019	0.071	0.019	0.004	0.014
	175°C	0.034	0.378	0.029	0.014	0.031

Fig. 1 Free energy of ether synthesis reaction pathways

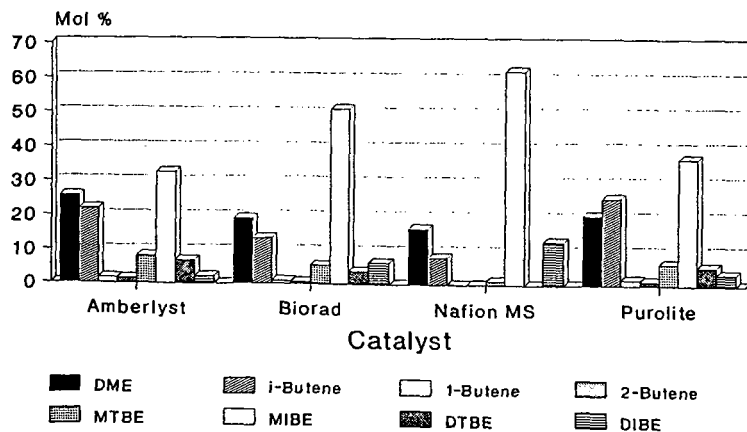
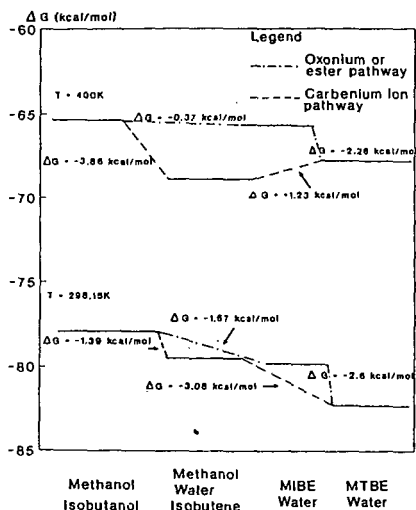


Fig. 2 Selectivity over organic catalysts for the methanol + isobutanol reaction at 90 °C.

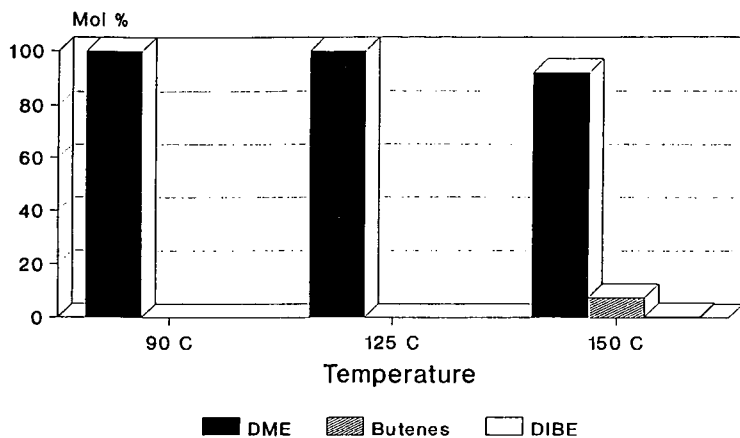


Fig. 3 Selectivity over H-mordenite for the methanol + isobutanol reaction at various temperatures.

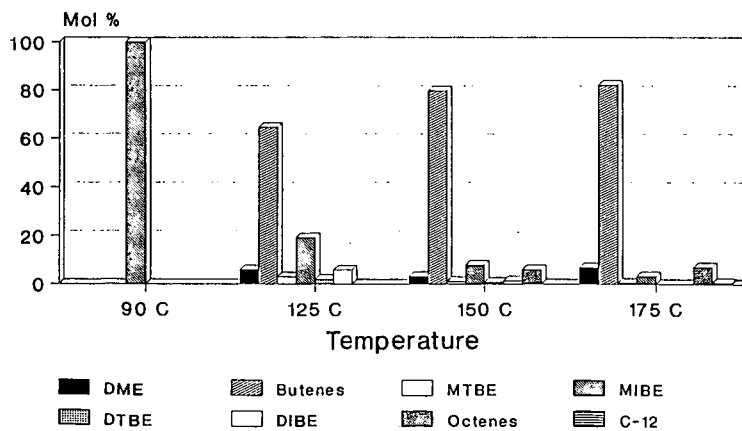


Fig. 4 Selectivity over ZrO<sub>2</sub>/SO<sub>4</sub> for the methanol + isobutanol reaction at various temperatures.

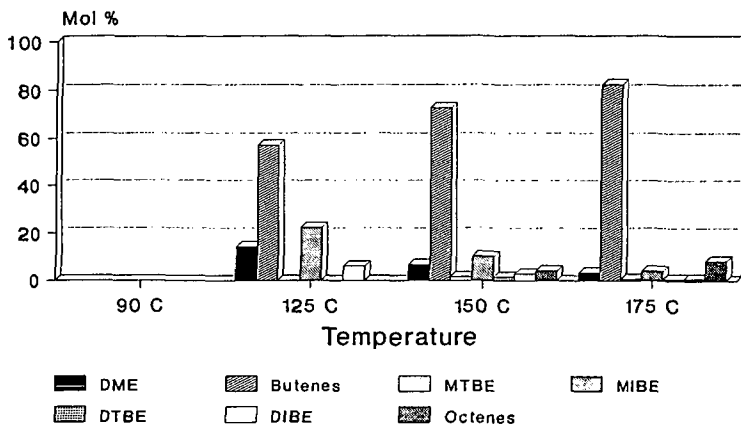


Fig. 5 Selectivity over SiO<sub>2</sub>/Al<sub>2</sub>O<sub>3</sub> for the methanol + isobutanol reaction at various temperatures.

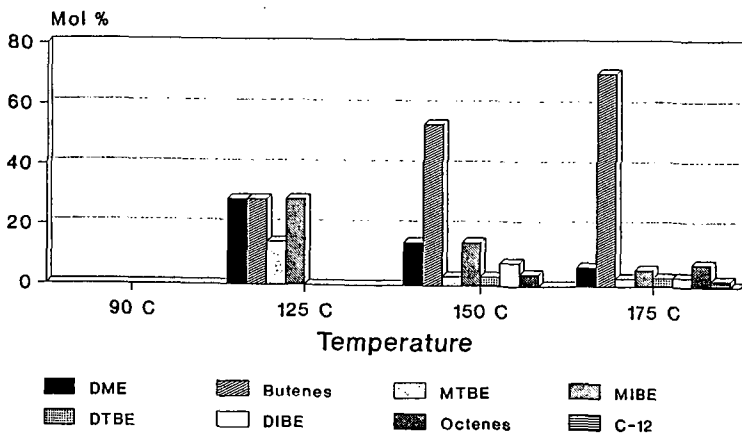


Fig. 6 Selectivity over Montmorillonite for the methanol + isobutanol reaction at various temperatures.

# ISOBUTYLENE SYNTHESIS OVER ZIRCONIA AND MODIFIED ZIRCONIA USING HYDROGEN LEAN SYNTHESIS GAS

by

Rayford G. Anthony, Walter Postula, Zhentao Feng, C. V. Philip, and Aydin Akgerman  
Kinetics, Catalysis and Reaction Engineering Laboratory  
Department of Chemical Engineering  
Texas A&M University  
College Station, TX 77843-3122

## INTRODUCTION

Early work on isobutylene and isobutane synthesis employed thoria based catalysts. Later isoalkenes were produced when zirconia was used at lower pressures and temperatures of 623 to 773 K. The difficultly reducible oxide catalysts such as  $\text{ThO}_2$  (1,2) and  $\text{Dy}_2\text{O}_3$ , (3) were used under very severe conditions. A  $\text{CdO}$  catalyst combined with acid supports was used under mild conditions. Recently, Maruya, et al.(4) and Onishi et al. (5) reported the use of  $\text{ZrO}_2$  at mild conditions, and methoxide species and formate ions have been observed on the surface of the  $\text{ZrO}_2$  catalysts. Maruya, et al. (6) also produced a  $\text{C}_4$  fraction with 99% isobutylene with carbon  $\text{C}_4$  selectivities in the range of 77 to 85%. The latter value was obtained when zirconia was impregnated with  $\text{NaOH}$ . The mechanism for formation of the branched alkanes has been postulated to be different than the mechanism for formation of linear alkanes.

Vedage et al. (7) postulated that linear products are produced by  $\text{CO}$  insertion into an alkoxide instead of an aldol-like condensation scheme in which a formyl species reacts with an enolate ( $\text{RCH}_2\text{-HCHO}$ ) at the carbon next to the carbonyl carbon. Mazanec (8) proposed a  $\text{CO}$  insertion scheme involving a bound aldehyde to produce a cyclic acyl which has two valence structures and the carbonyl carbon in one has carbenic character. Subsequent 1,2 shifts of hydrogen or R can lead to linear or branched products. Condensations reactions between eta-enolates and alkoxides were proposed to account for deviations from the Schulz-Flory distribution. Tseng et al. (9) and Jackson and Ekerdt (10) present the results of a comprehensive study and discuss proposed mechanisms on isosynthesis using zirconia. The formation of  $\text{C}_4\text{s}$  is postulated to be by addition and condensation reactions (4,6,9,10).

This manuscript reports data on isobutylene synthesis using zirconia prepared by coprecipitation and modified sol gel procedures.

## CATALYSTS SYNTHESIS AND CHARACTERIZATION

**Synthesis:** The two procedures used for synthesizing the catalysts presented herein were as follows: [1] Reaction of zirconyl nitrate with ammonium hydroxide which precipitates as zirconium hydroxide and is then dried and calcined at 500 °C for 2.5 hours. This catalyst is labelled Cat 1. [2] The sol gel procedures developed by Dosch et al. (11) were used to produce a sodium hydrous zirconium oxide, which was ion exchanged with  $\text{HCl}$  to remove the sodium, washed with acetone, dried and calcined at 500 °C for 4 hours. This catalyst is referred to as Cat 2.

**Characterization:** Differentiation between cubic zirconia and tetragonal zirconia by use of XRD has been reported to be very difficult to impossible. Cubic zirconia is normally formed at temperatures above 1200 °C except in the presence of alkali or alkaline salts. The cubic form can then be stabilized at lower temperatures. Inspection of XRD powder patterns suggests that one should be able to distinguish between the cubic and tetragonal forms. However, this is very difficult to accomplish except for highly crystalline zirconia. Catalysts prepared by procedure 1 could be made as tetragonal or monoclinic depending on the procedure used in calcination. Only the zirconia which had a monoclinic structure as indicated by an XRD powder pattern was used in this study.

The hydrous sodium zirconium oxide prepared by Dosch's method had an ion exchange capacity of approximately 4.5 meq/g. For the catalytic evaluations the sodium content was decreased to less than 0.3% using HCl exchange and then calcined at 500 °C for 4 hours. After calcination Catalyst #2 appeared to be monoclinic. Zirconia formed by this method should be more acidic than the zirconia prepared according to procedure #1.

## CATALYSTS EVALUATION

Two reactor systems, one constructed by us referred to as BR1 and an AE MSBTR 900 purchased from Autoclave Engineers, were used in the evaluation of the catalysts. For both systems the catalysts were loaded and purged with nitrogen at 400 °C for 4 hours prior to conducting the activity studies. Catalytic activity data reported herein for the precipitated catalysts, Cat. #1 batches 3 and 4, were obtained in the BR1 and AE MSBTR 900, and catalytic activity data reported for Cat. #2 were obtained using the AE MSBTR 900, only. Methanol and higher alcohols were detected as product from Cat. 1 when using the AE MSBTR 900, which had on-line analysis of the products. The analysis of the product for BR1 was off-line, and no alcohols were detected in the product stream. Figure 1 illustrates the activity and effect of pressure on CO conversion for zirconia using catalysts CAT 1&2. The space time,  $\tau$ , is defined as the bulk volume of the catalysts divided by the volumetric feed rate calculated at reaction conditions. The actual residence time is greater than the space time because of the decrease in the number of moles with reaction. However, at low conversions space time is a close approximation to residence time, which is dependent on the extent of reaction. Figure 1 shows that pressure does not have a significant effect on conversion at equal space times for a 1:3 or a 1:1 CO:H<sub>2</sub> ratio. Similarly results were obtained by Pichler and Ziesecke (1,2) for thoria catalysts. The data also indicate that Cat. #2 is not as active as Cat. #1. Figure 2 illustrates the expected trend for change in conversion with space time at 95 atm. and 400 °C and 50 atm and 425 °C. A space time of 90 seconds is required to obtain 20% CO conversion. Figure 3 illustrates the expected increase in conversion with increasing temperature for the two catalysts. The trends are the same indicating essentially the same reaction mechanism and activation energy.

In order to gain some insight into the type of reactions occurring several ratios were calculated, and are presented in Table 1. Table 1 illustrates the average values obtained for the isosynthesis profile, the branched to linear C<sub>4</sub>s and the isobutylene selectivity within the C<sub>4</sub> fraction. The isosynthesis profile was defined by Jackson and Ekerdt (10) as the ratio of C<sub>4</sub>s to (C<sub>2</sub>s + C<sub>3</sub>s), and is a measure of the relative importance of the condensation reactions. Ratios obtained in this study are comparable with the values reported by Jackson and Ekerdt (10).

Figures 4, 5, and 6 illustrate the effect of pressure, space time, and CO:H<sub>2</sub> ratio on the molar ratio of isobutylene to methane and the weight ratio of isobutylene to C<sub>2</sub>\* for Cat. #1. Figure 4 shows that for a 1:3 CO:H<sub>2</sub> ratio and low CO conversions (<5%) the isobutylene to

$C_5^+$  decreases as the pressure is increased, but the molar ratio of isobutylene to methane is essentially constant at 0.3. However, Figure 5 shows that for 95 atm and a 2:1 CO:H<sub>2</sub> ratio, the isobutylene to methane molar ratio varies from 0.5 to 0.75 as the CO conversion is increased with an increase in residence time. Figure 6 shows the effect of temperature and pressure on the ratio of isobutylene to  $C_5^+$ . Low pressures and high temperatures increases the ratio.

### CONCLUSIONS

The bench scale reactor systems have been successfully operated for a period of approximately one month with the collection of a substantial amount of data. The data reported above are for batches 3 and 4, Cat. 1. Data were also obtained on a catalyst prepared by catalyst preparation #2. Batches 3 and 4 for preparation of Cat. 1 were chosen because the XRD patterns and Raman spectra indicated they were predominately monoclinic, unlike the result obtained for other batches. Cat 2 was used to study the effect of acidity, and the effect of using a the modified sol gel method for preparing the catalyst. Experiments on Cat #1 in both reactor systems demonstrated the reproducibility of our experimental techniques. The activity of the zirconia catalysts are low and long residence times are required to obtain high CO conversions.

### ACKNOWLEDGEMENT

This work was done as a part of the U.S. Department of Energy on "Catalysts and Process Development for Synthesis Gas Conversion to Isobutylene," Contract No. DE-AC22-90PC90045, Texas A&M Research Foundation Project No. 6722

### LITERATURE CITED

1. Pichler, H., and Ziesecke, K-H., "Über die bei der Isosynthese entstehenden sauerstoffhaltigen Verbindungen, unter besonderer Berücksichtigung der Alkole," *Brennst. Chem.*, **31**, 360 (1950a).
2. Pichler, H., and Ziesecke, K-H., "The Isosynthesis," *Bur. Mines Bull.*, 488 (1950b).
3. Kieffer, R., G. Cherry, and R. E. Bacha, "Carbon Monoxide-Hydrogen Reactions. Mechanism of Isobutane Formation in Isosynthesis," *Mol. Chem.*, **2**(1), 11- 23 (1983).
4. Maruya, K., T. Maehashi, T. Haraoka, S. Narui, Y. Asakawa, K. Domen, and T. Onishi, "The CO-H<sub>2</sub> Reaction over ZrO<sub>2</sub> to Form Isobutene Selectively," *Bull. Chem. Soc. Jpn.*, **61**, 667-671 (1988).
5. Onishi, T., Maruya, K-I, Domen, K., Abe, H., and Kondo, J., "The Mechanism of CO Hydrogenation Over Zirconium Oxide Studied by FT-IR," *Catalysis: Theory to Practice*, Vol. 2 (M. J. Phillips and M. Ternan, Editors), Proceedings of the 9th International Congress on Catalysis, Calgary, (1988).
6. Maruya, K., T. Fujisawa, A. Takasawa, K. Domen and T. Onishi, "Effect of Additives on Selective Formation of Isobutene from the CO-H<sub>2</sub> Reaction over ZrO<sub>2</sub>," *Bull. Chem. Soc. Jpn.*, **62**, 11-16 (1989).
7. Vedage, G. A., P. G. Himerfarb, G. W. Simmons, and K. Klier, in "Solid State Chemistry in Catalysis" Eds. R. K. Grasselli and J. F. Bradzil, ACS Symposium Series No. 279 (1985).
8. Mazanec, T. J., "On the Mechanism of Higher Alcohol Formation Over Metal Oxide Catalysts" *J. Catal.* **98**, 115 (1986).

9. Tseng, S. C., N. Jackson, and J. G. Ekerdt, "Isosynthesis Reactions of Carbon Monoxide/Hydrogen Over Zirconium Dioxide," J. Catal. 109(2), 284-297 (1988),
10. Jackson, N. B. and Ekerdt, J. G., "The Surface Characteristics Required for Isosynthesis over Zirconium Dioxide and Modified Zirconium Dioxide," J. of Catal. 126, 31-45 (1990).
11. Dosch, R.G., Stephens, H. P., and Stohl, F. V., SAND89-2400, Sandia National Laboratories, 1990.

Table 1. Isothesis Characteristics of Catalyst 1 and Catalyst 2

Weight Ratios	Catalyst 1	Catalyst 2	Jackson & Ekerdt(10)
Isosynthesis Profile <sup>1</sup>	4.55 ± 1.28	2.29 ± 0.79	2.30
Branched C <sub>4</sub> /Linear C <sub>4</sub>	2.71 ± 0.67	2.97 ± 0.33	5.67
i-C <sub>4</sub> H <sub>9</sub> /All C <sub>4</sub> s	0.63 ± 0.06	0.37 ± 0.15	0.84

<sup>1</sup> Defined as (total weight of C<sub>4</sub> hydrocarbons)/(total weight of C<sub>2</sub>s and C<sub>3</sub>s).

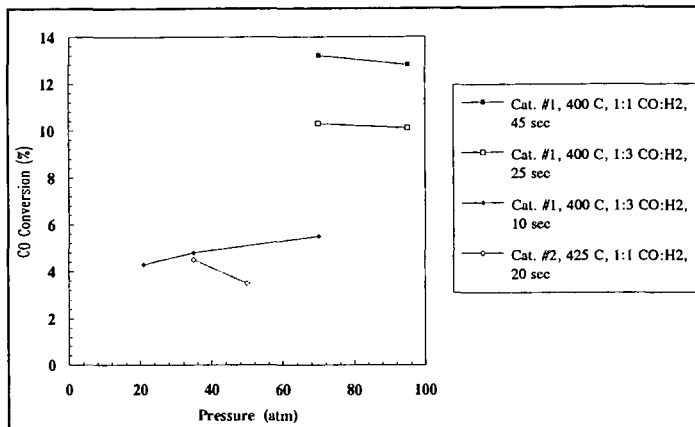


Figure 1. Effect of Pressure on Activity for Catalysts #1 and #2.

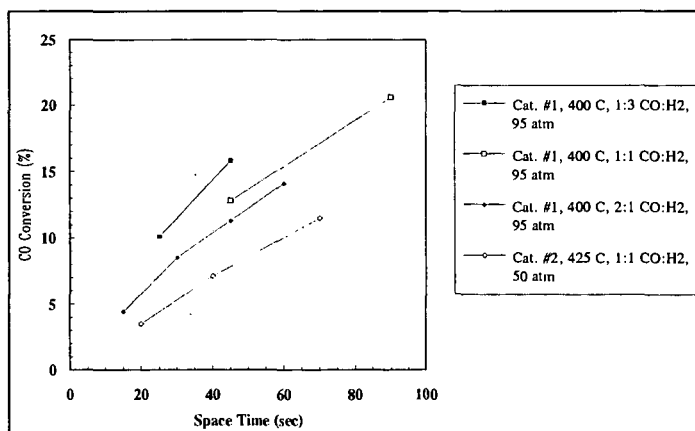


Figure 2. Effect of Space Time on Activity for Catalysts #1 and #2.

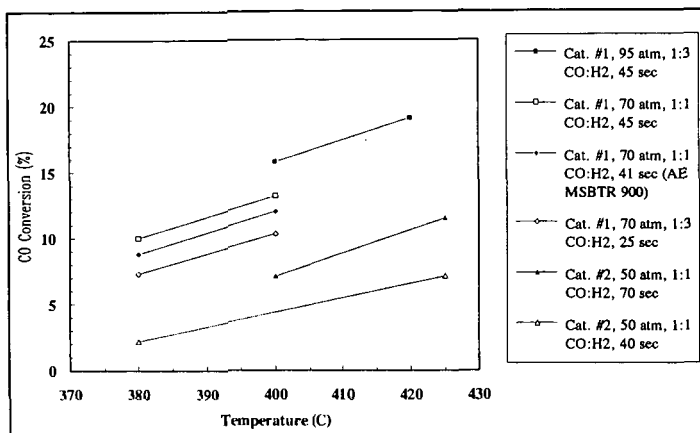


Figure 3. Effect of Temperature on Activity for Catalysts #1 and #2.

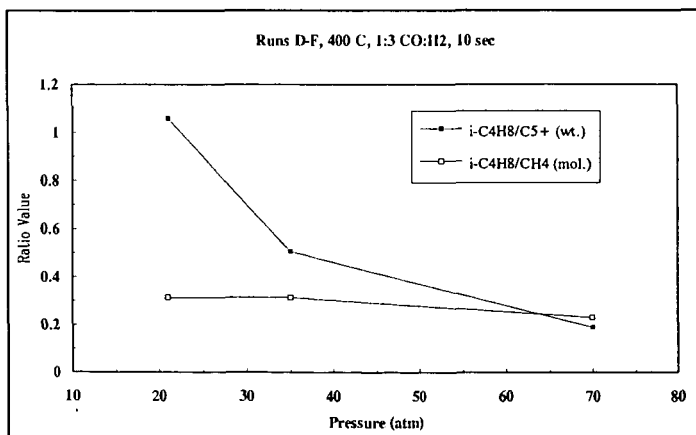


Figure 4. Effect of Pressure on Selectivities for Catalyst #1.

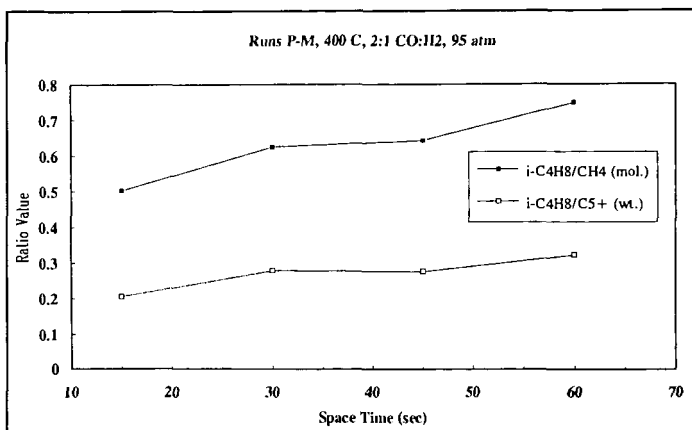


Figure 5. Effect of Space Time on Selectivities for Catalyst #1.

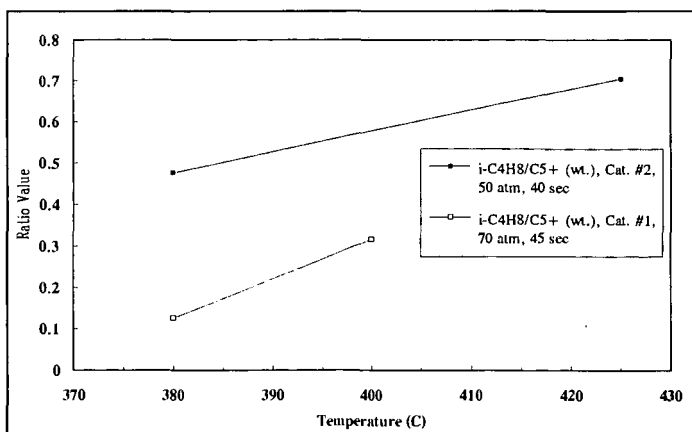


Figure 6. Wt. ratio of isobutylene/C<sub>5</sub>+ increases with temperature for Cat. #1 and #2.

## ACTIVITY, CHARACTERIZATION, AND SINTERING BEHAVIOR OF SULFATED IRON OXIDES IN LIQUEFACTION OF LOW PYRITE COALS.

V.R.Pradhan, J.W.Tierney, and I.Wender,  
Chemical and Petroleum Engineering Department,  
University of Pittsburgh, Pittsburgh, PA 15261.

Keywords: Highly dispersed catalysts, Direct coal liquefaction.

### Abstract

The activity of small amounts of iron and molybdenum added as finely divided sulfated oxide/oxyhydroxide catalysts ( $\text{FeOOH}/\text{SO}_4$ ,  $\text{Fe}_2\text{O}_3/\text{SO}_4$  and  $\text{Mo}/\text{Fe}_2\text{O}_3/\text{SO}_4$ ) for the direct liquefaction of low pyrite bituminous (Blind Canyon) and subbituminous coals (Wyodak) is reported in this paper. The quantification of dispersion and the composition of sulfated iron oxide/oxyhydroxide catalysts before and after coal liquefaction reactions is also reported. Catalytic dispersions (such as surface area and particulate size) were determined for the oxides and oxyhydroxides of iron containing 3-4 wt% of sulfate anion as such and after their transformation from the oxide phase to the sulfides during the course of coal liquefaction. The rates of these transformations were studied at 400°C and information on the size and composition of the resulting sulfide particles was obtained. It was found that the initially added sulfated iron oxides were completely converted to pyrrhotite,  $\text{Fe}_{1-x}\text{S}$ , after only five minutes of reaction at 400°C.  $\text{Fe}_7\text{S}_8$ , prepared by treating sulfated iron oxide with sulfur in the presence of tetralin, was also used as a catalyst for coal liquefaction and was found almost as effective as the initial sulfated iron oxide. 1000-5000 ppm of iron and 20-100 ppm of molybdenum were used in our catalytic systems with respect to coal. Molybdenum, used in small amounts, was more effective when used with the calcined form of the sulfated iron oxide than with its uncalcined form,  $\text{FeOOH}/\text{SO}_4$ .

### Introduction

Catalysis for direct coal liquefaction (especially for coal dissolution) by highly dispersed catalysts is a topic of considerable interest among researchers in this field<sup>[1]</sup>. Application of finely divided and chemically modified powdered solid catalysts, especially those based on cheap and environmentally benign iron, is very promising<sup>[2,4,5]</sup>. The objective of our research has been to develop novel catalytic systems based on the sulfate and molybdate anion-promoted oxides/oxyhydroxides of iron which can provide high dispersions and activity for coal liquefaction.

We have synthesized and characterized a number of sulfate-promoted oxides of metals such as Fe, Sn, Zr, Ti, and Hf.<sup>[3]</sup> We recently reported on the use of sulfate-promoted iron and tin oxides for the direct liquefaction and coprocessing of Argonne Illinois No.6 coal with tetralin and with Maya ATB heavy oil respectively<sup>[6,7]</sup>. The sulfate anion treatment of iron(III)oxides was found to enhance their acidic character and bring about a decrease in the particulate size. Sulfated iron oxides were also found to be active as catalysts at low iron concentrations (3500 ppm with respect to coal) for coal liquefaction. The sulfated iron oxide catalysts were completely converted to highly dispersed (average size = 15 nm) pyrrhotites ( $\text{Fe}_{1-x}\text{S}$ ) under coal liquefaction conditions in the presence of enough sulfur.

In this paper, we discuss the properties and activities of a new class of sulfated catalysts. These are based on sulfated oxyhydroxides of iron,  $\text{FeOOH}/\text{SO}_4$  and  $\text{Mo}/\text{FeOOH}/\text{SO}_4$ . A comparison is made between the activities of different sulfated iron oxyhydroxides promoted with molybdenum. The effects of small catalyst concentrations (20-100 ppm Mo and 1000-5000 ppm Fe) on conversion levels of a low-pyrite Blind Canyon coal were studied. An attempt was made to characterize the composition and the extent of dispersion of the sulfided catalysts obtained during coal liquefaction reactions. This includes study of the rate at which the initial sulfated metal oxide is converted to the corresponding sulfide under coal liquefaction conditions and also determination of the extent of catalyst particle agglomeration with time at reaction temperature.

## Experimental

**Catalyst Preparation and Characterization:** The sulfated oxides and oxyhydroxides of iron were prepared from either the sulfate, chloride, or nitrate salts precipitated with either ammonia water or urea depending on whether heterogeneous or homogeneous coprecipitation routes were followed. Small amounts of molybdenum (0.5-2 wt% of the iron oxyhydroxides) were introduced into the catalysts by the incipient wetness impregnation technique from an aqueous solution of ammonium heptamolybdate. The catalysts were characterized by BET-surface area analysis, sulfur analysis, thermogravimetry (TGA), acidity measurements, thermal stability measurements, X-ray diffraction, and electron microscopy. The residues of coal liquefaction experiments were also analyzed using X-ray diffraction and a JEOL 2000 FX STEM (100 kV beam) with an energy dispersive X-ray spectrometer (EDX) to determine composition and dispersion information about the catalytic phases formed under liquefaction conditions.

**Reaction Studies:** The low-pyrite Blind Canyon obtained from the Penn State Coal Research Bank and Wyodak (subbituminous) obtained from the Argonne Premium Coal Sample Bank were used for these studies. Elemental analyses of the two coals are shown in Table 1. Tetralin was used as the reaction solvent (3:1 by weight to coal) and elemental sulfur (2:1 by weight to catalyst) was used for catalyst sulfidation. Coal liquefaction reactions were carried out in both a 300 cc stainless steel autoclave reactor and a 27 cc tubing bomb microreactor. Elemental sulfur was used in excess for sulfiding catalysts in situ. Soxhlet extraction with methylene chloride was used to determine coal conversion. Soluble products were recovered by rotary evaporation at 45°C under vacuum. Pentane solubles (oils) were determined by adding 40 volumes of n-pentane to the methylene chloride solubles and using Soxhlet extraction with n-pentane. Pentane-insoluble but methylene chloride soluble material was referred to as asphaltenes.

## Results and Discussion

**Catalyst Characterization:** Specific surface areas of the sulfated iron oxyhydroxides and oxides, modified with small amounts of molybdenum, were determined by the BET method. In going from the unsulfated oxyhydroxides to the sulfated ones, surface areas increased from about 40  $\text{m}^2/\text{g}$  to 127  $\text{m}^2/\text{g}$ . Nitrogen adsorption porosimetry measurements indicated a bimodal distribution of the pores (essentially the void spaces between the primary crystallites). X-ray diffraction line broadening measurements and transmission electron microscopy indicated the particle size of the oxyhydroxides to be between 15-20 nm. The particles were elongated and needle-shaped. Differential thermal analysis studies of the sulfated oxyhydroxides indicated that crystallization to

the oxides occurred above 450°C. The presence of small amounts of the sulfate group in the oxyhydroxides, thus, delayed the crystallization (and therefore crystal growth) by about 150°C. Sulfated oxyhydroxides also exhibited a significant chemisorption of pyridine at high temperatures indicating a strong surface acidic character. A summary of catalyst properties is given in Table 2; the uncalcined sulfated iron oxyhydroxide has a specific surface area higher than its calcined form, sulfated iron oxide. The molybdate anion ( $\text{MoO}_4^{2-}$ ), added in small amounts (3 wt% of the oxide), exhibits a similar influence on the catalyst properties as does the sulfate anion.

### **Reaction Studies:**

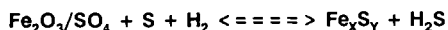
*1. Effect of Reaction Temperature :* The following three catalytic systems were used for the liquefaction of Argonne Wyodak coal (0.17 % pyrite) at different temperatures to determine the qualitative effect of reaction temperatures on the activities of these catalysts for coal conversion:  $\text{Fe}_2\text{O}_3 + \text{S}$ ,  $\text{Fe}_2\text{O}_3/\text{SO}_4 + \text{S}$ , and  $\text{Mo}/\text{Fe}_2\text{O}_3/\text{SO}_4 + \text{S}$ . As shown in Figure 1, the activities of sulfated catalysts for the production of oils (n-pentane solubles) from coal increased proportionately in going from 375 to 425°C.

*2. Sulfated Iron Oxyhydroxides and Molybdated Iron Oxide :* The  $\text{FeOOH}/\text{SO}_4$  and  $\text{Fe}_2\text{O}_3/\text{MoO}_4$  catalysts resulted in comparable levels of coal conversion to n-pentane solubles as did the sulfated iron oxide for the liquefaction of Wyodak coal (Figure 2) under similar reaction conditions. From these results we see that the effect of anions in modifying the catalytic properties of transition metal oxides is not anion-specific so long as the modifying anion is held by the oxide surface strongly even at high temperatures. The effect of adding sulfuric acid separately with the unsulfated iron oxide was not the same as that of previously sulfated iron oxide. The combination of pure iron oxide and dilute sulfuric acid resulted in a slightly higher conversion values than the iron oxide alone, but these conversions were lower than those obtained with presulfated iron oxide.

*3. Effect of Iron and Molybdenum Catalysts Loadings on Liquefaction of Low-Pyrite Blind Canyon Coal :* In order to study the effect of small catalyst loadings on coal conversion levels, it was necessary to use a coal containing as low an amount of pyritic iron as possible. For this reason, Blind Canyon coal was chosen for these studies. Sulfated iron oxyhydroxide, which was found as active as the sulfated iron oxide catalyst, was employed as catalyst for the runs carried out to determine the effect of small loadings of iron on coal conversion (1000-5000 ppm with respect to coal). The results are shown in Figure 3. It can be noted from Figure 3 that the catalytic effect of added iron (as 15 nm size  $\text{FeOOH}/\text{SO}_4$  catalyst) becomes significant only above 2500 ppm of iron with respect to coal. The incorporation of small amounts of molybdenum into this sulfated oxyhydroxide ( $\text{Mo}/\text{FeOOH}/\text{SO}_4$ ) was not as effective for coal conversion as that in the sulfated iron oxide ( $\text{Mo}/\text{Fe}_2\text{O}_3/\text{SO}_4$ ). The lack of high molybdenum dispersion due to the absence of a calcination treatment for the earlier catalyst might be part of the reason for its lower activity as compared with the calcined catalyst,  $\text{Mo}/\text{Fe}_2\text{O}_3/\text{SO}_4$ . The effect of molybdenum loadings between 20-200 ppm (with respect to coal) added with 2500 ppm Fe as  $\text{Mo}/\text{Fe}_2\text{O}_3/\text{SO}_4$  is shown in Figure 4. Additional amounts of molybdenum in an already active sulfated iron oxide do not bring about significant enhancement in total coal conversions (conversions increase from about 75 % in the absence of Mo to about 80 % in its presence), but the yield of light oil (n-pentane soluble products) is significantly enhanced in the presence of small amounts of Mo. This suggests that

molybdenum, due to its strong hydrogenation function (in the form of  $\text{MoS}_2$ ), helps to produce more oil at the expense of the asphaltenes.

**Catalyst Transformation and Sintering Studies:** It is well understood now that any iron-based catalyst precursor added at the beginning of coal liquefaction is converted to iron sulfides in the presence of enough sulfur under liquefaction conditions. The quantification of sulfided phases, thought to be catalytic, is essential for the understanding of the mode of action of the iron-based catalysts. We have made an attempt to investigate the rate of transformation (i.e. compositions of sulfides formed at different reaction times) and the extent of catalyst sintering (i.e. the degree of catalyst dispersion) of the iron-containing phases that result from addition of sulfated iron oxides during coal liquefaction. In general, the stoichiometry (or composition) of the iron phases formed during liquefaction is controlled by the following equation:



The objective here is to determine the atomic ratio (Fe/S) and the grain sizes of the iron-phases in the coal liquefaction residues using analytical tools such as X-ray diffraction and electron microscopy. The composition of the catalysts (sulfated and sulfided phases) and their sizes have been studied at different reaction times using the following model systems:

- (I) Active carbon + tetralin +  $\text{Fe}_2\text{O}_3/\text{SO}_4$  catalyst
- (II) Tetralin + S +  $\text{Fe}_2\text{O}_3/\text{SO}_4$  (Presulfidation)
- (III) Low-pyrite Blind Canyon coal + S + finely divided iron catalysts + tetralin

Active carbon was used instead of coal to avoid interference due to the mineral matter from coal. The reactions were carried out under identical conditions as coal liquefaction with the addition of elemental sulfur for metal sulfidation. When the reactions were carried out with a sulfated iron oxide catalyst for different reaction times, it was found that the initial sulfated iron oxide takes about five minutes at reaction temperature to convert completely to the sulfided iron phases, i.e., pyrite and finally pyrrhotites. The grain size changes occur primarily during this transformation. No further changes (increases) in the grain size of iron-containing phases was observed even when the reaction was carried out for two hours. The initially added sulfated iron oxide catalyst (particle size = 20 nm) were converted completely to pyrrhotite after five minutes of reaction (particle size = 10-50 nm). A similar transformation picture was seen when a soluble precursor of iron,  $\text{Fe}(\text{CO})_5$  was used. Figure 6 shows the transmission electron micrographs of the sulfated iron oxide before and after reaction treatment as in the model system (II) indicated earlier. As shown in Figure 5, all of the initial sulfated iron oxide had been converted to pyrrhotites, primarily,  $\text{Fe}_7\text{S}_8$ . There was no apparent increase in the grain size during this high temperature transformation. Figure 6 compares the particle sizes of the sulfided iron catalysts derived *in situ* from  $\text{FeOOH}/\text{SO}_4$  and  $\text{Fe}(\text{CO})_5$  precursors during direct liquefaction of Blind Canyon coal. The results of catalyst size and composition studies obtained using the model system (I) followed by examination of the residues by XRD, TEM, and EDX, are summarized in Table 3. Complete transformation of the initially added sulfated iron oxide catalyst to pyrrhotite occurred after five minutes at reaction temperature. The grain size change associated with this phase change was observed by electron microscopy, while particle sizes of the sulfided phases essentially remained the same without much further agglomeration or sintering for two hours of reaction time.

### Conclusions

The increase in total conversion as well as the increase in conversion to oils obtained with sulfated oxides is attributed primarily to enhanced "dispersion" (surface area/gm) with possibly a small contribution, made early on, from the high surface acidity of these oxides. Due to increase in the specific surface area and decrease in the average particle size of the oxides upon addition of small amounts of the sulfate group, conversion of the oxides to active catalytic sulfide phases, especially to non-stoichiometric sulfides of iron, is facilitated. More of the active catalyst surface of these sulfides becomes available for reaction and catalyst agglomeration is decreased. Sulfated iron-based finely divided catalysts result in better catalytic dispersion than soluble precursors such as  $\text{Fe}(\text{CO})_5$ . Addition of small amounts of molybdenum to the sulfated iron oxides increases its activity, especially for the production of oils.

### References

1. Derbyshire, F.J., Energy & Fuels, **1989**, 3, 273-277.
2. Suzuki, T., Yamada, H., Sears, P., Watanabe, Y., Energy & Fuels, **1989**, 3, 707-713.
3. Pradhan, V.R., Tierney, J.W., Wender, I., Prep. Pap., Am. Chem. Soc., Div. Fuel Chem., Vol. 35, No. 2, **1990**.
4. Cugini, A.V., Utz, B.R., Krastman, D., Hickey, R.F., Balsone, V., Prep. Pap., Am. Chem. Soc., Div. Fuel Chem., Vol. 36, No. 1, **1991**.
5. Herrick, D.E., Tierney, J.W., Wender, I., Huffman, G.P., Energy & Fuels, **1990**, 4, 231-235.
6. Pradhan, V.R., Huffman, G.P., Tierney, J.W., Wender, I., Energy & Fuels, **1991**, 5, 497-507.
7. Pradhan, V.R., Herrick, D.E., Tierney, J.W., Wender, I., Energy & Fuels, **1991**, 5, 712-720.

**Table 1. Elemental Analyses of Coals (All in weight percents)**

Coal	Carbon	Hydrogen	Nitrogen	Oxygen	Sulfur	Pyritic Sulfur
Wyodak	75.0	5.4	1.1	18.0	0.5	0.17
Blind Canyon	81.6	6.2	1.4	10.3	0.5	0.02

**Table 2. Summary of Catalyst Characterization Before Reaction**

Catalyst	Wt % SO <sub>4</sub>	Surface Area, m <sup>2</sup> /g	Average Size, nm (XRD)	Average Size, nm (TEM)
Fe <sub>2</sub> O <sub>3</sub>	0.0	26.8	46	65
Fe <sub>2</sub> O <sub>3</sub> /SO <sub>4</sub>	3.4	81.7	12	20
Mo/Fe <sub>2</sub> O <sub>3</sub> /SO <sub>4</sub>	3.1	81.5	12	20
FeOOH/SO <sub>4</sub>	10.2	127.0	12	25
Fe <sub>2</sub> O <sub>3</sub> /MoO <sub>4</sub>	0.0	88.0	09	15

**Table 3. Results of Catalyst Transformation and Sintering Studies on Model System (I)**

Reaction Time	Iron-Phases Detected	Average Particle Size (XRD)	(Fe/S) Atomic Ratio
0 min.	Fe <sub>2</sub> O <sub>3</sub> , Fe <sub>3</sub> O <sub>4</sub> , FeS <sub>2</sub> , Fe <sub>1-x</sub> S	14 nm	1.4
30 min.	Fe <sup>0</sup> , FeS <sub>2</sub> , Fe <sub>1-x</sub> S	16 nm	1.0
120 min.	Fe <sub>1-x</sub> S	16 nm	0.9

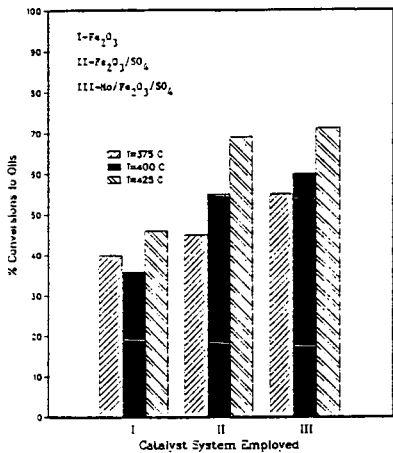


Figure 1. Activity of Sulfated Catalysts for Direct Liquefaction of Wyodak Coal at Three Reaction Temperatures

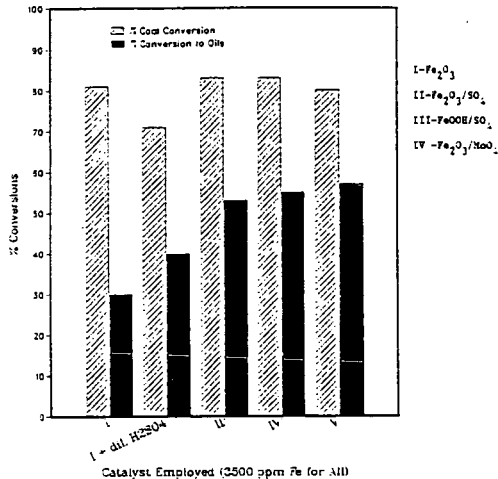


Figure 2. Activity of Oxyhydroxide and a New Molybdated Catalyst for Liquefaction of Wyodak at 400°C

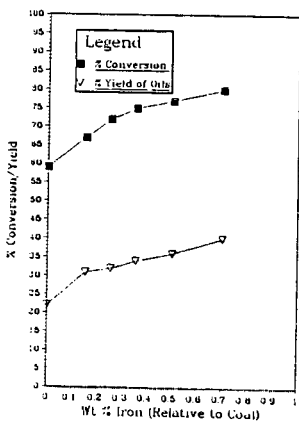


Figure 3. Conversion of Blind Canyon vs. Iron Concentration at 400°C

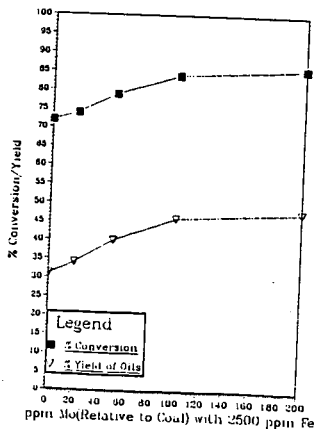


Figure 4. Conversion of Blind Canyon vs. Molybdenum Concentration at 400°C

*Before Reaction-*

Size = 20 nm



*After Reaction-*

Size = 20 nm

$Fe_7S_8$

$Fe_{11}S_{12}$



*From  $FeOOH/SO_4$*

size = 10-25 nm



*From  $Fe(CO)_5$*

size = 20-50 nm

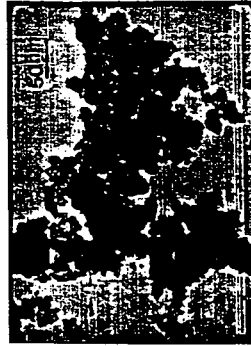


Figure 5. Sulfated Iron Oxide Catalyst: Before and After Sulfidation Reaction.

Figure 6. Dispersion of Fe-Containing Particles after Coal Liquefaction Reaction using Two Different Precursors.

## CATALYTIC REACTIONS OF SULFIDED IRON- AND MIXED METAL-PILLARED CLAYS

Edwin S. Olson and Mary L. Yagelowich  
Universal Fuel Development Associates, Inc.  
Grand Forks, ND 58201

and

Ramesh K. Sharma  
University of North Dakota Energy and Environmental Research Center  
Grand Forks, ND 58202

Key words: catalysts, pillared clays, coal liquefaction

### ABSTRACT

Iron-pillared montmorillonites were prepared by several methods and tested in hydrocracking and hydrogenation reactions. Rapid collection of the iron-intercalated clays was necessary for maximum activities, as was removal of residual sodium ions by exchange with ammonium ions. Calcination and sulfidation of the iron-pillared clays resulted in the formation of pyrrhotite, much of it in particles large enough to exhibit sharp XRD peaks. Thus the iron tends to migrate from its originally dispersed state, and surface area decreases with collapse of the layers. Alumina-pillaring prior to, or simultaneously with, intercalation of the iron resulted in more stable catalysts. The combined effects of clay acidity and hydrogen activation by the pyrrhotite resulted in high conversions in hydrocracking and hydrogenation tests. The presence of pyrrhotite resulted in minimal coking and condensation reactions.

### INTRODUCTION

The goal of the UFDA catalyst research program is the development of disposable, highly dispersed, high surface area catalysts for the direct liquefaction of coal. These catalysts consist of sulfided iron clusters intercalated into smectite clays. The smectite clays are swelling phyllosilicate minerals, commonly found as components of soils and sediments and often found as large, mineralogically pure deposits (1). These materials are highly useful in many chemical applications because of their small particle size ( $<2 \mu$ ), appreciable surface area for adsorption of organic molecules, and unique intercalating capabilities. Hence, they are utilized for supporting microcrystalline or metal cluster catalytic sites. Acid-modified smectites were used for a number of years as petroleum-cracking catalysts in the Houdry process, giving gasoline in high yields (1). In the mid 1960s they were replaced by more thermally stable and selective zeolite catalysts.

The use of large stable cations to pillar the aluminosilicate layers of clays results in the formation of porous networks analogous to zeolites. In these pillared clays, intercalation of hydroxylated or complexed metal cations maintains the clay layer structure after loss of water and generates a large micropore dimension. These structures are stable up to 450° to 500°C in contrast to the nonpillared clays which dehydrate and collapse at temperatures over 200°C. Acid zeolites are more stable at high temperatures; however, their pores are too narrow to be useful for coal macromolecules. The advantage of the pillared clay catalyst over the zeolites is that pore size can be controlled and made larger

than that of most of the zeolites. Therefore, these pillared clay catalysts may be more effective in cracking the large coal macromolecules than the conventional catalysts. The intent of this work is to discover how to obtain finely dispersed iron sulfide (pyrrhotite) catalytic sites in the pillared clay structure that will be useful for coal liquefaction.

## RESULTS AND DISCUSSION

Initial work was concerned with preparation methods for iron-pillared montmorillonites. The sodium form of this clay disperses to an extremely fine particle size in an aqueous medium with low concentrations of base. This form was preferred for metal ion exchange reactions that give the intercalated clays, since the clay layers are highly separated in this state and mass transfer is rapid. Iron in the form of a polyoxytriiron (III) complex (heptaacetatohydroxytriiron nitrate) was exchanged for the interlayer cations of the dispersed sodium montmorillonite (2). The iron-exchanged clays were subsequently calcined to form the stable polyoxyiron cation-pillared clays. For creation of catalytic sites for activation of hydrogen, the oxyiron species were converted to sulfide forms by treatment with hydrogen sulfide or carbon disulfide.

Intercalation of polyoxytriiron resulted in a change in particle-size distribution, with a substantial portion of larger particles (78%) being formed by agglomeration of the very fine particles. A fine particle fraction was also isolated by high-speed centrifugation. Calcination of the two fractions gave materials consisting of larger particles. X-ray diffraction studies of both calcined catalyst precursor fractions showed that hematite and maghemite (both  $\text{Fe}_2\text{O}_3$ ) had formed. The material from the fine clay particles contained hematite in greater abundance than that from the larger particles. The formation of these different compositions during the calcination of the iron-exchanged clays may be attributed to partial hydrolysis of the triiron clusters during washing and collection procedures. The fine particles were exposed to water for a much greater period of time. These data appear to be similar to those obtained by Lee and others (3) for pillaring with hydrolyzed ferric chloride, which indicated that hematite particles had formed. The  $d_{001}$  peak corresponding to the interlayer spacing was quite broad in the  $2\theta$  plot for both samples, indicating that spacings are irregular in the calcined products.

The difference in iron oxide composition between the calcined fine and larger particles of intercalated clay was further investigated by using a more rapid method in collection of the fine particles. X-ray diffraction of the calcined clays from the fine particles had a much smaller amount of hematite than the clay prepared by the former method. Thus the  $2\theta$  plots of catalyst precursors obtained from both the fine and larger particles in this preparation were very similar.

Methods for conversion of the oxyiron-intercalated clays to active sulfide forms were compared. Sulfidation was carried out either by heating the calcined precursor with a mixture of  $\text{H}_2\text{S}$  (100 psi) and  $\text{H}_2$  (900 psi) in the rocking heater at  $400^\circ\text{C}$  for 2 hr or by in situ reaction with 40 mg of carbon disulfide that was added with the test compound, decalin solvent, or coal, depending on the reaction being carried out. The catalysts prepared by treatment with  $\text{H}_2\text{S}$  exhibited major peaks corresponding to pyrrhotite. The pyrrhotite peaks were relatively narrow, indicating that the particle size of the iron sulfide in the catalyst may be larger than desired for high catalyst activity. Sulfidation under these conditions may have mobilized the iron in the pillars so that some larger iron sulfide particle formed, as described by Lee and others (3). In contrast, the

catalysts activated by in situ treatment with  $\text{CS}_2$  did not show significant peaks for pyrrhotite or pyrite. Since sulfidation did occur, the iron sulfide species in these catalysts must be very minute. As described below, these catalysts had superior hydrocracking activities.

When sulfidation was carried out with larger amounts of  $\text{H}_2\text{S}$ , x-ray diffraction showed that much of the iron was converted to pyrite rather than pyrrhotite. The pyrite-containing catalyst was easily converted back to the pyrrhotite form by further treatment with hydrogen at  $400^\circ\text{C}$ .

Surface areas of the fine particle and large particle iron-pillared clay catalysts were 156 and  $181 \text{ m}^2/\text{g}$ , respectively. However, on sulfiding the fine particle iron-pillared clay catalyst in  $\text{H}_2\text{S}$  and  $\text{H}_2$  at  $400^\circ\text{C}$  for 2 hours, the surface area dropped to  $17 \text{ m}^2/\text{g}$ . The reduction in surface indicates an undesired collapse of the interlayer structure or formation of iron sulfide agglomerates.

Hydrocracking activities of iron-pillared clay catalysts were determined by reacting with bibenzyl as the test compound. Reactions were carried out at  $350^\circ\text{C}$  for 3 hours in the presence of 1000 psi of molecular hydrogen in a 10-ml rocking autoclave reactor. The catalysts were recovered in quantitative amounts, and no retrograde reactions or coke were observed during reactions.

Comparison of the bibenzyl hydrocracking results for the initial sulfided catalysts prepared from the fine and larger iron-pillared clay particles showed that the catalyst from the hematite-containing fines had a much lower activity (62% conversion) than the catalyst from the large particles (80% conversion). The lower activity of the catalyst from the fines was attributed to hydrolysis reactions that occurred prior to calcining. For the second batch of pillared clays that were rapidly collected, the bibenzyl hydrocracking activities of the sulfided catalysts were essentially identical for the fine and larger particles (79 and 80% conversion, respectively). This observation was consistent with the low hematite content of both precursors as demonstrated by the similar  $2\theta$  plots described above.

Examination of the products obtained from the reactions of bibenzyl with sulfided iron-pillared clays provided information on the nature of the hydrocracking activity for the catalysts. The major products were benzene, toluene, and ethylbenzene. Benzene and ethylbenzene were the largest products, and the amount of benzene was considerably more than ethylbenzene, indicating the further cracking of the ethylbenzene to benzene. These products are indicative of the Brönsted acid catalysis mechanism. The mechanism involves the ipso protonation of an aromatic ring of bibenzyl, followed by aryl-methylene bond cleavage to form benzene and phenylethyl carbonium ion. The phenylethyl carbonium ion is reduced to ethylbenzene by hydride transfer or hydrogenation, or it could undergo a variety of reactions to give other products. This reaction mechanism is common in reactions catalyzed by clays and clay-supported catalysts. The formation of toluene probably occurs via a Lewis acid catalyzed mechanism, since the temperature is too low for homolytic cleavage of the central bond in bibenzyl. Reduction of carbonium ion intermediates in the reaction may or may not involve the iron sites.

The bibenzyl cracking products included many hundreds of other components, indicative of rearrangements and hydrogen addition as well as hydrocracking. Part of the single-ring aromatics was hydrogenated to give cycloalkanes in the reactions with sulfided catalysts. A substantial amount of methylcyclohexane was formed, probably from cleavage of the tertiary carbonium ion derived from

phenylethylcyclohexane or hydrogenation of the ring-protonated bibenzyl. Minor components formed as a result of hydrocracking were propylbenzene, butylbenzene, tetralin, ethylbibenzyl, and phenylethylbibenzyl, etc. The alkylbenzene products resulted from hydrogenation of bibenzyl followed by cracking reactions, probably involving Lewis acid sites.

A second factor in determining the activity of the catalysts was the concentration of iron introduced into the clay. Use of a smaller amount of iron might result in a lower number of pillars and, consequently, result in a larger micropore volume. Exchange of one-third of the total equivalents of sodium by the triiron acetate cation rather than using an excess of the triiron gave a catalyst, after calcination and sulfidation of the large particle fraction, that was as active in hydrocracking reactions (79% conversion) as the catalyst prepared previously with excess triiron complex. The fine particle fraction had a lower activity (33% conversion).

The presence of excess sodium in the catalyst brings up a question regarding the possible loss of Brönsted acid sites due to the presence of sodium cations. The sodium ions were exchanged out of one of the clays (from the fine particles) with ammonium ions following the iron-exchange. Calcination of this precursor to drive off ammonia gave a more active catalyst (64% conversion compared with 33%), because of regeneration of the Brönsted acid sites.

A comparison of the sulfided versus nonsulfided forms of the iron-pillared clays showed that the nonsulfided forms had a much lower hydrocracking activity (36 and 40% conversions for fine and large particles, respectively). These values are consistent with those obtained for other clay supports. Major products from nonsulfided catalysts were the same as those obtained with sulfided catalysts. The major difference in activity for the nonsulfided clays was the lower conversion, lower amounts of cyclohexanes, and lower proportion of ethylbenzene. Some of the reaction products were addition products of bibenzyl that may be regarded as Friedel Crafts addition products. However, extensive condensation and coke formation were not observed in the reaction. In comparison, acidic clay catalysts gave larger amounts of condensation products. Our results indicate that iron-pillared clays are effective in cleaving aryl-methylene and other C-C bonds at lower (350°C) temperature.

A general problem with the iron-pillared clays is that the calcination and/or sulfidation treatments appear to mobilize the iron and generate particles of the iron oxide and sulfide that are larger than desired for maximum utilization of the iron. Surface areas are also substantially decreased, owing to collapse of the layer structure. The use of discrete mixed alumina/iron-pillared clays or of alumina-pillared clays as supports for pyrrhotite active sites may give a more effective particle size for the iron sites and more stable pillared structures. The aluminum pillars are stable to calcining and sulfidation treatments.

Aluminum pillars were introduced by treatment of sodium montmorillonite dispersions with the oxaluminum cation, and various methods were investigated for intercalation of the iron. Several pillared clay catalysts with discrete pillars composed of alumina and of iron oxide were prepared by intercalation of sodium montmorillonite first with oxaluminum cations and then with oxiron cations (sequential pillaring). These materials differed in the amounts of alumina and iron oxide introduced. After calcining and sulfiding with hydrogen sulfide/hydrogen mixture, these catalysts exhibited high activities, with conversions of 85 to 88% in hydrocracking tests with bibenzyl. Neither the

concentration of alumina or iron had a significant effect on the activities, and a relatively low iron concentration (500 ppm) was quite active in the tests.

A second method for preparation of the discrete pillars was utilized. In this method, the oxyaluminum cations and the oxyiron cations were added simultaneously to the sodium montmorillonite in large excess. The catalyst obtained by calcining and sulfiding as above was nearly equally effective in hydrocracking tests with bibenzyl (83% conversion). Thus either the simultaneously or sequentially mixed pillared clays gave stable clays containing effective concentrations of pyrrhotite and acidic sites for catalysis.

The third method for preparing mixed pillared clays utilized a mixed oxymetal cation complex composed mainly of aluminum with a small amount of iron. This alloy-pillaring gave a catalyst with lower activity in hydrocracking tests (72% conversion). X-ray diffraction showed that iron from the alloy pillar had been converted to pyrrhotite by the sulfidation; hence, the lower activity is probably due to some collapse of the pillared structure during this transformation of the iron.

Since the presence of sodium ions was found to exert a significant negative effect on hydrocracking conversion, one of the sequentially pillared catalysts was treated with ammonium nitrate in order to exchange out any remaining sodium ions. After calcination to volatilize the ammonia and sulfidation, the catalyst gave a slightly better conversion in the bibenzyl hydrocracking test (89%).

The method of sulfiding the iron in the mixed metal-pillared catalyst was also varied. By adding a small amount of carbon disulfide to the reaction rather than presulfiding the catalyst with hydrogen sulfide/hydrogen, a significantly higher conversion of bibenzyl was obtained (94%). The reason for higher activity is suspected to be that the pyrrhotite particle size is smaller with this method of sulfiding (see discussion above).

In addition to effective catalysis of hydrocracking reactions at moderate temperatures, the iron-pillared clays were effective catalysts for catalyzing the hydrogenation of pyrene. Hydrogenation of pyrene with a sulfided ( $H_2S/H_2$ ) iron-pillared clay catalyst at 350°C for 3 hr gave an 88% conversion to hydrogenated pyrenes. The hydropyrene yields were better than those obtained with sulfided nickel molybdenum under identical conditions (69%). Conversion to the hexahydropyrenes had not proceeded very far in the latter case. A mixed metal-pillared catalyst was tested with pyrene at 400°C in the rocking microreactor with 1000 psi of hydrogen (measured at room temperature). A 68% conversion of the pyrene was obtained. The lower yield is consistent with the smaller equilibrium constant for hydrogenation at the higher temperature. Importantly, hydrocracking of the hydrogenated pyrenes was observed (20%) at the higher temperature. At 440°C, the conversion of pyrene dropped to 50%, and the yield of hydrocracked products increased slightly (23%).

Preliminary liquefaction testing with Wyodak subbituminous coal in tetralin solvent was performed using the discreet alumina/iron-pillared catalyst. The liquefaction reaction was carried out at 425°C for 1 hr in a 71-ml reactor with 1000 psi hydrogen (measured at ambient temperature). The catalyst was sulfided by adding a small amount of carbon disulfide. THF insolubles, THF solubles, and toluene solubles were measured by weighing. The pentane solubles consisted of coal-derived oil as well as tetralin solvent; therefore, the oil yield was determined by the difference between the isolatable products described above and the maf coal weight (thus the amount includes gases and reaction product water). For this reaction, yields of THF solubles were 19%, toluene solubles were 25%,

and oils/gases were 46%, with a total conversion to soluble products of 90%. The composition of the oil product was determined by gas chromatography of the pentane/tetralin solution. This analysis showed that the coal-derived oil product consisted of 9% phenolics and 25% hydrocarbons, based on maf coal. This product quality is better than previously attained with this coal in a 1-hr single-stage run. Further coal liquefaction tests are in progress.

#### ACKNOWLEDGEMENT

The support of the US Department of Energy is gratefully acknowledged.

#### REFERENCES

1. Ryland, L.B.; Tamale, M.W.; Wilson, J.N. Catalysis; Emmett, P.H. Ed.; Reinhold: New York, 1960, Vol. 7, Chap. 1.
2. Yamanaka, S.; Doi, T.; Sako, S.; Hattori, M. Mat. Res. Bull. 1984, 19, 161-168.
3. Lee, W.Y.; Raythatha, R.H; Tatarchuk, B.J. J. Catal. 1989, 115, 159-179.

Crystalline sodium or potassium silicon titanates prepared at temperatures of 200 °C or less as catalysts supports

R. G. Anthony<sup>a</sup>, C. V. Philip<sup>a</sup>, and R. G. Dosch<sup>b</sup>

<sup>a</sup>Kinetics, Catalysis and Reaction Engineering Laboratory, Department of Chemical Engineering, Texas A&M University, College Station, TX 77843-3122, United States

<sup>b</sup>Sandia National Laboratories, Div. 6212, Box 5800, Albuquerque, NM 87185, United States

## 1. INTRODUCTION

Hydrous sodium or potassium titanium and hydrous titanium/silicon oxides have been shown to be excellent precursors in the preparation of active hydrogenation catalysts (1,2,3,4). Anthony and Dosch (5) and Anthony et al. (6) recently reported the synthesis of six new layered crystalline titanates, and the catalytic activity of Pd and sulfided NiMo supported on these titanates. TS-1, a titanium-silicalite, is a mild oxidation catalyst for epoxidation of olefins and hydroxylation of phenols and aromatics when using hydrogen peroxide as the oxidant. Zorite, a natural molecular sieve with a Si/Ti ratio of 2.6, has been synthesized by Kuznicki, USP 4,853,202. He has also synthesized molecular sieves with Si/Ti ratios in the range of 2 to 10. Young, USP 3,329,481 synthesized a Si/Ti compound (TS 26), which he called a molecular sieve, but the XRD pattern is characteristic of a layered material.

This manuscript reports the synthesis and catalytic activity of sodium and potassium silicon titanates when used as precursors in preparation of sulfided NiMo catalysts. Catalytic activity is determined by using the model reactions, hydrogenation of pyrene at 300 °C and hydrodesulfurization of dibenzothiophene at 350 °C. Stephens et al. (7,8,9) have shown that rate constants for pyrene hydrogenation correlate with ultimate catalytic activity for coal liquefaction.

## 2. EXPERIMENTAL

The chemicals used in the preparation of a sodium silicon titanate (TAM-1) and a potassium silicon titanate (TAM-4) were tetraisopropyl orthotitanate, tetraethyl orthosilicate, an aqueous solution of sodium hydroxide, an aqueous solution of potassium hydroxide, a solution of tetramethylammonium hydroxide (TMAOH) in methanol, and tetraalkylammonium bromide (TRAB), where the alkyl group, R, was propyl, butyl or pentyl. The synthesis procedure was in two parts. First, an aqueous mixture containing all the reagents except the alkoxides was prepared. Second, the alkoxides were mixed and then added to the aqueous mixture while stirring and a gel formed. These ingredients were transferred to a reactor, which was placed in an oven preset to the appropriate temperature. Reaction times were 90 to 96 hours. The sodium silicon titanate was recovered by filtration and washing the precipitate with water and acetone. Typical molar ratios of Na or K:TMAOH:H<sub>2</sub>O:MeOH:TPAB:Si:Ti were 1:1.58:200:13:3:1:1 for TAM-1 and 2:0:175:0:2:1:1 for TAM-4. The procedure for preparing the sulfided nickel catalyst was the same as for the T2CT as reported by Anthony et al (6).

Activity experiments were conducted in minibatch reactors at 300 °C and 350 °C for pyrene hydrogenation and for hydrodesulfurization (HDS), respectively. The reactors were charged with 10 mg of catalysts, a solution containing 10% pyrene in hexadecane, and hydrogen pressure of 1000 psi at room temperature. The minibatch reactors were immersed in a constant temperature fluidized sand bath for a period of 15 minutes. After reaction the reactors were quenched, and the products were analyzed by gas chromatography. A similar procedure was followed for the HDS experiments, except dibenzothiophene was used instead of pyrene.

### 3. RESULTS AND DISCUSSION

#### 3.1 Catalyst Characterization

The XRD patterns for TAM-1 and TAM-4 are presented in Figures 1 and 2. TAM-1 had the following properties: The first peak of the XRD was at  $d_0$ -spacings of 1.47-1.5 nm. Other properties were surface areas of 150 to 170 m<sup>2</sup>/g, pore volumes of 0.9 to 1.0 cc/g, and a weight loss of 18 to 20% on heating for 10 hours in a vacuum at 170 °C. Weight loss on heating to 500 °C varied from 15 to 20% as compared to the 35 to 40% observed for TAM-4 and T2CT (6,7). The peaks at  $d_0$ -spacings of 5.4, 5.2, 3.71 and 3.60 nm disappeared after evacuation for 10 hours at 170 °C. The FTIR spectra shown in Figure 3 for TAM-1 has distinct peaks, a doublet or W shaped peaks in the range of 830 to 1020 cm<sup>-1</sup>. The relative intensities of the peaks at 1490 cm<sup>-1</sup> and 1640 cm<sup>-1</sup> are greater when tetrabutyl ammonium bromide is used in the synthesis compared to those when tetrapropyl ammonium bromide is used. The triplet at 4250 cm<sup>-1</sup> characteristic of quaternary ammonium compounds is present, but the absorption bands due to the primary C-H stretches are absent except when tetrapentyl ammonium bromide is used as the template. The average C:N ratio of  $6 \pm 1.2$  obtained for TAM-1 indicates incorporation of mostly TMAOH even though the TP<sub>3</sub>AB, TBAB, or TP<sub>4</sub>AB was used in the synthesis. When heating TAM-1 from 100 to 500 °C, the differential scanning calorimeter (DSC) recorded exothermic regions with peaks at 260 °C (376 mw/g) and 325 °C (543 mw/g). After heating TAM-1 for four hours at 500 °C or a shorter time at 700 °C, two phases as determined by XRD and electron microscopy characteristic of titania and silica were present.

The ion exchange capacity of TAM-1 was determined by using the following procedure. A 0.1 N HCl solution was added to a slurry of 50 mg TAM-1 in 50 ml of distilled, deionized water to maintain a pH of 3 for a period of 4 hours. Then it was filtered and rinsed with water and acetone and air dried. This procedure was repeated for the solids a second time. Eighty two percent of the sodium was removed in the first exchange and 86% of the remaining sodium was removed in the second exchange for a total sodium removal of 97.5 %. Hence, the ion exchange capacity was 4.1 meq/g, which is approximately equal to the initial sodium content (7.9 wt%).

TAM-4 had a  $d_0$ -spacing of 0.78 nm and a distinctly different XRD pattern from TAM-1. The quaternary ammonium compounds were not incorporated into the structure as indicated by the absence of the IR peak at 1490 cm<sup>-1</sup> in the FTIR spectra (Figure 4), and the low nitrogen content (<0.09%) from the CHN analysis. When heated to 500 °C for four hours or more the samples were converted to anatase titania and silica, and the percent volatiles was 40 to 45% (based on room temperature drying). If a sample was dried at 100 °C prior to calcination the volatiles were approximately 20%. TAM-4 was prepared with KOH/Ti ratios of 1.5 to 2.7, and variation of the concentration of the quaternary compounds appeared to have little effect on the XRD patterns of the final material. The DSC for TAM-4 was endothermic over the complete temperature range with a peak at 160 °C (-545 mw/g). Surface area of the as prepared TAM-4 was 194 m<sup>2</sup>/g

Analysis for titanium and silicon were determined by AA and ICP on selected TAM-1 and TAM-4 samples. The Si/Ti atomic ratios in the products were within 5% of the Si/Ti ratio in the charge solution.

Two U. S. patents (4,938,939, July 3, 1990, and 7,853,202, August 1, 1989) were issued in 1989 and 1990 to S. Kuznicki on the synthesis of small pore and large pore crystalline titanium/silica molecular sieves. These molecular sieves represent new structures with titanium in octahedral coordination and silicon in tetrahedral coordination. The Si/Ti ratios are in the range of 2 to 10 and preferably 5. The XRD patterns and compositions of these molecular sieves are significantly different than the titanates prepared in this study. However, work by Young, USP 3,329,481, claims the synthesis of a titanium silicate molecular sieve, TS-26. Examples presented by Kuznicki on Young's

work are a TS-26/ETS-1 are more fully characterized than the samples synthesized by Young. The bar spectra in Figure 2 is the XRD spectra for ETS-1/TS-26. TAM-4 appears to be a different material than ETS-1/TS-26 since the TAM-4 contains several new peaks, and not all of the remaining peaks match the bar spectra.

A material labelled ETS-2 was also synthesized by Kuznicki, but not claimed in the patent. The same procedure was used as in preparing TS-26, but no potassium was used in the synthesis. Even though the starting mixture contained approximately 1:1 Ti:Si, the material synthesized was "almost devoid of silica," and had significant peaks at 0.875, 0.370 and 0.316 nm with relative intensities of 85, 40, and 100, respectively. Obviously, this material is different than TAM-1 or TAM-4.

### 3.2 Catalytic Activity

A comparison of catalytic activity for hydrogenating pyrene to dihydropyrene using sulfided Ni/Mo supported on T2CT (6), TAM-1, TAM-4, hydrous titanium oxide, and hydrous silicon titanium oxide with the commercial catalysts, Shell 324 and Amocat 1C, is shown in Table 1. The data illustrate that sulfided Ni/Mo supported on T2CT (6), TAM-1, and TAM-4 have comparable activity on an active metal basis as the commercial catalysts and the Ni/Mo-Na<sub>0.5</sub>Ti amorphous catalyst, but the sulfided Ni/Mo Na<sub>0.5</sub>TiSi<sub>0.25</sub> amorphous catalyst has a much higher activity. For the amorphous Ti catalysts, as well as, T2CT(6), the majority (>98%) of the sodium was removed prior to loading with Mo and Ni by using 0.1 N HCl. However, TAM-1 and TAM-4 had sodium and potassium levels of 2.27% and 3.61%, respectively, prior to the loading even though ion exchange had been performed. Initial sodium and potassium levels of TAM-1 and TAM-4 varied from 8 to 12%. The ion exchange procedure used to determine the extent of exchange and the procedure used in the catalysts preparation were different. Aqueous mixtures of approximately 10% solids were used when preparing the catalysts instead of the 0.1% solids used in determining ion exchange capacity. Table 1 also illustrates the significant resistance to pore diffusion exhibited by the commercial catalysts.

The HDS activity of the TAM catalysts is shown in Table 1. The catalytic activity of TAM-1 and TAM-4 on a per gram of catalysts is considerably less than that of Shell 324. This difference is probably due to the low molybdenum loading since the activity of the TAM catalysts on a per gram of Mo basis is substantially greater than that for Shell 324. A significant difference occurs in the ratio of biphenyl to cyclohexyl benzene, which is much greater for the TAM catalysts than Shell 324 or the Sandia amorphous catalysts. The ratio also varies significantly for the TAM catalysts depending on the method of preparation.

### 4.0 CONCLUSION

Two new alkali silicon titanates have been synthesized which show high hydrogenation activities when used as precursors for sulfided NiMo catalysts. Based on the XRD patterns these are new materials. Even though the first reflection of TAM-4 and TS-26 and ETS-1 are the same, the remaining portion of the spectra indicates that TAM-4 is a different material. A characteristic of TAM-1 is the doublet that occurs between 830 and 1010 cm<sup>-1</sup> on the FTIR. Incorporation of template appears to be indicated by the peak at 1490 cm<sup>-1</sup> and the overtone bands at 4250 cm<sup>-1</sup>.

### 5. ACKNOWLEDGMENTS

This work was supported by the US Department of Energy at Sandia National Laboratories under contract DE-AC04-76DP000789 and by the Sandia National Laboratories for Texas A&M Research Foundation projects 6571 and 6806.

Table 1. Comparison of Catalysts Activities for Hydrogenation of Pyrene (pyr) and Hydrodesulfurization (HDS) of Dibenzothiophene

Catalyst	Form	Mo, % <sup>a</sup>	Ni, % <sup>a</sup>	SA, m <sup>2</sup> /g	$k_{pyr}$ (g cat g) <sup>-1</sup>	$k_{pyr}$ (g Mo g) <sup>-1</sup>	$\eta$ pyr. hyno.	$k_{HDS}$ (g cat g) <sup>-1</sup>	$k_{HDS}$ (g Mo g) <sup>-1</sup>	BP/CHB
Shell 324	1/32" Extrud.	13.2	2.7	152	0.041	0.31	0.24	0.016	0.121	1.6
Shell 324	-100 Mesh	13.2	2.7	152	0.120	0.91	0.72	ND	ND	ND
Shell 324	-200 Mesh	13.2	2.7	152	0.158	1.20	0.92	0.028	0.158	1.9
Amocat 1C	1/16" Extrud.	10.7	2.4	177	0.038	0.36	0.24	ND	ND	ND
Amocat 1C	-100 Mesh	10.7	2.4	177	0.059	0.55	0.38	ND	ND	ND
Amocat 1C	-200 Mesh	10.7	2.4	177	0.155	1.45	1.0	ND	ND	ND
NiMo-Type 2 CT (Batch #50)	-100 Mesh Sulfided @ 425 °C	5.35	1.76	160 <sup>c</sup>	0.065	1.22	0.8 <sup>d</sup>	ND	ND	ND
TAM-1, SV/T = 1.1	-100 Mesh/leached @ 500 °C/sulfided @ 425 °C	2.85	0.97	160 <sup>c</sup>	0.027	0.94	ND	0.0085	0.30	11.9
TAM-1, SV/T = 1.1	-100 Mesh/sulfided @ 425 °C	2.85	0.97	160 <sup>c</sup>	0.024	0.83	ND	0.0073	0.26	3.16
TAM-4, SV/T = 1.0	-100 Mesh/leached @ 500 °C/sulfided @ 425 °C	1.93	0.65	194 <sup>c</sup>	0.025	1.30	ND	0.0010	0.513	12.3
TAM-4, SV/T = 1.0	-100 Mesh/sulfided @ 425 °C	1.93	0.65	194 <sup>c</sup>	0.026	1.36	ND	0.0084	0.43	8.3
NiMo-N <sub>2</sub> O <sub>2</sub> IT <sup>b</sup>	-100 Mesh	11.2	3.7	130	0.186	1.66	ND	0.0302	0.302	2.8
NiMo-N <sub>2</sub> O <sub>2</sub> ITS <sub>133</sub> <sup>b</sup>	-100 Mesh	8.7	3.0	166	0.268	3.08	ND	0.0132	0.985	2.8

<sup>a</sup>Composition and surface areas of as-received Amocat 1C and Shell 324. Composition of HTO and CT-based Catalysts after calcination @ 500°C. <sup>b</sup> These are the latest and best of the HTO-Based NiMo Catalysts. <sup>c</sup>Prior to ion exchange and after degassing at 150 °C for 12 hours. <sup>d</sup> Effectiveness Factor; Effective Diffusivities based on pyrene for Shell 324 and Amocat 1C are 6.5 (10)<sup>-12</sup> and 3.2 (10)<sup>-11</sup> m<sup>2</sup>/s. The effectiveness factors were calculated assuming a pseudo first order rate equation and spherical particles. <sup>e</sup>Calculated based on an estimate of the effective diffusivity of pyrene. ND Not determined. BP/CHB Moles of biphenyl divided by the moles of cyclohexyl benzene. A high ratio indicates efficient utilization of hydrogen.

## 6. LITERATURE CITED

1. Dosch, R. G., H. P. Stephens, and F. V. Stohl, U.S. Patent No. 4,511,455 (April 16, 1985).
2. Dosch, R. G., H. P. Stephens, F. V. Stohl, B. C. Bunker and C. H. F. Peden, Hydrous Metal Oxide-Supported Catalysts: Part I. A Review of Preparation Chemistry and Physical and Chemical Properties, SAND89-2399, National Laboratories, 1990.
3. Dosch, R. G., H. P. Stephens and F. V. Stohl, Hydrous Metal Oxide-Supported Catalysts: Part II. A Review of Catalytic Properties and Applications, SAND89-2400, Sandia National Laboratories, 1990.
4. Stephens, H. P., R. G. Dosch and F. V. Stohl, *Ind. & Engr. Chem. Prod. Res. Dev.*, 24, (1985) 15.
5. Anthony, R. G. and R. G. Dosch, R. G., Pages 637-646, in *Preparation of Catalysts V* Ed. G. Poncelet, P.A. Jacobs, P. Grange and B. Delmon, Elsevier Science Publishers B. V., Amsterdam (1991).6
6. Anthony, R. G., C. V. Philip and R. G. Dosch, *Catalysis Today*, In press (Originally presented at the ACS meeting in NY in August, 1991).
7. Stephens, H.P. and R. N. Chapman, *PREPRINTS, Fuel Div.*, 28(5), (1983) 161.
8. Stephens, H.P. and F. V. Stohl, *PREPRINTS, Fuel Div., ACS*, 29(6), (1984) 79.
9. Stephens, H. P. and R. J. Kottenstette, *PREPRINTS, Fuel Div., ACS*, 30(2), (1985) 345.

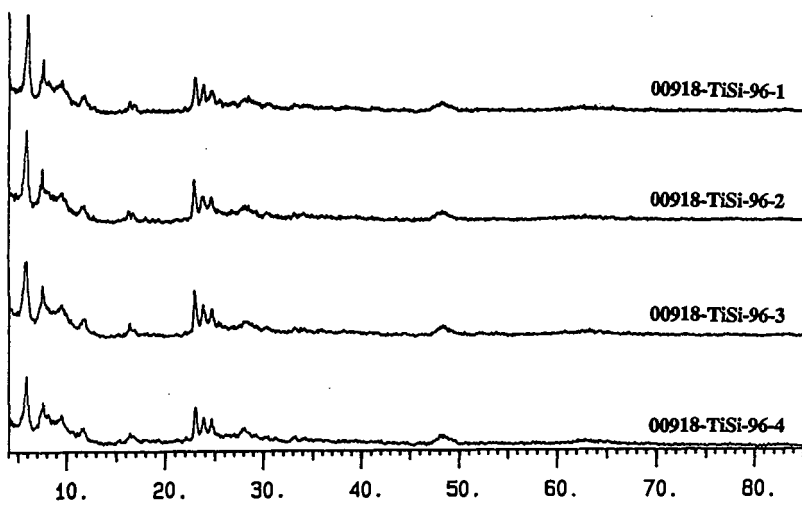


Figure 1. Comparison of XRD Patterns for TAM-1 Prepared with Different Charge Compositions.

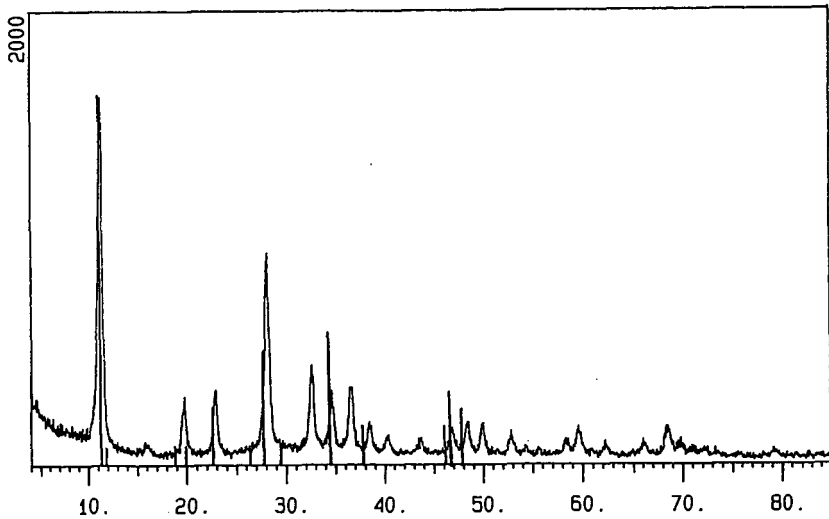


Figure 2. Comparison of XRD Powder Patterns for TAM-4 and ETS-1/TS-26 (Bars).

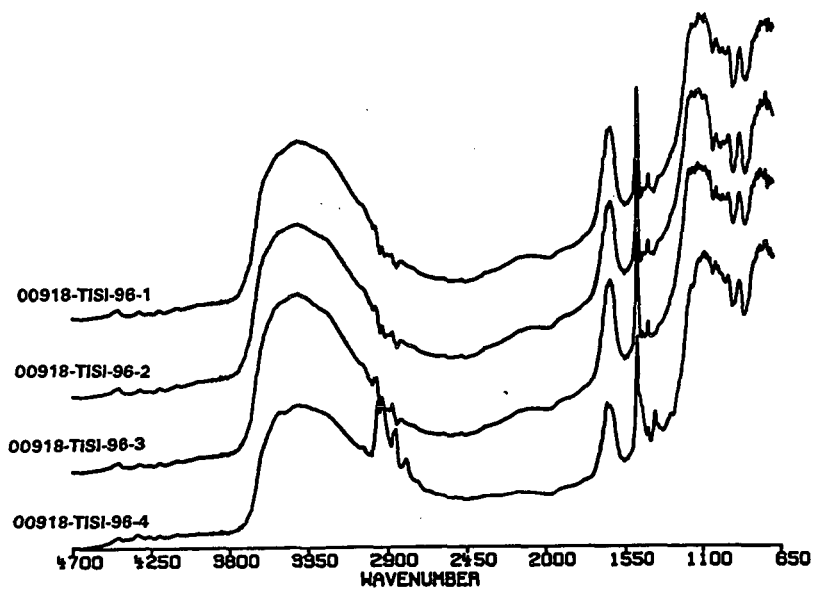


Figure 3. Comparison of FT-IR Spectra for TAM-1 Prepared Using TP<sub>3</sub>AB and TP<sub>5</sub>AB.

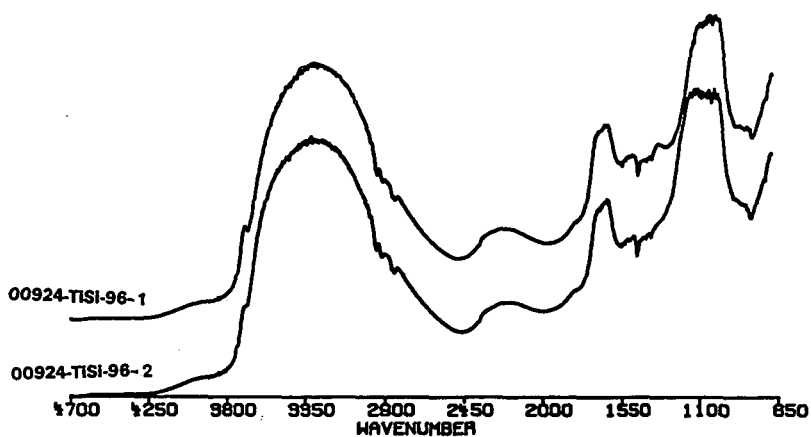


Figure 4. Comparison of FT-IR Spectra for Different Batches of TAM-4.

## ETHYLATION OF TETRAHYDROQUINOLINE USING Ru/Mo BIMETALLIC CATALYST PRECURSORS SYSTEM.

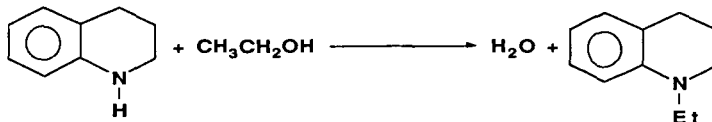
Sang-Man Koo, D. Ryan, and R. M. Laine  
The Department of Materials Science and Engineering and  
the Department of Chemistry, University of Michigan,  
Ann Arbor, MI. 48109-2136

Keywords: Ethylation ; Tetrahydroquinoline ; Bimetallic Catalyst Precursors.

Heteropolyanions (HPAs) offer the opportunity to develop soluble forms of surface confined catalysts. HPAs are inexpensive, well-characterized, water soluble metal oxide clusters, e.g.  $[EM_{12}O_{40}]^{4-}$  where E = Si or P and M = Mo or W.<sup>1</sup> They are easily modified to contain other transition metals such as Co, Ni or Ru and, can be made soluble in organic solvents.<sup>1-3</sup> The protic forms exhibit extremely high acidities with  $pK_a$ 's  $\approx$  0-2.<sup>1</sup> In addition, selectively modified HPAs can function as low temperature hydrogenation catalysts that exhibit microporosity.<sup>4</sup> HPAs are multi-functional catalysts that could be used to promote both hydroliquefaction and hydrotreating. The overall goal of the work reported here concerns our efforts to evaluate HPAs as soluble liquefaction and hydrotreating catalysts, with the goal of developing soluble analogs of surface confined catalysts.<sup>5,6</sup>

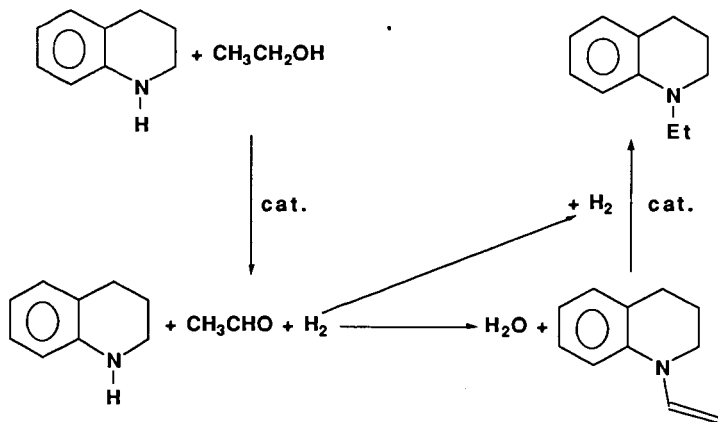
The primary purpose of the work reported here is to carefully delineate the reactivity patterns of RuMo bimetallic precatalysts. In particular, efforts were made to understand the reactivity of tetrahydroquinoline (THQ) at moderate temperatures. We have previously shown that bimetallic RuMo and trimetallic RuCoMo organometallic derived, supported catalysts will promote HDN of THQ at temperatures of 350°C.<sup>5,6</sup> Thus, we were interested to determine whether or not our recently developed, unsupported RuMo catalysts would have sufficient activity to work at temperatures below 250°C.

The preliminary results of this study are quite surprising and warrant further, more detailed studies. First, we find that THQ does not undergo HDN to products such as propylaniline, propylbenzene, propylcyclohexane, nor is it hydrogenated to decahydroquinoline. However, it does undergo a surprising reaction with the ethanol solvent wherein the nitrogen is ethylated according to the following reaction:



At 220°C, this reaction goes to 40% completion in 25 h at 1000 psig H<sub>2</sub> using a standard bimetallic precatalyst system [4 mL EtOH stock solution, 4.39 x 10<sup>-4</sup> M in Mo-HPA:1 mL stock solution, 5.74 x 10<sup>-4</sup> M in RuCl<sub>3</sub>/1.96 x 10<sup>-4</sup> M Ru<sub>3</sub>(CO)<sub>12</sub>, 50 μL CS<sub>2</sub>] as shown in Figures 1 and 3. What is extremely surprising about this reaction is that when it is run either with 4 mL of Mo-HPA stock solution or only 1 mL of RuCl<sub>3</sub> [or Ru<sub>3</sub>(CO)<sub>12</sub>] stock solution, where no synergistic effects are possible, almost no product is observed. In baseline tests, the Mo-HPA derived catalyst appears to function slightly better than the RuCl<sub>3</sub> derived catalyst [or nearly the same as Ru<sub>3</sub>(CO)<sub>12</sub>]. Apparently, it is necessary to have the bimetallic catalyst form in order to observe ethylation.

Another unexpected result comes from the observation that, for RuCl<sub>3</sub>/Mo-HPA catalyst precursor system, dropping the initial H<sub>2</sub> pressure from 1000 psig to 400 psig does not affect the rate of reaction at all (Figure 2). At least under the two pressures measured, it appears that H<sub>2</sub> pressure plays no role in the rate limiting step. Based on our previous work in this area, we can suggest a mechanism that explains this observation:<sup>7</sup>



In this reaction scheme, the first step involves dehydrogenation of ethanol to form acetaldehyde which condenses with THQ to form the enamine, shown in the lower right hand

corner. The enamine is then readily hydrogenated to **N-Et-THQ**.

In contrast to the RuCl<sub>3</sub>/Mo-HPA precatalyst system, the Ru<sub>3</sub>(CO)<sub>12</sub>/Mo-HPA system exhibits significant H<sub>2</sub> pressure dependence (Figure 4). The percent conversion rate (also TF value) reaches a maximum at 600 psig H<sub>2</sub> (~296 for TF and 32 for TF') as shown in Figure 4 and Table 1). The inhibition in catalyst activity observed above 600 psig H<sub>2</sub> is somewhat unexpected and further study will be needed.

Figure 5 and Table 2 show the effects of relative concentrations of bimetallic precatalyst on catalyst activity for **THQ** ethylation. Except at the lowest value of [Ru<sub>3</sub>(CO)<sub>12</sub>]/[Mo-HPA], increasing the relative concentration of Ru<sub>3</sub>(CO)<sub>12</sub> results in a decrease in percent conversion and lower TF (and TF') values. Maximum TF (or TF') values are obtained when a 1 mL/4 mL(Ru/Mo) precatalyst stock solution mixture is used.

Initial rates of reaction were determined for each temperature from 220 to 250°C with initial H<sub>2</sub> pressures of 600 psig. Raw reaction rate data are used to calculate initial TFs which are used as k<sub>obs</sub>.<sup>8</sup> These data allow us to calculate the energy of activation, E<sub>a</sub> = 27 ± 3 kcal/mole. When the reaction temperature was below 210°C, the percent conversion on to **N-Et-THQ** is much less than 1 %, even after 24 hours.

One possible conclusion as to why the bimetallic system is so much better than the individual metals is that one metal does one of the above catalytic operations well and the other poorly. The second metal then does the reverse. If this is the case, then from our hydrogenation studies, we would conclude that Mo catalyst sites are responsible for dehydrogenation and the Ru catalyst sites are responsible for hydrogenation.

In hydrotreating crude oil, oil shale and coal liquids; it is certain that primary and secondary alcohols will form during the process. Given that standard HDN catalysts contain sulfided Mo sites and Co sites, it is likely that these intermediate alcohols will alkylate any amine sources produced coincidentally. Although, Co is not as good a hydrogenation catalyst as Ru, at the elevated temperatures currently used for hydrotreating, it is possible that alkylation will occur quite readily.

### **Acknowledgements**

We wish to thank the Department of Energy and the Pittsburgh Energy and Technology Center for generous support of this work through contract no. DE-FG22-90PC90313.

### **References**

1. Heteropoly and Isopoly Oxometalates, M. T. Pope, Springer-Verlag Pub., Berlin, GDR,

1983.

2. R. F. Renneke and C. L. Hill, *J. Am. Chem. Soc.*, (1988) **110**, 5461.
3. R. K.C. Ho, W. G. Klemperer, *J. Am. Chem. Soc.*, (1978) **100**, 6774.
4. A. R. Siedle, R. A. Newmark, M. R. V. Sahyun, P. A. Lyon, S. L. Hunt, and R. P. Skarjune, *JACS* (1989) **111**, 8346.
5. "Bulk Ruthenium as an HDN Catalyst", A. S. Hirschon and R. M. Laine, *J. Energy and Fuels* (1988) **2**, 292-295.
6. "Use of Promoters to Enhance Hydrodenitrogenation and Hydrodeoxygenation Catalysis", A. S. Hirschon, L. L. Ackerman, R. M. Laine, and R. B. Wilson, Jr. *Proc. of the 1989 Internat. Conf. on Coal Science, Tokyo.* Vol. **II**, p. 923.
7. "Homogeneous Catalytic Cleavage of Saturated Carbon-Nitrogen Bonds." Y. Shvo, M. Abed, Y. Blum, and R. M. Laine, *Isr. J. Chem.* (1986) **27**, 267-275.
8.  $k_{obs}$  at each temperature is obtained from the slope of the equation,  $d[N-Et-THQ]/dt = k_{obs}[Q]^0$ , assuming zero order reaction from data obtained. The activation energy,  $E_a$ , is calculated from the expression  $k_{obs} = A e^{(-E_a/RT)}$ .

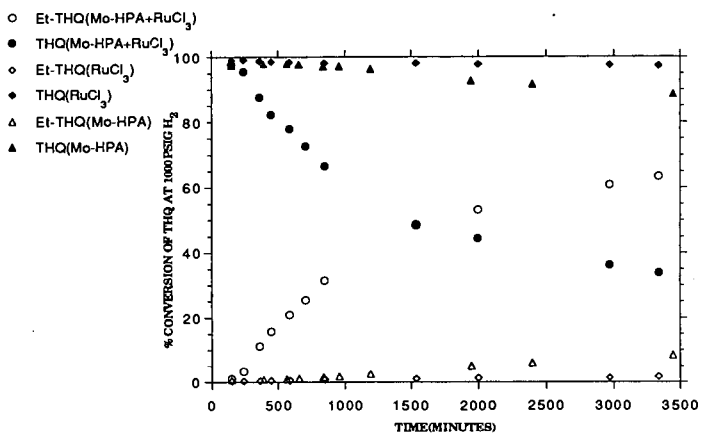


Figure 1. Percent Conversion of THQ to N-Et-THQ for Individual and Mixed Bimetallic Catalyst Precursors at 1000 Psig H<sub>2</sub> and 220 °C.

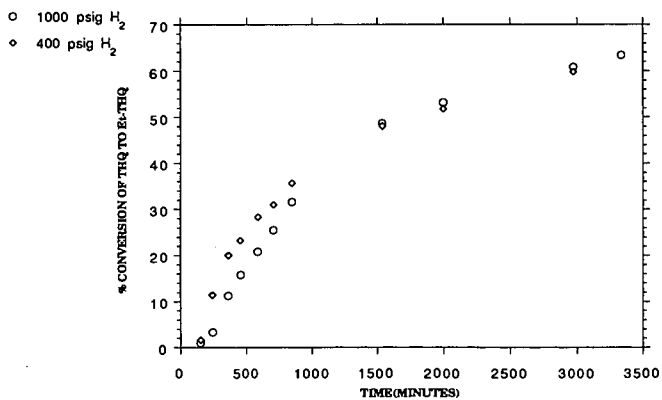


Figure 2. Percent Conversion of THQ to N-Et-THQ for Mo-HPA/RuCl<sub>3</sub> Bimetallic Catalyst Precursors in two different H<sub>2</sub> pressure at 220 °C.

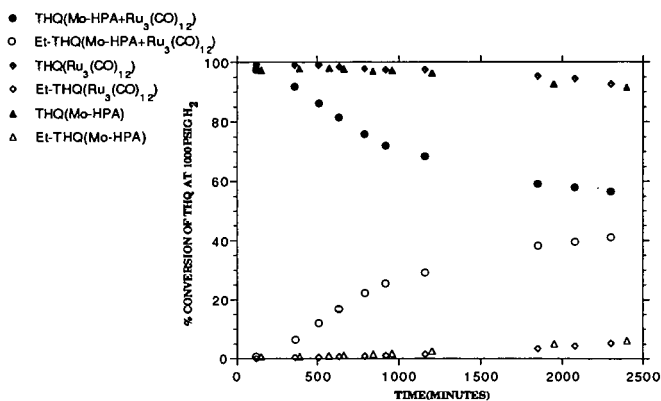


Figure 3. Percent Conversion of THQ to N-Et-THQ for Individual and Mixed Bimetallic Catalyst Precursors at 1000 Psig H<sub>2</sub> and 220 °C.

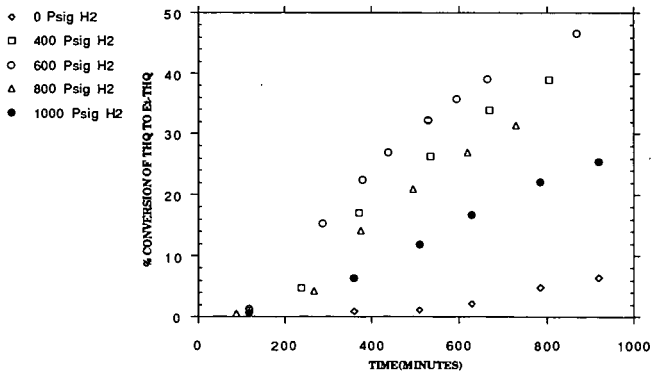


Figure 4. Percent Conversion of THQ to C<sub>2</sub>H<sub>5</sub>-THQ for Bimetallic Mo-HPA/Ru<sub>3</sub>(CO)<sub>12</sub> Precatalyst at Various Pressures.

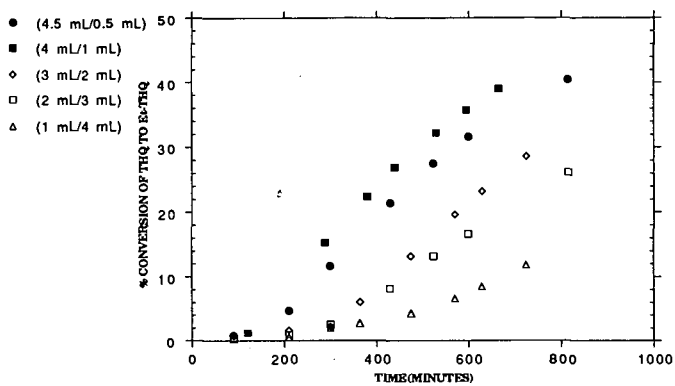


Figure 5. Percent Conversion of  $C_6H_8$ -THQ at Different Relative Concentration of Bimetallic Catalyst Precursors.

(Mo-HIPA/Ru<sub>3</sub>(CO)<sub>12</sub>)/w, 1 mL Mo-HIPA=1.1 × 10<sup>-4</sup> M and 1 mL Ru<sub>3</sub>(CO)<sub>12</sub>=1.98 × 10<sup>-4</sup> M)

**Table 1. Turnover Frequencies of Mixed Bimetallic Catalyst Precursors at different H<sub>2</sub> Pressure and 220 °C.**

H <sub>2</sub> Pressure	TF(Total no. of moles of catalyst precursor)	TF(Total no. of moles of Metal atoms)
0 psig	61 ± 17	7 ± 2
400 psig	221 ± 20	24 ± 2
600 psig	296 ± 14	32 ± 2
800 psig	190 ± 20	21 ± 2
1000 psig	140 ± 10	15 ± 1

\*TF(TF) = no. of moles of product, N-Et-THQ/no. of moles of catalyst (or metal atoms)/h

\*The total no. of moles of catalyst precursor is  $6.34 \times 10^{-6}$  moles [Mo-HPA/Ru<sub>3</sub>(CO)<sub>12</sub> =  $4.38 \times 10^{-6}$ /1.96 × 10<sup>-6</sup>].

\*The total no. of moles of metal atoms is  $5.85 \times 10^{-5}$  moles (Mo/Ru = 5.26 × 10<sup>-6</sup>/5.87 × 10<sup>-6</sup>).

**Table 2. Turnover Frequencies of Mixed Bimetallic Catalyst Precursors at different Relative Concentration. (600 psig H<sub>2</sub> and 220 °C)**

Relative volume (Ru/Mo) of catalyst precursor soln	Concentration	no. of moles of Ru <sub>3</sub> (CO) <sub>12</sub> catalyst precursor (× 10 <sup>-6</sup> moles)	Total no. of moles of metal atoms (× 10 <sup>-5</sup> moles)	TF(Catalyst)	TF(Metal)
0.5 mL/4.5 mL	0.98/4.93	5.91	6.21	273 ± 38	26 ± 3
1 mL/4 mL	1.95/4.38	6.34	5.85	236 ± 14	32 ± 2
2 mL/3 mL	3.91/3.29	7.19	5.12	214 ± 24	30 ± 3
3 mL/2 mL	5.87/2.19	8.06	4.39	144 ± 19	27 ± 3
4 mL/1 mL	7.82/1.1	8.92	3.66	81 ± 15	20 ± 4

\*TF and TF's are defined as in table 1.

## EXAFS Studies of Mo-Y-Zeolite Catalysts

Qiwu Wang and Dale Sayers

Department of Physics, North Carolina State University, Raleigh, NC 27695

Miming Huang, Chunhua Yuan and Shiqiang Wei

Department of Modern Chemistry, University of Science and Technology of  
China, Hefei, Anhui, P. R. China

### Introduction

In recent years there has been an increasing interest in molybdenum containing zeolite catalysts as effective bifunctional catalysts.<sup>1-4</sup> Different techniques have been used to prepare and characterize the Mo-zeolites. It is difficult to exchange the cations of a zeolite for molybdenum ions directly because high valence cationic molybdenum can only exist in very acidic solution where ion-exchange equilibria are unfavourable and many zeolites are unstable. Ion exchange with neutral and anionic species results in a large amount of surface loading. In order to overcome the difficulties of aqueous ion exchange, molybdenum is introduced into zeolites by the solid-ion exchange method. A special procedure was developed recently for initiating controlled immigration of  $\text{MoO}_2(\text{OH})_2$  into the zeolite pore of HY with  $\text{MoO}_3$  in the presence of water vapor.<sup>5</sup>

EXAFS is an effective physical method for determination of the local structure of specific atoms in complex systems such as highly dispersed supported metal catalysts. It has been successfully applied to some metal zeolite catalysts: viz. Pt-Y-zeolite<sup>6</sup>, Cd-Y-zeolite<sup>7</sup> and Ni, Mo-Y-zeolite<sup>8</sup> and other bimetallic catalysts<sup>9-10</sup>. However, an EXAFS study of Mo-zeolite prepared with solid-ion exchange method has not been published. In this work, we studied by EXAFS the change of the local environment around Mo in the preparation of Mo-Y-zeolite directly to see if Mo incorporated into the framework of Y-zeolites. As prepared, reduced and dehydrated samples were studied.

### Experimental

#### Samples

The HNaY zeolite was prepared by exchange of NaY with 0.1 N  $\text{NH}_4\text{NO}_3$  solution at 365K for 1 hour, followed by a direct calcination at 823K for 5.5 hours in a closed vessel. The modified solid ion exchange was performed as following: a mixture of 27 g HNaY and 1.2g  $\text{MoO}_3$  was ground in a mortar

(hereafter denoted as MoHY), placed in a quartz tube and then calcined at 723K, water vapor at 323K (118 torr) was carried through the mixture using H<sub>2</sub> as the vector gas with a flow of 45ml/min. The sample obtained after calcination was then denoted as MoHYR. This sample then underwent dehydration at 673K (MoHYRD). The contents of the samples were then analyzed by AAS, Na contents were determined by ICP, and X-ray powder diffraction measurements were made using a Cu-target x-ray tube.

### X-ray absorption measurement

X-ray absorption experiments were performed on beam line X-11A of the National Synchrotron Light Source (NSLS), Brookhaven National Laboratory. The X-ray absorption spectra for Mo K-edge were recorded with the ring operating at 2.5 GeV beam energy and a beam current of 40-180 mA. The pressed powder samples were mounted on the holder and measured at liquid nitrogen temperature in the transmission mode.

Data analysis was carried out with using standard methods<sup>11</sup> and the fitting was done using experimentally determined Mo-O (from ZnMoO<sub>4</sub>), Mo-Mo (from metallic Mo) and theoretically calculated Mo-Si (using FEFF)<sup>12</sup> phase shifts and backscattering amplitudes. Both single or multiple shell models were assumed for fitting the various filtered Fourier transform (FT) peaks.

## Results and Discussion

### 1. XAS of Mo-Y-zeolites

The normalized X-ray absorption curves of MoO<sub>3</sub>, MoHY, MoHYR, MoHYRD and Mo metal are shown in Fig.1. The high pre-edge peak on the MoHY curve provides strong evidence for the presence of a short M=O bond characterizing MoO<sub>3</sub> in the mixture of MoO<sub>3</sub> and HY.<sup>13</sup> This feature of MoO<sub>3</sub> almost disappears after calcination of the mixture at 723K in the presence of water vapour which means that the incorporation of Mo from MoO<sub>3</sub> into zeolite has taken place. XRD measurement also showed that MoO<sub>3</sub> diffraction peaks located at  $d=6.907, 3.801$  and  $3.255\text{\AA}$  were absent in these samples.<sup>14</sup> Further changes of the spectrum occurred when the sample was calcined in H<sub>2</sub> (MoHYR) and then dehydrated (MoHYRD). The comparison between  $k^3\chi(k)$  of MoO<sub>3</sub> and MoHYRD (see Fig.2) indicates that a great change of the environment around Mo in them clearly takes place because of the solid-ion exchange process. Further comparison of the Fourier transforms as shown in Figure 3 also show significant changes but no strong evidence for the formation of the metallic phase. From these comparisons

we assume that there is no significant change of the oxidation state of Mo after incorporation of MoO<sub>3</sub> into the zeolite.

## 2. Fitting results

Fitting to the Fourier isolated shells in each sample was done using the reference compounds cited above. A summary of the results are listed in Table 1 for the three catalysts studied as well as MoO<sub>3</sub>. For the first three shells in MoHY, a good fit was only obtained with a short Mo=O bond along with two Mo-O bonds. Any other combination of Mo oxygen bonds had variances at least a factor of two greater than the resulted shown here. It is also consistent with the observation of the absorption profiles (Fig.1) and Fourier transforms (Fig.3) where the first Mo=O peak changed.

When Mo is incorporated into the supercages of the zeolite, fitting shows that two new longer Mo-O bonds, 2.03-2.05 Å and 2.66-2.67 Å, are formed instead of 1.70 and 1.96Å bonds in MoO<sub>3</sub>. For the first two peaks in the FT of MoHYRD, the isolated  $k^3\chi(k)$  and the fitting curve with two longer Mo-O models are overplotted in Fig.4. The agreement is excellent. It was observed previously that the longer metal-oxygen bond around 2.6 Å can be present in metal-Y-zeolites.<sup>15</sup> The Mo-Mo interaction fitting results (see CN and R for Mo-Mo in Table 1) show that initially when Mo has been exchanged with the cationic ions in zeolite the Mo-Mo coordination is relatively large with an average Mo-Mo bond about 3.40Å but that this is significantly changed after reduction and dehydration. The Mo coordination number decreases from 6 (MoHY) to 1 (MoHYRD). This means that Mo was dispersed into the supercages of Y-zeolite, probably in octahedral clusters as [-Si-MoO<sub>4</sub>-MoO<sub>4</sub>-Si-]. Also a new third coordination shell around Mo in MoHYR and MoHYRD develops which is a combination of both Mo and Si(or possibly Al). The fitting of the third Fourier transform peaks in MoHYR and MoHYRD with both Mo-Mo and Mo-Si models greatly reduces the fitting variation between the experimental and calculated EXAFS data by up to 10-15 times compared to those with Mo or Si only as the neighbor. From Fig. 5 and 6, it can be seen that the two shell fitting gives the best results. The presence of Si around Mo from the zeolite framework, the decrease of the Mo-Mo coordination and the appearance of a long Mo-O bond all support the hypothesis that the solid-ion exchange method produces a Mo-substituted zeolite.

## References

1. Meszaros-Kis, A. and Valyon, J., in "Zeolites as Catalysts, Sorbents and Detergent Builders" Edited by Karge H. G. and Weitkamp J., Elsevier, 1989, p.251
2. Laniecki, M., *ibid* P. 259

3. Harris, I. M., Dwyer, J., Garforth, A.A., Mc Ateer, C. H. and Ball, W. J., *ibid* P.271
4. Howe, R. F. and Huang M., *Proceeding of 9th International Conference on Catalysis, Canada, 1988*, p. 1585
5. Huang, M. and Howe, R. F., *J. Catal.* 108 (1987) 283
6. Yokoyama, T., Kosugi, N., Asakura, K., Iwasawa, Y. and Kuroda, H., *J. Physique* 47, C8-273, 1986
7. Moller, K., Eddy, M. M., Stucky, G.D., Herron, N. and Bein, T., *J. Am. Chem. Soc.*, 1989, 117, 1564
8. Clozza, A., Bianconi, A., Garcia, J., Corma, A and Buratini, E., *XAFS V* edited by Mustre de Leon, J., Stern, E. A., Sayers, D. E., Ma, Y. & Rehr, J.J., North-Holland, 1988, p.162
9. Wang Q. and Wei S., *Kehue Tongbao* 6, 435, (1990)
10. Wang Q. and Wei S., *Chinese J. Chem. Phys.* 3, 49, (1990)
11. Stern, E. A., Sayers, D. E. and Lytle, F. W., *Phys. Rev. B: Solid State* 11, 4836-4845, 1975
12. Rehr, J. J., *Physica B* 158 (1989) 1-4 (XAFS V)
13. Garner, C. D., *EXAFS and Near Edge Structure IV*, *J de Physique* 47, C8-1111, 1986
14. Huang, M., Yuan, C., Wei, S. and Wang, Q., *in press*
15. Koningsberger, D. C., *XAFS VI*, 6th International Conference on XAFS, York, 5-11 August, 1990, p.28

**Table 1. Mo Coordination Shells in Mo-Y-Zeolites and Mo Trioxide**

MoHY					MoO3			
Model	CN	R(Å)	DWF.10 <sup>2</sup>	d-E <sub>0</sub> (eV)	CN	R(Å)	DWF.10 <sup>2</sup>	d-E <sub>0</sub> (eV)
Mo=O	1.1±.1	1.58±.01	-0.59±.03	12.8±.5	1.0±.1	1.63±.01	-0.35±.03	12.0±1.0
Mo-O	3.4±.3	1.77±.01	-0.24±.06	-2.1±.2	2.5±.2	1.78±.01	0.27±.02	-7.0±.7
Mo-O	2.4±.2	1.98±.01	-0.56±.09	-2.1±.2	1.5±.1	1.97±.01	-0.68±.06	-2.0±.2
Mo-Mo	5.7±.2	3.36±.02	0.73±.01	3.2±.3	8.9±.8	3.48±.02	0.18±.02	-7.7±.8
Mo-O	2.5±.2	3.92±.02	-0.84±.08	-8.9±.8	7.6±.5	3.90±.02	-0.57±.05	-8.9±.9
MoHYR					MoHYRD			
Model	CN	R(Å)	DWF.10 <sup>2</sup>	d-E <sub>0</sub> (eV)	CN	R(Å)	DWF.10 <sup>2</sup>	d-E <sub>0</sub> (eV)
Mo-O	2.5±.2	2.03±.01	-0.27±.02	-7.9±.6	2.7±.2	2.05±.01	-0.23±.01	-6.7±.7
Mo-O	1.3±.1	2.67±.01	-0.52±.05	2.0±.2	1.3±.1	2.65±.01	-0.72±.01	6.6±1.0
Mo-Si	1.6±.1	3.45±.02	-0.27±.01	-10.7±.8	0.7±.1	3.45±.01	1.10±.01	-7.7±1.0
Mo-Mo	1.8±.1	3.75±.02	-0.28±.02	-5.6±.5	1.1±.1	3.75±.01	-0.22±.01	0.9±.1

Note: The experimental standard data are used for fitting: Mo-O (CN=4, R=1.78Å) from ZnMoO<sub>4</sub> and Mo-Mo (12, 2.73Å) from metal Mo foil.

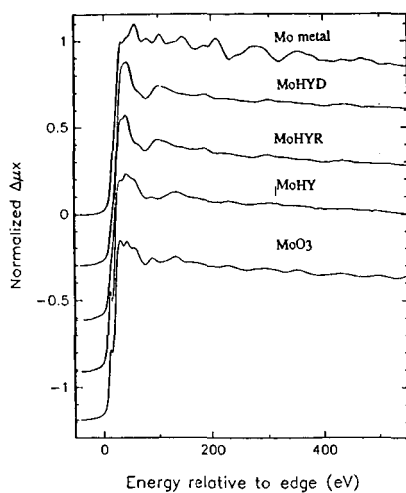


Figure 1. The normalized x-ray absorption spectrum versus energy for Mo metal, Mo in Y-zeolite which has been reduced and dehydrated as described (MoHYRD), Mo in Y-zeolite which has been reduced (MoHYR), Mo in Y-zeolite as prepared (MoHY) and MoO<sub>3</sub>. The energy scale is relative to the binding energy of the Mo 1s state (20,000 eV).

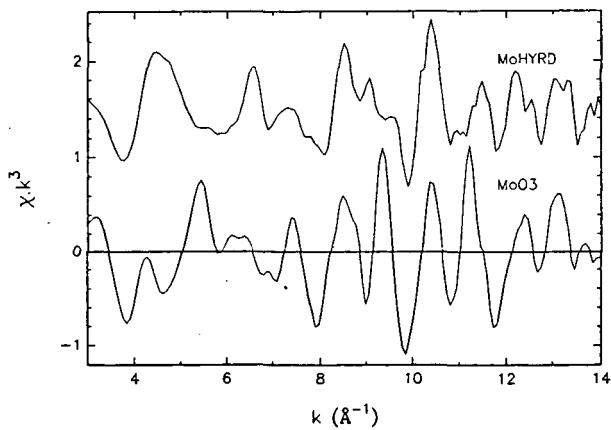


Figure 2. A comparison of the weighted spectra  $k^3\chi(k)$  versus  $k$  of MoHYRD and MoO<sub>3</sub>.

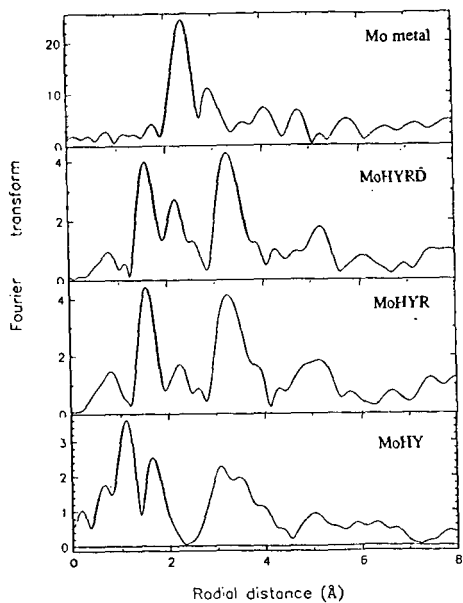


Figure 3. A comparison of the magnitudes of the Fourier transforms of the weighted EXAFS for Mo metal, MoHYRD, MoHYR, and MoHY versus  $R$ . The transforms are all of  $k^3\chi(k)$  and taken over a  $k$ -space range of 3-14  $\text{\AA}^{-1}$ .

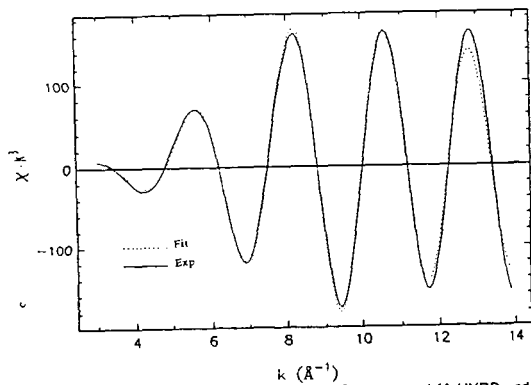


Figure 4. An overplot of the Fourier filtered  $k^3\chi(k)$  data of MoHYRD and the best fitting results (see Table 1) versus  $r$ . The filtering range was from 1 to 2.8  $\text{\AA}^{-1}$ . The fitting included two Mo-O bonds only.

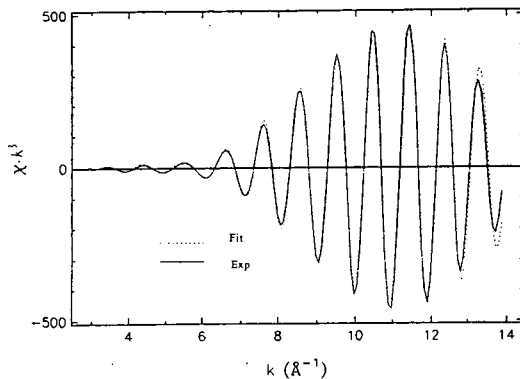


Figure 5. An overplot of the Fourier filtered  $k^3\chi(k)$  third shell data of MoHYR and the best fitting results (see Table 1) versus  $R$ . The filtering range was from 2.8 to 4.1  $\text{\AA}^{-1}$ . The fit included both Mo-Mo and Mo-Si contributions.

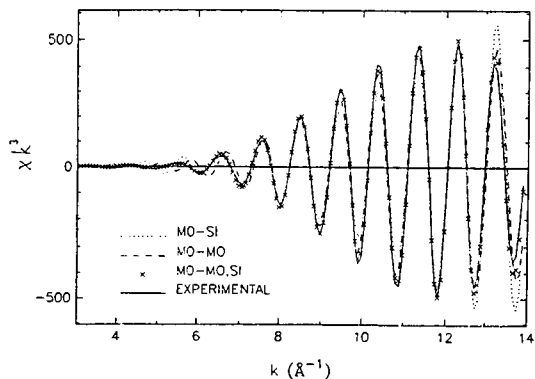


Figure 6. A comparison of the Fourier filtered  $k^3\chi(k)$  third shell data of MoHYR and fits containing Mo-Mo only (---), Mo-Si only (···), and Mo-Mo and Mo-Si (xxx) versus  $R$ . The filtering range was from 2.8 to 4.1  $\text{\AA}^{-1}$ .

## HETEROPOLYANIONS, SOLUBLE PRECATALYSTS FOR QUINOLINE HYDROGENATION.

Sang-Man Koo, M.L. Hoppe, and R. M. Laine  
The Department of Materials Science and Engineering and  
the Department of Chemistry, University of Michigan,  
Ann Arbor, MI. 48109-2136

Keywords: Heteropolyanions ; Quinoline Hydrogenation ; Bimetallic Catalyst Precursors.

Within the past two decades, inorganic chemists have developed a growing fascination for metal cluster chemistry, especially metal cluster catalysis chemistry. The sources of this fascination are the potential benefits cluster catalysis can provide to: (1) further the development and understanding of heterogeneous catalysis through modeling studies; (2) advance the development of new, industrially important, homogeneous catalysis chemistry, and (3) provide a sound basis for the development of "surface confined" metal cluster catalysis chemistry. The latter area being the translation of metal cluster catalysis chemistry to the development of new heterogeneous catalysts.

In this study, we describe initial efforts to evaluate a set of heteropolyanions (HPAs,  $[EM_{12}O_{40}]^{4-}$  where E = P and M = Mo or W, Mo-HPA, W-HPA) as potential liquefaction and hydrotreating catalysts. We develop a standard set of reaction parameters for quinoline (Q) hydrogenation to tetrahydroquinoline (THQ) by delineating the effects of variations in temperature,  $H_2$  pressure, catalyst and Q concentrations on the catalytic activity of a set of precatalysts. These standard parameters are then used to survey other potentially useful catalysts.

At the outset, it was anticipated that soluble HPAs would serve as precatalysts to the true, active species. It was also recognized that under the reaction conditions employed, the soluble HPAs might be transformed to heterogeneous species. We find that under the reaction conditions employed; the precatalysts described here, decompose to give heterogeneous catalyst particles that actively catalyze hydrogenation of Q to THQ. The following studies establish the parameters of the process leading to formation of active catalyst and define conditions used to survey of other potential catalysts.

The effects of variations in  $H_2$  pressure ( $P_{H_2}$ ) on catalyst activity are shown in Figure 1. There appears to be an almost linear relationship between  $H_2$  pressure and catalyst activity (turnover frequency, TF).<sup>1</sup> Under the conditions studied, it was not possible to ascertain the  $P_{H_2}$  required to reach the falloff region, where the relationship  $TF/P_{H_2}$  is no longer linear.

Figure 2 shows the effect of total metal concentration on catalyst activity for Mo-HPA.

The highest catalyst concentration used in this study ( $5.5 \times 10^{-4}$  M) is less than 0.02 mole percent of the Q concentration used. Within the range of catalyst concentrations studied, except at very low concentrations, there appears to be a linear relationship between catalyst concentration and TF. These results are extremely valuable because, as discussed below, the active catalyst is heterogeneous. At low metal concentrations, the linearity of the conc./TF relationship is lost because of errors in reproducibility at very low conversions.

The Figure 3 results indicate that under the reaction conditions studied, the rate of Q hydrogenation to THQ is not linearly dependent on initial Q concentration. The turnover frequency reaches its maximum (TF = 20) at [Q] = 4.23 M at [Mo-HPA] =  $5.5 \times 10^{-4}$  M. Considering the extremely high Q concentrations used, there are three likely explanations for the observed falloff. One is that above [Q] = 4.23 M, the reaction conditions are pseudo first order, with H<sub>2</sub> pressure being the only variable and the falloff above these concentrations resulting from experimental error. Alternately, at these high concentrations, Q competes successfully with H<sub>2</sub> for active catalyst sites thereby slowing the rate of hydrogenation. A third explanation is that at these high Q concentrations, the reaction solution composition is quite different--there is much less EtOH. Consequently, the solvation of the precatalyst changes or the decomposition mechanism and therefore the surface area of the active catalyst produced is diminished.

Initial rates of reaction were determined for each temperature from 150 to 225°C with initial H<sub>2</sub> pressures of 400 psig. Raw reaction rate data are used to calculate initial TFs which are used as  $k_{obs}$ .<sup>1</sup> These data allow us to calculate an activation energy of  $E_a = 16 \pm 3$  kcal/mole.

Figure 4 indicates that the bimetallic Mo-HPA/RuCl<sub>3</sub>·xH<sub>2</sub>O precatalyst system offers the highest catalytic activity (TF ~ 10) of the precatalysts surveyed. The absence of catalytic activity for W-HPA and (NH<sub>4</sub>)VO<sub>3</sub> were somewhat unexpected considering the modest activities of the polyoxomolybdate catalysts.

The baseline studies presented above were conducted to: (1) develop a set of standard conditions for testing HPA precatalyst systems; (2) identify promising precatalysts for further study at higher temperatures, and (3) establish hydrogenation reactivity patterns of the prospective catalyst systems. These studies were designed to answer several important questions concerning the utility of HPAs as hydrotreating and hydroliquefaction precatalysts. The questions include: (1) Do HPA derived catalysts function as heterogeneous or homogeneous catalysts?; (2) What advantages do HPAs offer over conventional catalysts?; and (3) Are polymetallic HPA derived catalysts better than conventional or monometallic HPA catalysts?

How Do HPA Derived Catalysts Function: As noted above, the HPA systems function as heterogeneous catalysts rather than homogeneous catalysts. Proof of heterogeneity comes from the fact that catalyst activation requires: (1) hydrogen reduction; (2) CS<sub>2</sub>, and (3) an induction period (10-15 min at 200°C) prior to onset of catalyst activity. All of these components are necessary to obtain catalytic activity. In addition, once the heterogeneous catalyst has been formed, removal of all of the reaction solution (by decantation in air) followed by readdition of more Q and EtOH (but not CS<sub>2</sub>) and repressurization to the initial H<sub>2</sub> pressure, gives the same catalyst activity as obtained initially--without an induction period. Thus, the heterogeneous particles formed by reduction, sulfidation and degradation of the HPAs is the true, active catalyst. One important observation is that there is a linear correlation between precatalyst concentration and catalyst activity (Figure 2). This linear relationship occurs despite the fact that catalysis occurs after conversion of the homogeneous precatalyst to the active, heterogeneous form.

It can be argued that increases in precatalyst concentration should lead to lower, relative catalyst surface areas (leading to lower TF/mole metal) as initially nucleated catalyst particles serve as growth sites for the decomposition of additional HPA molecules. Given that the correlation is linear, we presume that nucleation is a solution phase rather than a surface phenomena. Thus, all of the catalyst particles may be expected to be of approximately the same dimensions. Scanning electron microscopy supports this idea, given that the fresh catalyst particles, seen at highest magnification, are all submicron and therefore offer very high surface areas.

What Advantages Do HPAs Offer Over Conventional Catalysts: Several potential advantages are offered by HPAs relative to conventional catalysts. First, HPAs are soluble in a variety of polar and slightly polar solvents including water, MeOH, EtOH, and acetonitrile. Consequently, under liquefaction conditions, it should be possible to tailor the HPA/solvent system to optimize coal swelling and coincidentally catalyst dispersion. By comparison, conventional soluble catalysts such as ammonium heptamolybdate; which exhibits essentially the same activity as Mo-HPA (see Figure 4), is soluble only in water.

Bimetallic HPAs were also examined. Surprisingly, studies with the bimetallic precatalyst,<sup>2</sup> (NH<sub>4</sub>)<sub>6</sub>[Co<sub>2</sub>Mo<sub>10</sub>O<sub>38</sub>H<sub>4</sub>]·7H<sub>2</sub>O, reveal catalytic activities somewhat less than exhibited by Mo-HPA and the heptamolybdate on a per-mol of metal basis. The most likely explanation is that the effectiveness of "CoMo" and NiMo bimetallic catalysts derives from their ability to promote C-N bond hydrogenolysis rather than hydrogenation of Q to THQ. Indeed, one could argue from our data on Mo-HPA, (NH<sub>4</sub>)<sub>6</sub>[Co<sub>2</sub>Mo<sub>10</sub>O<sub>38</sub>H<sub>4</sub>]·7H<sub>2</sub>O, and the heptamolybdate that hydrogenation of Q must occur almost entirely on sulfided molybdenum sites. The bimetallic compound, (NH<sub>4</sub>)<sub>6</sub>[Co<sub>2</sub>Mo<sub>10</sub>O<sub>38</sub>H<sub>4</sub>]·7H<sub>2</sub>O,<sup>2</sup> with some cobalt should

generate catalyst particles with some portion of the surface "protected" by cobalt. Consequently, if sulfided molybdenum sites are indeed responsible for hydrogenation and surface areas are comparable, one would expect the  $(\text{NH}_4)_6[\text{Co}_2\text{Mo}_{10}\text{O}_{38}\text{H}_4] \cdot 7\text{H}_2\text{O}$  derived catalyst to exhibit lower TFs for Q hydrogenation, as observed.

Polymetallic HPA Precatalysts vs Conventional or Monometallic HPA Precatalysts: We have conducted one set of tests based on our previous discovery that RuMo bimetallic systems were exceptionally active HDN systems.<sup>3</sup> Our previous studies were conducted with the objective of optimizing Ru/CoMo/ $\alpha$ -alumina catalysts for the HDN of Q to propylbenzene.<sup>3</sup> It was assumed that the major function of Ru in this trimetallic system is to promote C-N bond cleavage at low temperatures. Limited efforts were made to determine the effects of ruthenium on the individual metals (Co and Mo) with the finding that a RuMo organometallic surface confined catalyst exhibits the same synergistic activity for production of propylbenzene as the trimetallic catalyst. However, no effort was made to explore the effects of Ru on Q hydrogenation activity in this catalyst system.

Figures 5 and 6 show Q to THQ conversions as a function of time for typical reactions run using Ru/Mo-HPAs bimetallic systems where Ru is introduced either as  $\text{RuCl}_3$  or  $\text{Ru}_3(\text{CO})_{12}$ , and for the individual precatalysts. These Figures also show the simple sums of the conversion percentages of the individual catalysts for comparison with the true bimetallic catalysts. In both instances, the actual bimetallic catalyst offers activities some 20% higher than the sums of the two metals used individually. The results clearly point to a synergistic system. However, it is too early to speculate on the reasons for these results.

Hydrogenation Modeling Studies vs HDN Activity vs. Coal Liquefaction Behavior. The RuMo precatalyst system, which shows good Q to THQ conversion activity, was studied based on the exceptional abilities of a supported RuMo material to promote THQ HDN catalysis as previously reported from these laboratories.<sup>3-8</sup> Although it is tempting to claim that the hydrogenation activities parallel the previously observed C-N bond hydrogenolysis activities, we believe that the parallel is coincidental. For example, both Rh and Pd catalysts are quite effective hydrogenation catalysts but exhibit only moderate HDN activity.<sup>9,10</sup>

The current studies with a Ru/Mo-HPA precatalyst system works well and will be explored extensively in the future. However, this system can only serve as a baseline for liquefaction studies because the precatalyst system consists of a mixture of soluble forms of both Ru and Mo. In direct liquefaction studies, a major concern will be our ability to create the same bimetallic catalyst properties in single particles following impregnation of coal with the two independent, soluble species. We view this as unlikely with the current set of precatalysts.

### **Acknowledgements**

We wish to thank the Department of Energy and the Pittsburgh Energy and Technology Center for generous support of this work through contract no. DE-FG22-90PC90313. We would also like to thank Dr. A. Hirschon of SRI International for helpful discussions.

### **References**

1.  $k_{\text{obs}}$  at each temperature is obtained from the slope of the equation,  $d[\text{THQ}]/dt = k_{\text{obs}}[\text{Q}]^0$ , assuming zero order reaction from data obtained. The activation energy,  $E_a$ , is calculated from the expression  $k_{\text{obs}} = Ae^{(-E_a/RT)}$ .
2. G. Tsigdinos, Dissertation Abstract, University of Michigan, B22, 732 (1961)
3. "Modeling the Hydrodenitrogenation Reaction Using Homogeneous Catalyst Model Systems." A. S. Hirschon, R. B. Wilson, Jr.; and R. M. Laine, *New J. Chem.*, **11**, 543-547 (1987).
4. "New Catalysts for Hydrotreating Coal Liquids." A. S. Hirschon, R. B. Wilson Jr., and R. M. Laine, *Am. Chem. Soc. Div. Fuel. Prepr.* **31**, 310-317 (1986).
5. "New Approaches to Enhance Hydrodenitrogenation of Coal Liquids" A. S. Hirschon, R. B. Wilson, Jr., R. M. Laine, in Adv. in Coal Chemistry, Theophrastus Publ, Athens 1988, p 351.
6. "Ruthenium Promoted Hydrodenitrogenation Catalysts." A. S. Hirschon, R. B. Wilson Jr., and R. M. Laine, *J. Appl. Cat.* **34**, 311-316 (1987).
7. "Bulk Ruthenium as an HDN Catalyst", A. S. Hirschon and R. M. Laine, *J. Energy and Fuels* **2**, 292-295 (1988).
8. "Use of Promoters to Enhance Hydrodenitrogenation and Hydrodeoxygenation Catalysis", A. S. Hirschon, L. L. Ackerman, R. M. Laine, and R. B. Wilson, Jr. *Proc. of the 1989 Internat. Conf. on Coal Science, Tokyo.*, Vol. **II**, p. 923.
9. S-I Murahashi, Y. Imada, and Y. Hirai, "Rhodium Catalyst Hydrogenation of Quinolines and Isoquinolines under Water-Gas Shift Conditions", *Bull. Chem. Soc. Jpn.* **62**, 2968 (1989).
10. M. J. Guttieri and W. F. Maier, *J. Org. Chem.* **49**, 2875 (1984).

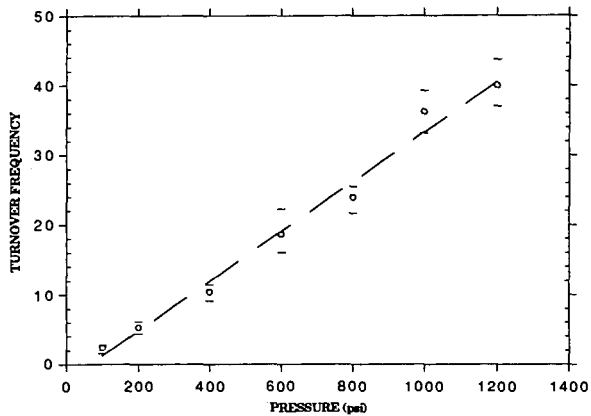


Figure 1. Turnover Frequency as a Function of Initial  $H_2$  Pressure.  
Pressures shown are measured at room temperature.

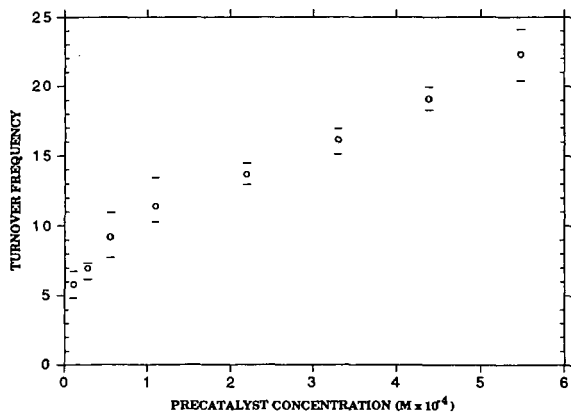


Figure 2. Turnover Frequency as a Function of [Mo-HPA]  
Activities were determined based on less than  
25% conversion of Q to THQ

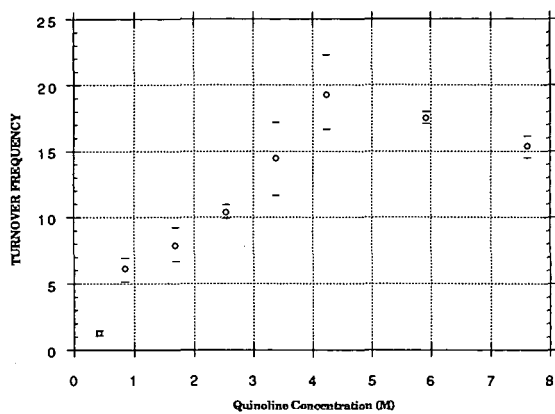


Figure 3. Turnover Frequency as a Function of Changes in [Quinoline]

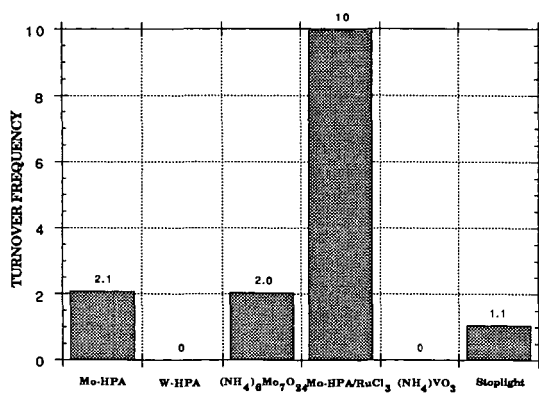


Figure 4. Initial Turnover Frequencies at 175 °C, 400 psig H<sub>2</sub> for Selected Precatalysts. TFs calculated based on total moles of metal. Error limits are +6%.

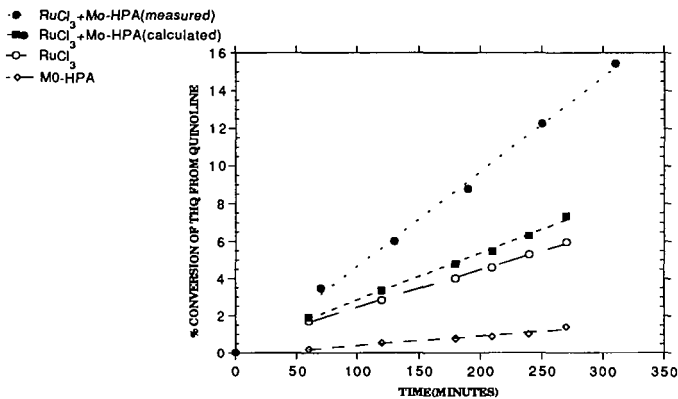


Figure 5. Percent Conversion of THQ from Quinoline for Bimetallic Precatalyst Systems (Mo-HPA, Mo-HPA/RuCl<sub>3</sub>·3H<sub>2</sub>O, and RuCl<sub>3</sub>·3H<sub>2</sub>O). Reactions run at at 175 °C, 400 psiiH<sub>2</sub>.

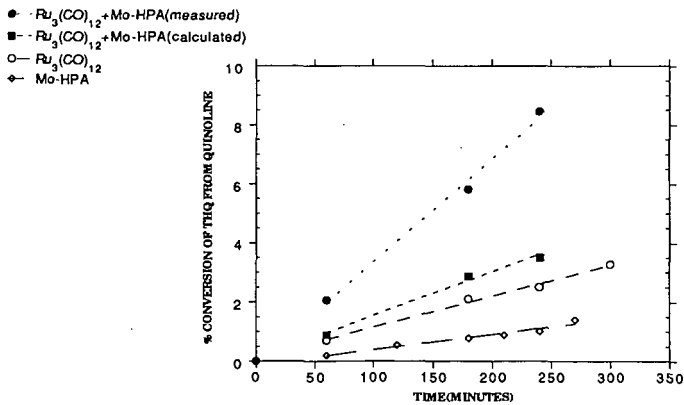


Figure 6. Percent Conversion of THQ from Quinoline for Bimetallic Precatalyst Systems (Mo-HPA, Mo-HPA/Ru<sub>3</sub>(CO)<sub>12</sub> and Ru<sub>3</sub>(CO)<sub>12</sub>). Reactions run at 175 °C, 400 psiiH<sub>2</sub>.